TECHNISCHE UNIVERSITÄT MÜNCHEN

Lehrstuhl für Biotechnologie der Nutztiere

Identification and characterization of the novel planar cell polarity gene *Flattop* (*Fltp*)

Moritz A. Gegg

Vollständiger Abdruck der von der Fakultät Wissenschaftszentrum Weihenstephan für Ernährung, Landnutzung und Umwelt der Technischen Universität München zur Erlangung des akademischen Grades eines

Doktors der Naturwissenschaften

genehmigten Dissertation.

Vorsitzender: Univ.-Prof. Dr. H. Luksch

Prüfer der Dissertation:

1. Univ.-Prof. A. Schnieke, Ph.D.
2. Univ.-Prof. Dr. H. Lickert

Die Dissertation wurde am 17.09.2012 bei der Technischen Universität München eingereicht und durch die Fakultät Wissenschaftszentrum Weihenstephan für Ernährung, Landnutzung und Umwelt am 08.02.2014 angenommen.

Danksagung

In den nächsten Zeilen möchte ich all jenen danken die es mir ermöglicht haben mein Studium und meine Promotion erfolgreich abzuschließen.

Ganz herzlich danke ich Herrn Professor Dr. Heiko Lickert für die Möglichkeit meine Diplomarbeit sowie meine Promotion in seiner Arbeitsgruppe anzufertigen. Deine Motivationsgabe ist erstaunlich! Danke für das Korrekturlesen dieser Arbeit.

Frau Professor Dr. Angelika Schnieke danke ich sehr herzlich für die Möglichkeit am WZW zu promovieren.

Herrn Professor Dr. Harald Luksch danke ich für die unkomplizierte und selbstverständliche Übernahme des Vorsitzes der Prüfungskommission.

Dr. Ingo Burtscher danke ich für die exzellente Fähigkeit der knock in Maus Generierung, die Einführung in Antikörperfärbungen sowie konfokal Mikroskopie und Antworten auf (fast) alle meine Fragen die ich während meiner Anstellung am Helmholtz Zentrum München hatte.
Mein herzlicher Dank gebührt Dr. Anika Böttcher für die Unterstützung bei dem – nicht immer einfachen – Fltp Projekt. Ich habe viel gelernt und es wäre schön gewesen wenn du früher zu uns gekommen wärst. Lass dich nicht unterkriegen…das läuft schon!
Anne, ohne dich hätte ich mindestens zwei Jahre länger gebraucht. Vielen Dank für die unzähligen PCRs, Sequenzierungen, Maushausbesuche, Apfelpausen, MOMA Asylanträge und lustigen Urlaubskarten. Der Inhalt deiner Schublade hat mir oft genug den Laboralltag versüßt.
Des Weiteren danke ich Daniela Padula, Wenke Barkay, Heide Oller, Silvia Engert, Steffan Hasenöder, Jacob Mutter, Alexandra Tregubova und der gesamten AG Lickert für die Hilfe im Labor und beim Fltp Projekt. Ich fand’s eigentlich jeden Tag sehr lustig im Labor und es hat mich sehr gefreut in einem so netten Team gearbeitet zu haben. Claude Van Campenhout danke ich für die Betreuung während des Dlg Projekts. Daraus resultierten meine Diplomarbeit und ein wunderbares paper. Wer hätte gedacht dass sich die Wege dieser beiden Projekte zu einem späteren Zeitpunkt kreuzen. Danke für die Dlg-Venus Maus und all die fertigen Konstrukte die uns das Arbeiten erleichtern.
Besonderer Dank gebührt all den verschiedenen Kooperationspartnern. Vielen Dank für die daraus resultierenden paper.

Allergrößter Dank gilt meinen Eltern die mir mein Studium ermöglicht, mich immer unterstützt und mir das kostspielige Leben in München mitfinanziert haben. Danke für Alles.

Danke dass du am frühen Morgen am Chinesischen Turm gesessen bist und wir uns nach sehr langer Zeit wieder getroffen haben. Danke dass es dich gibt Sari.

Contents

1 Abstract

How exactly signaling from the endoderm during early development patterns endodermal as well as mesodermal tissues and which set of genes play important roles is not completely understood. Therefore, spatial and temporal inactivation of genes especially and exclusively in the endoderm is of great interest. One of the earliest factors specifying the endodermal lineage is *Foxa2*. In this thesis we generated a new *Foxa2-iCre* mouse line for the analysis of conditional gene deletions during endoderm formation as well as in endoderm-derived tissues like the pancreas or the lung. Moreover, this *iCre* line can be used for genetic lineage tracing of cells that express *Foxa2*, more precisely of progenitor cells of the endoderm and stem cells of distinct tissues. With availability of this mouse line a big step towards the direction of understanding the key transcription factor networks, growth factors, and signaling molecules in the endoderm, endoderm derived organs, notochord, and floor plate is made. Functionality of the strategy was proven by the specific deletion of *Mib1* in the DE showing that Notch signaling is used iteratively to control cell fate choices during pancreatic development (Horn et al., 2012).

Recently, we discovered *Flattop* (*Fltp*; *17000009p17Rik*) in a microarray-based screen to identify potential *Foxa2* target genes and novel mouse gastrula organizer genes (Tamplin et al., 2008). *Pitchfork* (*Pifo*), another organizer expressed gene identified in the same screen is essential for cilia disassembly (Kinzel et al., 2010). Interestingly, both genes were also found in a screen for mRNAs abundant in tissues rich in highly ciliated cells such as the olfactory epithelium, the testis, and the lung, suggesting that both *Pifo* and *Fltp* encode for proteins involved in ciliogenesis (McClintock et al., 2008). To investigate the expression and function of *Fltp* in more detail, we generated a knock-in/knock-out construct ($Fltp^{ZV}$) where we replaced the complete open reading frame by introducing a *lacZ* (*Z*) and *Venus* (*V*) reporter gene. Additionally, we generated an iCre recombinase knock-in mouse line ($Fltp^{T2AiCre}$) for conditional gene targeting in distinct mono- and multiciliated tissues (Lange et al., 2012). In this thesis I describe the generation of the $Fltp^{ZV}$ mouse line as well as the analysis of the temporal and spatial expression pattern of the *Fltp* gene using the β-galactosidase and Venus fluorescent reporter proteins. Additionally, I report the analysis of the $Fltp^{ZV/ZV}$ knock-out phenotype.

Expression of *Fltp* is restricted to distinct mono- and multiciliated tissues that depend on planar cell polarity (PCP). PCP is a conserved mechanism that regulates, via a set of core PCP genes, the polarization and subsequently the orientation of cells within the plane of an epithelium. Our observation suggests that inactivation of *Fltp* results in developmental defects in the inner ear, the lung, the limbs, and during neural tube closure resulting in a phenotype usually observed in PCP mutants. We demonstrate that *Fltp* genetically interacts with the core PCP gene *Celsr1* in the inner ear as well as during limb bud development. Additionally, we could show that normal localization of Discs large 3 (Dlg3) is disrupted in *Fltp* homozygous mutants most likely due to defective transport. In air liquid interface culture of cultured multiciliated tracheal cells we could show that upon *Fltp* deletion basal bodies are not positioned uniformly at the apical surface but are stuck in the cytoplasm. We therefore hypothesize that *Fltp* is a new PCP effector gene acting in the basal body transport and positioning pathway together with Dlg3, basal body proteins, and secretory pathway proteins. The analysis of the $Fltp^{ZV}$ phenotype was additionally impeded by the strong background dependency of this gene.

2 Introduction

2.1 Early embryonic development of the mouse

Murine embryonic development starts with the fertilization of the egg in the oviduct followed by subsequent, tightly regulated, lineage specification events resulting in a multicellular organism (Figure 1). 24 hours after fertilization the zygote starts its first cell division. At the eight-cell stage, the blastomeres increase in size and start a process called compaction which results in apical-basal polarized blastomeres (Figure 1). The larger polarized outer cells will generate the trophectoderm (TE), the smaller inner cells form the *Oct3/4* and *Nanog* positive inner cell mass (ICM) (Figure 1, grey and orange cells) (Dietrich and Hiiragi, 2007; Niwa et al., 2005). In 1981 Martin showed that isolated ICM cells are pluripotent and serve as embryonic stem (ES) cells (Martin, 1981). At embryonic day 3.5 (E3.5) the developing embryo is called blastocyst and comprises the TE and the ICM. The TE will give rise to the extraembryonic tissues such as the placenta. A subset of the ICM will give rise to the embryo proper while the other ICM cells generate the primitive endoderm (PE) (Figure 1, grey, yellow, and blue cells). The PE surrounds the ICM on the surface of the blastocyst and will contribute to extraembryonic membranes; the other ICM cells will form the primitive ectoderm (epiblast) (Figure 1, grey, yellow, and blue cells). The whole embryo proper will develop from cells of the epiblast. At the same time the blastocyst implants into the uterine wall after it hatched out of the *zona pellucida*.

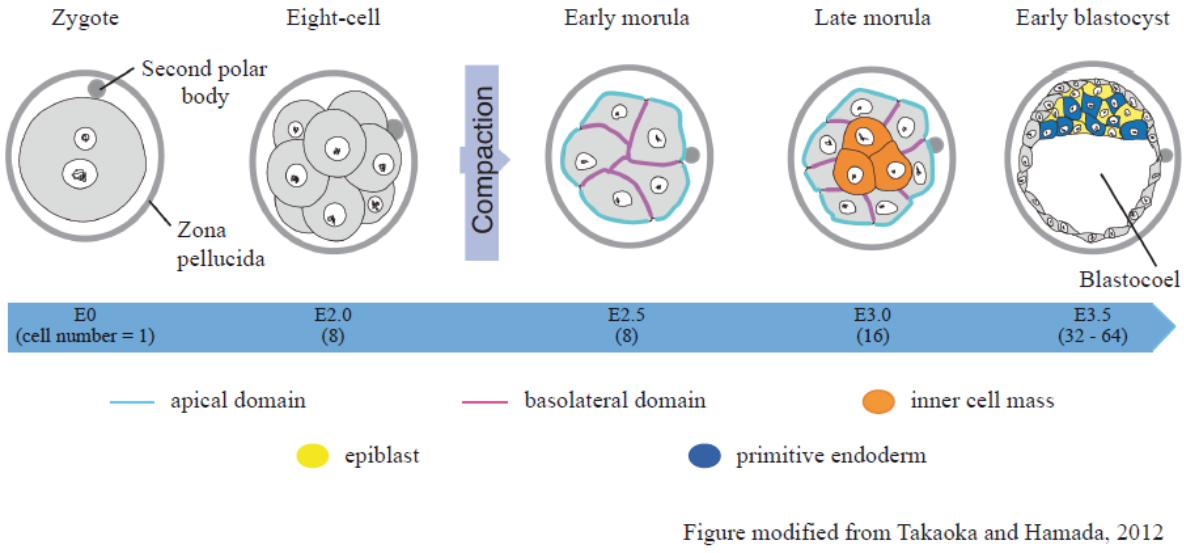

Figure modified from Takaoka and Hamada, 2012

Figure 1 Early cleavage in the mouse embryo – from zygote to blastocyst

The morphological changes and cell fate specification events taking place from zygote to early blastocyst stage. The zygote is protected by the *zona pellucida*. After 3 divisions compaction occurs and the morula forms. During compaction the cells establish apical-basal polarity (light blue and purple cell membranes). In the late morula ICM cells (orange cells) can already be distinguished from outer lying extraembryonic cells. At blastocyst stage ICM cells can be seen at the top of the blastocyst (yellow and blue cells). ICM cells give rise to the embryo proper and the outer layer, the TE, gives rise to extraembryonic structures (gray cells at early blastocyst stage).

The PE expands, covers the whole inner surface of the mural TE, and will later become parietal endoderm. The rest of the PE will form the visceral endoderm (VE) which covers the developing cup-

shaped epiblast (Figure 2). The cup-shaped embryo now consists of an embryonic and an extraembryonic part (Figure 2, border between grey and yellow cells). Before E5.5 the distal VE (DVE) forms at the distal tip of the embryo and starts to migrate towards the future anterior side of the embryonic cup (Figure 2, green cells) (Beddington and Robertson, 1998; Perea-Gomez et al., 2002; Piccolo et al., 1999). Through expression of the Nodal and BMP antagonists *Cer1* and *Lefty* by the anterior VE (AVE), the underlying epiblast is specified to future anterior identity (Belo et al., 1997; Piccolo et al., 1999). The epiblast on the opposite side of the embryo is out of reach for the inhibitory signals and thus these cells are able to induce primitive streak (PS) formation through *Nodal* and *Wnt3* expression (Figure 2, streak on the posterior side of the embryo) (Beddington and Robertson, 1998). PS formation is the onset of gastrulation which is a crucial step in embryonic development. During gastrulation the three germ layers - ectoderm, mesoderm, and endoderm - are being formed. One very important transcription factor for early embryonic patterning is Foxa2 (forkhead box transcription factor a 2; HNF3β). The forkhead family contains two other related helix turn helix transcription factors Foxa1 (HNF3α) and Foxa3 (HNF3γ) (Lai et al., 1990; Lai et al., 1991). *Foxa2* expression starts at E6.5 in the pre-streak-stage embryo in the posterior epiblast and the VE where Foxa2 positive cells intermingle slightly with brachyury (T) positive cells (Ang et al., 1994; Burtscher and Lickert, 2009). By the mid-streak-stage (E7.0) these two populations separate and Foxa2 positive cells orientate towards the proximal whereas T positive cells orientated towards the distal part of the posterior epiblast. Later, the T population gives rise to mesodermal cells, whereas the Foxa2 positive epiblast cells give rise to polarized and epithelialized structures such as the DE and the axial mesoderm including the cells of the node and notochord. Some Foxa2 positive epiblast cells turn on T immediately after epithelial-mesenchymal transition (EMT) and contribute to axial mesoderm formation. The important role of *Foxa2* during gastrulation is emphasized by the fact that *Foxa2* is essential for the expression of *Dkk1* (Glinka et al., 1998), *Cer* (Piccolo et al., 1999) and *Lefty* (Perea-Gomez et al., 2002) three important Wnt and Nodal antagonists in the VE at pre- to early-streak-stages (Kimura-Yoshida et al., 2007).

By E7.5 the murine embryonic node forms as an accumulation of cells at the distal tip of the embryo which is the anterior end of the PS. Isochronal the VE is completely replaced by DE. The node is an important transient structure of the late gastrula embryo that functions as an organizing center and is crucial for subsequent patterning of the embryo (Beddington, 1994; Blum et al., 1992). Organizer regions are, by definition, able to induce a secondary embryonic axis when transplanted ectopically. This ability was first observed in transplantation experiments in the newt by Spemann and Mangold and published in 1924. When they transplanted the dorsal blastopore lip of a dark pigmented newt in the ventral region of a non-pigmented newt they could observe the induction of a complete secondary axis (Spemann and Mangold, 1924). Analogous structures with organizing functions were identified in other model organisms such as the fish (shield) (Shih and Fraser, 1996), the chick (Hensen's node) (Hensen, 1876; Wetzel, 1925), the rabbit (Waddington and Waterman, 1933), the *Xenopus* (gastrocoel roof plate), and the mouse (Beddington, 1994; Kinder et al., 2001; Tam et al., 1997). The organizer cell population of the murine embryonic node consists of a dynamic population with varying potential to induce secondary axis depending on the stage of gastrulation (Kinder et al., 2001). During early gastrulation (E6.5) these cells contribute to the most anterior lying DE (ADE) and the prechordal plate whereas at later stages (midgastrulation), when the PS has elongated till the middle of the posterior side of the embryo, they contribute to the notochord, the ADE, and the axial mesoderm. At the late gastrula stage the node lies at the distal tip and contributes to the more distal lying parts of the notochord and the floor plate (Kinder et al., 2001). Despite the fact that the

organizing region was identified somewhat 88 years ago, only a few organizer specific genes are known up to now.

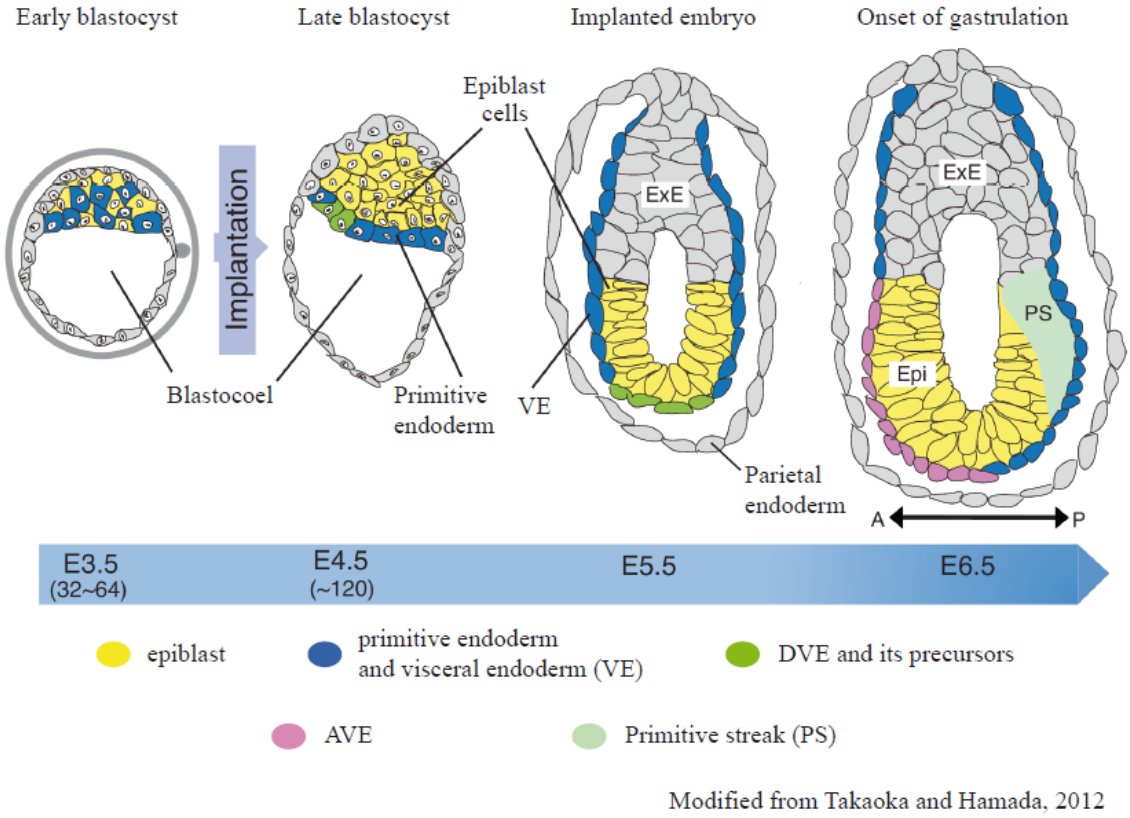

Figure 2 From implantation to gastrulation

The morphological changes and cell fate specification events taking place from early blastocyst to gastrulation stage. Implantation occurs between the early and late blastocyst stage. After implantation the ICM can be divided in epiblast cells and PE cells (yellow and blue cells). The green PE cells in the late blastocyst are the precursors of the DVE. At E5.5 the embryo elongates and develops an internal cavity. Now, it consists of an embryonic and an extra-embryonic part (ExE), is covered with VE (blue cells), and the DVE has formed (green cells). DVE cells migrate to the future anterior part of the embryo. The onset of gastrulation is marked by the appearance of the PS (light green stripe) on the future posterior side of the cup shaped embryo. It starts to elongate anteriorly till it reaches the distal tip. During gastrulation the 3 germ layers are formed.

Foxa2 expression is necessary for these organizer populations. *Foxa2*$^{-/-}$ mice are embryonic lethal and lack organizer cell populations (Ang and Rossant, 1994). The absence of the organizer cell populations leads to secondary defects in somitogenesis, organization of the notochord, and defects in development of the fore- and midgut (Ang et al., 1994; Weinstein et al., 1994).

2.1.1 Establishment of left-right asymmetry in the mouse embryo

The embryonic node is a transient structure in the midline of the murine embryo formed during gastrulation at the anterior end of the PS (see 2.1). The node has a pit shaped structure and the nodal pit cells are monociliated with a 9+0 axonemal structure but nevertheless motile (see 2.5). Monociliated crown cells surround the pit cells in a horseshoe shaped pattern. During the late headfold stage 200 to 300 motile monocilia are rotating counterclockwise in the node cavity thus generating a leftward flow (nodal flow) of the extracellular fluid surrounding the node (Nonaka et al.,

1998). At this stage the embryo breaks bilateral symmetry and establishes left-right asymmetry. Recently, it has been shown that only two functional motile monocilia are sufficient to break bilateral symmetry (Shinohara et al., 2012). Interestingly, if nodal cilia are absent like in *Kif3A* or *Kif3B* mutants or paralyzed such as in *inversus viscerus* (*iv*) mutants, where the *left-right dynein* (*Lrd*) gene is absent, the nodal flow cannot be generated and left-right axis determination is disturbed (Supp et al., 1997). This is a very strong argument for the hypothesis that the nodal cilia are indispensable for proper left-right asymmetry establishment.

2.2 Development of the murine lung

As already mentioned, the endoderm germ layer forms during gastrulation between the ectoderm and the mesoderm. The endoderm derived gut tube completely closes during embryonic turning at E8.5-E9.0. The endodermal organs such as the thymus, the thyroid, the lung, the pharynx, the liver, the pancreas, the stomach, the gastrointestinal tract, and the epithelial part of the ureter and the bladder are induced at distinct positions along the anterior-posterior axis of the gut tube through interactions with their mesodermal neighbors. The lung arises from the anterior foregut when it divides longitudinal to generate the dorsal esophagus and the ventral trachea (Que et al., 2006). The respiratory domain is marked by the transcription factor Nkx2.1 and the endodermal transcription factor Foxa2. At the distal site of the tracheal bud two buds appear which later branch into the characteristically tree shaped tubular network of airways (Metzger et al., 2008). This stereotypic branching requires tight regulation and communication between the epithelium and the surrounding mesenchyme mediated by Wnt, Shh, Bone morphogenetic protein (Bmp), FGF, and retinoic acid (RA) signaling (Morrisey and Hogan, 2010). At around E16.5, branching morphogenesis stops and maturation of the most distal airways starts by generation of saccules that later develop into alveoli.
During branching morphogenesis all the cell types of the mature lung have to be generated or at least precursor cells have to be created. At the distal tip of the extending branches multipotent Sox9 (HMG-box transcription factor) and Id2 (basic helix loop helix (bHLH) transcription factor) positive epithelial progenitors have been found that are able of generating all epithelial cell types including neuroendocrine cells (Rawlins et al., 2009a). Multiciliated cells are first arising at E14.0 in the trachea as well as in the main stem bronchi (Rawlins et al., 2007). The first ciliated cells appear in a salt-and-pepper fashion increasing in amount from proximal to distal.
The main function of the lung is to mediate gas exchange between the blood and the surrounding environment. The gas exchange takes place in the alveoli, located in the most distal part of the bronchioles. More proximal, a branched tubular network of conducting airways transports the gas to and from the alveoli. The alveolar epithelium consists of type one and type two alveolar epithelial cells (AEC1/2) and are absent of multiciliated cells. AEC1 cells are flat and take up almost the whole surfaces area of the alveoli whereas AEC2 cells have a cuboidal shape. AEC1 cells are the major functional unit for gas exchange. AEC2 cells are thought to be progenitors for AEC1 cells. The conducting airways are lined by a columnar epithelium which consists of multiciliated and secretory cells. Secretory cells generate mucus and multiciliated cells, beating in a uniform direction, move the mucus out of the respiratory airways. Through this mechanism, called mucociliary clearance, inhaled particles and pathogens are transported out of the lung. One cell type among the secretory cells is the Scgb1a1 secreting Clara cell. Rawlins et al. suggest that Scgb1a1 positive cells self-renew and are able to generate multiciliated cells (Rawlins et al., 2009b). The pseudostratified epithelium of mouse and human contains relatively undifferentiated basal cells. These cells have the capability of self-

renewal and are able to differentiate into ciliated cells as well as secretory cells (Rock et al., 2009). Therefore, basal cells are considered the stem cells among lung epithelial airway cells. The transcription factor *Trp63* is expressed in basal cells from E10.5 onwards. These proliferative cells mature - Notch dependent - into early progenitors that are intermediates between stem cells and differentiated cells (Rock et al., 2010).

2.3 Development and function of the inner ear

The vertebrate inner ear (IE) is an organ that mediates multiple sensory inputs including the sense of hearing, balance, and acceleration. To meet these diverse functions the membranous labyrinth is divided into two different functional parts: The dorsal, vestibular portion, which mediates the sense of balance and acceleration, and the ventral, auditory part, which is the place of sound perception.
The first optical manifestations of the developing IE are bilateral thickenings located near the developing hindbrain at E8.5 that mark the otic placode. In the course of development the ectodermal derived placodes descent under the surface ectoderm and form the otic cups and later the otic vesicles (Figure 3) (Barald and Kelley, 2004). By E10.5 neuroblasts delaminate from the ventral region of the otocyst that later will give rise to the statoacoustic ganglion (SAG) which is innervating the vestibular as well as the auditory part of the IE (Carney and Silver, 1983; Rubel and Fritzsch, 2002). One day later the endolymphatic duct starts to bud out of the dorsal otocyst and at the ventral side the first evidence of the cochlear duct is visible. At E12.5 the six prosensory patches that will later differentiate into the six sensory regions made up of mechanosensory hair cells and non-sensory supporting cells can be identified as epithelial thickenings. The six sensory regions include: the three cristae with the associated semi-circular canals, the utricular and the saccular maculae, and the organ of Corti embedded in the cochlea. The three cristae are responsible for maintaining balance, the two maculae are involved in perception of linear and angular acceleration and the organ of Corti mediates the sense of hearing. The cochlea grows during development till it reaches its final length of one and three quarter turns. The elongation of the cochlea takes place at the apical tip where newly formed sensory and supporting cells mature into their fully differentiated form.

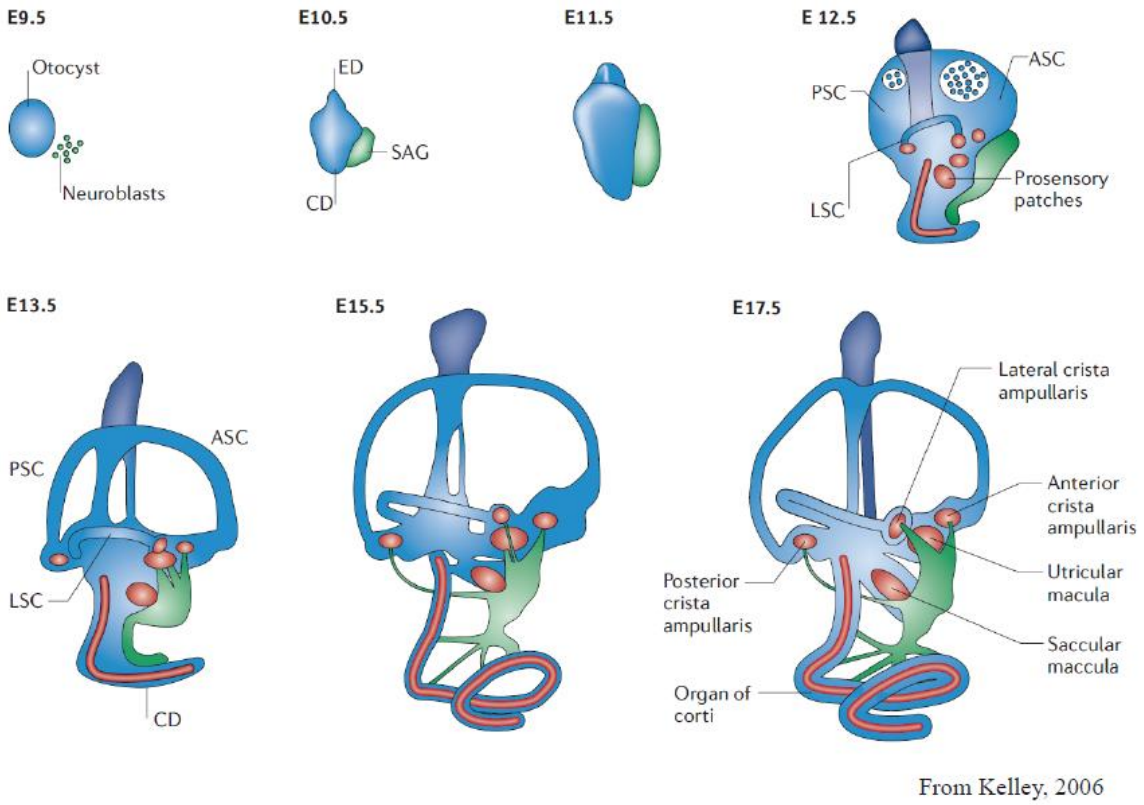

Figure 3 Development of the inner ear

Neuroblasts delaminate from the ectodermal derived otocyst at E9.5 to form the statoacoustic ganglion (SAG) by E10.5. The protrusions on the ventral and dorsal part are later giving rise to the cochlear duct (CD) and the endolymphatic duct (ED). By E12.5 the 6 prosensory patches can be identified (red). Additionally, the 3 semicircular canals appear: The anterior (ASC), the posterior (PSC), and the lateral semicircular canal (LSC). The blue dots indicate cell resorptions that are important to establish the mature canal phenotype. By E13.5 the cochlear duct elongates and the SAG starts to connect to the sensory patches. At E15.5 all sensory patches are innervated by the SAG neurons and the IE growth till it reaches its final morphology at E17.5.

The organ of Corti is embedded in the snail-like shaped cochlea and shows the highest degree of polarization of all sensory patches within the IE. It consists of four hair cell rows that are divided into one inner hair cell (IHC) row located on the medial side and three outer hair cell (OHC) rows located on the lateral side of the organ of Corti. Between these hair cell rows nonsensory supporting cells that provide structural and physiological support are distributed (Figure 4). Five to seven distinct types of supporting cells in the IE are known. However, a remarkable aspect of the organ of Corti is the precise alignment of the hair and supporting cells into highly ordered rows. These hair cells project actin-filled stereocilia arranged in a staircase manner on their apical surface. Moreover, viewed from the top onto the apical surface, these stereocilia show a “V”- or rather “W”-shaped arrangement that adopts a specific orientation on the apical surface of the hair cell that is crucial for its function and determined by the planar cell polarity (PCP) pathway. The organ of Corti is a highly polarized tissue not only because of the intrinsic polarity of the stereociliary bundle within each hair cell but also because of the uniform alignment of all hair cells across the whole length of the organ of Corti. Stereocilia develop from microvilli on the apical surface of the hair cells in the organ of Corti starting at around E15.5. First, the microvilli are all of a uniform height. In the center of the sensory cell, in the immature bundle, the kinocilium appears (Frolenkov et al., 2004). The actin filaments of

the stereocilia are anchored at the actin rich cuticular plate that is located right beneath the stereocilia. On the lateral side of the cuticular plate directly on the vertex of each "V"-shaped stereociliary bundle is an opening that accommodates the basal body (BB) and the kinocilium. The kinocilium is located directly next to the tallest stereocilia. By E16.5 the kinocilium starts to migrate to the lateral side of the cell surface membrane. The staircase arrangement maturation starts between E17.5 and postnatal day one (P1) and is finished latest at P7. At E18.5 the kinocilium-stereocilia-complex is relatively close to its final position. At P0 the BB is positioned in a way that the daughter centriole is localized closer to the lateral membrane and the mother centriole, which nucleates the kinocilium, is a bit more medial. Postnatally, the stereociliary bundle gets locked in its final place (Frolenkov et al., 2004). The kinocilium in the organ of Corti gets resorbed at P7.

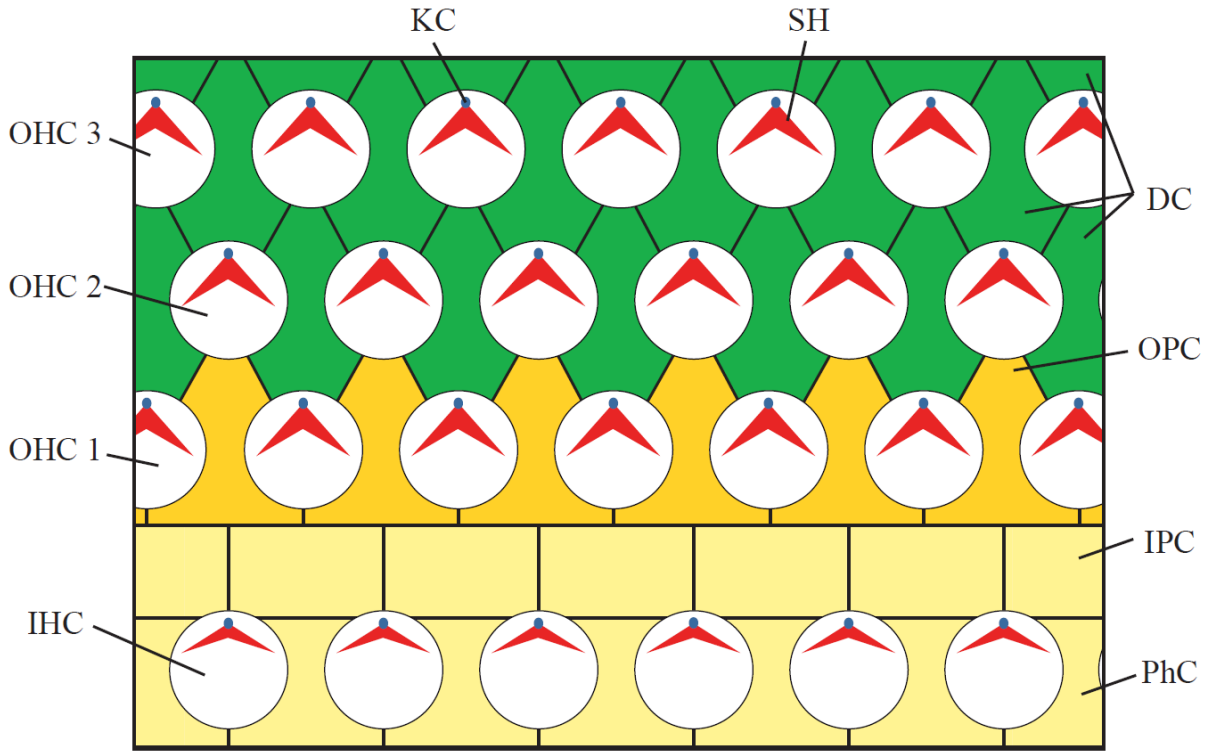

Figure 4 Diagram of the luminal surface of the organ of Corti

Hair cells (white) are arranged into 4 parallel rows. The single row of inner hair cells (IHC) is separated by inner pillar cells (IPC, beige) and outer pillar cells (OPC, yellow) from 3 rows of outer hair cells (OHC). Single IHCs are separated from each other by phalangeal supporting cells (PhC, beige). The 1st row of OHCs is separated by OPC and the 2nd and 3rd row is separated by Deiters' cells (DC, green). Each hair cell projects a single kinocilium (KC, blue) and a row of stereociliary hair bundles (SH, red) into the lumen of the cochlear duct.

The sensory organs of the vertebrate IE show distinct forms of PCP and provide an excellent opportunity to study the role of primary cilia in PCP. The IE and is a very sensitive model to study PCP defects because each sensory cell in the organ of Corti shows a coordinated and stereotype positioning of its primary cilium (kinocilium) at one defined side. The position of the kinocilium is dependent on the transport of the centrosome/BB to the lateral side. Therefore, I want to introduce the lifecycle of the centrosome in the next paragraph.

2.4 Centrosomes, centriole biogenesis, and basal bodies

To understand how a cilium forms it is crucial to understand the lifecycle of the organelles that build the cilium. The major player that in the end nucleates the whole cilium is the mother centriole of the centrosome, in this case called BB.

Centrosomes function as the microtubule (MT) organizing centres of animal cells thus influencing their shape, polarity, motility, as well as spindle formation, chromosome segregation, and cell division (Luders and Stearns, 2007). Centrosomes consist of two cylindrical MT based structures called centrioles which are surrounded by pericentriolar material (Figure 5). These two centrioles differ in age and maturity, therefore consequently called mother and daughter centrioles. Importantly, the mother centriole serves as the BB for cilia and flagella formation. During the past years more and more human syndromes, including ciliopathies, brain disease, and cancer, have been identified where centriole/BB formation and function are the pathogenic reason.

Whenever a cell enters the cell cycle it has only one centrosome and duplication of centrosomes has to be tightly controlled in order to avoid over duplication. Every centrosome consists of two centrioles. Adjacent to each existing centriole exactly one new centriole forms resulting in two centrosomes with one mature and one newly synthesized centriole. Two types of controls are needed to assure a constant centriole number. First, the cell cycle control guarantees that every centriole duplicates only once per cell cycle and, second, the copy number control, which allows the synthesis of only one new centriole next to a pre-existing one. In multiciliated tissues each cell harbours up to 200 cilia with adherent BBs which have formed adjacent to deuterosomes and amorphous proteinaceous structures that are unique to these cell type (Figure 5). '*De novo*' formation of centrioles was thought to be a rare event but now it is known that cells depleted of BBs are able to '*de novo*' synthesise new centrioles (Khodjakov et al., 2002). The centriole biogenesis starts at the transition form G1- to S-phase of the cell cycle by formation of one procentriole connected by the S-M linker (SML) to each pre-existing parental centriole (Figure 5). The procentrioles elongate throughout the S- and G2-phase and keep contact to the mother centriole by their SML (Figure 5). A mature centriole can be recognised by its distal and subdistal appendages which are important for MT anchoring and ciliogenesis. The pericentriolar material (PCM) encloses proteins with various functions such as the recruitment of centriole duplication factors (CEP152, CEP192) or the recruitment and assembly of PCM components (CEP215) (Cizmecioglu et al., 2010; Conduit et al., 2010; Dzhindzhev et al., 2010; Hatch et al., 2010). Late in cell division when centrioles are mature the SML is disintegrated. Beside of providing an attachment for the two centrioles the SML is an important control unit of centriole duplication. One model assumes that centriole re-duplication is prevented as long as the SML connects both mother and daughter centriole ('engaged') and that disintegration ('disengagement') serves as a signal for a subsequent round of centriole duplication (Tsou and Stearns, 2006). The second type of connection is the G1-G2 tether (GGT) that provides a rather loose connection between the proximal ends of mother and daughter centrioles at G1 and is by S connecting the two duplicating parental centrioles (Figure 5). Establishment of GGT occurs in G1 cells coeval with the disengagement of the SML. Live cell imaging of our centrin-GFP fusion cell line shows movement of the centrioles over micrometres confirming the rather loose GGT connection. The GGT allows the duplicated centrosomes to function as single MT organizing center during interphase until this tether is lost when bipolar spindle formation and subsequent chromosome segregation during mitosis take place. As already mentioned above, the two centrioles differ from each other. The mother centriole of a G1 cell has distal and subdistal appendages which are absent on the daughter centriole. The subdistal appendages are important for cell division as

they function in organizing the interphase MT cytoskeleton. The distal appendages dock the distal part of the mother centriole to the plasma membrane where it now functions as the BB nucleating a cilium (Hoyer-Fender, 2010). After cell division the mother centriole gets inherited to one of the daughter cells whereas the former daughter centriole gets inherited to the other daughter cell and functions as the new mother centriole. Through this cycle every daughter centriole becomes a mother centriole and stays a mother centriole. The cell with the former mother centriole is able to build a cilium much faster than the cell with the former daughter and, as a consequence, respond different to Shh signaling (Anderson and Stearns, 2009).

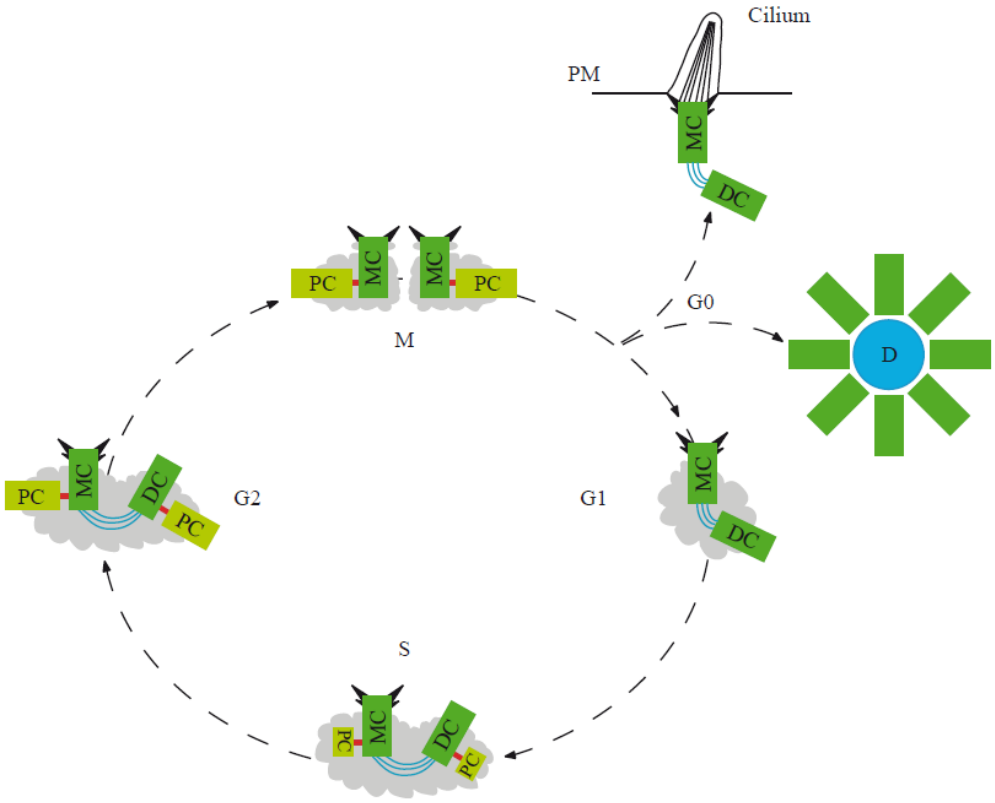

Figure 5 Centriole biogenesis

At the transition from G1- to S-phase the centriole starts to duplicate. Each mature centriole from the G1 centrosome (mother centriole, MC, dark green) starts to assemble a pro-centriole (PC, light green). The mother centriole has distal and subdistal appendages whereas the daughter centriole (DC) has not. Pro-centriole elongation continues through G2 until 2 centrosomes, each consisting of 2 centrioles, are present. These centrosomes move to the cell poles and ensure centrosome segregation during M-phase. In early M-phase the 2 “older” centrioles lose their tight association in a process called disengagement. After the M-phase the cell can enter a quiescent stage (G0) and nucleate a primary cilium from the MC in monociliated cells or assemble deuterosomes (D) in multiciliated cells. From G1- to early G2-phase the 2 mature centrioles are held together by the G1-G2-tether (GGT; blue). From the S- till the early M-phase the centrioles and the pro-centriole are connected via the S-M-linker (red).

With this basic knowledge we can start to understand how a cilium is assembled.

2.5 A bifunctional organelle - the motile and sensory function of the cilium

The cilium was first described by light microscopic analysis by Karl Wilhelm Zimmermann over 100 years ago in kidney tubular epithelial cells (Zimmermann, 1898). Around 50 years later its ultrastructure was observed in detail and during the last ten years the cilium became object of intense scientific studies. The interest increased because the cilium was pathogenic in ciliopathies such as *situs inversus* and polycystic kidney disease.

Cilia are MT based cellular organelles that extend form the plasma membrane of almost every cell type of the murine and human body. The MT based axoneme is covered by the cells' plasma membrane. Cilia can only be built when the cell exits the cell cycle into a quiescent G0 state (Figure 5). Reentry into the cell cycle implies the resorption of the cilium. To assemble a cilium the cells transport machinery has to deliver specific ciliary proteins to the BB that nucleates the cilium. Because no protein synthesis does occur in the cilium all proteins have to be transported along the cilium. This process is dependent on intraflagellar transport (IFT) and therefore mutations in genes coding for IFT particles causes defects in basically all cilia (Pazour et al., 2000; Rosenbaum and Witman, 2002). The microtubule + ends of the axoneme are located at the ciliary tip and intraflagellar transport towards the tip (anterograde) is mediated by a family of proteins called kinesins whereas transport from the tip towards the lumen (retrograde) is accomplished via dyneins.

In general cilia are able to fulfill two different functions. Motile cilia can actively move cells through their environment and transport extracellular fluid over the surface of an epithelium. Immotile cilia sense environmental signals that influence the cells behavior. It is a fact that cilia of various organs are remarkably diverse in their signaling capabilities and that both sensory and motile functions can be separate or mixed in these cilia (Bloodgood, 2010). Because of their function cilia are classically grouped in motile (9+2) and in immotile "primary" (9+0) cilia (Figure 6). The term 9+2 refers to the nature of the ciliary axoneme.

In case of a motile cilium, the ciliary axoneme consists of nine outer MT doublets that surround a pair of inner MTs and contain associated structures like radial spokes and inner and outer dynein arms. Motile cilia are present in large numbers on epithelial cells of the trachea, the lung, the choroid plexi, the ventricles, and the oviduct. Most of these cilia are able to move extracellular fluid over epithelial linings (Figure 6 A, D). Multiciliated cells in the epithelial lining of the trachea and the lung move mucus out of the respiratory system (mucociliary clearance). The motile cilia on the multiciliated ependymal cells generate the ependymal flow which corresponds to the movement of the cerebrospinal fluid in the brain ventricles. A specialized form is the flagella of the sperm tail which is propelling the sperm through the uterus towards the female egg cell. Primary nodal cilia constitute an exception of this classification because they have a 9+0 axonemal structure but nevertheless are motile. Recent studies argue that there are even two types of cilia in the node that are both essential to break bilateral symmetry (McGrath et al., 2003). The set of cilia covering the nodal pit cells is motile and generates the nodal flow whereas the cilia covering the nodal crown cells are immotile and respond to that fluid flow. It is of great importance that the motile cilia are tilted to the posterior side relative to the cellular axis and their axonemes rotate counter clockwise to generate the nodal flow which is indispensable for establishment of left-right asymmetry (Nonaka et al., 2005).

Compared to motile cilia a primary cilium lacks specific components for active motility such as the dynein arms and additionally the axoneme is buildup of nine outer MTs with the inner MT pair missing (Figure 6). After standing in the shadow of their motile siblings for a long time, sensory cilia are now in the limelight of scientific research. Because of their immotility primary cilia were thought to be vestigial motile cilia with no function. The kinocilium is another form of a specialized cilium.

Regardless its 9+2 axonemal structure it is present as a single immotile cilium in sensory hair cells of the vestibular as well as the auditory part of the IE. Together with the BB and the PCP machinery the kinocilium is important for establishment of the stereotypic arrangement of the sensory hair cells in the IE. Primary cilia are immotile and serve as an antenna to sense extracellular signals. Primary cilia are always – if present on an epithelial cell – located to the luminal site of the organ and possess a 9+0 axonemal structure (Figure 6 B, E). In other cellular types it is more complicated to study primary cilia because they are squeezed between adjacent cells or the extracellular matrix. In a couple of organs the functionality of these cilia strongly depends on the position and orientation of the axoneme in the 3D space. It has been shown recently that cilia can mediate different types of signal transduction (e.g. Shh, platelet derived growth factor receptor (PDGFR), and non-canonical Wnt signaling (PCP)) via its various receptors and channels accumulating at the ciliary membrane (Huangfu et al., 2003; Ross et al., 2005; Schneider et al., 2005). The density of receptors and channels accumulated at the ciliary membrane could influence the ability of cilia to respond more or less towards outside signals. In some organs multiciliated and monociliated cells can be found next to each other (e.g. uterine tube).

The hedgehog (HH) signaling pathway is dependent on ciliary function because loss of HH activity resembles the phenotype observed in IFT mutants including holoprosencephaly, polydactyly, craniofacial defects, and skeletal malformations (McMahon et al., 2003). The IFT machinery is extremely important for HH signaling transduction downstream of the receptor patched-1 and upstream of activated transcriptional targets. The importance of cilia for HH signaling is again underlined by the fact that the major transcriptional targets of HH the glioma (Gli) proteins as well as the suppressor of fused (Sufu) are located to the distal tip of the cilium in primary limb bud cell culture (Haycraft et al., 2005). Furthermore, there is accumulating evidence that Gli3 is processed at the ciliary tip into its repressor form $Gli3^R$ that represses HH target genes. In the absence of HH ligand patched does not release Smoothened (Smo) bound in a vesicle and Gli3 is constantly proteolysed into its repressor form. By the IFT machinery and dynein motors $Gli3^R$ is transported to the nucleus and represses target gene activation. When the HH ligand binds to patched, Smo is released from the vesicle and can suppress the proteolysis of Gli3 resulting in the activator form of Gli3 which in turn is transported to the nucleus and activates target genes.

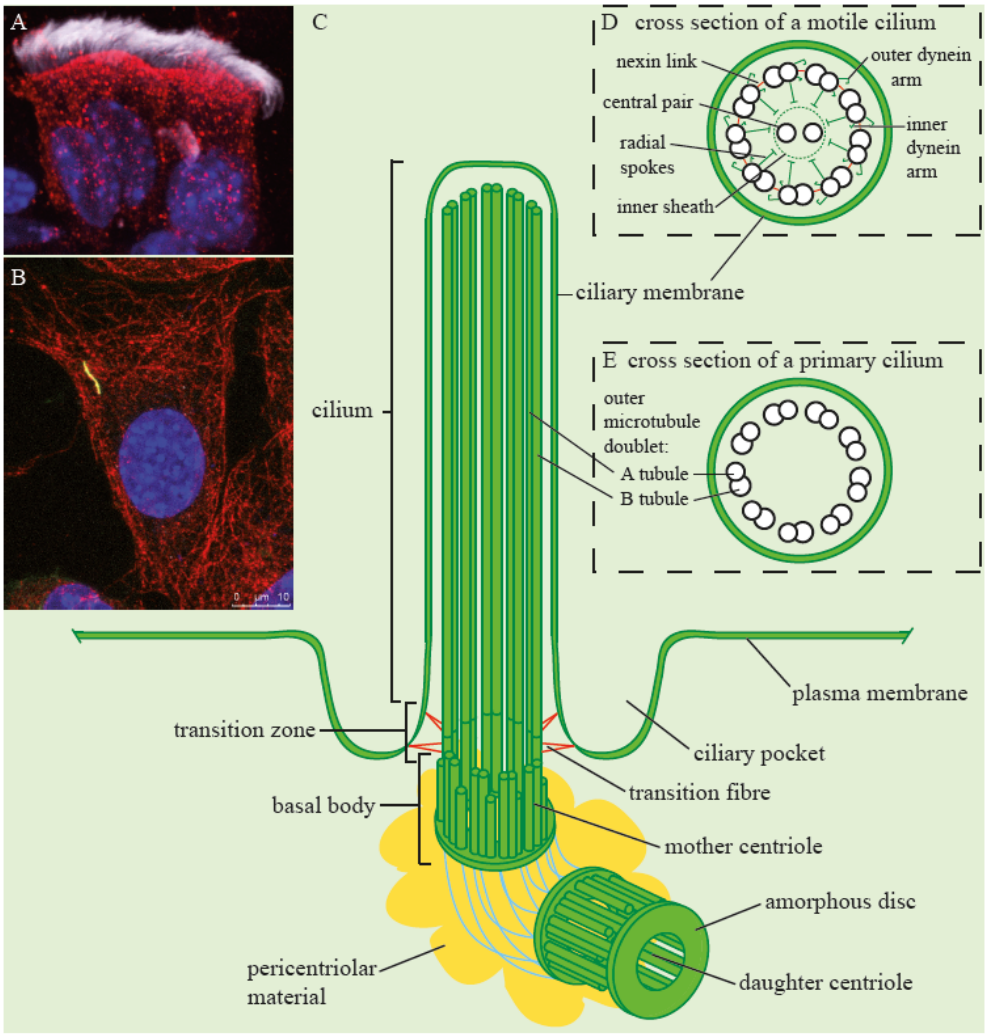

Figure 6 The cilium

Every cilium is nucleated via the mother centriole (basal body, BB).
(**A**) Immunofluorescence image of multiciliated bronchial epithelial cells (red: BB; white: cilia; blue: nucleus).
(**B**) Immunofluorescence image of a primary cilium on an IMCD3 cell (red: α-tubulin; yellow: cilium; blue: nucleus).
(**C**) Schematic diagram of a primary cilium. The BB is surrounded by the pericentriolar material and builds the axoneme. The transition fibers anchor the mother centriole at the plasma membrane. In the transition zone the microtubule (MT) triplets of the BB are converted into doublets of the axoneme. The ciliary membrane is separated from the plasma membrane and contains an accumulation of signaling receptors and channels.
(**D**) Cross section of a motile cilium. The central MT pair is surrounded by 9 MT doublets which are connected via nexin links. Inner and outer dynein arms are crucial for motion. The radial spokes have a stabilizing function.
(**E**) Cross section of a primary cilium. In contrast to a motile cilium, the central MT pair and the dyneins are missing.

Soon after the finding that cilia are important signaling organelles several human disease and syndromes turned out to be caused by defects in ciliary motility, -transport, and -signal transduction. These ciliopathies include polycystic kidney disease, Bardet-Biedl syndrome (BBS), Meckel-Gruber syndrome, orofaciodigital syndrome, nephronophthisis, hydrocephalus, *situs inversus*, blindness, chronic bronchitis, obesity, hearing loss, and most likely also cancer and diabetes.

In some cells of specialized ciliated tissues (e.g. the IE and the node) the cilium has to be positioned on a defined place on the apical surface in order to fulfil its designated function. In those cases a defined class of molecules guide the way for the BB and subsequently the cilium. This mechanism is called ciliary positioning. The current knowledge of ciliary positioning suggests that docking of the mother centriole to the plasma membrane is the initial step of the positioning process. To understand the docking process it is of great importance to understand how cilia become localized always at the same position on the plasma membrane. Docking of the BB is a prerequisite in every cell that has a cilium but its position differs from cell type to cell type. Depending on the tissue some cells are copying their neighbours in regard of ciliary positioning and others are independent of surrounding cells. It is clear that the site of BB docking to the apical surface (translational orientation) as well as the orientation of the basal foot of the BB in respect to the cells polarity (rotational orientation) affects ciliary function (Marshall and Kintner, 2008). In tubular organs primary cilia always emerge from the center of the luminal side of the cell. In the sensory epithelium of the mammalian IE the actin filled stereocilia rely on the proper position of the microtubular kinocilium on the apical surface of the epithelium (Dabdoub and Kelley, 2005). The precise position of the BB, the kinocilium, and the stereociliary bundle is coordinated by a specific signaling pathway called PCP pathway (Goetz and Anderson, 2010). In early developmental stages of the cochlea the BB is docked in the center of the IE hair cell and repositions to the lateral side when polarity is established (Jones and Chen, 2008).
It is not surprising that also some multiciliated tissues depend on distinct BB and ciliary axoneme positioning. The ependyma, the respiratory tract, or the reproductive tract harbors actively beating cilia that show a coordinated beating in the same direction.

2.6 Establishment of apical-basolateral polarity

During embryonic development, more precisely during compaction of the blastomeres of the early morula, the apical-basolateral (AB) polarity is the first polarity the embryo establishes (see 2.1). This initial polarization is essential for the formation of epithelia, for asymmetric cell division, and for directed migration. Due to AB polarity the late morula begins to specify the future ICM cells and the outer lying future extraembryonic cells.
In general, the AB polarity of cells results in at least two different plasma membrane compartments with different functions. First, the apical surface facing the external medium and shielding the more inner laying compartments from the outside, and second, the basolateral membrane domain which connects the cells to their neighbors and the connective tissue. AB polarity is most prominent in epithelial cells. Epithelial cell sheets can only function because of cell junctions holding the cells together. The most apical laying junctions are the tight junctions (TJ) that constitute the border between the apical and the basolateral membrane domain (Figure 7). These junctions basically fulfill two functions: first, they constitute a diffusion barrier to fluid and seal the intercellular space; second they maintain the AB polarity of epithelial cells by inhibiting diffusion of membrane molecules along the lateral cell membrane. The building blocks of TJs are the transmembrane proteins occludin, claudin, and junctional adhesion molecules (JAM). Together with the TJs the more basally localized adherens junctions (AJ) form the apical junctional complex (AJC) (Shin et al., 2006). The core of AJs is built of the cadherin-catenin complex and the nectin-afadin complex. The extracellular domains of cadherin and nectin form homophilic interactions that stabilize the AJ (Figure 7).

Establishment and maintenance of AB polarity requires three distinct complexes: the Crumbs complex, the Par complex, and the Scrib-Lgl-Dlg complex. Members of this polarity machinery are well known to interact with signaling pathways like Wnt, HH, and Hippo, as well as with the cytoskeleton and, during mitosis, they are important for asymmetric cell division.

The Crumbs (Crb) complex is important for establishment of the apical membrane identity by stabilizing apical cell junctions and interacting with TJ proteins (Figure 7). Therefore, proteins found in this complex localize to the apical membrane and the TJs. The eponymous member of the Crb complex is Crb itself. Through gene duplication mammals generated three homologs of the *Drosophila Crb* (*Crb 1-3*) (Medina et al., 2002). The second member of the Crb complex is PALS1. This molecule is the adaptor protein to mediate the indirect interaction of Crb and PATJ (Figure 7). PATJ (PALS1-associated tight junction protein) is the third member of the Crumbs complex. PATJ provides the link between the lateral (Occludin, ZO3) and the apical (Crb, PALS1) components of TJs and additionally stabilizes the Crb complex (Figure 7).

Another complex is the Par (partitioning-defective) complex which defines the apical basal membrane border (Figure 7). Here, the eponymous members are the Par proteins. Its members are Par3, Par6, aPKC (atypical protein kinase C), and CDC42 (cell division control 42). The main function of Par6 is to enable aPKC to interact with its downstream effectors like Lgl (Yamanaka et al., 2003). Par3 in polarizing cells is located to the Par6 complex and later in polarized cells interacts with cell adhesion molecules and associates with other TJ proteins like ZO-1 (Figure 7) (Kohjima et al., 2002). In mammals two aPKC isoforms exist denoted as aPKCλ and aPKCζ. aPKC functions also in the Par complex and is phosphorylating Par3 and Lgl (Nagai-Tamai et al., 2002; Plant et al., 2003). In Madin Darby canine kidney (MDCK) cells aPKC and the rest of the Par complex localizes at TJs (Figure 7) (Izumi et al., 1998).

The Scrib-Lgl-Dlg complex is located in mammals to the AJs and in *Drosophila* to the septate junctions (SJ) and by this defining the basolateral membrane compartment (Figure 7). Its members are Scribble (Scrib), Discs large (Dlg), and Lethal giant larvae (Lgl). In polarized cells Scrib is associated with β-catenin at the AJs. Scrib and E-cadherin are mutually dependent to localize both to the AJs (Navarro et al., 2005). In *Drosophila* the main function of Scrib is to exclude apical proteins like the Crb complex from the basolateral domain (Bilder and Perrimon, 2000). Dlg physically interacts with Scrib in *Drosophila* (Mathew et al., 2002). Due to gene duplication five mammalian *Dlg* homologs (*Dlg 1-5*) are known. *Lgl* in mammals is also duplicated (*Lgl 1-4*). Lgl1/2 are phosphorylated by aPKC and localized at the lateral membrane below the AJs. During polarity establishment Lgl can be found in a complex with Par6 and aPKC and disengages when Lgl is being phosphorylated (Yamanaka et al., 2003).

The first step of AB polarity establishment in epithelial cells is the formation of adhesive homophilic interactions from puncta through Par3, E-cadherin, and junctional adhesion molecule A (JAMA) (Adams et al., 1998). These first junctions contain molecules from AJs and TJs and spread along the whole basolateral membrane (Tsukita et al., 2009). During the next steps the AJs and TJs are being formed. First PAR3 has to be excluded from the junctional complex and localized to the subapical region where it forms a complex with Par6 and recruits aPKC to the subapical domain. E-cadherin in the junctional complex activates Cdc42 which in turn phosphorylates aPKC. Through phosphorylation of Par3 by aPKC, Par3 is subducted from the TJs subsequently allowing TJ formation and the separation of apical and subapical domain (Horikoshi et al., 2009). Subsequently, aPKC phosphorylates Lgl and Lgl dissociates from the Par6-aPKC complex and complexes with Dlg and Scrib at the basolateral membrane (Plant et al., 2003). It is known from *Drosophila* that Dpatj is able to modulate the phosphorylation of Crb by aPKC and phosphorylated Crb is important for correct

localization of aPKC and Dpatj to the apical membrane compartment and also for Scrib to the basolateral domain (Sotillos et al., 2004). Cbr3 and Par6 interact directly or via Pals1 and promote differentiation of the premature junctional complex into the mature epithelial structures including TJs (Hurd et al., 2003; Lemmers et al., 2004). The Scrib complex restricts the Cbr and the Par complex to the apical side where they interact to form TJs. These three complexes are not only interacting with each other but also with the cytoskeleton to influence cell shape.

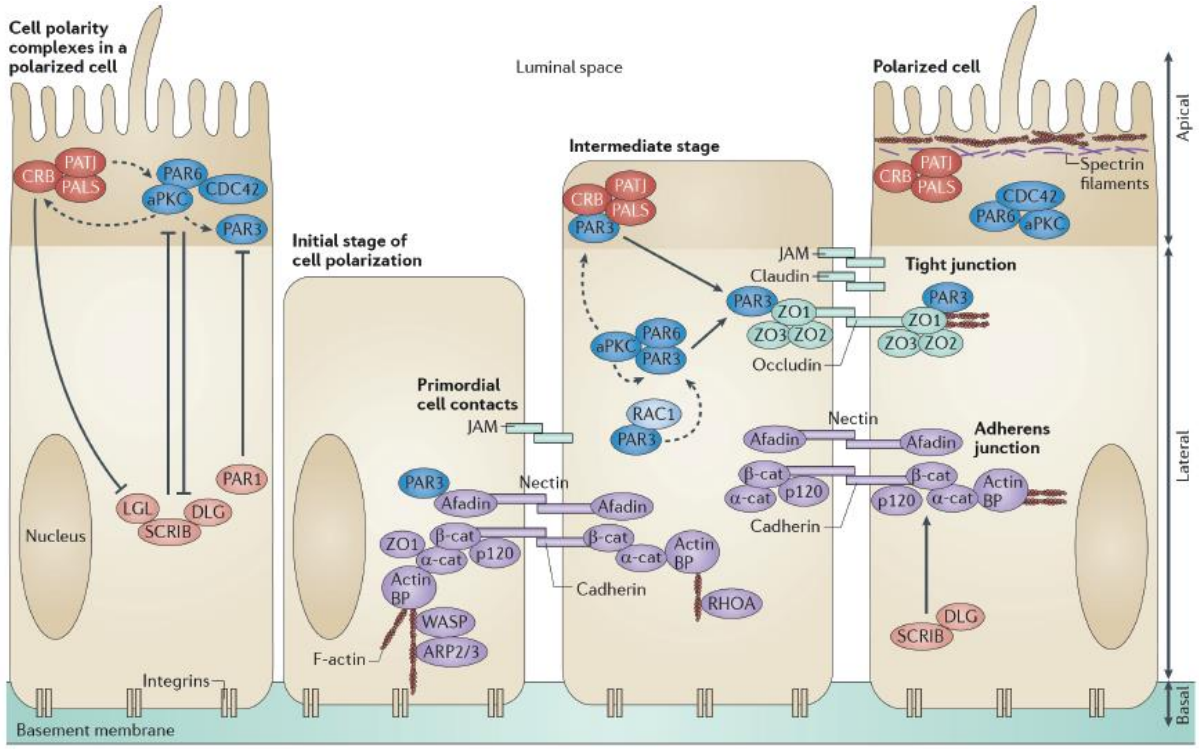

Martin-Belmonte and Perez-Moreno, 2012

Figure 7 Epithelial cell polarity complexes

Together with TJs and AJs 3 major complexes regulate apical-basolateral (AB) polarity establishment: the Crb complex (red) is responsible for the apical membrane identity and unifies the transmembrane protein Crb and its associated cytoplasmic proteins PALS1 and PATJ; the Par complex (blue) required for establishment of the apical-lateral membrane border and comprising Par3, Par6, aPKC, and CDC42; and the Scrib complex (rosa) which defines the basolateral membrane compartment and consists of Scrib, Dlg, and Lgl. During AB polarity establishment these 3 complexes antagonize each other and interact with the cytoskeleton as well as with membrane proteins of TJs and AJs. At the initial stage of cell polarization Par3 binds to Afadin and this generates the first primordial adhesions which later give rise to the AJs and TJs. Subsequent steps include exclusion of Par3 through phosphorylation by aPKC from the primordial adhesions as well as from Par6-aPKC and Crb complex establishing the apical-lateral border and the apical membrane compartment. The Scrib complex antagonizes the Par and the Crb complex by restricting them to the apical surface and defining the basolateral domain.

2.6.1 The neoplastic tumor suppressor gene *Discs large 3*

Discs large (*Dlg*) was identified in *Drosophila* as a neoplastic tumor suppressor gene. This scaffolding molecule accumulates at the SJ together with Lgl and Scrib to form a complex essential for establishment of the basolateral polarity (see 2.6) (Woods et al., 1996). Studies in *Drosophila* showed

that these three molecules control both, cell polarity and cell proliferation. Mutations in these neoplastic tumor suppressor genes lead to over proliferation of the imaginal disc cells in *Drosophila* and due to loss of cell polarity to metastatic cancer formation (Bilder et al., 2000). Due to gene duplication five mammalian *Dlg* homologs (*Dlg 1-5*) are known. Dlgs are members of the MAGUK (membrane associated guanylate kinase) family of proteins and contains besides its three postsynaptic density-95/Dlg/zonula occludens-1 (PDZ) one Src homology domain-3 (SH3) and one guanylate kinase-like (GUK) domain. Via these protein-protein interaction domains Dlg can interact with a large amount of different proteins involved in signaling, membrane organization, ion channel function, and scaffolding (Sans et al., 2003). The phenotypes of mouse mutants with defective Dlg proteins manifest mostly in the central nervous system. A mutation in the human DLG3 gene results in nonsyndromic X-linked mental retardation (Tarpey et al., 2004). Recently, Van Campenhout et al. published a paper where we could show a function for Dlg3 in establishing apical-basal polarity, epithelial junction formation, and PCP in the IE (Van Campenhout et al., 2011). We could show that mice with a gene trap or a null allele of *Dlg3* show embryonic lethality with low penetrance. The mice with mutations in *Dlg3* show turning defects, posterior truncations, and a lack of anterior neural induction. Loss of *Dlg3* affects localization of AJ proteins like E-cadherin and mis-localizes TJ proteins like ZO-1. The enlarged node region is a hint for convergent extension (CE) movement defects which are common disorders in PCP mutants. A screen to identify potential Dlg3 interaction partners identified TJ-associated protein 1 (TJAP1/Pilt), protein phosphatase 1 that is part of the AJC and regulates Par-3/aPKC activity (Hendrickx et al., 2009; Traweger et al., 2008), the motor protein Dynein that regulates vectorial transport of vesicles to the apical surface (Lafont et al., 1994), the E3-ubiquitin ligase Nedd4-2 which is involved in protein trafficking, and the Nedd4 binding protein 3 (N4BP3) (Murillas et al., 2002). These interaction partners provide a clear hint for Dlg3 involvement in polarity establishment. To strengthen this hypothesis we co-immunoprecipitated Dlg3 and Nedd4 in polarized conditions whereas the amount of precipitate in unpolarized cells was less. Immunohistochemistry revealed a strong interaction of both at the apical membrane and the AJC of polarized cells. Mapping analysis showed that the interaction is mediated through a binding motif between the second and the third PDZ domain (Van Campenhout et al., 2011). Additionally, it has been shown that Dlg3 interacts with the exocyst complex Sec8 to mediate trafficking of neuro transmitter filled vesicles from the endoplasmic reticulum to the synaptic membrane. Lgl and Dlg3 function in the same complex and both interact with the exocyst complex (Gangar et al., 2005; Sans et al., 2003). The interaction of Dlg3 with the exocyst complex and the motor protein is also abolished upon removal of the Dlg3 Nedd4 binding site (Van Campenhout et al., 2011).
Finally, we could show a new function of Dlg3 and Nedd4 in the establishment of TJ formation as well as an involvement in the PCP pathway. Up to now Dlg3 was thought to locate to the basolateral membrane domain. The current model proposes that Dlg3-Nedd4 interaction is trafficking a subset of Dlg3 molecules to the apical surface of polarized cells by interacting with the exocyst complex and the cellular motor proteins.

2.7 The Wnt signaling pathway

The Wnt signaling pathway is involved in a variety of diverse functions including cell fate determination, cell migration, cell polarity, neural patterning, and organogenesis during embryonic development. Wnt/β-catenin signaling has been implicated in early endoderm development as well as early lung formation (Burtscher and Lickert, 2009; Goss et al., 2009). Activation of the receptor

upon ligand stimulation can either result in the canonical pathway (Wnt/β-catenin dependent) or the noncanonical pathway (Wnt/β-catenin independent) which can be divided into the PCP and the Wnt/Ca^{2+} pathway (Habas and Dawid, 2005). Wnt signaling must be tightly regulated and defects result in severe malformations of the developing embryo or later in pleiotropic pathologies including cancer, skeletal defects, and birth defects (Logan and Nusse, 2004). The ligand of the Wnt signaling pathway is the secreted glycoprotein Wnt and the receptor is a seven-pass transmembrane protein called Frizzled (Fz). In humans, 19 Wnt signaling proteins and ten Fz receptors have been identified. In addition to the Fz receptor the low-density lipoprotein receptor-related protein 5/6 (LRP5/6) is needed for canonical Wnt signaling. After the ligand has bound to the receptor complex the first key player in intracellular signal transduction is the phosphoprotein Dishevelled (Dsh/Dvl). Dsh is the branching point of the canonical and the noncanonical Wnt pathway. Till now it is not clear how Dvl is mediating the split of the signal in these two branches. The outcome of the canonical Wnt signaling pathway is stabilization of intracellular β-catenin and subsequent transcriptional activation of Wnt target genes.

2.7.1 The Wnt signaling pathway and its connection to cilia

Compared to the extensive dataset about connection of HH signaling and cilia, the role of Wnt signaling through cilia is much more elusive. One of the first reported connections between canonical Wnt signaling and cilia were described when Inversin (Inv) was shown to localize to the cilium and interacts with one of the core Wnt pathway components Dvl (Wallingford and Mitchell, 2011). From the early studies it was thought that Inv and thus signaling over the cilium is influencing the transduction of the Wnt signal via Dvl rather negatively. Inv is a Dvl modulator and is thought to act as a switch between canonical and noncanonical Wnt signaling pathways. Later experiments showed that defective IFT and mutations in some of the Bardet-Biedl syndrome (BBS) genes cause a hyperactive Wnt response in cultured cells (Gerdes et al., 2007). Similar observations were made shortly after in mice and again the presence of a primary cilium rather influences Wnt responsiveness of cells negatively. Contradicting to these results it was also shown that loss of cilia does not at all affect Wnt signaling in regard to Wnt loss-of-function phenotypes or expression levels of Wnt target genes. Nevertheless, more and more studies support a role of cilia in negatively regulating Wnt signal transduction in mouse, zebrafish, and *Xenopus*. However, it has to be considered that mutations in core ciliogenesis genes do not display defects in Wnt mediated developmental processes like it is the case for defects in HH signaling due to loss of cilia. The impact of ciliary signal transduction in canonical Wnt signaling is cell type specific and much more subtle as HH signaling.

2.8 The planar cell polarity pathway

For proper function of cells and development of tissues a lot of different factors are needed. Beside the ubiquitous AB polarity (see 2.6) another not that well understood pathway is required: The planar cell polarity (PCP) pathway. PCP is also known as the noncanonical Wnt pathway because it shares components (Dsh, Fz) with the canonical Wnt-β-catenin signaling pathway. Downstream of Dsh/Dvl the canonical pathway inhibits the degradation of cytoplasmic β-catenin. The noncanonical pathway instead activates a Jun kinase/Rac/Ror pathway downstream of Dsh/Dvl. These kinases regulate cytoskeletal rearrangement processes and are thought to assist in the repolarization events taking part after PCP pathway stimulation (Habas et al., 2001; Marlow et al., 2002; Strutt et al.,

1997). The PCP signaling pathway not only functions to establish a defined polarity in single cells but is translating this information to a uniform orientation of all cells located in this tissue. Therefore, global guidance cues for directional information, cellular factors to interpret the directional signals and establish the PCP axis, and tissue specific effectors for executing the function in individual cells are needed (Klein and Mlodzik, 2005; Lawrence et al., 2007; Ma et al., 2003). PCP was originally identified in *Drosophila*, but during the last years PCP in vertebrates has more and more moved into the spotlight of investigation. In *Drosophila*, inactivation of PCP genes leads to disorganized orientation of wing hair cells, body bristles, and ommatidia in the eye. Further investigation of these phenotypes and characterization of the underlying genes resulted in a set of core PCP factors including the four-pass transmembrane protein Van Gogh (Vang), the seven-pass transmembrane atypical cadherin Flamingo (Fmi), the seven-pass transmembrane protein Frizzled (Fz), and the cytoplasmic proteins Diego (Dgo), Prickle (Pk), and Dishevelled (Dsh). Classically, these six factors become distributed to opposite sides of the cell by means of inhibiting each other as well as directed transport. Through this asymmetric distribution the cell gains information additionally to the AB polarity which is important to define the proximal and distal side of the cell. Cell-cell communication between these core components orientates all cells in the tissue in a uniform direction.

Instructed through the action of morphogens like *Wg* and *Decapentaplegic*, the two atypical cadherins *Fat* (*Ft*) and *Dachsous* (*Ds*) are expressed in opposing gradients in imaginal discs of the *Drosophila* larvae. Ft and Ds restructure and condense the microtubule network at the apical surface providing the scaffold for the migration of core PCP molecules (Fmi, Fz) to the distal sides initializing the asymmetric distribution. If the MT network is disrupted Fz is not localized to the membrane anymore resulting in mis-localized prehair formation because of defective PCP signaling (Shimada et al., 2006). If this mechanism is also true for vertebrate cells is not finally proven. In *Drosophila* Vang complexes with Pk and localizes to the proximal side of the cell whereas Fz, Dsh, and Dgo are located to the obverse side. Fmi is distributed on both sides and is important for signaling between the alongside lying cells. The asymmetric distribution of the PCP factors is often transient and precedes the actual morphological event making it difficult to define the proper time point for the analysis.

Through intensive studies in the last decade PCP is also implicated in a variety of vertebrate processes including gastrulation movements of convergence and extension (see 2.8.1) (Wallingford et al., 2000), IE morphogenesis (see 2.8.5) (Wang et al., 2006), hair and cilia polarization (Mitchell et al., 2009), as well as tangential neuronal migration (Jessen et al., 2002). Quite recently, PCP was additionally implicated in establishment of coordinated ciliary beating of multiciliated tissues (see 2.8.5). All core PCP molecules of *Drosophila* have vertebrate orthologs, their function is conserved, and they are even distributed the same way. Additional complexity is generated by duplication of many genes involved in regulation of PCP in vertebrates. In mouse, ten *Frizzled* (*Fzd1-10*), two *Van Gogh like* (*Vangl1-2*), three *Fmi* homologs called *Celsr1-3*, two *Prickle* (*Pk1-2*), and three *Dishevelled* (*Dvl1-3*) homologs are known. Because single gene mutations of only the core PCP genes cause a severe PCP phenotype the analysis of the PCP pathway in vertebrates requires the generation of complex genotypes. The phenotypes of single or double mutants of *Vangl1*, *Vangl2*, *Fzd3*, *Fzd6*, *Dvl1*, *Dvl2*, and *Celsr1* show a combination of classical PCP phenotypes like open neural tube, disrupted IE hair cells, and open eye lids but are, nevertheless, distinguishable from each other.

A nice study in the vestibular part of the IE shows that the position of the kinocilium is not necessarily depending on a distinct set of PCP molecules. In contrast to the always lateral localized kinocilia in the cochlea the kinocilium in the vestibular epithelium can be positioned at the medial or the lateral side. The individual hair cells on one side of the asymmetry axis always localize their cilia towards the axis. Interestingly, although the positions of the cilium are variable, the localization of the core PCP

components Fzd6 and Pk2 are not reversed (Deans et al., 2007). This important finding shows that additional molecules have to act on the BB to transport/localize it on the right side of the cell.

2.8.1 Planar cell polarity regulates convergent extension movements

Conducting studies in *Xenopus*, PCP molecules are important for early embryonic development due to their function in CE movements. During gastrulation CE movements elongate the embryonic tissues in anterior-posterior direction. Defects in CE movements result in broader and wider neural plates and consequently in neural tube malformations (see 2.8.2). Mouse mutants carrying loss-of-function alleles of distinct PCP genes show abnormally shorter and broader body axis suggestive for a CE defect during gastrulation. In those mutants the cochlea of the IE also shows a shortened and broader appearance which suggests defects in CE movements (Wang et al., 2005). Different allelic series of *Protein tyrosin kinase 7* (*Ptk7*) and the *Celsr1*^{crsh} mouse line for example display such body axis defects. One of the possible mechanisms underlying the CE phenotypes is that the actin cytoskeleton is no longer correctly polarized in PCP mutants (Wallingford, 2006). This is also compatible with the fact that Celsr1 is a molecule important for cell-cell signaling and therefore might also influence the rearrangement of the cytoskeleton. Embryonic development also depends on precise movement of cells and PCP dependent appropriate polarization of the actin rich lamellipodia of migrating cells is a prerequisite for precise movement.

2.8.2 Planar cell polarity regulates neural tube closure

Primary neurulation starts at around the five somite stage with the closure of the neural tube at the base of the future hindbrain (closure one). At the twelve somite stage closure two initiates at the forebrain-midbrain boundary and closure three at the rostral extend of the forebrain. Cranial closure is completed by the 17 somite stage whereas the closure of the spine continues with the elongation of the embryo till the complete closure ends in the posterior neuropore at the 30 somite stage (Paudyal et al., 2010). During primary neurulation the two edges of the neural plate first form the neural folds, than fold up and fuse at the midline to become the closed neural tube. There are several types of neural tube closure defects reported and they all depend on the region where the closure is affected. Anencephaly for example results from an incomplete closure of the head whereas spina bifida appears when the posterior neuropore closure is defective. The most severe case of closing defect - the craniorachischisis - results in a complete failure of closure of the neural tube ranging from the midbrain region to the tail region. Both, anencephaly and craniorachischisis, are perinatal lethal because of disrupted brain formation. Only eleven genes are associated with craniorachischisis among them the homozygous mutations of *Vangl2*, *Celsr1*, *Scrib* and *Ptk7*, as well as double heterozygous mutations in *Dvl1/2*, *Dvl2/3*, and *Fz3/6*. This phenotype is probably arising because of the large spatial distance between the two neural fold rims due to CE movement defects and/or cytoskeletal rearrangement defects (Copp et al., 2003). *Scrib* has originally been identified as a gene involved in apical-basolateral polarity together with *Dlg* and *Lgl* but recently has been shown to influence establishment of PCP in the IE and genetically and physically interacts with *Vangl2* (see 2.6) (Montcouquiol et al., 2003). Most recently, a mutation in *Sec24b* has been shown to exhibit craniorachischisis and is influencing PCP through regulation of Vangl2 protein trafficking (Merte et al., 2010; Wansleeben et al., 2010).

2.8.3 Planar cell polarity regulates limb development

In vertebrates additional players in the planar polarity pathway have been identified and mutants exhibit classical PCP phenotypes. In contrast to *Drosophila* where no Wnt ligands regulating PCP have been identified till now, there are at least three Wnts in vertebrates that stimulate noncanonical Wnt signaling: Wnt11 (Zhou et al., 2007), Wnt5a (Qian et al., 2007), and possibly Wnt9b (Karner et al., 2009). Till now it is unclear if these Wnts play an instructive or permissive role in establishment of PCP. It is known that noncanonical Wnts regulate PCP processes in vertebrates ranging from CE movements to IE hair cell polarization. Morphogen gradients play important roles in directing cells towards defined lineages where they influence not only cell morphology but also the spatial and temporal component of differentiation. It is fairly unknown if, and if yes, how exactly signaling gradients can affect the cells' polarity. The initial cue for PCP establishment in vertebrates remains to be identified. Recently, Gao et al. showed that a gradient of Wnt5a induces asymmetrical Vangl2 distribution and this is important for proper mammalian limb bud patterning (Gao et al., 2011). Wnt5a genetically interacts with Vangl2 and signals through the receptor tyrosine-kinase Ror2 (Angers and Moon, 2009; Kikuchi et al., 2009; Qian et al., 2007). Ror2 is a single-pass transmembrane protein with a tyrosine kinase domain that binds extracellular Wnt5a through its cysteine rich Wnt binding domain (Oishi et al., 2003). Mutations in *Ror2* can lead to Brachydactyly type B and combined with a mutation in *HOXD13* to Brachydactyly type B and E. Both are very rare human skeletal syndromes characterized by disproportionately short fingers and toes. Mutated *Ror2* can also lead to Robinow disease, also a very rare human skeletal syndrome characterized by dwarfism, limb shortening, and facial abnormalities. Gao et al. observed similar phenotypes in *Wnt5a*$^{-/-}$, *Ror2*$^{-/-}$, and *Vangl2*$^{Lp/Lp}$ *looptail* (*Lp*) mice suggesting that the syndromes of these diseases resemble PCP defects and therefore are results of disrupted PCP signaling. The asymmetrical localization of Vangl2 in chondrocytes is missing in *Wnt5a*$^{-/-}$ and *Ror2*$^{-/-}$ mice. Moreover, *Ror2* genetically interacts with *Vangl2* because double homozygous animals show a more severe phenotype including open neural tube, skeletal deformations, and misorientated IE hair cells. Since it is known that Ror2 is part of the Wnt5a receptor complex activated Ror2 could possibly regulate asymmetrical Vangl2 distribution. The phosphorylation of Ror2 through the binding of Wnt5a is depending on the presence of Fz and Dsh. Activated Ror2 is now able to phosphorylate Vangl2 resulting in asymmetric distribution of Vangl2 in chondrocytes of limb buds. Phosphorylated Vangl2 becomes enriched at the proximal side of these chondrocytes and thus, at the side of lower Wnt5a activity. Taken together, these data show that PCP in chondrocytes plays an important role in proper limb development.

2.8.4 Planar cell polarity and cilia

As described above mostly all cells of the vertebrate body project at least a single cilium - specialized cells can project a few hundred cilia - from their apical surface (see 2.5). Recently, it has been shown that core components of the PCP pathway (Vangl2, Dvl, Inv) are localized directly at or at the base of cilia. As already mentioned (see 2.7.1) Inv interacts with Dvl which is involved in both, canonical and noncanonical Wnt signaling. Loss of *Inv* gene function leads to CE defects and thus implicates Inv to function in vertebrate PCP as a modulator of Dvl activity leading to activation of either the canonical or the noncanonical Wnt signaling pathway. To strengthen the hypothesis that cilia are involved in PCP signaling it has been shown that some BBS proteins co-localize together with one of the core PCP proteins Vangl2 to the axoneme and the BB and even genetically interact in double heterozygous

animals (Ross et al., 2005). Characteristic phenotypes include open eyelids, neural tube closure defects, and misorientation of stereociliary hair bundles (Klein and Mlodzik, 2005).
In vertebrates the cilium is thought to serve as an antenna to sense extracellular cues for establishment of PCP. Evidence in the mammalian system comes from the IE of the conditional *Ift88* mutant mouse. Conditional inactivation of *Ift88* in the organ of Corti results in absence of the MT based kinocilium. The mutation does not influence the assembly of the actin based stereocilia but their intrinsic polarity. The phenotype observed in the conditional mutants displays misorientation of stereociliary hair cells but the asymmetric localization of the core PCP genes is not affected. That would mean that the kinocilium regulates planar polarity independently or downstream of PCP signaling (Jones and Chen, 2008; Jones et al., 2008). This observation is confirmed by the fact that mutation of *Ift88* leads to defective ciliary beating in multiciliated mouse ependymal cells. The core PCP protein Vangl2 is again not altered in its asymmetric distribution (Guirao et al., 2010). The BBs of ependymal cells are polarized in two ways, first, they show rotational polarity, and second, translational polarity which results in asymmetric positioning of cilia on the apical surface (see 2.8.5). When ciliogenesis of ependymal cells is disrupted through conditionally ablating *Kif3a* in progenitor cells (radial glia cells) translational polarity is still present. In contrast, if ciliogenesis is already defective in radial glia cells, ependymal cells do not show translational polarity anymore (Mirzadeh et al., 2010). This mechanism is shown to be independent of PCP signaling (Hirota et al., 2010). This suggests that translational polarity of ependymal cells is already determined by the cilium in radial glia cells.
Additionally, recent reports indicate that at least some PCP molecules are important for ciliogenesis. The first two implied in ciliogenesis were the PCP effector genes *Inturned* and *Fuzzy*. They are expressed in highly ciliated cells and ablation leads to defective ciliogenesis and consequently to disrupted HH signaling. Vertebrate Inturned is apically enriched in multiciliated cells and has been shown to regulate actin assembly, Rho localization, and docking of BBs in *Xenopus* (Park et al., 2008b). The second gene is *Fuzzy* which does not play a role in BB docking but rather is important for vesicular transport to the BB and further from the BB to the ciliary tip (Gray et al., 2009). These two genes play a role in PCP in *Drosophila* wing cells but it stays elusive if they do so in vertebrate PCP controlled developmental processes like CE movements. Mutant mice either for *Inturned* or *Fuzzy* do not display craniorachischisis that is associated with mutations of core PCP genes.
The accumulation of all this data described above would strongly argue for a role of ciliary proteins in PCP but caution is needed to interpret all this data. Mostly, genetic interactions of genes involved in PCP with core PCP genes are measured by the intensity and rates of neural tube defects (see 2.8.2). Interestingly, genes associated with a complete failure of cilia formation do not display craniorachischisis as they should when PCP signaling is dependent on functional cilia. These mutants rather show exencephaly that is characterized by an open forebrain.

2.8.5 Planar cell polarity influences basal body transport, docking, and positioning

PCP has been implicated to play an important role in apical actin organization. Assembly of apical actin is mediated by molecules like Inturned, Fuzzy, as well as the actin regulators Ezrin and RhoA and defects in apical actin assembly abolish BB docking (Park et al., 2008b). This fact provides a mechanistically hint for the important role of planar polarity for BB transport and positioning. In mammals the processes of BB transport and orientation are not well understood.

It has been shown that Dvl together with the PCP effector Inturned and the Rho GTPase mediate docking of BBs to the apical membrane at least in the *Xenopus* epidermis (Park et al., 2008b). Moreover, they showed that Dvl-dependent association of BBs with membrane-bound vesicles and Sec8, a component of the vesicle-trafficking machinery, is transporting the BBs to the apical surface. Interfering with Dvl function in nodal and ependymal cells did not lead to the same phenotype as in *Xenopus* epidermis suggesting that redundancy and/or other yet undiscovered genes play a role in BB transport/positioning in mouse (Hashimoto et al., 2010; Hirota et al., 2010). It is very likely that core PCP molecules together with PCP effector molecules regulate the process of BB transport and positioning.

One example for a tissue where BB positioning is crucial for its function is the node. To generate the leftward nodal flow BBs have to be repositioned from a central position to the posterior side of the node cells (Nonaka et al., 2005). Pk2 and Vangl1 are localized to the anterior, whereas GFP-Dvl2 and Dvl3 have been shown to localize to the posterior side of the cell. Additionally, it has been shown that Dvl is important for the repositioning of the nodal cilia (Hashimoto et al., 2010). Analysing the phenotype of the *Vangl1* and *Vangl2* double mutant provided another hint for the involvement of PCP in ciliary positioning. These mutants show normal developed nodal cilia but are not able to reposition their cilia to the posterior side (Song et al., 2010). This results in common asymmetry defects such as failure of embryonic turning at E8.5 and heart looping defects. This observation confirms that PCP signaling in the node is downstream of ciliogenesis but upstream of ciliary positioning.

Another excellent example for the influence of PCP signaling on BB positioning provides the cochlea of the IE. Defects in BB positioning result in defective alignment of the stereociliary hair cells which is a common feature of PCP mutants. In the organ of Corti, it has been shown, that the core PCP molecules Vangl1, 2 and Fzd3, 6 localize to the medial side of the hair cell whereas Dvl1, 2, 3 localize to the lateral side (Etheridge et al., 2008; Wang et al., 2006). Controversial, mosaic labeling showed that fluorescent labeled Fzd3 localizes to the lateral side whereas immunohistochemistry of Pk2 showed a medial localization (Deans et al., 2007). Loss-of-function of one of these molecules leads to disruption of the typical highly ordered structures displayed in the organ of Corti. In PCP mutants, initial cell polarity is never established and as a consequence the stereociliary bundles show loss of orientation. The *Vangl2*$^{Lp/Lp}$ mouse shows a completely randomized organization of IE hair cells and Fzd3 is absent from the cell membrane. A similar phenotype can be observed in *Celsr1*$^{crsh/crsh}$ mutants where due to loss-of-function of Celsr1 Vangl2 is not distributed asymmetrically any more (Montcouquiol et al., 2006).

In multiciliated tissues such as the fallopian tube, the lung, and the ependymal cells of the brain the directional beating of cilia is always coordinated with the direction of fluid flow. Looking closer at the cerebrospinal fluid (CSF) flow in the developing mouse brain Guirao et al. suggest that both, PCP and fluid flow is needed for proper orientation of ependymal cilia (Guirao et al., 2010). The BBs in ependymal cells first dock randomly at the apical surface and get repositioned later by a combination of hydrodynamic forces and PCP signaling. The force is generated by a pressure gradient of CSF in the lateral ventricle because it is released in the choroid plexus and absorbed in the foramen of Monroe. They also show that Vangl2 is transiently asymmetrically localized in the ependymal cells until their ciliary orientation is locked. Vangl2 alone was not sufficient to correctly polarize the BBs in the absence of cilia in *Kif3a* or *Ift88* mutants but apical docking was not influenced (Guirao et al., 2010). This is in clear contrast to what has been shown in *Xenopus* skin where the BBs do not dock at the apical surface and ciliogenesis is impaired in *Vangl2* mutants (Mitchell et al., 2009). How PCP and hydrodynamic forces could interact is possibly through the signaling function of the transmembrane

protein Vangl2 that is located in the ciliary membrane. One possibility is that this signaling activates a cytoskeletal rearrangement cascade that subsequently positions the BBs in direction of fluid flow. Mutations in other core components of the PCP pathway like *Celsr2* and *Celsr3* double mutants show defects in the apical docking process of multiciliated ependymal cell BBs leading to fatal hydrocephalus (Tissir et al., 2010). Moreover, in this mutant other core PCP components like *Vangl2* and *Fzd3* are mislocalized.

2.8.6 Mutation of *Celsr1* leads to neural tube and inner ear defects

The *Crash* (*Crsh*) mutant mouse was identified in an N-ethyl-N-nitrosourea (ENU) screen together with another mutant mouse named *spin cycle* (*Scy*) (Curtin et al., 2003). Both mouse mutants underlie a mutation in one of the core tissue polarity genes, encoding for the seven-transmembrane protocadherin molecule Cadherin EGF LAG seven-pass G-type receptor (Celsr1). *Celsr1* is one of three mammalian homologs of *Drosophila flamingo* (*Fmi*), which has been shown to be essential for PCP in *Drosophila* (see 2.8) (Adler and Lee, 2001).
Celsr1 mRNA expression can be detected in the PS at E7.5 whereas *Celsr2* is present in the anterior neural ectoderm. *Celsr2* is strongly expressed in the ventral limb bud at E9.5 and becomes restricted to the apical ectodermal ridge (AER) by E10.5. In contrast, *Celsr1* is expressed in a weak and broader manner in the limb bud at E10.5. Additionally, *Celsr1-3* are expressed in the eyelids, in the ventricular zones of the brain, the choroid plexus, in the whole olfactory epithelium of the vomeronasal organ, in the cochlea of the organ of Corti as well as in the cochlea ducts, in the vestibular epithelium of the IE, and in the neuroepithelium. At E14.5 *Celsr1-3* are expressed in ureteric buds in the kidney. *Celsr1, 2* are expressed in the esophagus, in the stomach, in the developing lung, and kidney epithelium (Formstone and Little, 2001; Shima et al., 2002; Tissir et al., 2002).
Crsh heterozygous mice exhibit head-shaking behavior, belly curling, and spinning during tail suspension. Investigation of the cochlea revealed that a large number of OHCs particular in the apex are heavily rotated indicating a defect in PCP (Curtin et al., 2003). IHCs appeared to be unaffected. The general organization of one IHC row and three OHC rows seems not to be affected in *Crsh* heterozygous animals. The IE phenotype was significantly stronger in homozygous *Crsh* mice. Heavily rotated OHCs could be observed along the whole cochlea duct. At E16.5 near the apex when PCP starts to influence the positioning of the kinocilium the failure of establishment of polarity is visible in not correctly positioned kinocilia. Additionally, these mice show craniorachischisis that leads to perinatal mortality. $Celsr1^{Crsh/Crsh}$ animals display a delay or failure of eyelid closure which is considered a PCP phenotype. The forebrain and rostral midbrain shows normal neural tube closure but in the future cervical region the neural tube fails to close at E8.5. The failure of neural tube closure could be due to a defect in CE movements during the neurulation process. Sequencing of *Celsr1* cDNA from *Crsh* mutants identified a single point mutation (A3126G) that results in an aspartate to glycine substitution at codon 1040. The ENU mutagenesis was performed in the F1 generation of [C3H/HeH x 101/H]. These mice were then mated to BALB/c mice and the F1 generation was analyzed for the *Crsh* phenotype.

2.9 Aim of this thesis

Foxa2 plays an important role in generation of the organizer cell population and till now only a few of its targets are known. Beside this, better tools for analyzing endoderm and organizer development are needed. Therefore, we generated the novel *Foxa2*^{T2AiCre} mouse line. Now, key transcription factors, growth factors, and signaling molecules can be conditionally deleted in the endoderm and endoderm-derived organs for a better understanding of endoderm development.
Both genes, *Pifo* and *Fltp* where originally identified as potential *Foxa2* target genes and the initial benefit of this analysis should lie in the better understanding of the patterning of the organizer population in the node. Together with *Pifo*, *Fltp* is of particular interest because it shows a restricted expression at the node at E7.5. In a previous publication Kinzel et al. focused on the identification of the Riken clone *1700027A23rik* (*Pifo*) and could show an involvement of *Pifo* in cilia disassembly (Kinzel et al., 2010). Our interest lies on the other newly identified Riken clone - *1700009P17rik* (*Flattop*; *Fltp*) - and its hypothetical role in ciliated tissues. Because of its restricted expression pattern and the fact that the function of *Fltp* is unknown we decided to analyze this new gene functional and molecular by generating a knock-in/knock-out mouse line (*Fltp*^{ZV}) as well as an iCre mouse line (*Fltp*^{T2AiCre}) for genetic lineage tracing of the descendants of *Fltp* expressing cells.

3 Results

3.1 Generation and analysis of the *Foxa2*^{T2AiCre} mouse line

The forkhead box transcription factor *Foxa2* is the first gene expressed in the mesendoderm precursor cells and essential for endoderm and organizer formation (Monaghan et al., 1993; Sasaki and Hogan, 1993). It is involved in generation of the node and the notochord which are missing in *Foxa2*$^{-/-}$ animals (Ang and Rossant, 1994; Burtscher and Lickert, 2009). Due to earlier lineage tracing studies in our laboratory using a knock-in strategy to express the codon-improved Cre (iCre) recombinase (Shimshek et al., 2002) from exon one (E1) of the *Foxa2* gene (*Foxa2*^{iCre} mouse line), we know that *Foxa2* expressing cells are the progenitor population for all endoderm-derived organs (Uetzmann et al., 2008). Moreover, Foxa2 positive cells are present in stem cell niches of the intestinal crypt and the lung. However, at the time when we generated the *Foxa2*^{iCre} mouse line we did not know that *Foxa2* has a second promoter downstream of E1 that enhances expression in the endoderm, which was reflected by the fact that the *Cre* reporter gene did not label every single cell of the *Foxa2* expression domain. Additionally, this knock-in strategy generated a hypomorphic allele, which makes the interpretation of conditional knock-out approaches difficult. To circumvent these problems and to analyze the effect of deleting genes in the early endodermal progenitors as well as to genetic lineage trace the early endodermal progenitors, Cre lines that accurately reflect the endogenous expression pattern are needed.

For this purpose we have employed a new strategy by replacing the translational stop codon of *Foxa2* by a 2A-like sequence from the *Thosea asigna* virus (T2A) (Pringle et al., 1999) followed by the iCre recombinase. Here, the recombinase expression reflects the expression of the gene most precisely because all cis-regulatory elements including promoters and enhancers are present and not altered through the knock-in strategy. Moreover, the 20 amino acid (aa) viral T2A peptide allows for co-translational cleavage and equimolar production of the iCre recombinase as well as the Foxa2 protein (Donnelly et al., 2001). In the past, multicistronic gene vectors were often cloned by using an internal ribosomal entry site (IRES) to generate single proteins. The problem of this strategy was that the cistrons were not expressed at same levels due to differential translational initiation. This is now circumvented by the T2A strategy. By crossing the Cre line into Cre-reporter lines, such as fluorescent reporters or reporters harboring the β-galactosidase (β-gal) gene *lacZ*, allows for continuous tracing of cells that express the gene of interest as well as the progeny of these cells that do not necessarily have to express the gene anymore, but are irreversible labeled. On the other hand, these Cre lines allow conditional gene targeting to analyze the influence of specific pathways on endoderm differentiation and organ formation. For this, the Cre line is crossed into conditional mouse lines where one specific gene of interest is irreversibly deleted in cells expressing the *Cre* recombinase.

3.1.1 Design, generation, and verification of the *Foxa2*^{T2AiCre} targeting vector

The objective of our cloning strategy was to create a knock-in mouse line where the T2A (Donnelly et al., 2001) and the iCre recombinase (Shimshek et al., 2002) are fused directly to the ORF of the *Foxa2* locus by removing its stop codon, followed by the endogenous *Foxa2* 3´-untranslated region (3´-UTR). The knock-in construct was designed as shown in Figure 8 A. To generate this mouse line we replaced the stop codon and fused the 18 aa long viral T2A sequence followed by an iCre recombinase at the 3' end of the *Foxa2* ORF (Figure 8 A, red box and red arrow). Upstream of the *iCre*

recombinase a perfect *Kozak* sequence is introduced to allow efficient initiation of translation of the iCre protein (Figure 8 A, red arrow). Downstream, a translational stop codon was inserted. Following the stop codon the *Flippase (Flp) recognition target* (*FRT*)-flanked phospho-glycerate kinase (PGK)-driven *neomycin* (*neo*) resistance gene was introduced (Figure 8 A, yellow box and white arrow). The detailed generation of the targeting vector for Foxa2 is described in the "Material and methods" section (see 5.2.1.3).

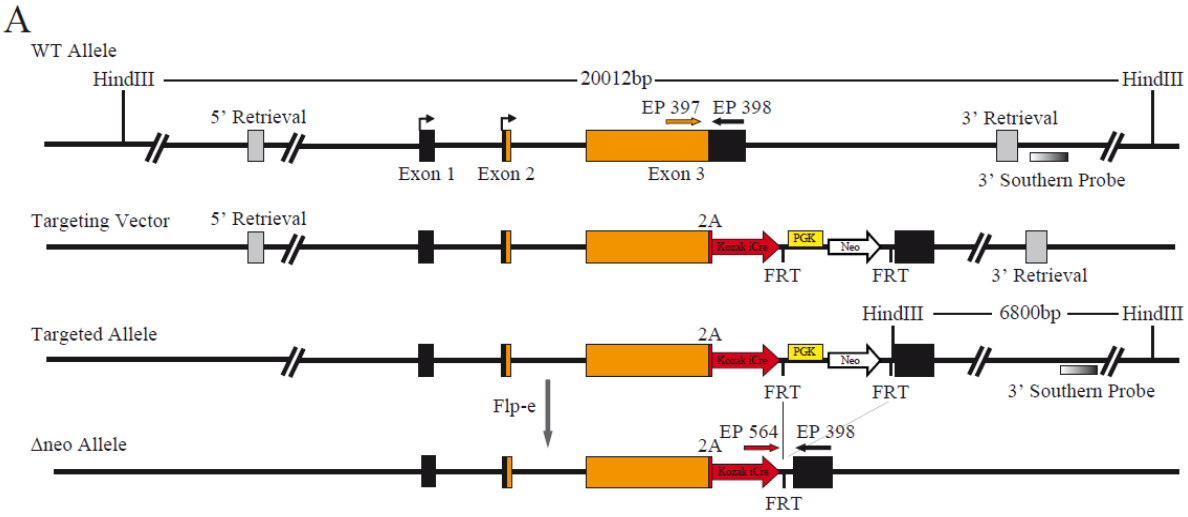

Figure 8 Targeting strategy of the *Foxa2*^{T2AiCre} allele

(**A**) Targeting strategy for the *Foxa2*^{T2AiCre} allele. A targeting construct has been generated to introduce a T2A sequence and an iCre recombinase into exon 3 of the *Foxa2* allele. Upon germline transmission the *neomycin* selection cassette was removed by Flp-e mediated excision. *Foxa2* exons are depicted as black boxes and the ORF as orange boxes. Genotyping primers are designated EP397, EP398, and EP564. The restriction enzyme sites for *HindIII* and the external 5'- and 3'- Southern probe are as indicated. Homology regions to generate the targeting constructs are indicated as 5'- and 3'- Retrieval. The figure is on scale.

IDG3.2 ES cells (Hitz et al., 2007) were electroporated with the *AscI*-linearized *Foxa2*^{T2AiCre} targeting vector and neomycin resistant clones were selected using 300 µg/ml G418 (Invitrogen). Homologous recombination at the *Foxa2* locus was confirmed by Southern blot analysis of *HindIII*-digested genomic DNA using the *Foxa2* 3'-probe (730 bp) located outside of the targeting vector (EP322 fwd *HindIII*; EP323 rev *XhoI*; see 5.1.9.1). 4 out of 138 clones showed homologous recombination (Figure 9 A). Germline chimeras were generated by CD1 morula aggregation and the *FRT*-flanked *neo* selection cassette was subsequently removed in the germline by intercrossing with *Flp-e* (*enhanced Flippase*) mice (Dymecki, 1996). After deletion, mice were backcrossed to C57Bl/6J to eliminate the *Flp-e* allele. Only those mice negative for the *Flp-e* allele were used for backcrossings to C57Bl/6J and further analyses were carried out with *Foxa2*$^{T2AiCre\Delta neo/+}$ mice backcrossed onto a pure C57Bl/6J background for five generations. The targeting was done by Dr. Ingo Burtscher and Wenke Barkay.
For genotyping of the *Foxa2*^{T2AiCre} mouse line the primer EP397, EP398, and EP564 were used and resulted in a PCR product for the *wild-type* (*WT*) allele of 207 bp and 457 bp for the targeted *Δneo* allele (Figure 9 B; for genotyping protocol see 5.2.4.1). Western blot analysis was performed on lung lysate of a *WT*, *Foxa2*$^{T2AiCre/+}$, and *Foxa2*$^{T2AiCre/T2AiCre}$ mice to show that both proteins, Foxa2 as well as iCre, are synthesized and no uncleaved Foxa2-T2A-iCre fusion protein remains (Figure 9 C).

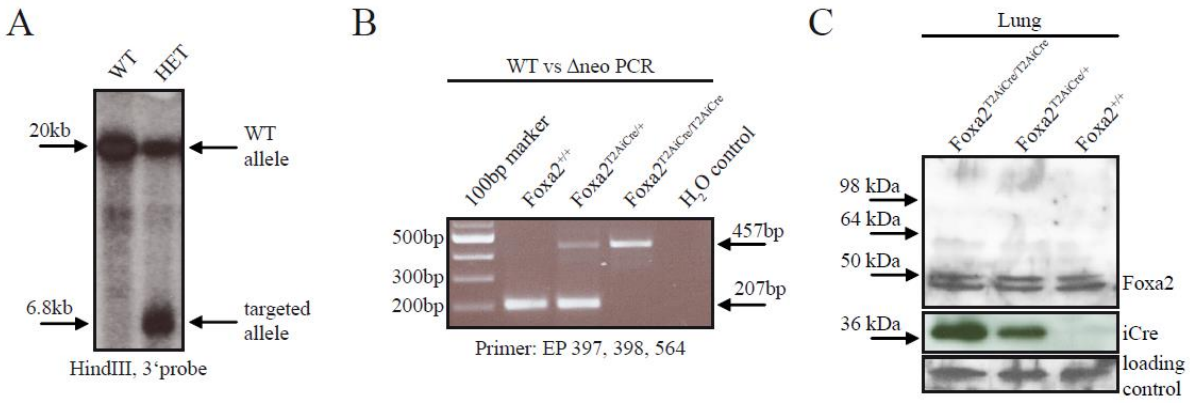

Figure 9 Verification of the *Foxa2*^{T2AiCre} allele

(**A**) Southern blot of ES cells digested with *HindIII* and hybridized with the external 3'-probe, showing the *WT* allele (20.012 bp) and the targeted allele (6.800 bp).
(**B**) Genotyping PCR of tail tip DNA derived from *Foxa2*$^{T2AiCre/+}$ intercrosses after removal of the *neomycin* cassette. Primer EP397, EP398, and EP564 were used to distinguish between *WT* (207 bp) and *Foxa2*$^{T2AiCre\Delta neo}$ (457 bp) allele.
(**C**) Western blot of lung lysates of *WT*, *Foxa2*$^{T2AiCre/+}$, and *Foxa2*$^{T2AiCre/T2AiCre}$ mice analyzed for Foxa2 (~48 kDa) and iCre (~39 kDa) synthesis and T2A peptide co-translational cleavage. Note that no remaining Foxa2-T2A-iCre fusion protein can be detected.

3.1.2 Analysis of the *Foxa2*^{T2AiCre} mouse line

3.1.2.1 Recombination activity of the Foxa2-iCre recombinase during early embryonic development

To test whether the created *Foxa2*^{T2AiCre} mouse line accurately reflects endogenous *Foxa2* expression, we crossed it into the ROSA26 Cre-reporter line (R26R) (Soriano, 1999) and analyzed the heterozygous offspring. Here, the iCre mediates recombination of the *loxP* site flanked neo cassette which allows subsequent *lacZ* expression under the control of the constitutively active ROSA26 promoter. In the next section the temporal and spatial recombination pattern of *Foxa2*$^{T2AiCre/+}$; *R26*$^{R/+}$ embryos during early embryonic development is analyzed.
At embryonic day 6.5 (E6.5), before gastrulation starts no recombination of the *R26R* reporter in the visceral endoderm (VE) could be observed (data not shown). At E7.5, strong β-gal activity can be detected in the epiblast and DE (definitive endoderm) cells anterior to the primitive streak (PS) and posterior to the node. Additional recombination takes place in the anterior visceral endoderm (AVE) and the anterior definitive endodermal (ADE) cells, both cell populations that contribute to the head organizer (Kinder et al., 2001) (Figure 10 A). By E8.5, at somite stage iCre-mediated recombination of the *R26R* was restricted to the foregut pocket, the developing heart, the floor plate of the arising neural tube, the notochord, the regressing node, as well as the hindgut pocket (Figure 10 B, D). At E9.5, reporter gene expression can be detected in the fore- mid- and hindgut, the developing heart, the floor plate, the notochord, and in the liver primordium (Figure 10 C, E). Interestingly, lineage positive cells could also be detected in the head mesenchyme indicating that the progenitor of head mesenchyme is a Foxa2 positive epiblast cell. Additional expression could be observed in the neural tube dorsally to the floor plate indicating that *Foxa2* expressing cells from the floor plate populate

more ventrally located parts of the neural tube (Figure 10 E). At E10.5 β-gal activity was observed throughout the whole gut including the stomach, along the anterior-posterior (A-P) axis of the floor plate and the notochord, in the right main bronchi (RMB) and the left lung lobe (LLB) of the developing lung, as well as in the liver primordium (Figure 10 F, K). Additionally, we could observe strong expression in the heart ranging from the outflow tract over the common ventricular chamber, the aortic sac, the atrio-ventricular channel, and both ventricles (Figure 10 G, H, I, J). Curiously, β-gal activity was weaker and dispersed in the right atrial wall as well as in the left atrial wall indicating that Foxa2-lineage positive cells give only rise to the anterior part of the murine heart (Figure 10 I, J). In summary, the *Foxa2*^{T2AiCre} mouse line is a valuable tool to study mesendoderm formation and lineage relationships.

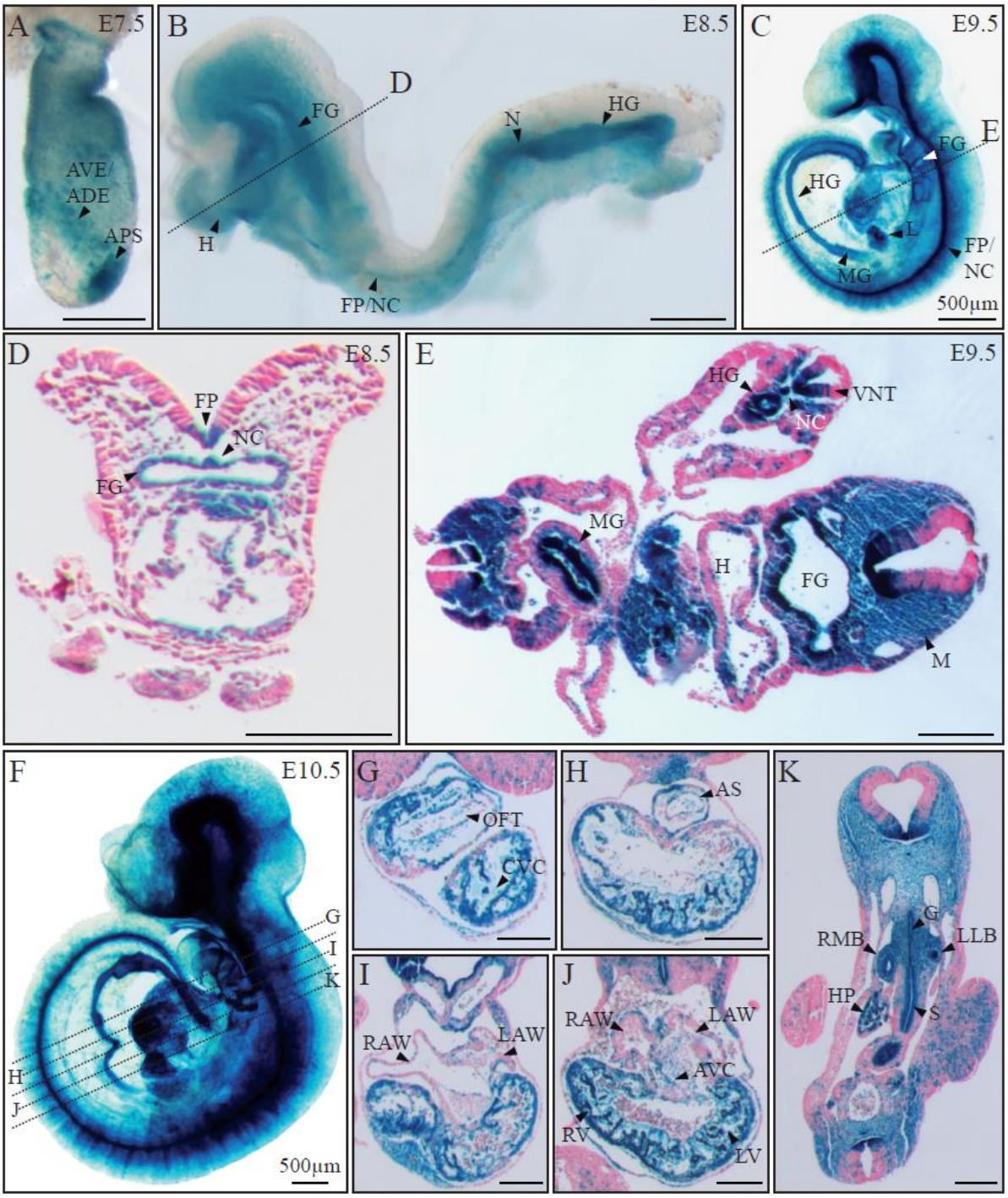

Figure 10 Foxa2-iCre recombination activity during early embryonic development

(**A**) Lateral view of an E7.5 *Foxa2*$^{T2AiCre/+}$; *R26*$^{R/+}$ mouse embryo. β-gal activity is most prominent in the anterior primitive streak (APS) region. Additionally, the intermingled cells of the anterior visceral endoderm (AVE) and the anterior definitive endoderm (ADE) are reporter positive.

(**B, D**) At E8.5, X-gal (bromo-chloro-indolyl-galactopyranoside) staining can be observed in the epithelium of the fore- (FG) and hindgut (HG) pocket, in the heart (H), the regressing node (N), the notochord (NC), and the floor plate (FP) of the developing neural tube.

(**C, E**) A BABB (benzyl alcohol/benzyl benzoate 1:2) cleared E9.5 embryo, Foxa2 lineage positive cells reside throughout the entire gut tube (FG, MG, HG), the ventral neural tube (VNT), the notochord (NC), the heart (H), the head mesenchyme (M), and the liver primordium (L).

(**F, K**) A BABB cleared E10.5 embryo, β-gal activity can be detected in the floor plate of the neural tube, in the notochord, in the entire gut tube (G), in the stomach (S), in the heart, in the right main bronchus (RMB) and the

left lung lobe (LLB), and the hepatic primordium (HP).
(**G-J**) Enlargements of heart sections of an E10.5 embryo in the regions indicated in F. Recombination in heart progenitor cells of the outflow tract (OFT), the common ventricular chamber (CVC), the aortic sac (AS), the atrio-ventricular channel (AVC), and the right and the left ventricle (RV, LV) can be observed. β-gal activity in the right and left atrial wall (RAW, LAW) is not very prominent.
If not indicated scale bars are 200 μm.

To analyze Foxa2 lineage versus expression at gastrulation stage, we made use of the *CAG-CAT-GFP* mouse line (Kawamoto et al., 2000), which expresses the *GFP* reporter gene upon Cre activation. At E7.0, endogenous nuclear Foxa2 localization can be detected in the cells of the DE and in a few epiblast cells as marked by a Foxa2 antibody staining. At this time point, lineage, indicated by cytoplasmic localization of the CAG-CAT-GFP reporter, does not differ much from the actual expression and is thus found in the DE and the epiblast (Figure 11 A, B, C). By E7.5, the lineage positive cells can be found at more anterior positions of the epiblast suggesting that these cells derive from Foxa2-positive cells and later contribute to notochord or floor plate induction. Additional, expression of both, *Foxa2* and the lineage reporter *GFP*, can be detected in DE cells (Figure 11 D, E, F). At E7.75, the GFP reporter positive domain moved even further to the anterior region of the epiblast where these cells contribute to axial mesendoderm and ADE. Again, the DE is stained for both, Foxa2 protein as well as the lineage reporter GFP (Figure 11 G, H, I).
Taken together, Foxa2 positive anterior epiblast cells move towards the anterior side of the embryo and stay lineage positive, but lose Foxa2 protein. This suggests that not all Foxa2 positive cells in the epiblast undergo epithelial-mesenchymal transition (EMT). Some Foxa2 positive cells, or their daughter cells, stay in the epiblast and move anterior to contribute to anterior structures, such as the floor plate. Cells of the DE stay Foxa2 positive and constitute the progenitor cells of the endoderm-derived organs.

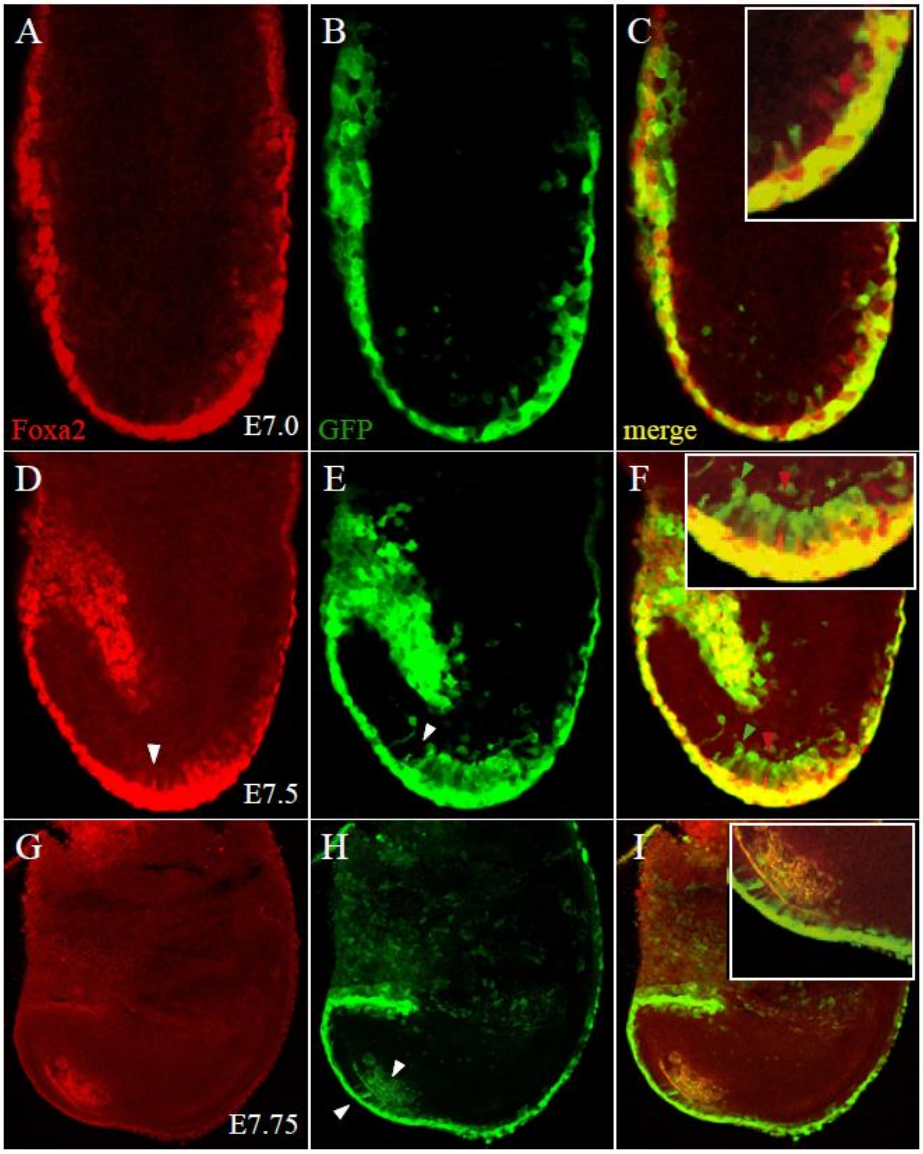

Figure 11 *Foxa2* expression compared to Foxa2 lineage during gastrulation

Confocal pictures of murine *Foxa2*$^{T2AiCre/+}$; *CAG-CAT-GFP/+* embryos at the indicated stages.
(**A-C**) Antibody staining of an E7.0 embryo. *Foxa2* expression is marked by an anti-Foxa2 antibody in red (nuclear staining) whereas Foxa2 lineage positive cells are marked by an anti-GFP antibody in green (cytoplasmic staining). Foxa2 and Foxa2 lineage positive cells can be found in the visceral and the definitive endoderm as well as in the epiblast anterior to the end of the primitive streak.
(**D-F**) At E7.5 Foxa2 lineage positive and Foxa2 negative cells are present more anterior of the epiblast (white arrow head in E) whereas *Foxa2* expressing cells only reach till the distal tip of the epiblast (white arrow head in D). Cells of the definitive endoderm are Foxa2 positive as well as lineage positive.
(**G-I**) By E7.75 the lineage positive cells have reached more anterior parts of the epiblast (white arrowhead in H) and the definitive endoderm is still positive for both (white arrowhead in H).

3.1.2.2 Recombination activity of the Foxa2-iCre recombinase during organogenesis

After primitive gut tube formation the primordia of most endoderm-derived organs are specified by E9.5. Therefore, organogenesis of lung, liver, pancreas, and gastrointestinal (GI) tract starts. To

analyze the contribution of Foxa2 progenitor cells to different organs we examined organs from E12.5 till adulthood.

At E12.5, β-gal activity is visible in the ureteric bud of the developing kidney and in the lung epithelium (Figure 12 A, B). As mentioned earlier β-gal activity in the lung, liver, and intestine primordia starts during embryonic development and these tissues are still lacZ positive (data not shown; 3.1.2.1). At E14.5 β-gal activity can be detected in the lung, in the primordium of follicle of vibrissa as well as in hair follicles of the head, and in the pancreatic bud (Figure 12 C-G). Foxa2 lineage positive cells in the pancreas are restricted to the endoderm derived progenitor cells of the endocrine and exocrine pancreas whereas the surrounding mesenchyme is *lacZ* negative (data not shown).

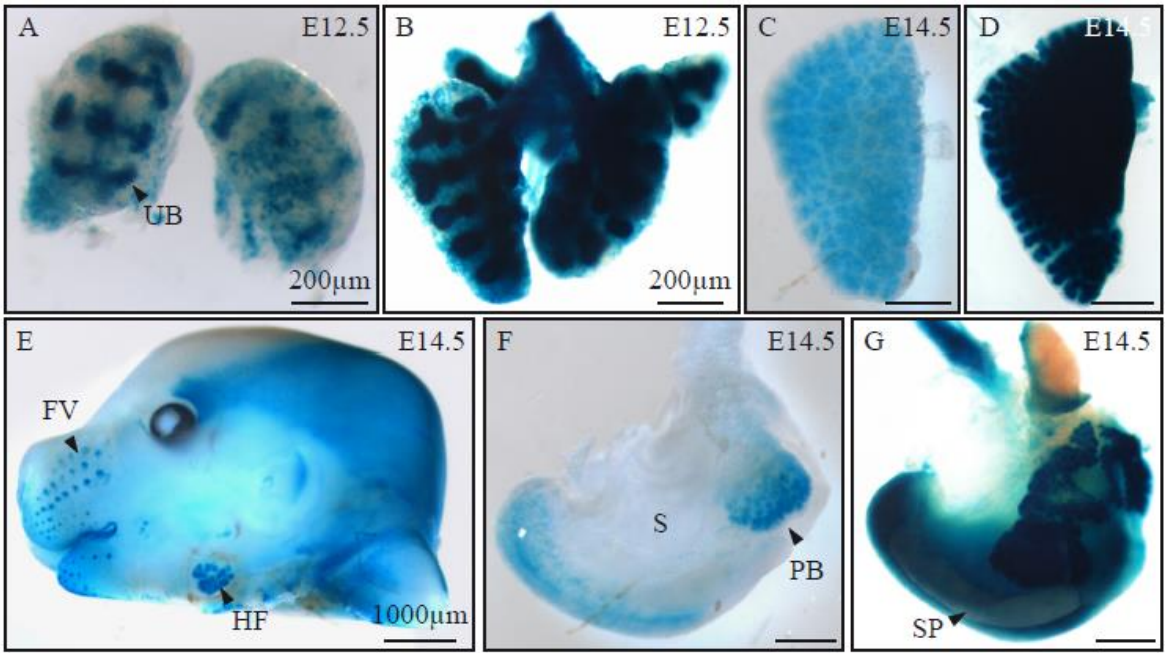

Figure 12 Foxa2-iCre recombination activity during organogenesis

(**A-G**) LacZ stained tissues of *Foxa2*$^{T2AiCre/+}$; *R26*$^{R/+}$ embryos.
(**A**) At E12.5 β-gal activity in the developing kidney is visible in the ureteric buds (UB).
(**B**) LacZ staining in the epithelium of a whole lung of an E12.5 embryo stained for 2 days.
(**C**) 1 day lacZ staining of an E14.5 lung.
(**D**) 2 day lacZ staining of an E14.5 lung. Staining is restricted to the lung epithelium.
(**E**) β-gal activity in the head can be detected in the primordium of the follicle of vibrissa (FV) and other hair follicle (HF).
(**F**) β-gal activity in the pancreatic bud (PB) of an E14.5 embryo stained for 1 day. The stomach (S) should normally be lacZ positive.
(**G**) LacZ staining for 2 days reveals staining in the pancreatic bud and the stomach but the spleen (SP) is negative.
If not indicated scale bars are 500 µm.

A closer look at the limbs of *Foxa2*$^{T2AiCre/+}$; *R26*$^{R/+}$ mice revealed a *lacZ* expression pattern somehow reminiscent of *Gli1* expression, which is a Sonic hedgehog (Shh) target gene (Ahn and Joyner, 2004). The lineage positive cells are more prominent in the posterior part of the limb bud at E12.5, where Shh signaling is active (Figure 13 A-D, dotted white line). At E16.5 β-gal activity can be found in the joints of the digits as well as in the carpus (Figure 13 E-H). The forelimbs are developmentally older

than the hindlimbs therefore the joint reporter gene expression might be visible later in development. Together, this suggests that *Foxa2* is not only a Shh target gene in the floor plate (Sasaki et al., 1997), but possibly also during limb bub development.

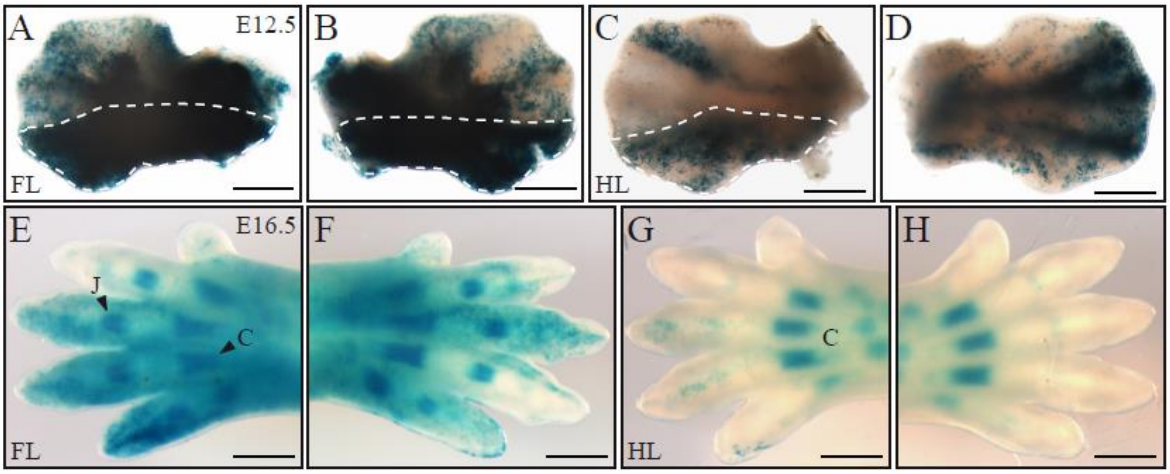

Figure 13 Foxa2 lineage in the limbs shows similarity to *Gli1* expression

(**A-H**) LacZ stained limbs of *Foxa2*$^{T2AiCre/+}$; *R26*$^{R/+}$ embryos. Stages as indicated.
(**A, B**) At E12.5 lineage positive cells accumulate in the posterior part of the limb from proximal to distal of the left and right forelimb (dotted white line).
(**C, D**) β-gal activity in the left and right hindlimb seems to be accumulated in the distal part at least in C (dotted white line).
(**E, F**) At E16.5 *lacZ* expression is restricted to the metacarpal–phalangeal joints (J) of the digits and the metatarsals (C) of the left and right forelimbs.
(**G, H**) In both hindlimbs lineage positive cells are visible in the carpus (C). The joints seem to be lacZ negative.
Scale bars are 500 μm.

In summary, these results convincingly show that Foxa2-iCre marks an early endodermal progenitor cell population that gives rise to a majority of the endoderm-derived organs. Additionally, we could show that Foxa2 lineage positive cells are not restricted to the floor plate of the neural tube but expand in more dorsal regions of the neural tube and partially contribute to the cardiac mesoderm as well as to the head mesenchyme. Due to uniform expression of the iCre recombinase in all Foxa2 positive tissues we show that we generated a reliable tool for conditional gene targeting, which was already used to study Notch signaling during pancreas development (Horn et al., 2012).

3.2 Identification of *Flattop*, a novel gene expressed in the mouse gastrula organizer

As already discussed in the previous section (2.1), *Foxa2* is one of the most important organizer genes, as its loss leads to the absence of the node and its derivatives: AME, notochord, DE, and floor plate. To get a better understanding how the organizer tissue and the endoderm forms as well as to find new Foxa2 target genes, expression profiles of *Foxa2* mutant embryos was compared to *WT* stage-matching embryos using Affymetrix whole genome arrays (Tamplin et al., 2008). Taken together, this data set identified novel Foxa2 target genes validated through the identification of known target genes and the expression of these genes in tissues absent in *Foxa2*$^{-/-}$ animals. To validate possible novel organizer genes regulated by *Foxa2* a whole mount *in situ* hybridization

screen was performed to identify their expression domains. Ten genes were found to be expressed in the organizer region. Among them two which are exclusively expressed in the node at E7.5: *1700009P17rik* and *1700027A23rik* (*Pitchfork*) (Kinzel et al., 2010). We named this yet unknown Riken clone (*1700009P17rik*) *Flattop* (*Fltp*) because of its loss-of-function phenotype in multiciliated epithelial lung cells (see 3.4.2.4). It is well known that the node is indispensable for generation of left-right asymmetry in the early murine embryo and therefore a very interesting transient anatomic structure to study (Shinohara et al., 2012). It was shown that *Pitchfork* (*Pifo*) haploinsufficiency causes a unique node cilia duplication phenotype, left-right asymmetry defects, and heart failure (Kinzel et al., 2010). Whereas *Pifo* is only expressed in the nodal pit cells, *Fltp* is expressed in both, in nodal pit as well as in crown cells. Interestingly, both genes are also found in a screen for mRNAs highly enriched in ciliated tissues like in the lung, the olfactory epithelium, and the testis, suggestive for a function related to ciliogenesis, ciliary function or ciliary positioning (McClintock et al., 2008). Not many node specific genes and potential targets of *Foxa2* involved in ciliary function are known; therefore we decided to investigate *Fltp* function in mouse more closely. In the following section I will focus on the generation and the analysis of the $Fltp^{ZV}$ reporter knock-in and gene knock-out mouse line.

3.2.1 Bioinformatic analysis of the novel organizer gene *Flattop*

Because *Fltp* is a novel gene and only limited expression data is available, we first characterized the gene locus, the mRNA expression, and the protein domains as well as synthesis.

3.2.1.1 The *Flattop* gene

Fltp is located on chromosome one at position 173,044,049 – 173,057,098. The genomic region (exons plus introns) comprises 5.31 kilo bases (kb). This gene of unknown function consists of six exons, has three predicted promoters (Figure 14, yellow boxes, Genomatix software suite v2.5), and two predicted transcriptional start sites (TSS) (Figure 14, red boxes). The promoter that is used to transcribe the gene is located around the second exon and the start codon ATG is also located to the second exon. This promoter is supported by one CAGE (Cap Analysis Gene Expression) tag. CAGE tags are based on the analysis of sequence tags corresponding to 5’ ends of mRNAs at the cap sites. The translational stop codon lies in the middle of exon six (Figure 14). The transcript is 1034 bp long with a 5’ UTR of 282 bp reaching from the beginning of exon one to the TSS as well as a 3’ UTR of 131 bp from the stop codon till the end of exon six. There are seven alternative transcripts predicted, but our RT-PCR analyses (Lange et al., 2012) indicated that the transcript of 1034 bp starting in exon two and ending in exon six is the one expressed in most tissues analyzed (Figure 14, red box AK005804 (1700009P17Rik)). This transcript is verified experimentally in *Mus musculus* adult testis (Genomatix). The rest of the transcripts would result in proteins of less molecular weight than the AK005804 or are not supported by current biological evidence.

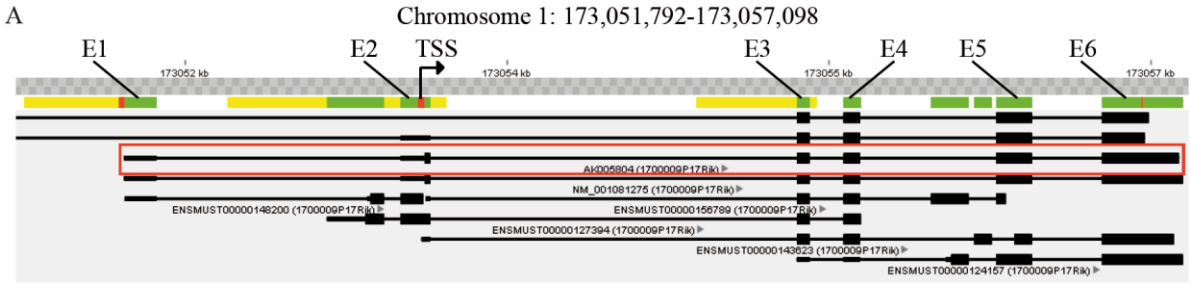

Figure 14 *Fltp* locus

(**A**) *Fltp* is located on chromosome 1. The 6 exons (E1-E6) of *Fltp* are shown in green. Yellow boxes indicate the predicted promoters. The filled red boxes show the predicted transcriptional start sites (TSS). The possible transcripts are shown in black. The thin black boxes show untranslated regions and the fat black boxes stand for the open reading frame. The clear red box marks the transcript with the highest expression probability. Figure modified from Genomatix.

The following sequence shows the whole Fltp cDNA from exon one till the end of exon six. In red the cDNA of the *Fltp* ORF is shown.

acctgcttcc ccctataccc tcttctcact tcacgtggac ttttgttctt gttgtttggt
tgttgagata aggcctttct atgcatccct gactggcctg gaacttacta tgtaaacctg
gttggctcac atttagaggt ctgactcctc caagttctga gagagaaagg aagagggtag
tgtaaaccac agaatgtagc ccaacccctg ctgaccggga gtaactccca gaaggctggc
cttctgcagt tgccaggcaa caagtgtaaa cagcactgga tcatggccac taactacagt
gccaaccagt atgaaaaagc ttacttaccc acgtacctgc agaactggtc tcctgccagg
ccaacgaaag agaaaatcgc tgcccatgaa ggttacactc agatcatcgc caacgatcga
gggcatctct tgccttcagt gccccgttcc aaggcaagtc cttggggttc cttcatgggc
acctggcaaa tgcccctgaa gatcccacct gctaaggtga ccttgaccgc ccgtacaact
acagctgccg acaacctcac caaatggata cacaagaatc ctgatctact caacgcctgt
aatgggctgc gtcctgaaat ctcaggcaag cccttcgatc ctgacagtca gacgaaacag
aagaaatctg tcaccaagac tgtacaacaa gcaccaaatc caaccataat tcccagctcc
ccggttatcc aaggagacaa cccagatgaa ccgcaaagct cgcacccctc tgcaggtcac
actccaggtc cccaaactcc agtcaactct cccaacaacc cacctccgag cccttgtaag
agcaccaagt aggtcctagt ctagctgagg tccagatcta tgccatgctg gggtgacatt
ttagagactg accgaaatag gtgagaccct gcctgtattc agaaatgtgg aacagagaaa
tggtgggcca ggagtgaagg cagatttagg gaaataaaca ttgtgtgtta aatcttttac
tgacctgggt tttc

I also analyzed the *Fltp* ORF as well as the promoter region one kb upstream of exon one for potential Foxa2 and Foxj1 binding sites, because *Fltp* was identified as a target gene of *Foxa2* and additionally is expressed in ciliated tissues where *Foxj1* is thought to be a master regulator for ciliogenesis (Brody et al., 2000; Chen et al., 1998). With the help of the Genomatix software forkhead domain factor binding consensus target sites were identified. In total one predicted Foxj1 binding site and four Foxa2 binding sites could be identified. The potential Foxj1 binding site is located in the promoter region in front of the second exon and the TSS (Figure 15, blue box). Directly upstream of the TSS a Foxa1 and 2 binding site is located. Additionally, one Foxa2 and one Foxa1 and 2 binding site are located between the second and the third exon. The last Foxa2 binding site is in the intron between exon four and exon five (Figure 15, blue box). This indicates that *Fltp* might be a direct target of some forkhead transcription factors, which needs to be tested in further details.

The fact that *Fltp* is expressed in ciliated tissues and a Foxj1 binding site lies directly in the *Fltp* promoter raise the intriguing possibility that Foxj1 protein regulates *Fltp* expression in ciliated cells.

Moreover, *Fltp* was identified in a screen for potential Foxa2 target genes. The identification of Foxa2 binding sites in the *Fltp* gene locus and the resulting potential regulation of *Fltp* through Foxa2 would confirm the initial findings obtained from the expression profiling (Tamplin et al., 2008).

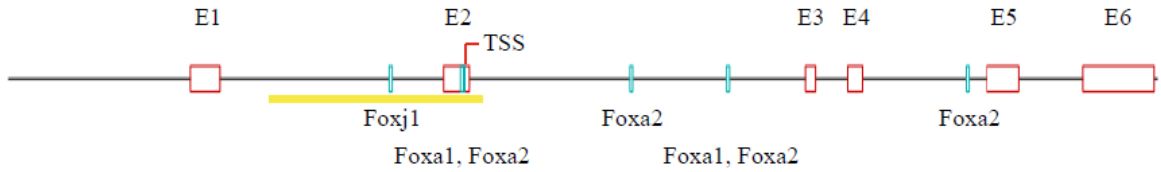

Figure 15 Forkhead domain factor consensus target sites across the *Fltp* locus

The 6 exons (E1-E6) of *Fltp* are indicated as clear red boxes. The yellow box shows the promoter with the transcriptional start site indicated as TSS. Foxj1, Foxa1, Foxa2, and Foxa2 binding sites are depicted by light blue boxes.

3.2.1.2 The Flattop protein

The protein encoded by the Fltp transcript has a length of 190 aas.

```
MATNYSANQY EKAYLPTYLQ NWSPARPTKE KIAAHEGYTQ IIANDRGHLL PSVPRSKASP
WGSFMGTWQM PLKIPPAKVT LTARTTTAAD NLTKWIHKNP DLLNACNGLR PEISGKPFDP
DSQTKQKKSV TKTVQQAPNP TIIPSSPVIQ GDNPDEPQSS HPSAGHTPGP QTPVNSPNNP
PPSPCKSTK-
```

Mammalian orthologs of Fltp can be found in human (*Homo sapiens*; C1orf192), in rat (*Rattus norvegicus*; RGD1562658), in cattle (*Bos taurus*; C3H1orf192), in chimpanzee (*Pan troglodytes*; LOC457454), and in dog (*Canis familiaris*; LOC488655). Orthologs in other species are present in model organisms such as the zebrafish (*Danio rerio*; C23H1orf192), the african clawed frog (*Xenopus laevis*; LOC734862), as well as the fly (*Drosophila virilis*; GJ15715). An alignment of the proteins of different species shows that the N terminus is highly conserved till aa 76 whereas the C terminus shows rather low conservation (Figure 16 A). *Drosophila* Fltp protein is with 265 aa the longest ortholog. The human and the murine form show the highest conservation. The red box shows the peptide used for generation of the antibodies (Figure 16 A). Using protein domain prediction tools (MyHits, http://hits.isb-sib.ch/cgi-bin/motif_scan; Scansite, http://scansite.mit.edu), we could identify two proline rich repeats (PRR) (Figure 16 A, green boxes).

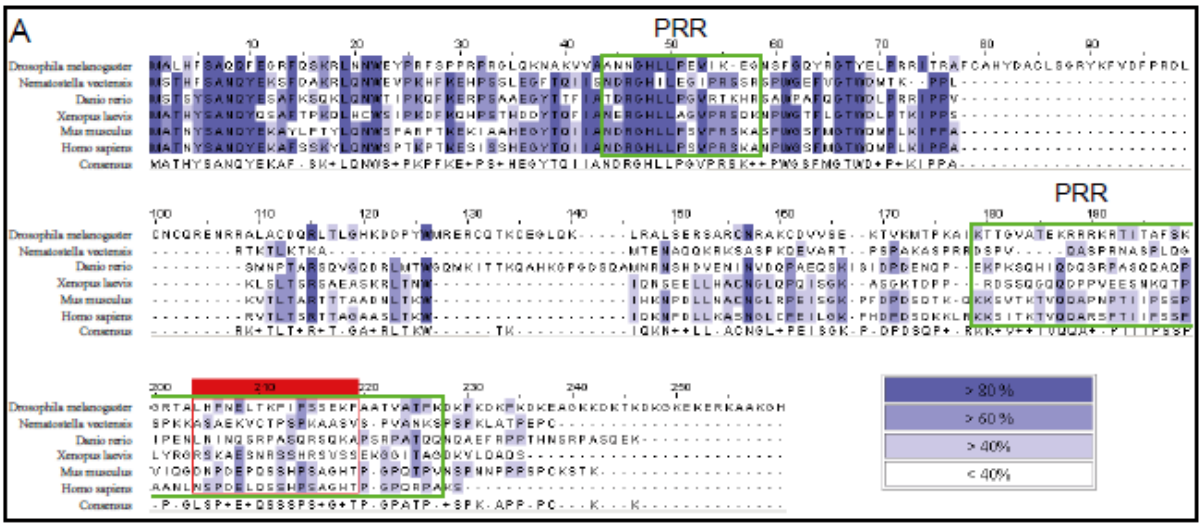

Figure 16 Fltp protein alignment

(**A**) Fltp protein alignment between different species shows conservation in the first 76 amino acids. The clear green boxes highlight the predicted proline rich repeats (PRR). The *Drosophila* and the *Danio rerio* protein have additional amino acids compared to the orthologs. The mouse and human proteins show high homology. The red box shows the peptide sequence used for generating the Fltp antibodies. Dark blue indicates conversation over 80%. Lighter colors indicate less conservation.

PRRs are known to interact with SRC homology 3 (SH3) domains (Lock et al., 2000). The classical SH3 domain is a protein-protein interaction domain, which is found in a variety of intracellular proteins (adaptor proteins, kinases, GTPases). The first, higher conserved PRR is located near the N terminus (at aa 44-58 in mouse) and harbors a PSVP (proline/serin/valin/proline) binding motif that belongs to the classical PxxP (proline/x/x/proline) SH3 binding motif (Figure 17, red). In general the conservation of Fltp protein at the N terminal region is higher than at the C terminus. The second PRR (at aa 138-184 in mouse) comprises three SH3 PxxP binding motifs (PssP, PdeP, PqtP) but is not as conserved as the first one (Figure 17, red). Additionally, we could identify a Gab2a motif: sPaRPtKekiaa (pPpRPpKpxxxe), several motifs that bind to Mona/Gads: RxxxxK (RptkeK), RxxK (RptK), and two KxxK (KqkK, KstK) motifs which all are SH3 binding motifs. PxxP motifs outside of the PRRs are: PfdP, PnnP, and PpsP.

MATNYSANQY EKAYLPTYLQ NWSPARPTKE KIAAHEGYTQ IIANDRGHLL PSVPRSKASP
WGSFMGTWQM PLKIPPAKVT LTARTTTAAD NLTKWIHKNP DLLNACNGLR PEISGKPFDP
DSQTKQKKSV TKTVQQAPNP TIIPSSPVIQ GDNPDEPQSS HPSAGHTPGP QTPVNSPNNP
PPSPCKSTK-

Figure 17 SH3 binding motifs in the Fltp amino acid sequence

Underlined regions indicate the proline rich repeats. SH3 binding motifs of the PxxP type are shown in red, motifs of the KxxK type in green, and the RxxxxK as well as the RxxK motif in light blue.

The prediction tool MyHits provided additional information about two predicted N-glycosylation sites (at aa 4-7 and 91-94 in mouse), one expected Casein kinase II phosphorylation site (at aa 87-90 in mouse), one theoretical N-myristoylation site (at aa 62-67 in mouse), and three potential protein kinase C phosphorylation sites (at aa 82-84, 114-116, 187-189 in mouse). Potential N-myristoylation

and N-glycosylation might indicate that the Fltp protein is targeted to the membrane or functions in the secretory pathway, respectively.

3.2.2 Generation of affinity purified polyclonal *Flattop* antibodies

To analyze the Fltp protein biochemically and cell biologically, we raised two affinity purified polyclonal antibodies in rabbit (FltpI and II) and one in guinea pig (FltpIII) against mouse Fltp using the peptide sequence: DNPDEPQSSHPSAGHT (Pineda, Berlin, Germany). The epitope lies in the PRR of the less well conserved C terminal part of the Fltp protein (Figure 16 A, red box). Nevertheless, the human and murine sequences are nearly completely similar. Lately, we got evidence from human lung sections, which indicate that the FltpI antibody can detect human FLTP (unpublished data from Dr. Barkha Srivastava). The specificity of these antibodies was tested on Western blot and in immunofluorescence analysis. For Western blot analysis we transfected human embryonic kidney (HEK293T) cells with a vector encoding for an *enhanced green fluorescent protein* (*eGFP*) fused to the 5' region of *Fltp*, a vector encoding for *Fltp* fused to the 5' region of an *enhanced yellow fluorescent protein* (*eYFP*), *Fltp* alone, a vector expressing only *eGFP*, and untransfected HEK293T cells as control (Figure 18 D). In the *Fltp* only transfected cells a specific band could be detected at around 25 kDa with the FltpI and FltpIII antibody (Figure 18 A, B). The Fltp protein generated by the transcript AK005804 (1700009P17Rik) has a calculated molecular weight of 20.55 kDa. The discrepancy between the calculated and observed size could be due to posttranslational modifications like phosphorylation, glycosylation, or myristoylation. Sites for all these modifications are located in the Fltp protein (see 3.2.1.2). The fusion bands are, as expected, visible at 50 kDa (25 kDa Fltp + 25 kDa eGFP/eYFP) in the eYFP/eGFP Fltp transfected HEK293T cells. Lower bands are likely degradation bands. The antibodies specifically detect Fltp protein, as no bands are visible in the *eGFP* only transfected cells as well as in the non-transfected control (Figure 18 A, B). Additionally, we used *WT*, $Fltp^{ZV/+}$, and $Fltp^{ZV/ZV}$ murine testis lysate to proof the specificity of our antibodies. As expected, Fltp protein can be detected in *WT* and $Fltp^{ZV/+}$ but not in knock-out $Fltp^{ZV/ZV}$ animals (Figure 18 C).

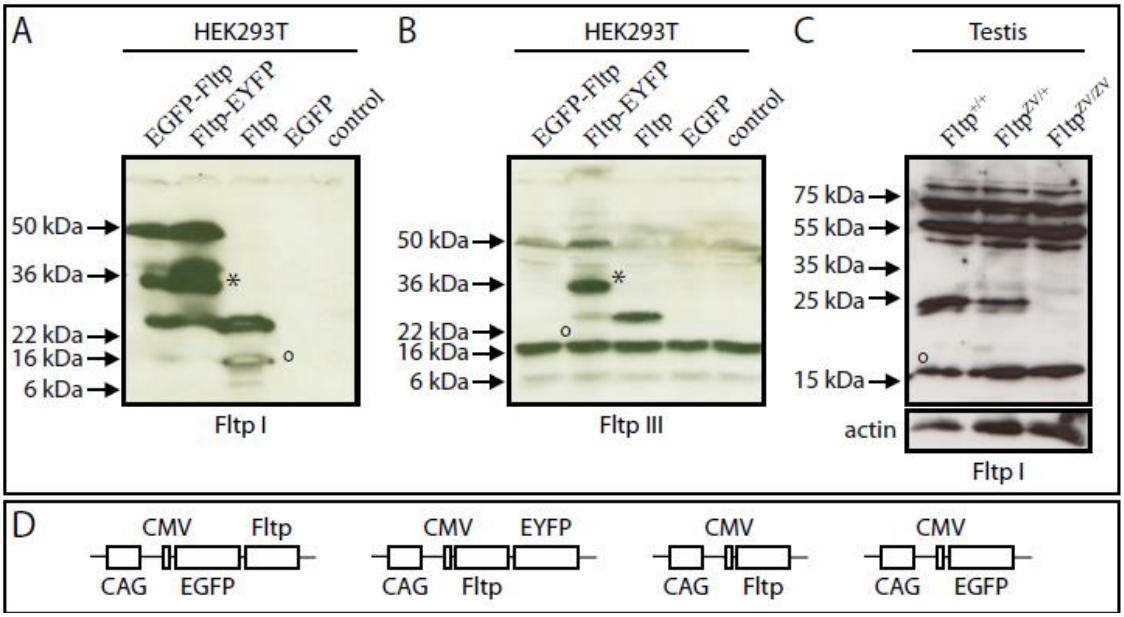

Figure 18 Fltp antibody specificity in Western blot

(**A-B**) HEK293T cells were transiently transfected with eGFP tagged murine Fltp cDNA, Fltp-eYFP, only Fltp cDNA, and eGFP alone. An untransfected control is shown in the last panel. Lysates were analyzed with the FltpI and FltpIII antibody. Proteolytic degradation products are marked with an asterisk.
(**C**) Western blot analysis of testis lysate of *WT*, *Fltp*$^{ZV/+}$, and *Fltp*$^{ZV/ZV}$ animals with the FltpI antibody.
(**D**) Scheme of constructs used for transient HEK293T cell transfection.
(Abbreviations: CAG = The CMV early enhancer/chicken β-actin promoter; CMV = cytomegalovirus)

To test whether the antibodies also work in immunohisto- and cytochemistry, we overexpressed Fltp protein fused to eYFP in a transient transfected mouse embryonic fibroblast cell line (NIH3T3). As shown in Figure 19 A-D overexpressed Fltp protein co-localizes with eYFP protein indicating that this antibody is able to detect Fltp protein in immunohisto- and cytochemistry. The Fltp positive red dots in the non-transfected cells reflect endogenous Fltp localization at or around the centrosomes of these cells. Additionally, we transfected inner medullary collecting duct (IMCD3) cells that harbor long primary cilia on their surface with a construct containing *Arl13b-BFP*, *Cep97-tagRFP*, and *Fltp-Venus* (Figure 19 M). Antibody staining for Fltp protein with two different antibodies (FltpI and FltpII) showed localization at the primary cilium as indicated by a co-staining with ciliary localized Arl13b and alpha-tubulin (Figure 19 F-L). Immunohistochemistry on the murine embryonic node of an E7.75 *WT* embryo revealed localization of the Fltp protein exclusively to the node cells in accordance with the mRNA expression data (Tamplin et al., 2008), as well as the β-gal activity data (Figure 19 N, O; Figure 25 H-M) (Lange et al., 2012). On subcellular level, Fltp protein is enriched at the apical membrane of node cells, maybe due to N-myristoylation/N-glycosylation dependent membrane targeting. Moreover, we could detect Fltp at the primary nodal cilia (Figure 19 N, O). Fltp is located to both, the motile primary cilia of the nodal pit cells as well as to the immotile primary cilia of the nodal crown cells (Lange et al., 2012). Taken together, these experiments indicate that the generated antibodies are useful tools to detect overexpressed as well as endogenous Fltp protein in Western blot and immunohisto- and cytochemical analysis. Moreover, the specificity is proven by the absence of Fltp detection in the knock out tissue as well as by the localization of two different Fltp antibodies to the same subcellular structures *in vivo*.

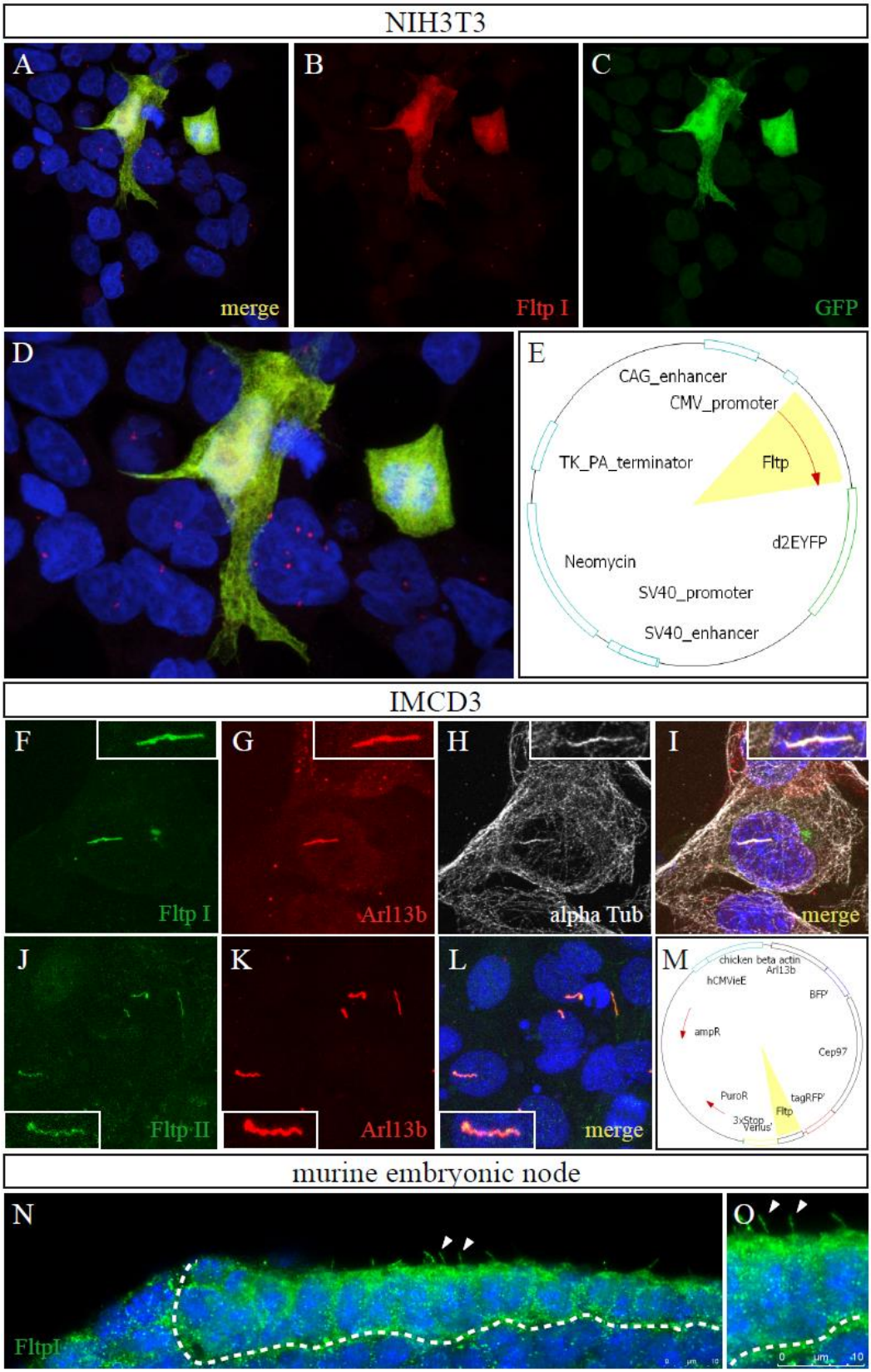

Figure 19 Fltp antibody specificity in immunohistochemistry

(**A-D**) Confocal pictures of Fltp-eYFP transfected NIH3T3 cells. Fltp staining by the anti-Fltp antibody FltpI is shown in red, staining for eYFP is performed with an anti-GFP antibody in green. The yellow staining shows the merged picture.

(**E**) The construct used for transfection of the NIH3T3 cells.

(**F-L**) Confocal pictures of *Arl13b-BFP*, *CEP97-tagRFP*, and *Fltp-Venus* transfected IMCD3 cells.
(**F-I)** The FltpI antibody shows staining of the cilium (green) as shown by co-staining with an anti-Arl13b antibody (red) and α-tubulin staining (white).
(**J-L**) Fltp protein is localized to the cilium as shown by FltpII antibody staining (green) and Arl13b staining (red).
(**M**) The construct used to transfect the IMCD3 cells. Note that *CEP97-tagRFP* did not show any expression.
(**N, O**) Confocal picture of an E7.75 murine embryonic node (surrounded by the dotted white line) where Fltp protein is localized at the cilia (white arrow heads) and in the cytoplasm enriched at the apical surface as shown by FltpI antibody staining (green).

3.2.3 Generation of monoclonal *Flattop* antibodies

In addition to the polyclonal rabbit antibodies, we generated mouse monoclonal Fltp antibodies against the same peptide sequence as the polyclonal antibodies with the help of Dr. Kremmer (Institute for Molecular Immunology) (see 3.2.2). These antibodies were tested for their specificity on Western blot as well as in immunofluorescent analysis. First we tested the antibodies on cell lysates of HEK293T cells overexpressing the Fltp protein fused to a GFP. Antibodies that recognized the protein on Western blot were further characterized in immunocytochemistry. Therefore, we transfected NIH3T3 cells with Fltp-GFP fusion protein and quantified their co-expression. The results for different antibodies can be seen in Figure 20.

Monoclonal Fltp antibodies					
Antibody no.	WB	IF	Antibody no.	WB	IF
Rik2-1B6	no signal	not tested	Rik2-3F7	A	AA
Rik2-1E5	no signal	not tested	Rik2-3H7	A	A
Rik2-1E4	AA	AAA	Rik2-3H10	A	no signal
Rik2-1F8	A	A	Rik2-4B5	A	A
Rik2-1G7	AAA	AAA	Rik2-4D7	AAA	AAA
Rik2-2A4	no signal	not tested	Rik-C 4D9	A	AA
Rik2-2A9	no signal	not tested	RIK-2+C 4E3 G3	AAA	AAA
Rik2-2A10	no signal	not tested	Rik2-4E9	A	AA
Rik2-2A11	no signal	not tested	Rik2-4E12	A	A
Rik2-2C5	no signal	not tested	Rik2-4F2	A	AA
RIK-2+C 2D3 2a	AAA	AAA	Rik2-5H9	no signal	not tested
Rik2-2D7	no signal	not tested	RIK-2+C 6D10 G3	no signal	not tested
Rik2-2D10	no signal	not tested	Rik2-6H3	A	AA
RIK-2+C 2E3 2a	A	A	Rik2-7A10	A	A
Rik2-3C10	no signal	not tested	Rik2-7A12	AA	A
Rik2-3D3	A	A	Rik2-7C6	no signal	not tested
Rik2-3E3	AA	A	Rik2-7F6	no signal	not tested

Figure 20 Monoclonal Fltp antibody specificity

Table of all tested monoclonal Fltp antibodies. All antibodies were first tested on Western blot (WB) on cell lysates of HEK293T cells overexpressing *Fltp-GFP*. Antibodies with positive signal in WB were further tested on immunofluorescence. For this purpose NIH3T3 cells transfected with *Fltp-GFP* were used. A means the staining is o.k., AA means the staining is good, and AAA the staining is very good.

3.2.4 Generation of the T2A antibodies

For the purpose of genetic lineage tracing as well as conditional gene inactivation in distinct mono- and multiciliated cells, we generated the *Fltp*^{T2AiCre} mouse line (Lange et al., 2012). Here the iCre is separated by a T2A sequence from the ORF of Fltp. The consensus sequence of the T2A peptide is characterized by the following 18 aas: EGRGSLLTCGDVEENPGP. The 2A part consists of the first 17 aas and the 2B part of the last aa. The cleavage is performed between the last glycine of the 2A sequence and the proline of the 2B. The 2A part always remains on the C terminal end of the upstream protein making it a very useful tag to generate antibodies against proteins where no commercial antibodies are available. The T2A antibodies will provide an excellent tool for analyzing the subcellular localization of the T2A tagged Fltp protein in *Fltp*^{T2AiCre} mice. The rat monoclonal T2A antibodies were generated against the 2A part (EGRGSLLTCGDVEENPG) of the T2A peptide by Dr. Kremmer (Institute for Molecular Immunology). To test whether the generated T2A antibodies are specific we transiently transfected IMCD3 cells with an *Arl13b-BFP-T2A-hPifo-Venus* construct (Figure 21 A). This allows us to stain these cells for cilia with an anti-Arl13b, anti-T2A, and anti-GFP antibody. Two monoclonal T2A antibodies (1G8 and 5E6) clearly show a ciliary staining (Figure 21 B, red) proven by co-localization with an anti-Arl13b (Figure 21B, green, top two panels) or an anti-GFP antibody in transfected cells (Figure 21 B, green, lower two panels). The Arl13b antibody also marks cilia in untransfected cells (Figure 21 B, green, top two panels on the right), whereas the GFP antibody does not (Figure 21 B, green, lower two panels on the right). In addition, the T2A antibody reacts with a protein of 55 kDa in HEK293T cells transfected with a Venus-T2A-tagged murine *Fltp* cDNA. No signal is observed in non-transfected or SF-TAP-tagged *Fltp* cDNA transfected cells (Lange et al., 2012).

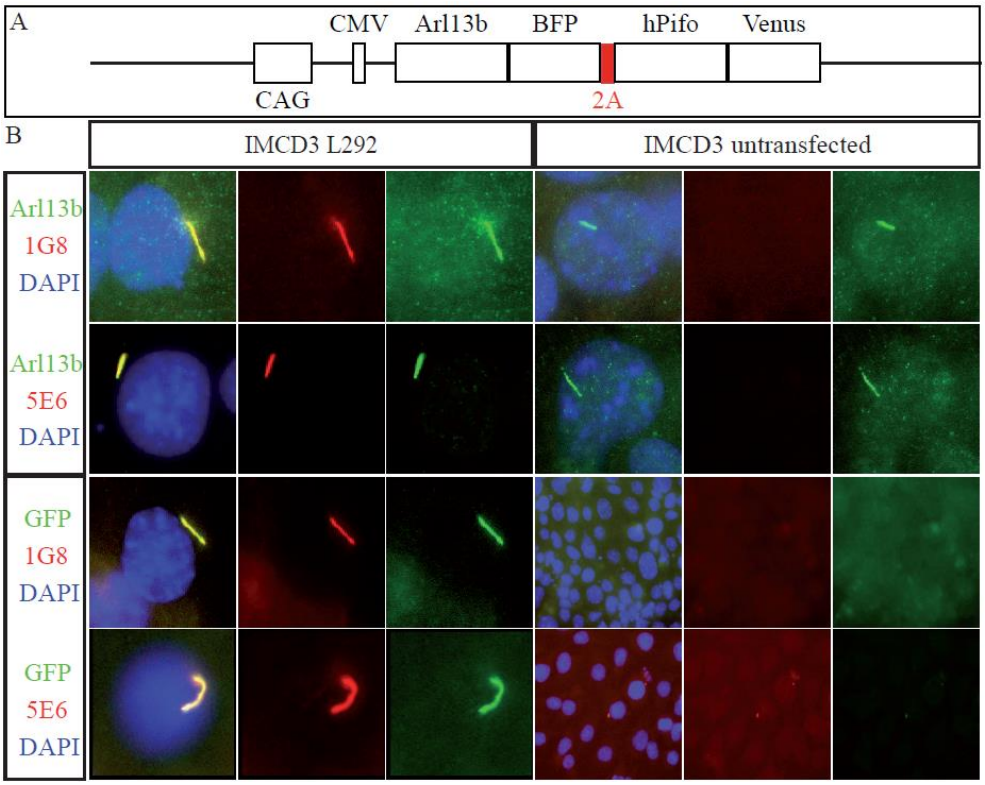

Figure 21 T2A antibody specificity in immunohistochemistry

To show T2A antibody specificity transiently transfected IMCD3 cells were analyzed by immunohistochemistry.

(**A**) The construct (L292) used for transient transfection. *Arl13b-BFP* is separated by the *T2A* sequence from *hPifo-Venus*.
(**B**) Transfected IMCD3 cells show localization of T2A antibody exclusively at the cilia (red) which is verified by an anti-Arl13b staining (green, upper two panels). Note that the Arl13b antibody also recognizes the cilia in untransfected cells whereas the T2A antibody does not. The lower two panels show again antibody staining for the T2A protein. Localization of the T2A protein (red) is at the cilium as proven by a co-staining for the BFP tagged Arl13b with the GFP antibody (green). Note that the hPifo is not detectable in these cells.

In Figure 22 all T2A antibodies we tested are listed with comments if and how good they work in Western blot and immunofluorescence.

Monoclonal T2A antibodies					
Antibody no.	WB	IF	Antibody no.	WB	IF
Mouse-EGR 1A1-2A	no signal	A	Rat-EGR 3D2-2C	no signal	no signal
Rat-EGR 1C4-G1+2a	AAA	AAA	Rat-EGR 3D11-2A	AA	no signal
Rat-EGR 1C4-G1+2a g	AAA	AAA	Mouse-EGR 3E1-2A	no signal	no signal
Mouse-EGR 1F9-2A	no signal	no signal	Rat-EGR 4A3-2a	no signal	no signal
Rat-EGR 1G5-G1	AA	AAA	Rat-EGR 4C9-G1	no signal	no signal
Rat-EGR 1G8-G1+2a+2c	AA	AAA	Rat-EGR 5E6-G1+2a	AAA	AAA
Mouse-EGR 2A11-G1	no signal	no signal	Rat-EGR 5E6-G1+2a g	AAA	AAA
Rat-EGR 2A11-2a	AA	AAA	Mouse-EGR HB9-2A	no signal	no signal
Rat-EGR 2G1-2a	A	no signal			

Figure 22 T2A antibody specificity

Table of all tested monoclonal T2A antibodies. All antibodies were first tested on Western blot (WB) on cell lysates of HEK293T cells overexpressing *Fltp-GFP*. Antibodies with positive signal in WB were further tested on immunofluorescence. For this purpose NIH3T3 cells transfected with *Fltp-GFP* were used. A means the staining is o.k., AA means the staining is good, and AAA the staining is very good.

Taken together, we could show that the *Fltp* gene locus expresses an mRNA that is translated and potentially post-translationally modified. The resulting protein migrates at around 25 kDa in gel electrophoresis. On the cellular level Fltp protein is localized to the cells of the murine embryonic node which is consistent with the mRNA expression data (Tamplin et al., 2008). Subcellular it localizes to the apical surface as well as to motile and immotile primary cilia of the node. These observations could be confirmed with two polyclonal antibodies against the endogenous Fltp protein and two monoclonal antibodies against the T2A tagged endogenous Fltp protein. Because we identified an interesting novel gene expressed in the embryonic organizer, more precisely, in the node and its cilia, we generated a knock in/knock out allele to analyze *Fltp* function *in vivo*.

3.3 Generation of the genetically modified *Flattop* mouse line

To analyze the spatial and temporal expression pattern and the function of *Fltp* we generated a knock in/knock out allele. Through homologues recombination in ES cells we replaced the whole ORF by a reporter gene cassette consisting of a nuclear tagged *lacZ* gene and a Histone-tagged *Venus* fluorescent reporter gene.

3.3.1 Generation of the *Fltp*^{ZV} mouse line

3.3.1.1 Design and generation of the *Fltp*^{ZV} targeting vector

The targeting vector used for recombination in ES cells was designed as demonstrated in Figure 23. The ORF was replaced by a cassette containing a nuclear localization signal (NLS) fused to a *lacZ* gene encoding for β-gal (Figure 23, light blue box, LacZ). It also contains a coding sequence for Histone-2B (H2B) fused to a *Venus* fluorescent reporter gene (Venus) that is separated by a T2A sequence (2A; see 3.1.1) from the NLS-LacZ (Figure 23, red, green, and yellow boxes). Downstream of the reporter cassette an artificial intron and an exon encoding for the Simian Virus 40 polyadenylation signal sequence (SV40-pA) follows (Figure 23, purple box and brown arrow). The *loxP*-flanked PGK promoter-driven *neo* resistance gene follows the polyadenylation signal in the opposite orientation (Figure 23, pink box and white arrow plus red arrows marking *loxP* sites). After the last *loxP* site the original 3' UTR follows. The detailed generation of the targeting vector for the *Fltp*^{ZV} allele is described in the "Material and methods" section (see 5.2.1.4).

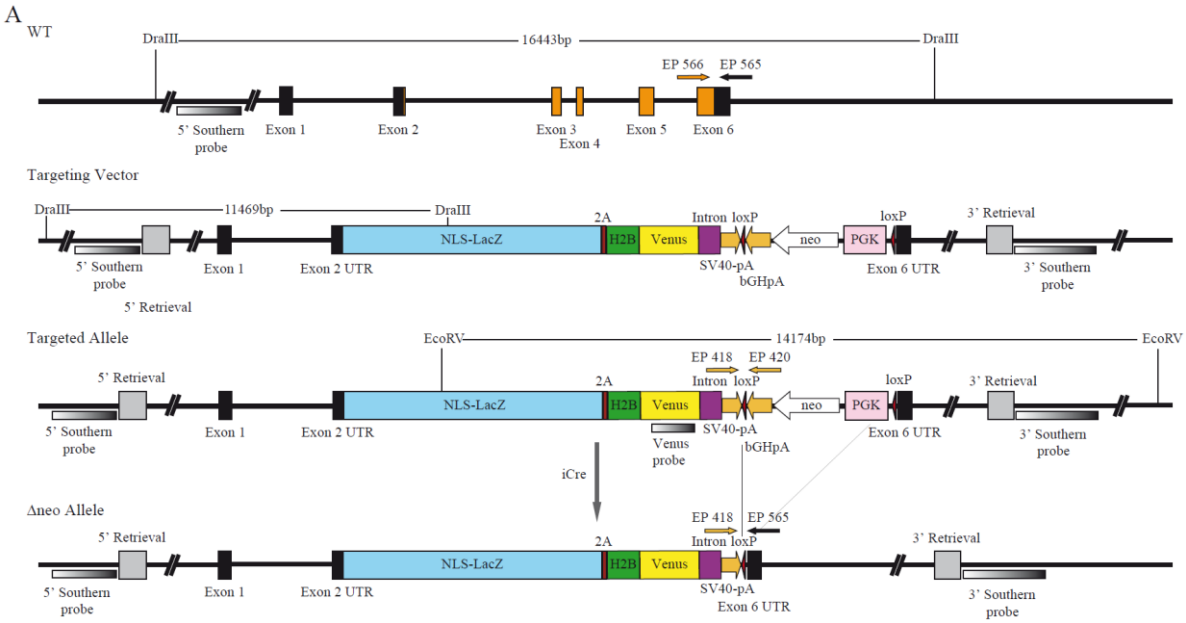

Figure 23 Targeting strategy of the *Fltp*^{ZV} allele

(**A**) To delete the whole open reading frame of *Fltp* a targeting vector ranging from exon 2 till exon 6 was introduced. To delete the selection cassette an iCre recombinase has to be introduced. The exons are numbered and shown as black and orange boxes. The orange boxes indicate the open reading frame. Primers for genotyping are designated EP418, EP420, EP565, and EP566. The external 5'- as well as the 3'-probe are as indicated in the figure. Restriction enzyme sites for *DraIII* and *EcoRV* are shown. Homology regions for recombination of the targeting construct are indicated as 5'- and 3'-Retrieval. The figure is on scale.
(Abbreviations: NLS-LacZ = nuclear localization signal-beta-galactosidase; 2A = viral T2A sequence; H2B = histon-2B; Venus = yellow fluorescent reporter gene; SV40-pA = Simian Virus 40 polyadenylation signal; loxP = site of Cre mediate recombination; bGHpA = bovine Growth Hormone polyadenylation signal; neo = neomycin resistance cassette; PGK = phospho-glycerate kinase; UTR = untranslated region)

To generate targeted ES cells we electroporated IDG3.2-F1 ES cells (C57BL/6J x 129S6/SvEvTac) (Hitz et al., 2007) with the *AscI*-linearized *Fltp*^{ZV} targeting vector and neomycin resistant clones were

selected using 300 µg/ml G418 (Invitrogen). Homologous recombination at the *Fltp* locus was confirmed by Southern blot analysis of *DraIII*-digested genomic DNA using the Fltp 5'-probe (620 bp) located outside the recombination border of the integration site of the targeting vector (Figure 23) (5' Southern Fltp FWD *XhoI*; 5' Southern Fltp REV *XbaI*, see 5.1.9.2). 8 out of 100 clones (in total: 22 positive clones out of 289) showed homologous recombination. Due to restriction fragment length polymorphisms (RFLP) of the Bl/6J and 129S6 alleles and an isogenic Bl6 targeting vector, homologous recombination occurred preferentially on the Bl/6J allele and reduced the size of the restriction fragment from 16.443 bp to 11.469 bp. The 129S6 WT band is smaller in size than the Bl/6J WT band and is not targeted (Figure 24). Out of two different ES clones (E2/2 and E3/1) germline chimeras were generated by CD1 morula aggregation and the *loxP*-flanked *neo* selection cassette was subsequently removed in the germline by intercrossing with an ubiquitous expressed Cre recombinase deleter mouse strain (*ROSA26-Cre*) (Soriano, 1999). Both ES cell clones gave birth to ∆neo animals but for the analysis we concentrated on the E2/2 clone and founded the animal colony on this clone. After deletion mice were backcrossed to C57Bl/6J to eliminate the *Cre* allele. Only those mice negative for the *Cre* allele were used for backcrossings to C57Bl/6J, 129S2/SvPasCrlCD1, or CD1 and further analyses were carried out with $Fltp^{ZV\Delta neo/+}$ mice backcrossed several generations in C57Bl/6J, 129S2/SvPasCrlCD1, or CD1. For genotyping of $Fltp^{ZV}$ animals the primer EP418, EP565, and EP566 were used and resulted in PCR products of 317 bp (WT) and 387 bp (targeted ∆neo allele) (Figure 24 B; for genotyping protocol see 5.2.4.1). Western blot analysis was performed on testis lysate of a *WT*, a $Fltp^{ZV/+}$, and a $Fltp^{ZV/ZV}$ mouse to show that the introduced knock out construct generates a null allele and results in absence of Fltp protein as expected due to the deletion of the complete ORF (Figure 24 C). The targeting was done by Dr. Ingo Burtscher, Wenke Barkey, and Patrizia Gillardino.

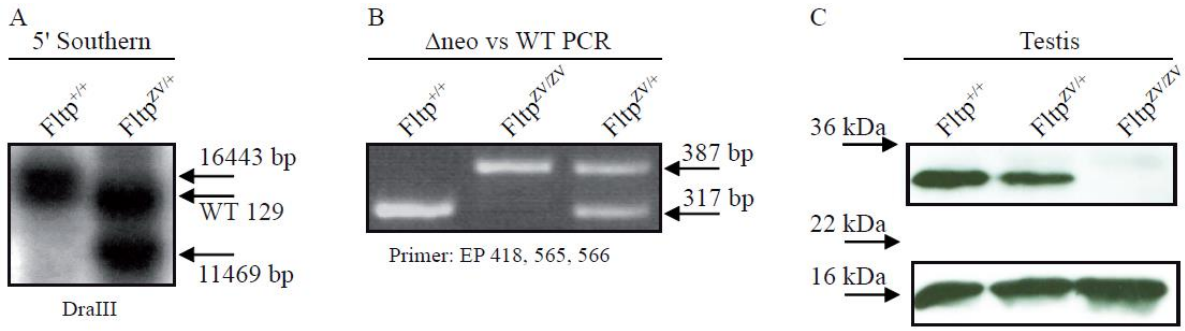

Figure 24 Verification of the $Fltp^{ZV}$ allele

(**A**) Southern blot of *WT* ES cell versus $Fltp^{ZV/+}$ ES cell digested with *DraIII* and hybridized with the external 5' Southern probe showing the Bl6 (16443 bp) and 129 *WT* allele as well as the Bl6 targeted allele (11469 bp). Notice the shift of the WT band due to restriction length polymorphism.
(**B**) Genotyping PCR for discrimination between *WT*, $Fltp^{ZV/+}$, and $Fltp^{ZV/ZV}$. Primers used: EP418, EP565, and EP566. WT band (317 bp); targeted ∆neo band (387 bp).
(**C**) Western blot to show absence of Fltp protein in the $Fltp^{ZV/ZV}$ mouse compared to the *WT* and $Fltp^{ZV/+}$ mouse. Fltp protein band is detectable at around 25 kDa (calculated weight 20 kDa).

The Mendelian distribution for *Fltp* G2 in CD1 heterozygous intercrosses did not show a dramatically altered decrease of $Fltp^{ZV/ZV}$ animals (Table 1). In *Fltp* G1 CD1 heterozygous intercrosses we found the later mentioned exencephaly phenotype (3.4.2.1; Figure 37).

Fltp CD1 G2 intercrosses			
WT	HOM	HET	total
49	45	81	175
28,0%	25,7%	46,3%	100,0%

Table 1 Fltp CD1 G2 intercrosses

For heterozygous intercrosses of *Fltp*^{zv} animals inbred into the 129S6/SvEvTac mouse line for two generations the Mendelian ratio shifted towards WT and HET animals. The expected Mendelian ratio for HOM animals dropped dramatically (Table 2).

Fltp 129S6/SvEvTac G2 intercrosses			
WT	HOM	HET	total
35	2	23	60
58,3%	3,3%	38,3%	100,0%

Table 2 Fltp 129S6/SvEvTac G2 intercrosses

For heterozygous intercrosses of *Fltp*^{zv} animals inbred into the 129S6/SvEvTac mouse line for three generations the expected Mendelian for HOM animals increased whereas the one for HET decreased (Table 3).

Fltp 129S6/SvEvTac G3 intercrosses			
WT	HOM	HET	total
12	15	12	39
30,7%	38,5%	30,7%	100,0%

Table 3 Fltp 129S6/SvEvTac G3 intercrosses

For heterozygous intercrosses of *Fltp*^{zv} animals inbred into the 129S6/SvEvTac mouse line for four generations the expected Mendelian for HOM animals again decreased (Table 4).

Fltp 129S6/SvEvTac G4 intercrosses			
WT	HOM	HET	total
15	5	20	40
37,5%	12,5%	50,0%	100,0%

Table 4 Fltp 129S6/SvEvTac G4 intercrosses

3.4 Analysis of the novel planar cell polarity gene *Flattop*

3.4.1 *Flattop* reporter gene expression is restricted to mono- and multiciliated tissues

As *Fltp* is a newly discovered gene and very little expression information is available, we first analyzed the tissue and cell-type specific reporter expression. To characterize the temporal and spatial pattern of expression we mated $Fltp^{ZV/+}$ animals with CD1 and analyzed *Fltp* reporter gene expression in embryos and the offspring. To monitor *Fltp* expression we made use of the *lacZ* and the *Venus* reporter gene knock in under the control of the endogenous *Fltp* promoter.

3.4.1.1 *Flattop* reporter gene expression during early embryonic development

As expected, β-gal activity in $Fltp^{ZV/+}$ animals starts at E7.5 in the embryonic node which is consistent with endogenous mRNA expression (Tamplin et al., 2008) and immunohistochemical studies as well as lineage tracing studies (Figure 25 A, B, H-M) (Lange et al., 2012). Immunohistochemical analysis of whole-mount *WT* E7.75 embryos revealed that endogenous Fltp is localized exclusively to the cytoplasm of the node cells as well as to the primary nodal cilia (Figure 25 H-M). In co-localization studies we could show that endogenous Fltp protein marked by FltpI antibody co-localizes with MTs at the apical surface of node cells as well as to the primary cilium (Figure 25 K-M). To confirm endogenous Fltp localization shown by the FltpI antibody and to show the presence of the Fltp-TAP-T2A fusion protein *in vivo* in the $Fltp^{T2AiCre}$ mouse line we used the T2A antibody for whole-mount immunofluorescence stainings of E7.75 embryos. Laser scanning microscopy (LSM) revealed that the T2A antibody specifically recognized the tagged Fltp protein in the pit and crown cells of the embryonic node. Interestingly, the tagged Fltp protein specifically localized to the node cilia suggestive for a function in the process of ciliogenesis (Lange et al., 2012). At E8.5, the cells of the node move to the posterior of the embryo and are still expressing the *lacZ* reporter gene (Figure 25 C). At E9.5, *lacZ* reporter gene expression starts in the prechordal plate in the developing brain (data not shown). During early organogenesis at E10.5, *lacZ* reporter gene activity reaches from the prechordal plate in the developing brain through the whole floor plate of the neural tube till the tail region. Strong expression is also visible in the developing choroid plexi (cp) of the first, second, third, and fourth ventricle as well as in the apical ectodermal ridge (aer) of the fore- and hindlimbs (Figure 25 D; Figure 36 A, B). β-gal activity in the aer of the hindlimb is weaker because the hindlimb is developmentally younger than the forelimb and only the onset of expression can be visualized. At E11.5, β-gal activity is strong in the floor plate and in all four cp. The expression in the aer of the fore- and hindlimb is still present and additional expression in the bone forming tissue of all limbs arises (Figure 25 E; Figure 36 C, D). By E12.5, β-gal activity is additionally visible in the inner ear (IE; data not shown). Figure 25 G shows the *lacZ* reporter gene expression at E13.5 in the IE, the cp, and the floor plate.

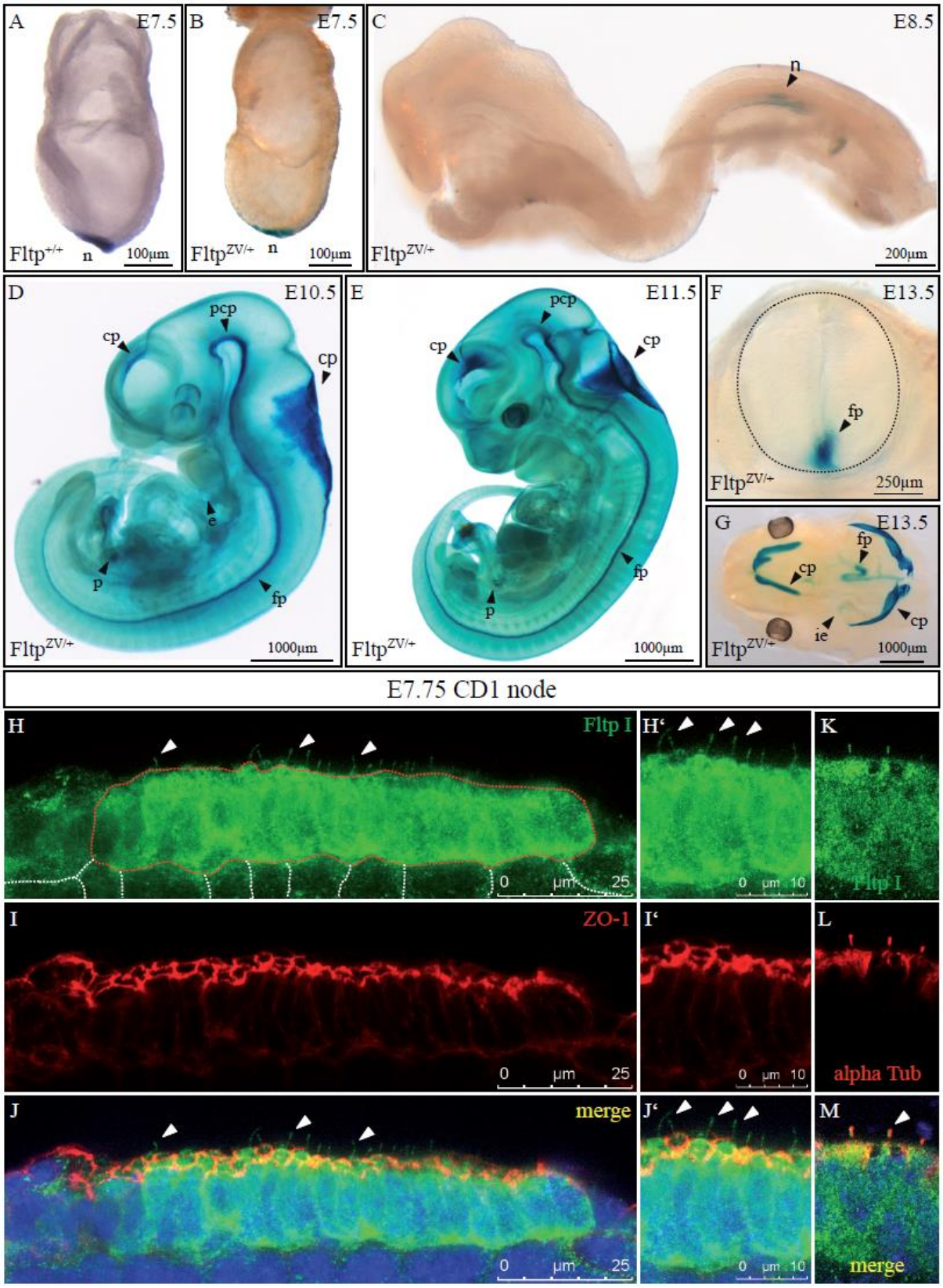

Figure 25 Early embryonic expression pattern of *Fltp*

Fltp reporter gene expression is restricted to distinct ciliated tissues during early embryonic development. (**A**) Fltp *in situ* hybridization on a gastrulating embryo at E7.5. mRNA expression is restricted to the node (n). (**B**) E7.5 *Fltp*$^{ZV/+}$ embryo. *LacZ* reporter gene expression is restricted to the node (n).

(**C**) E8.5 *Fltp*$^{ZV/+}$ embryo. β-gal activity is restricted to the node (n) which moved to the posterior side of the embryo.
(**D, E, G**) *Fltp*$^{ZV/+}$ embryos dehydrated by a methanol series and finally incubated in BABB.
(**D**) By E10.5 *Fltp*$^{ZV/+}$ embryos show *lacZ* expression in the developing choroid plexi (cp) of the first, second, third, and fourth ventricle, in the prechordal plate (pcp), in the developing eye (e), in the floorplate (fp) and in the pancreatic primordium (p).
(**E**) At E11.5 no additional expression domains are visible.
(**F**) Cross section of the neural tube at E13.5. The dotted line marks the border of the neural tube. Reporter gene expression is visible in the fp of the neural tube.
(**G**) Top view of an E13.5 head. Expression in the four cp, the fp, and the IE (ie) can be detected.
(**H-M**) Confocal pictures of an immunohistochemical analysis of an E7.5 embryonic node.
(**H**) Endogenous Fltp (marked by FltpI rabbit antibody, green) can be detected in the cytoplasm of the nodal cells, which are marked by the red dotted line, as well as in the node cilia (white arrow head). The white dotted line marks the epiblast cells.
(**H'**) Enlargement of H.
(**I**) ZO-1 staining (red) marks the apical surface of the node cells.
(**I'**) Enlargement of I.
(**J**) Overlay of H and I. Cell nuclei are stained by DAPI (blue), endogenous Fltp expression is shown in green, and ZO-1 in red. White arrow heads show Fltp positive cilia.
(**J'**) Enlargement of J.
(**K**) Antibody staining with the FltpI antibody.
(**L**) α-tubulin staining of the apical tubulin network and the cilia of node cells.
(**M**) Overlay of K and L.

Taken together, we could show that endogenous Fltp protein (validated by three different antibodies, FltpI, FltpII, and T2A) and *Fltp* reporter gene activity can be observed in distinct mono- and multiciliated tissues during early embryonic development that depend on PCP. Moreover, we could prove that Fltp reporter activity as well as endogenous protein localization accurately reflects endogenous mRNA expression.

3.4.1.2 *Flattop* reporter gene expression in the six sensory patches of the inner ear

Due to PCP related phenotypes (see below) and expression of *Fltp* in tissues that depend on PCP, we analyzed *Fltp* expression in the IE because it is a well-established model to analyze PCP in the mouse. The IE consists of six ciliated regions (sensory regions): the three cristae associated with the semi-circular canals (posterior crista ampullaris (pca); lateral crista ampullaris (lca); anterior crista ampullaris (aca)), the utricular macula (uma), the sacular macula (sma), which together constitute the vestibular system of the IE and the cochlea with its sensory organ the organ of Corti (oc) which is termed the auditory system (Kelley, 2006).
LacZ reporter gene expression in the IE starts at E12.5 in all six sensory regions (data not shown). At E13.5, the *Fltp*^{ZV} allele is expressed in a thin stripe at the base and the expression pattern gets broader in the region of the apex. Additional reporter gene expression is visible in the three cristae, the uma, and sma (Figure 26 A). By E14.5, the reporter expression gets more condensed in the sensory patches of the vestibular system whereas the cochlea staining is still ranging from thin restricted expression in the base to broader expression in the apex (Figure 26). From E15.5 onwards, β-gal activity in the vestibular region is well defined to the sensory cells and the cochlea is stained

from the base to the apex in a thin line that might correspond to the sensory hair cells (Figure 26). *Fltp* expression in the IE persists till adulthood.

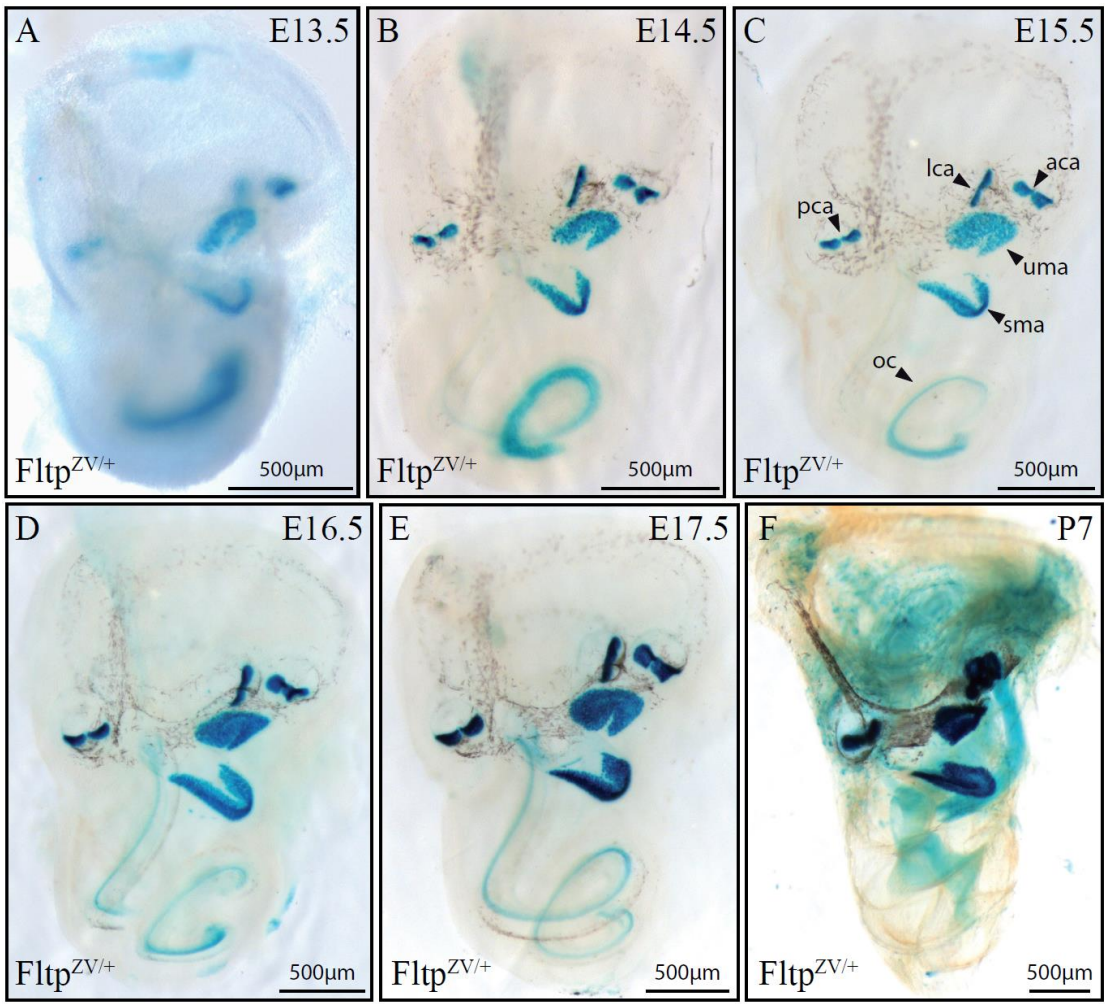

Figure 26 *Fltp* reporter gene activity in the inner ear is restricted to the six sensory patches

LacZ reporter gene is expressed in the 6 sensory regions of the IE. Onset of expression is at E12.5. (**A-F**) IEs of *Fltp*$^{ZV/+}$ embryos. Stages as indicated. *LacZ* expression can be detected in the posterior crista ampullaris (pca), the lateral crista ampullaris (lca), the anterior crista ampullaris (aca), the utricular macula (uma), and the sacular maccula (sma) of the vestibular part of the IE. Additional, expression can be observed in the organ of Corti (oc) embedded in the cochlear duct of the auditory region of the IE. IEs of *Fltp*$^{ZV/+}$ embryos in B-F are dehydrated by a methanol series and finally incubated in BABB.

To analyse the cell-type specific expression in the IE we performed immunohistochemical studies on the sensory patches of the IE. Fltp Venus reporter activity could be observed in the sensory cells of the cochlea as well as in the sensory cells of the vestibular region (data not shown). Moreover, we could show that endogenous Fltp protein is localized in the cytoplasm between the nucleus and the apical surface of sensory hair cells of the cochlea, which most likely represents localization of newly synthesized protein in the Golgi and/or trans-Golgi network. Additionally, Fltp protein is localized at the apical membrane on top of the cuticular plate, which is marked by an anti-Phalloidin antibody (Figure 27 A-C). These cells are not yet polarized and do not poses a kinocilium because they did not

form stereociliary hair bundles at their apical surface indicated by the absence of Phalloidin staining. In more mature cells Fltp protein is located asymmetrically on the basolateral membrane in sensory hair cells as well as on the apical surface (Figure 27 D-F). Antibody staining with an anti-GFP antibody marks Venus reporter positive cells. To analyze the subcellular localization of Fltp protein in sensory cells of the cochlea we made use of the T2A antibodies. Immunohistochemistry of *Fltp*$^{T2AiCre/+}$ animals revealed that Fltp protein is located in both, the kinocilium and the primary cilium of the supporting cells. Moreover, Fltp localization is restricted to the lateral side and is localized at the basolateral and the apical membrane. It co-localizes with the MT network as can be shown by anti-acetylated-tubulin antibody staining. Interestingly, Fltp protein surrounds the BB, as indicated by the black hole in the basal view, which might suggest that it has a function in BB transport, docking, and/or positioning (Figure 27 G).

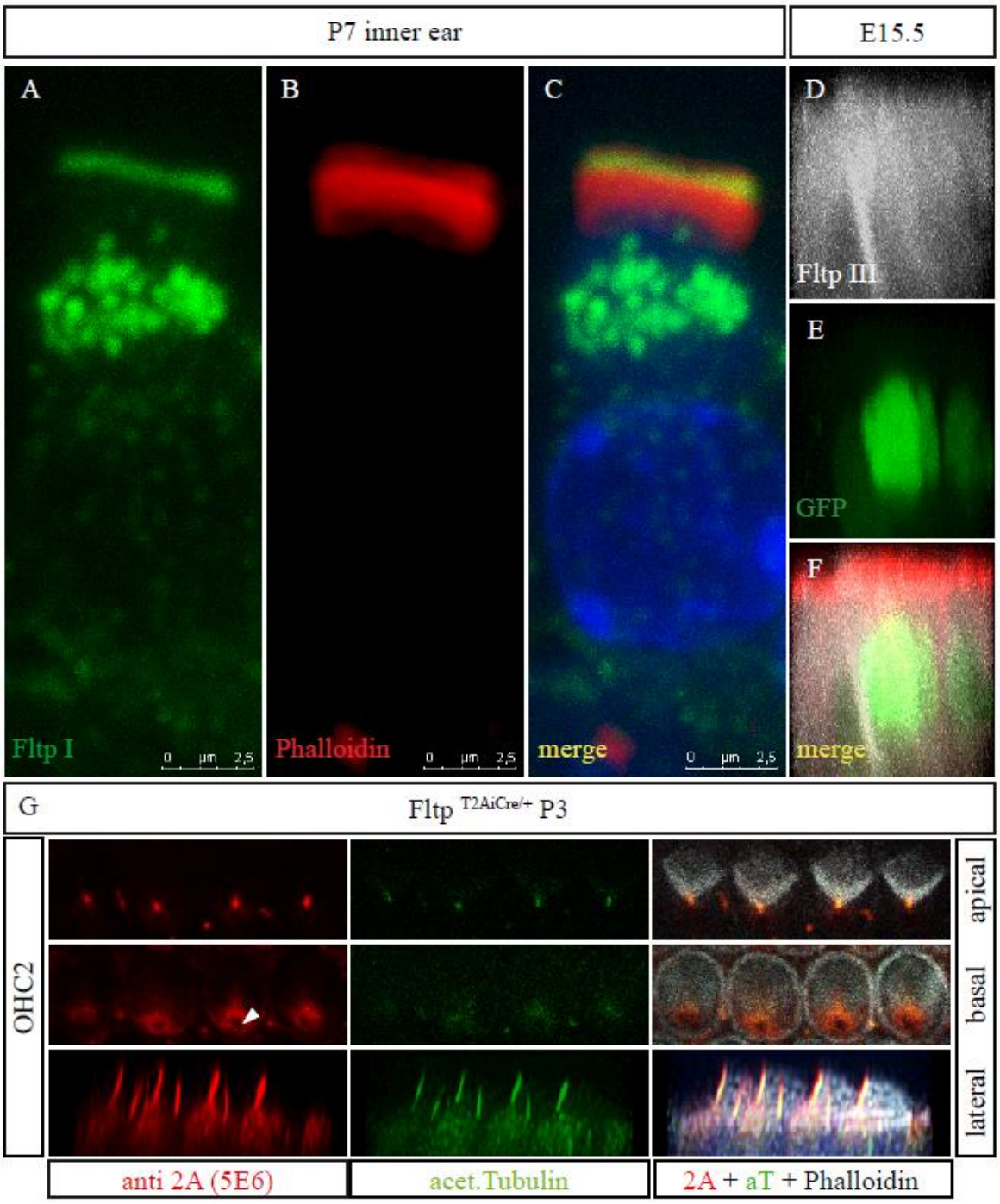

Figure 27 Fltp protein localization in sensory hair cells of the inner ear

(**A-G**) Confocal pictures of the cochlea of the IE.
(**A-C**) Fltp protein (green) is located in the cytoplasm and at the apical surface of *WT* polarizing IE hair cells. Phalloidin staining (red) marks the cortical actin cytoskeleton. Note that this cell has not established stereociliary hair cell bundles as can be seen by negative Phalloidin staining above the apical surface.
(**D-F**) Fltp protein (FltpIII antibody) is located asymmetrically in IE hair cells (white) of $Fltp^{ZV/+}$ animals. *Fltp* expressing cells are marked by *Venus* reporter gene expression stained by an anti-GFP antibody. Red marks the apical surface.
(**G**) T2A tagged Fltp protein (red) is located at the kinocilium and around the BB (region of BB is marked by the white arrow head) at the basolateral side of IE hair cells of $Fltp^{T2AiCre/+}$ animals as proven by co-localization with an anti-acetylated-tubulin antibody (green). The Phalloidin staining marks the stereociliary hair bundles (white). The first row shows an apical view, the second row is more basally at the height of the docked BB, and the third row shows a lateral view of the outer hair cell row 2.

3.4.1.3 *Flattop* reporter gene expression in the lung is restricted to ciliated cells

Ciliated cells in the lung are present in the trachea, main bronchi, bronchi, and the terminal bronchi. The alveoli are absent of ciliated cells and are important for gas exchange. At E13.5, the murine embryonic lung is free of *Fltp* reporter gene expression (Figure 28 A). *LacZ* reporter gene expression starts in the trachea and the main bronchi at E14.5, which is consistent with the spatial and temporal onset of ciliogenesis in this organ (Figure 28 B) (Toskala et al., 2005). Lineage tracing of Fltp positive cells using the *Fltp*^{T2AiCre} mouse line crossed into *ROSA26* reporter mouse line revealed an onset of reporter gene expression at E13.5 (Lange et al., 2012). By E15.5, all airways till the terminal bronchioles are lacZ positive (Figure 28 C). A cross section of an adult lung shows *lacZ* reporter gene expression in the airway epithelium (Figure 28 H). *Fltp* reporter expression directly stops at the bronchoalveolar duct junction (BADJ) as can be seen in Figure 28 I. The BADJ marks the junction between bronchi and alveoli in which ciliated cells are absent, strongly suggesting that *Fltp* is expressed in ciliated cells.

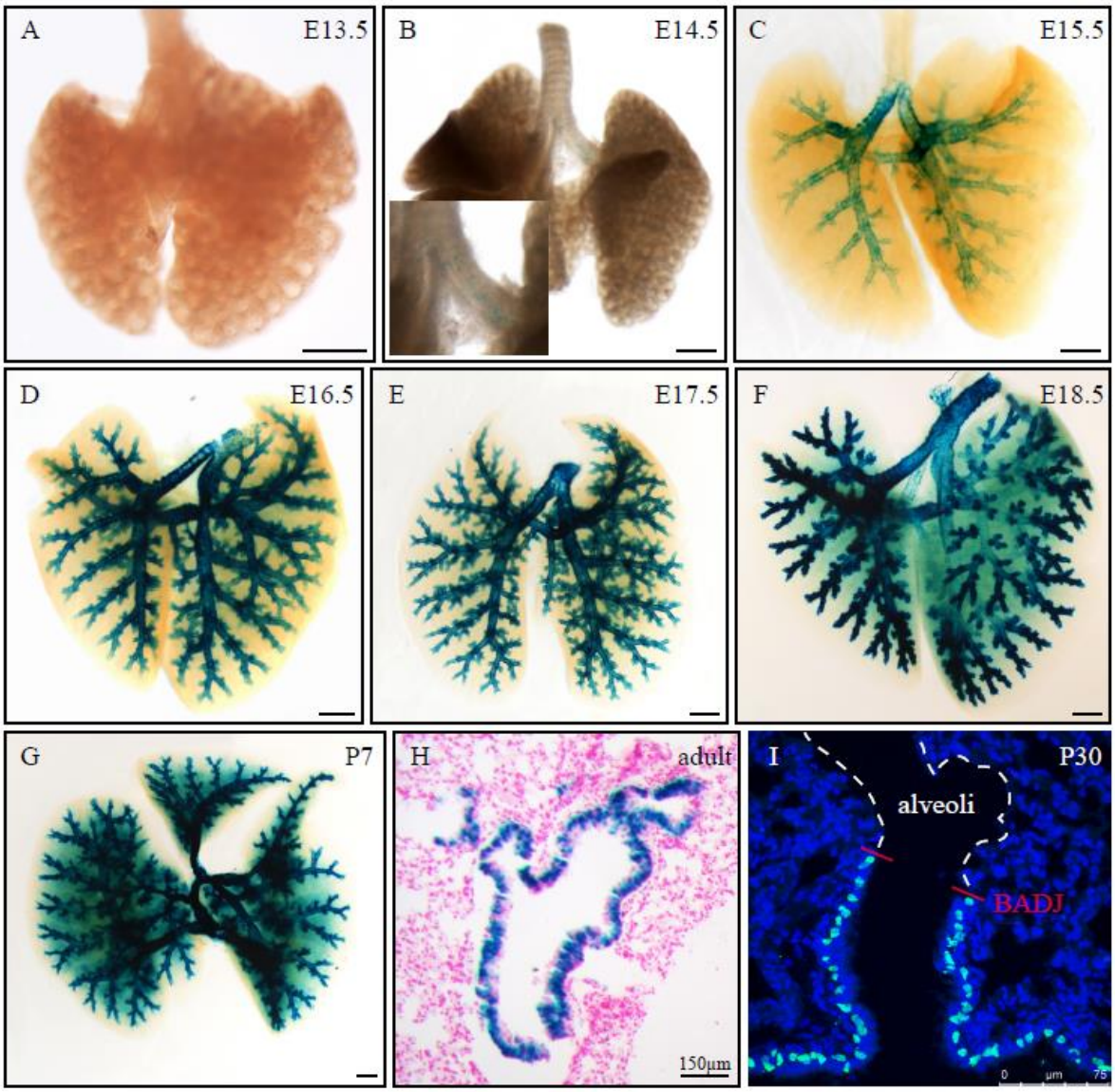

Figure 28 *Fltp* reporter gene expression in the lung is restricted to the airway epithelium

(**A-G**) LacZ staining of whole mount lungs of *Fltp*$^{ZV/+}$ mice.
(**A**) No *lacZ* reporter gene expression is visible in the lung at E13.5.
(**B**) β-gal activity starts in the main bronchi at E14.5.
(**C-G**) Lungs are cleared with BABB. Reporter gene expression is restricted to the lung epithelium.
(**H**) Histological section through an adult lung showing β-gal activity in the lung epithelium.
(**I**) Confocal picture of an *Fltp*$^{ZV/+}$ animal. Fltp positive cells are marked by *Venus* reporter gene expression stained by an anti-GFP antibody. Expression directly stops at the broncho-alveolar-duct junction (BADJ). The alveoli are absent of *Fltp* reporter gene expression.
Scale bars are 500 µm unless indicated anything else.

We confirmed the expression in multiciliated epithelia lung cells by immunohistochemical analyses. *Venus* reporter gene expression is located to multiciliated lung epithelial cells as can be shown by co-staining with an anti-acetylated-tubulin antibody (Figure 29 A-D). Nuclear localized Venus is present in only a few T1α positive basal stem cells, but mainly restricted to the multiciliated cell population (Figure 29 A-D).

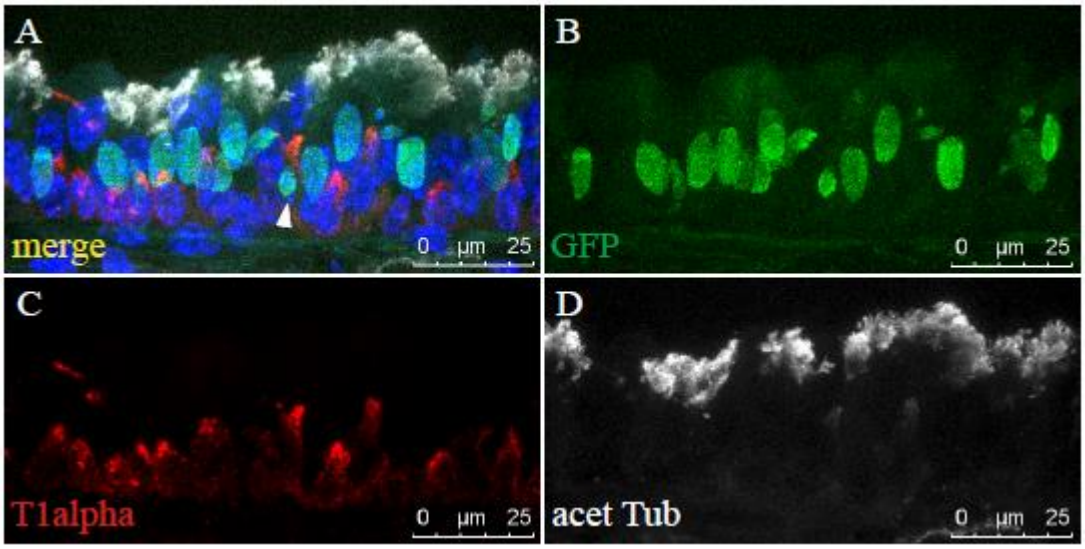

Figure 29 *Fltp* reporter gene expression in the lung is restricted to multiciliated epithelial cells as well as to a subset of basal cells

(**A-D**) Confocal pictures of the lung epithelium of an adult *Fltp*$^{ZV/+}$ animal. *Fltp* reporter gene expressing cells are marked by Venus enhanced by an anti-GFP antibody staining (green). T1α (red) marks basal cells, a precursor cell population in the lung. Anti-acetylated-tubulin antibody staining (white) marks ciliated cells. Note that nearly every Fltp reporter positive cell is ciliated. Very few slightly GFP, T1α double positive cells might be ciliated precursor cells (white arrow head).

Additionally, we performed immunohistochemical analysis on *WT*, *Fltp*$^{ZV/+}$, and *Fltp*$^{ZV/ZV}$ animals with the anti-FltpI antibody. Although this polyclonal rabbit antibody gave high background, it is important to notice that the Fltp protein in the lung is localized to the apical part of multiciliated epithelial lung cells – maybe even to the cilia – as can be shown by co-staining for the *Venus* reporter gene which is expressed in multiciliated cells (Figure 30 G-I). Almost all *Venus* reporter gene positive cells are also Fltp positive. Only few cells do not show FltpI antibody staining. This could be due to higher protein stability of the Venus reporter protein compared to the Flattop protein or different affinities of the antibodies (Figure 30 D-F). In *Fltp*$^{ZV/ZV}$ animals stained by the FltpI antibody we could show that Fltp immunoreactivity is absent confirming the specificity of the antibody (Figure 30 A-C).

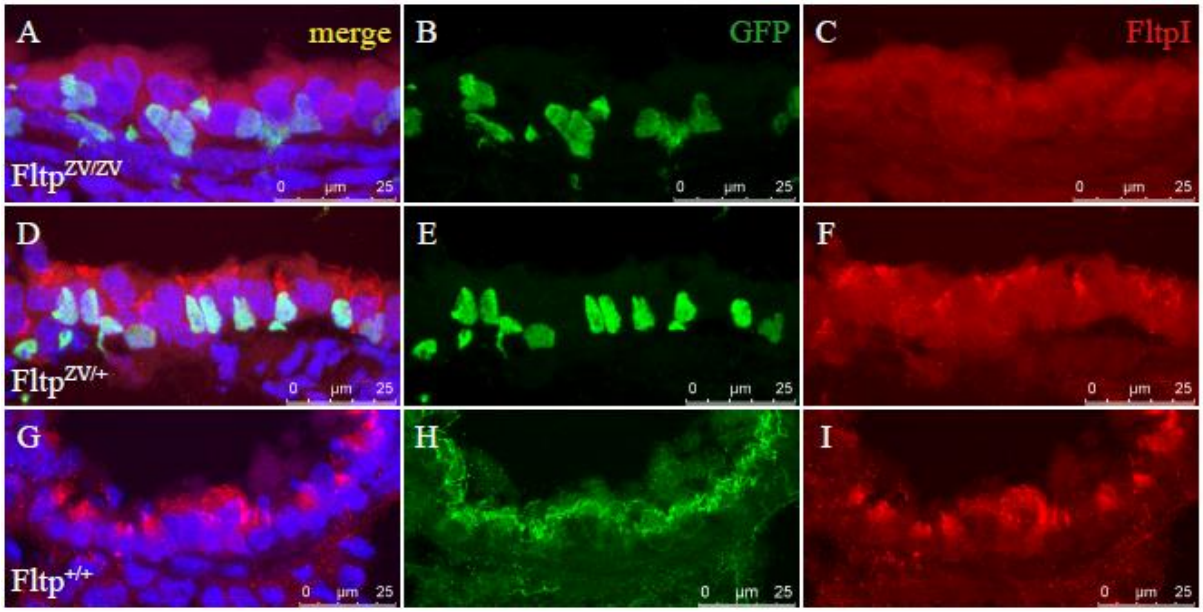

Figure 30 Endogenous Fltp localization in the lung epithelium

(**A-I**) Confocal pictures of lung epithelia of mice with indicated genotypes.
(**A-C**) Endogenous Fltp protein (red) could not be detected in Fltp reporter positive cells (green) of *Fltp*$^{ZV/ZV}$ animals by an anti-Fltp antibody (FltpI).
(**D-F**) In *Fltp*$^{ZV/+}$ animals endogenous Fltp protein expression (red) correlates with *Venus* reporter gene expression marked by anti-GFF antibody staining (green).
(**G-I**) In *WT* animals endogenous Fltp protein is restricted to distinct cells and is located in the cytoplasm.

Taken together, we showed that *Fltp* is expressed in multiciliated cells of the lung epithelium and in a few precursor cells marked by the expression of *T1α*. Its onset correlates with the onset of ciliogenesis in the lung and expression stops at the BADJ. This strongly suggests that Fltp functions in the process of ciliogenesis in multiciliated lung cells.

3.4.1.4 *Flattop* reporter gene expression in stem cell niches of ciliated tissues

3.4.1.4.1 The male reproductive system

The testes are the site of spermatogenesis and during this process fully functional spermatozoa are being generated out of germ cells with the help of Sertoli cells (Phillips et al., 2010). The spermatogonial stem cells (SSC) arise from the primordial germ cells (PGC) at around E7-7.25. The PGCs migrate to the genital ridges and populate them by E12.5. By E13.5 the PGCs give rise to the gonocytes. The SSCs maintain spermatogenesis throughout post pubertal life. The spermatogenic cycle in mice can be divided in twelve stages and the maturation proceeds from the basement membrane to the lumen of the seminiferous tubule until the mature spermatozoa is released. Some important intermediates are the different types of A spermatogonia (A1-A4) that develop over an intermediate stage to B spermatogonia that give rise to primary spermatogonia which then are entering the mitotic cycle and mature over 16 stages to spermatozoa. In *Drosophila* each of the cells has four centrioles that migrate to the cell membrane and build transient small cilia that are disassembled again and function as centrosomes for the next cell division (Rodrigues-Martins et al., 2007).

Venus as well as *lacZ* reporter gene positive cells can be observed in the primary spermatocytes that are characterized by their spatial location in the seminiferous tubule (Figure 31 C, D). The reporter gene is expressed in a spatial restricted pattern and these spermatocytes are appearing as multiples of two. This might indicate that the cells are direct daughters of SSCs. Later in development the spermatocytes loose *Fltp* reporter gene expression.

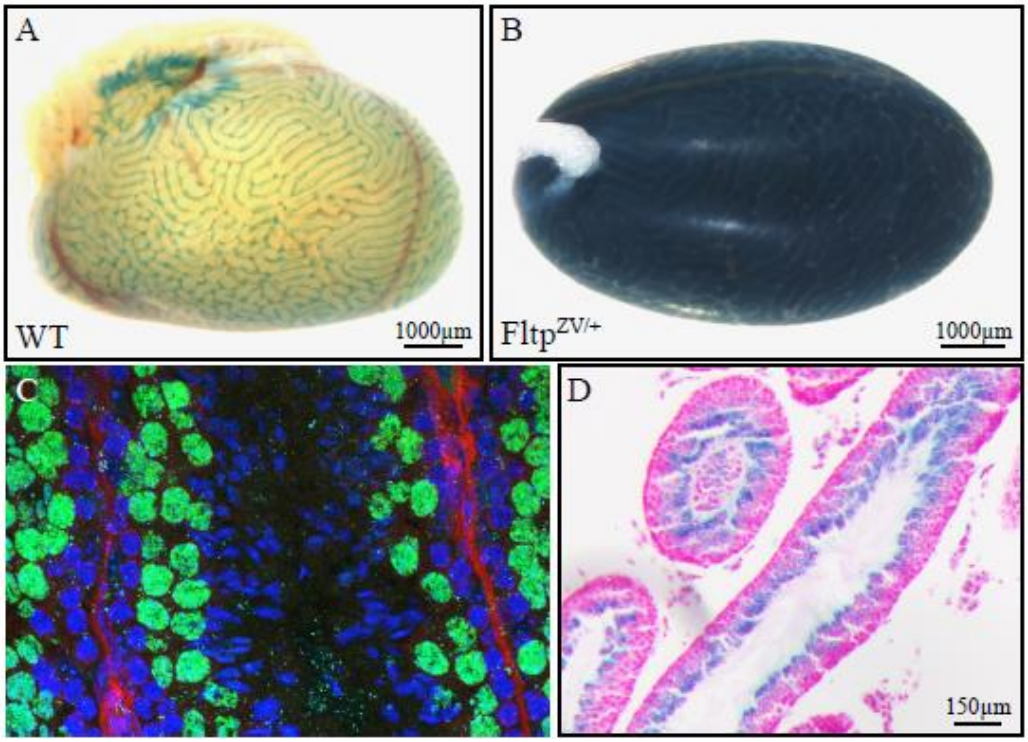

Figure 31 *Fltp* reporter gene expression in the testis

(**A-B**) Whole mount lacZ staining of adult *WT* and *Fltp*$^{ZV/+}$ animals.
(**C**) Confocal picture of the seminiferous tubule. *Venus* reporter gene positive cells can be observed in the primary spermatocytes.
(**D**) Histological section of the seminiferous tubule. β-gal activity is visible in the primary spermatocytes.

3.4.1.4.2 The intestinal crypt compartment

We investigated the intestinal crypt compartment with the method of crypt isolation and cultivation. Immunohistochemical staining for the *Venus* reporter gene revealed expression in cells near the bottom of the crypt compartment where the crypt stem cells reside. Due to their large and granular morphology on sections as well as in movies of live imaging we assume that these cells are Paneth cells. Paneth cells are known to provide the niche for crypt stem cells. It is interesting that the Venus positive cells seem to appear as doublets during mitosis. This might mean that they derive through a symmetric division of a differentiating crypt stem cell, which will have to be tested in further detail. Some of these Paneth cells are clearly lacking E-cadherin expression (Figure 32 A-K). Histological sections of part of the intestine also showed *Venus* reporter gene expression in the crypt stem cell compartment (Figure 32 L-O).

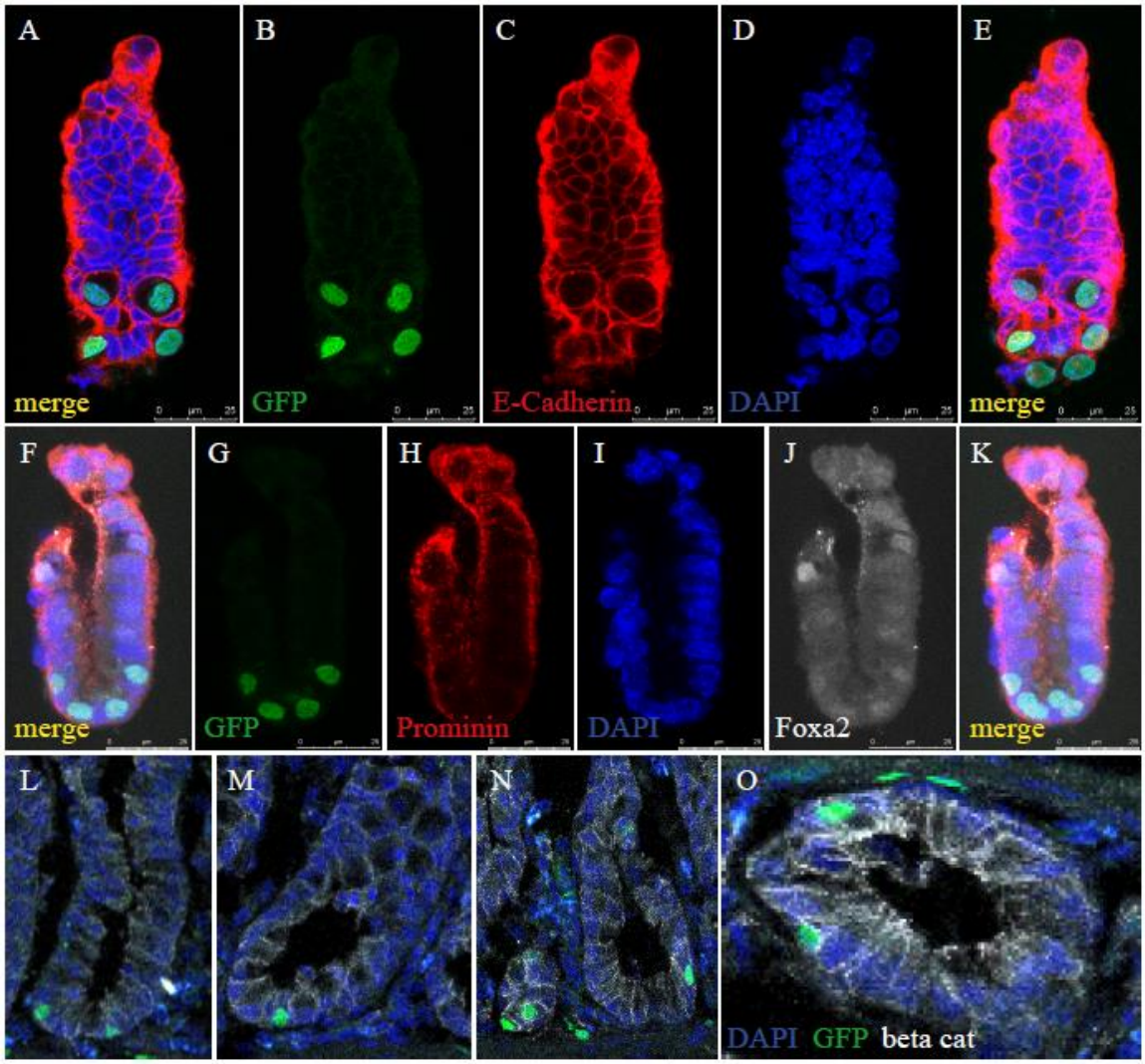

Figure 32 *Fltp* reporter gene expression in isolated intestinal crypts

(**A-K**) Confocal pictures of isolated intestinal crypts of adult *Fltp*$^{ZV/ZV}$ animals.
(**A-E**) *Fltp* reporter gene positive cells are marked by anti-GFP antibody staining (green). Cell membranes are stained by an anti-E-cadherin antibody (red). Fltp positive cells reside in the crypt stem cell compartment. Note that these cells are mostly a multiple of 2. A maximum projection of the isolated crypt can be seen in E.
(**F-K**) Fltp reporter positive cells are marked by GFP. Foxa2 potentially marks stem cells in the crypt region. Some cells are Foxa2 and Fltp double positive. A maximum projection of the isolated crypt can be seen in K. Again, Fltp positive cells mostly appear in multiples of 2.
(**L-O**) Confocal pictures of an *Fltp*$^{ZV/ZV}$ animal. Fltp reporter positive cells (green) are visible in the crypt compartment. Cell membranes are stained by an anti-β-catenin antibody.

3.4.1.4.3 The neurogenic regions of the brain

LacZ reporter gene expression in the brain starts at E10.5 in the developing cp (Figure 25 D). At E13.5 strong β-gal activity can be detected in the cp of the first, second, and third ventricle as shown on the whole mount head picture and the coronal histological sections. Additionally, expression is visible in the ependymal cells, a specialized multiciliated epithelium lining the lateral, third and fourth ventricles (Figure 33 A-C). The beating cilia of the ependymal cells are important for generation of the cerebrospinal fluid flow in the brain.

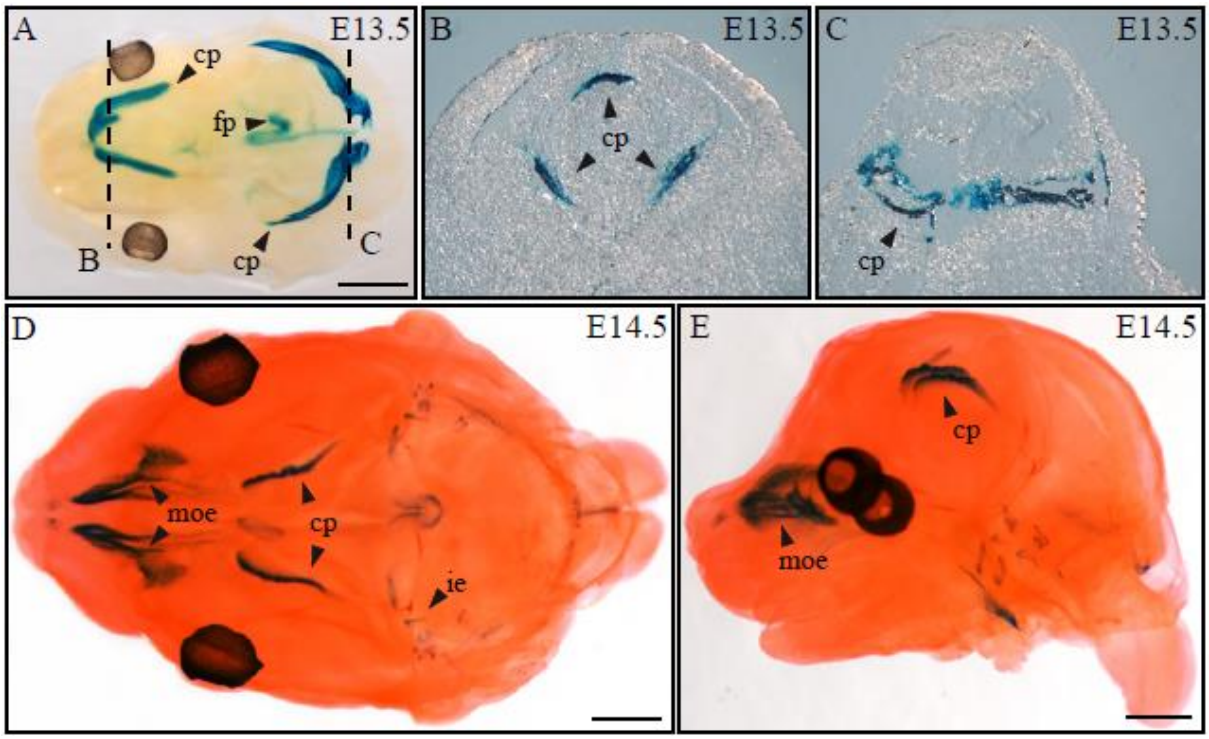

Figure 33 *Fltp* reporter gene expression in the brain

(**A, D, E**) BABB cleared heads of *Fltp*$^{ZV/+}$ animals.
(**A**) LacZ staining of an E13.5 head with the most prominent expression patterns in the choroid plexi (cp) and the floor plate (fp) of the neural tube. B and C indicate the planes of the sections represented in B and C.
(**B, C**) Coronal sections of an E13.5 *Fltp*$^{ZV/+}$ head. The lacZ staining marks the cp of the different ventricles.
(**D, E**) By E14.5 the main olfactory epithelium (moe), the cp, and the IE (ie) are reporter positive.
Scale bars are 1000 µm.

We also performed immunohistochemistry on sagittal sections of the brain to detect cellular *Fltp* reporter gene expression. Venus positive cells could be observed in the cp, the ependymal lining of the ventricles and dentate gyrus (Figure 34 A-D). The sub-ependymal region and the dentate gyrus are regions of adult neurogenesis in the brain. Whether the stem cells in the sub-ependymal region express *Fltp* is not known. In the dentate gyrus we speculate because of the position of the cells that *Fltp Venus* reporter is expressed in transient amplifying cells rather than in the stem cells, which could be confirmed by co-labeling of proliferating cells (Figure 34 C). In addition to these obvious expression domains Venus reporter positive cells were observed interspersed basically throughout the whole brain (most strongly in the midbrain) except the olfactory bulb and the cerebellum.

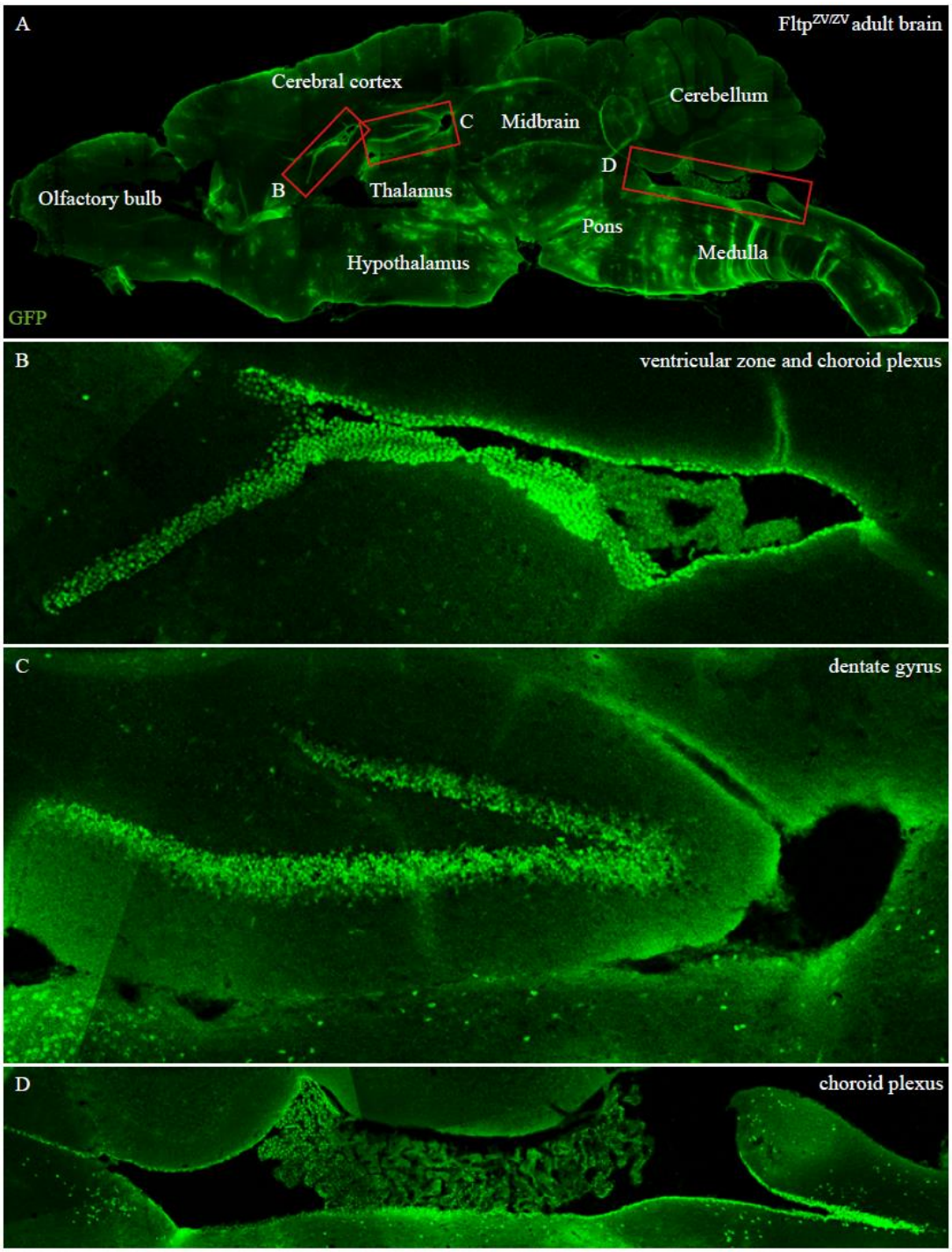

Figure 34 *Fltp* reporter gene is expressed in ciliated as well as neurogenic regions of the brain

(**A-D**) Tile scan confocal pictures of an adult *Fltp*$^{ZV/ZV}$ brain. Most prominent reporter gene expression (green) is visible in the ventricular zone and their choroid plexi as well as in the dentate gyrus. Note that individual cells are spread throughout the rest of the brain.

Taken together, it is obvious that *Fltp* reporter gene expression can be detected in stem cell compartments and is most likely important for the differentiation of stem cells into postmitotic ciliated tissues possibly by symmetric division as indicated by lineage tracing analysis (unpublished data from Dr. Anika Böttcher).

3.4.1.5 Main olfactory epithelium

In the main olfactory epithelium (MOE) multiciliated olfactory sensory neurons (OSN) are located between supporting cells (Mombaerts, 2004). These ciliated cells are derived from multipotent basal progenitor cells in the MOE indicating that Fltp might also play a role during OSN differentiation. In contrast to multiciliated cells in the lung these OSN only project a small number of cilia (six to eight) into the extracellular space. These neurons display a highly defined position of their cilia emerging from the apical surface as can be seen by the circular arrangement of their BBs (Jenkins et al., 2009). β-gal activity in the MOE starts at E14.5 and does not change over lifetime (Figure 35). The reporter expression of Fltp in the MOE is consistent with the results obtained from the screen for mRNA highly enriched in ciliated tissues (McClintock et al., 2008). We did not further analyze the MOE.

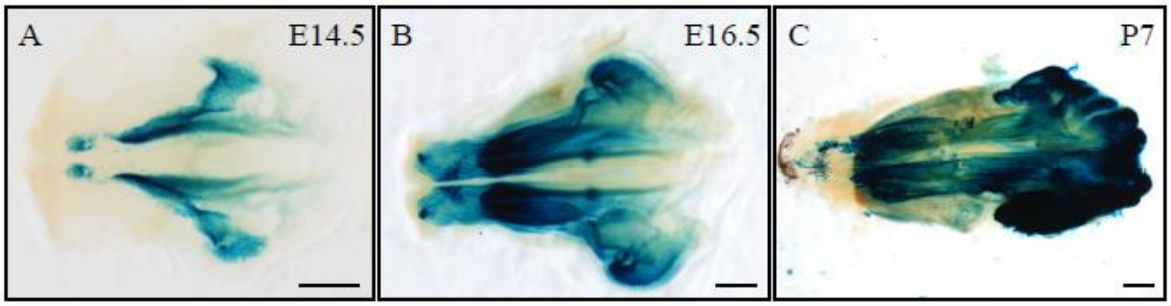

Figure 35 *Fltp* reporter gene is expressed in the main olfactory epithelium

(**A-C**) BABB cleared main olfactory epithelia of $Fltp^{zv/+}$ animals. β-gal activity is visible in the main olfactory epithelium most likely in the ciliated olfactory sensory neurons.
Scale bars are 500 µm.

3.4.1.6 *Flattop* reporter gene expression during limb development

Another interesting observation was made by analyzing the Fltp β-gal reporter activity in the developing limbs. The first lacZ positive cells could be observed at E10.5 in the AER and in the proximal region where the chondrocytes form (Figure 36 A, B). The AER is an important organizer tissue for proper limb development. Defects in these tissues can result in defects in the amount and structure of the limbs. Defects in chondrocyte maturation can later result in skeletal deformations. At E11.5, the AER is still positive and the chondrogenic region is marked by high expression of the reporter gene (Figure 36 C, D).

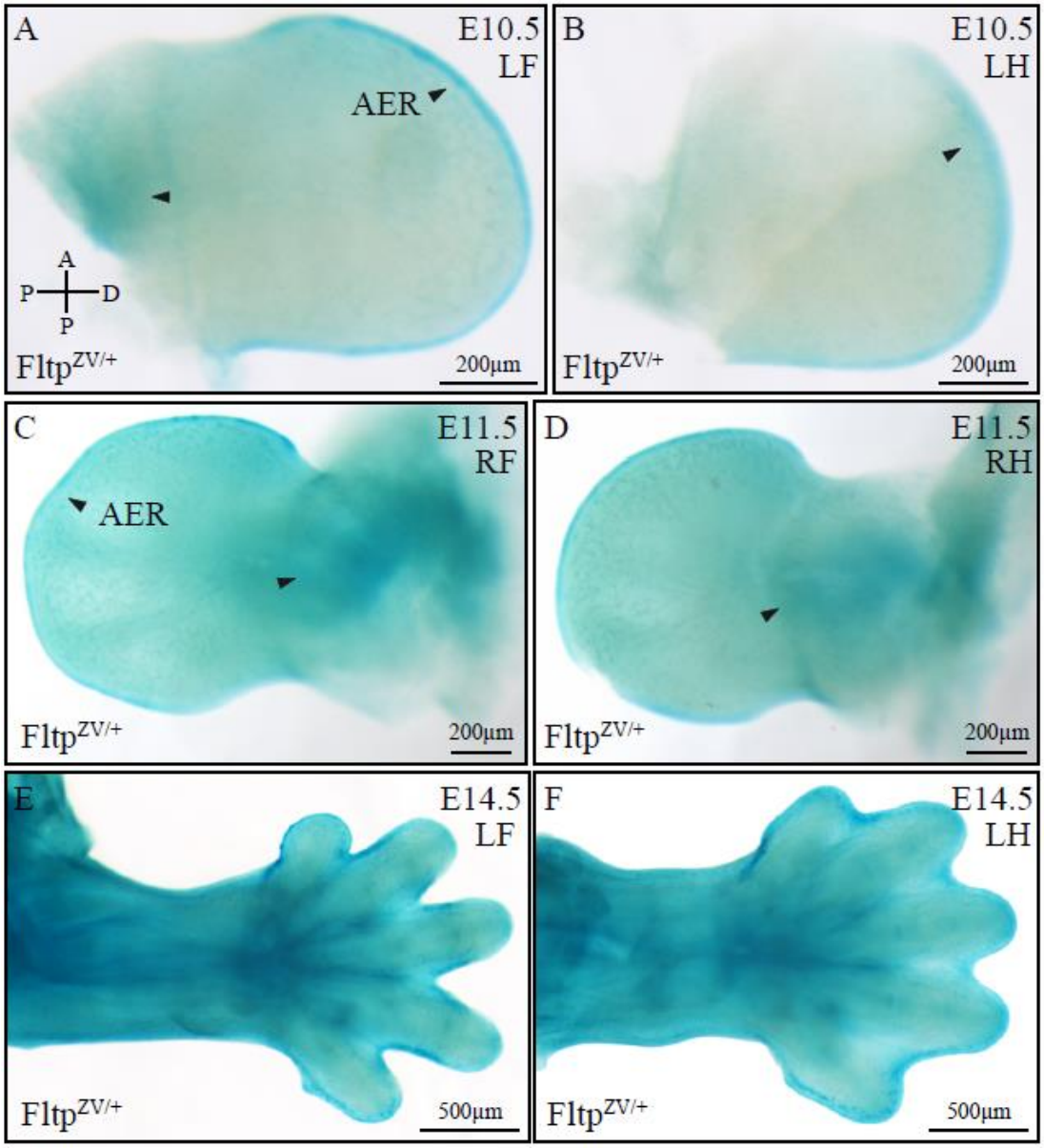

Figure 36 β-gal activity during limb development

(**A-F**) LacZ stained fore- and hindlimbs of *Fltp*$^{ZV/+}$ animals at indicated stages.
(**A, B**) At E10.5 *lacZ* expression is visible in the apical ectodermal ridge (AER) of the developing fore- and hindlimb as well as in the chondrocyte forming region (black arrow head in A).
(**C, D**) The same expression can be seen in E11.5.
(**E, F**) By E14.5 *lacZ* expression is visible in the AER as well as in the chondrocyte forming tissue. From E16.5 expression in the limbs is absent.

These results might suggest that Fltp plays a role during limb patterning.

Taken together, we analyze *Fltp* reporter gene expression during early embryonic development, followed it till birth and ended at adulthood. *Fltp* reporter gene expression was restricted to distinct mono- and multiciliated tissues at every time point of the analysis. *Venus* reporter gene and *lacZ* expression cannot be observed in all ciliated tissues but in those depending on PCP. *Fltp* expression is absent from cells of tubular organs with primary cilia emerging from the center of the luminal side of the cell. Fltp might direct the response of PCP signaling in distinct ciliated tissues towards precise BB

positioning. In *Fltp* negative tissues with active PCP signaling the BBs might not require a distinct position at the apical surface.

3.4.2 *Flattop*$^{ZV/ZV}$ animals show phenotypes in distinct ciliated tissues

In the next section I will focus on the potential function of *Fltp* by analyzing the knock-out phenotype. Candidate regions to look for a phenotype are all regions where *Fltp* is expressed. We first focused on the IE and the lung.

3.4.2.1 *Flattop*$^{ZV/ZV}$ animals show an exencephaly phenotype

In some of our first heterozygous intercrosses after removal of the *neo* selection cassette we could identify three *Fltp*$^{ZV/ZV}$ animals that exhibit an incomplete closure of the brain at E13.5 (Figure 37 A-C). This phenotype was variable between the failure of closing the whole brain like it is the case in Figure 37 A or milder phenotypes where only part of the brain shows incomplete closure as in Figure 37 B and C. *Fltp*$^{ZV/+}$ littermates show normal brain closure. Additionally, it seems that the expression domain of *Fltp* reporter gene is changed, probably secondary due to changes in head morphology (Figure 37 B, cp expression is shifted to the posterior part of the brain). This phenotype showed low penetrance and was not observed in animals outcrossed onto the C57BL/6J and 129S6/SvEvTac genetic backgrounds.

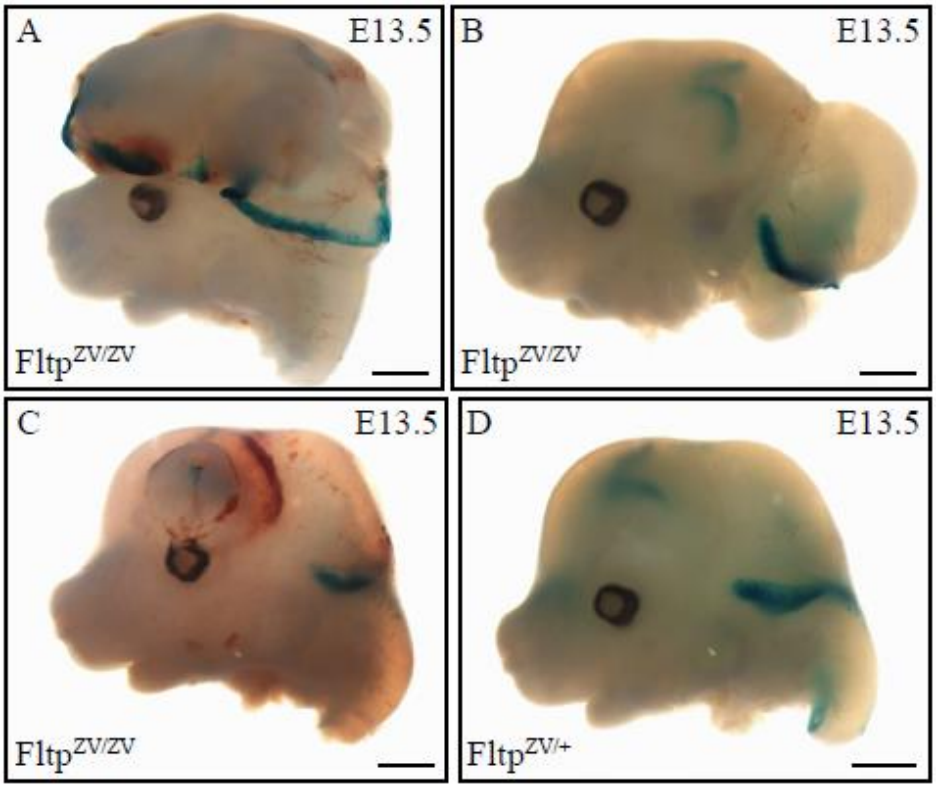

Figure 37 *Fltp*^{ZV} animals show exencephaly phenotypes

(**A-C**) Heads of *Fltp*$^{ZV/ZV}$ animals show exencephaly phenotypes.
(**D**) A *Fltp*$^{ZV/+}$ littermate control shows normal *Fltp* reporter gene expression and head morphology.

Nevertheless, because neural tube closure defects have shown to be associated with PCP defects, we started analyzing the *Fltp*^{ZV} mouse for common PCP phenotypes, such as defects in IE hair cell polarity.

3.4.2.2 Flattop mutants display defects in cochlea hair cell arrangement

Mutants with open neural tube phenotypes often show disrupted PCP. A very well studied organ to address PCP defects is the IE with its highly defined orientation of sensory hair cells in the cochlear duct. Thus we decided to analyze the IE of *Fltp* mice in more detail. Morphological the IE looked normal and the cochlear duct is not significantly shortened or widened suggesting that convergent extension (CE) movements are not affected (data not shown). Widening (additional rows of hair cells) and shortening of the cochlear duct are often associated with PCP mutants like the *Vangl2*^{LP} mouse or the *Fz3/6* double mutants (Montcouquiol et al., 2003; Wang et al., 2006). The semicircular canals are also unaffected. These mice do not show head-shaking behavior suggesting that the vestibular part of the IE is functional. Therefore, the vestibular region was not the primary target of investigation. We performed some simple auditory tests (handclap) on adult *Fltp* mice which suggested that the mice are not deaf.

The following analysis focuses on the cochlea of the IE. Phalloidin staining of a *WT* cochlear epithelium showed the typical arrangement of one inner hair cell (IHC) row and three outer hair cell (OHC) rows with uniformly polarized arrangement of stereociliary bundles in the basal regions of the organ of Corti from E18.5 heterozygous fetuses (Figure 38 A). In contrast, Phalloidin staining in the basal and middle region of heterozygous mutant cochlea revealed that large areas with four OHC rows were present suggestive for a defect in differentiation of prosensory cells or a failure in CE movements (Figure 38 B, C). Additional hints for CE movement defects are the presence of four to seven rows of OHC in the apex of *Fltp*$^{ZV/+}$ animals (data not shown). In the IHC row single cells were often localized out of line (Figure 38 B). Additionally to the extra hair cell row, the hair cells of all rows show misalignment of the stereociliary bundles which points to a loss of polarity in these hair cells (Figure 38 B, C). Because of the presence of the kinocilium a ciliary defect causing for loss of polarity can be excluded (data not shown). We quantified the rotation of the IE hair cells by measuring their angle of rotation in relation to the common tissue polarity of the organ of Corti where the stereociliary bundles are always positioned towards the lateral side (Figure 38 D). A clear difference between *WT*, heterozygous, and homozygous animals could be observed. The OHC rows three and four show the most sever loss of polarity (Figure 38 E). We only analyzed one *Fltp*$^{ZV/ZV}$ mouse that exhibited a clear phenotype. The other *Fltp*$^{ZV/ZV}$ animals showed a relative normal IE morphology in comparison to the *Fltp*$^{ZV/+}$ animals. The mice used for this study were backcrossed for three generations on 129S2/SvPasCrlCD1.

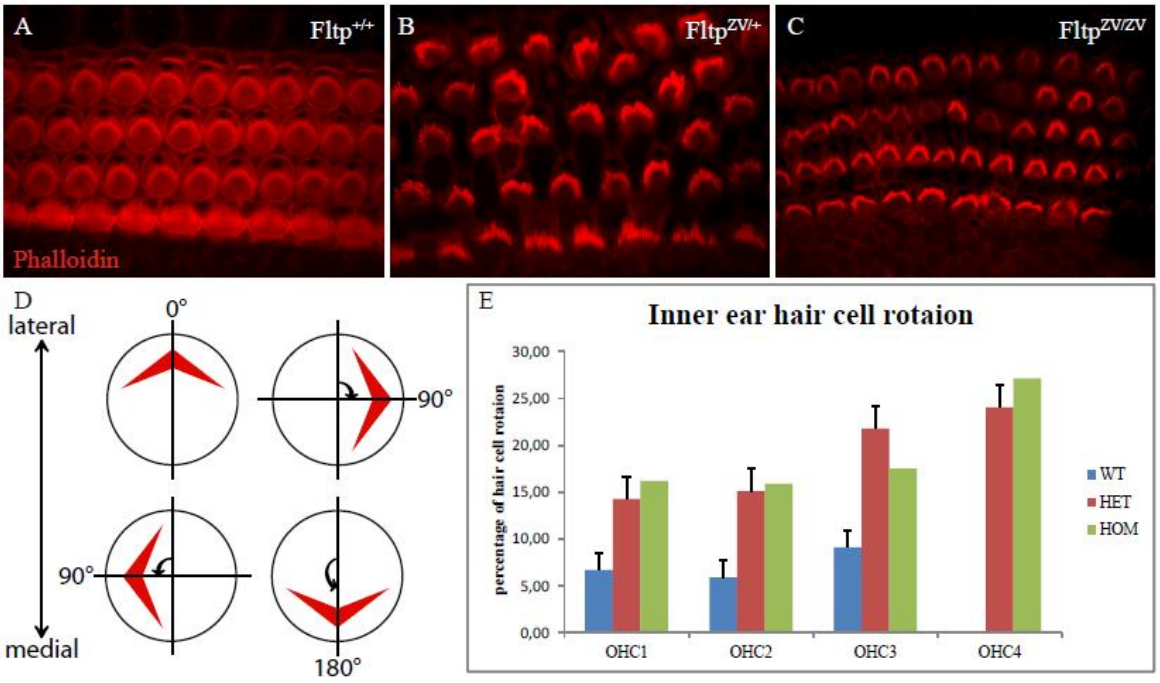

Figure 38 *Fltp*^{ZV} animals show a PCP like inner ear defect

(**A-C**) Phalloidin staining of the cochlea of IEs of indicated genotypes.
(**A**) *WT* animals show the stereotypically aligned IE hair cells.
(**B**) In *Fltp*$^{ZV/+}$ animals the hair cell rows are rotated and large areas with an additional outer hair cell row are present.
(**C**) In *Fltp*$^{ZV/ZV}$ animals the hair cell rows are less rotated than in the *Fltp*$^{ZV/+}$ animals and only very few areas show an additional outer hair cell row.
(**D**) Model how the rotation of the IE hair cells was measured.
(**E**) Chart showing the average rotation of cells of the different hair cell rows (OHC1-OHC4). Note that the WT does only have 3 OHC rows. Analysis of 17 different IEs of *WT* mice (blue bars) revealed an average rotation of 6.72° for OHC row 1 (n=159), 5.91° (n=158) for OHC row 2, and 9.13° (n=155) for OHC row 3. For *Fltp*$^{ZV/+}$ animals (red bars) we analyzed 5 different mice and these revealed an average rotation of 14.28° for OHC row 1 (n=44), 15.09° (n=39) for OHC row 2, 21.78° (n=41) for OHC row 3, and 24.02° (n=17) for OHC row 4. For the *Fltp*$^{ZV/ZV}$ animals (green bars) we analyzed 1 mouse and this revealed an average rotation of 16.18° for OHC row 1 (n=11), 15.89° (n=12) for OHC row 2, 17.50° (n=11) for OHC row 3, and 27.14° (n=3) for OHC row 4.

Nevertheless, this data shows that *Fltp*^{ZV} mutants have disrupted PCP resulting in loss of polarity of the hair cells in the cochlear duct of the IE.
Moreover, we analyzed the localization of proteins involved in PCP in the IE of *WT* and *Fltp*$^{ZV/ZV}$ animals. Scribble (Scrib) antibody staining on *WT* (*Fltp*$^{T2AiCre/+}$) mice showed a horseshoe like localization of the protein at the basolateral side of IE hair cells. As expected for the localization of a PCP protein, the crescent-like localization was always towards the lateral side of the OHC rows one to three of the IE (Figure 39 E-H). Compared to controls the localization of Scrib in *Fltp*$^{ZV/ZV}$ animals showed a more random distribution of the horseshoe arrangement (Figure 39 A-D).

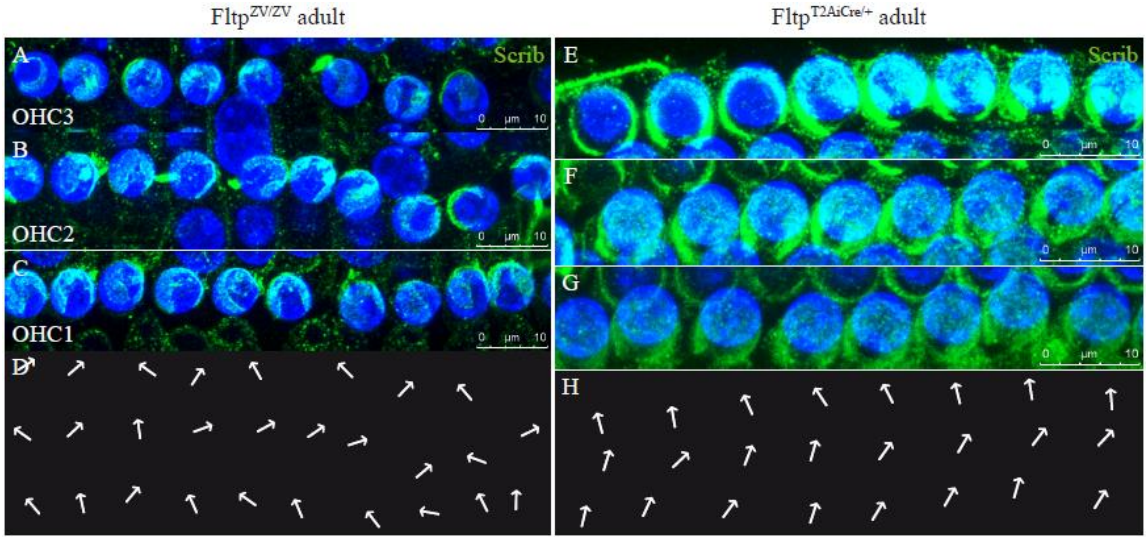

Figure 39 Scrib protein shows altered localization in *Fltp^{ZV}* mutants

(**A-H**) Confocal pictures of IE hair cell rows of genetically modified animals. Genotypes as indicated.
(**A-C**) Outer hair cell (OHC) row 1-3 of an adult *Fltp$^{ZV/ZV}$* animal. Antibody staining for Scribble (Scrib, green) shows a rather misorientated distribution of Scrib localization in comparison to E-G.
(**D**) Scheme indicating the orientation of the Scrib protein in an adult *Fltp$^{ZV/ZV}$* animal.
(**E-G**) Outer hair cell (OHC) row 1-3 of an adult *Fltp$^{T2AiCre/+}$* animal. This situation is considered as WT situation. Scrib staining shows a rather orientated distribution towards the lateral side of hair cells.
(**H**) Scheme indicating the orientation of the Scrib protein in an adult *Fltp$^{T2AiCre/+}$* animal.

3.4.2.3 *Flattop^{ZV}* animals show constricted distal airways

While the canonical Wnt pathway has been shown to influence murine lung development (Okubo and Hogan, 2004) the role of the non-canonical Wnt pathway in the lung is still elusive. Recent observation of lungs of two mutants with mutations in core PCP genes showed impaired lung branching morphogenesis (Yates et al., 2010). Therefore, we started to investigate whether Fltp mutant lungs also show a phenotype characteristic to the reported PCP phenotypes in the lung. The gross morphology of *Fltp$^{ZV/ZV}$* animals showed no obvious differences to *Fltp$^{+/+}$* animals. All lungs show the characteristically five lung lobes: the apical lobe, the cardiac lobe, the azygous lobe, the diaphragmatic lobe, and the left lobe. I analyzed the β-gal stained left lung lobe and compared the branching of *WT*, *Fltp$^{ZV/+}$*, and *Fltp$^{ZV/ZV}$* animals. As a *WT* control we made use of the *Fltp$^{T2AiCre/+}$* mouse line crossed into the *ROSA26* reporter line. Counting of the main bronchi revealed that neither *Fltp$^{ZV/+}$* nor *Fltp$^{ZV/ZV}$* animals showed altered number of main bronchi compared to the control (Figure 40 A-C). We could observe that the distal airways showed altered morphology due to β-gal staining. The first difference we noticed was that the most distal airways of *Fltp$^{ZV/+}$* as well as *Fltp$^{ZV/ZV}$* animals showed constriction compared to control animals. It was most evident in the distal airways of the main fifth and sixth bronchus (Figure 40 B-F). Additionally, the epithelial morphology in these airways looked somehow rough and not as smooth as in the control and the heterozygous *Fltp$^{ZV/+}$* animals (Figure 40 E, F). Measurements of the most distal β-gal positive parts of these airways revealed a clear difference in airway diameter of *WT*, *Fltp$^{ZV/+}$*, and *Fltp$^{ZV/ZV}$* animals (Figure 40 G). For this analysis the diameter of all terminal airways of the left lung lobe were counted. Control (*Fltp$^{T2AiCre/+}$*; *R26$^{R/+}$*) animals showed an average distal airway diameter of 132.25 µm (n=4), *Fltp$^{ZV/+}$* animals showed an

average distal airway diameter of 99.68 µm (n=7), and *Fltp*$^{ZV/ZV}$ animals showed an average distal airway diameter of 90.06 µm (n=6; Figure 40 G first three bars). Because it appeared that the most constricted airways are the distal airways of bronchus five and six, their diameter without accounting for the rest of the airways was measured. Control (*Fltp*$^{T2AiCre/+}$; *R26*$^{R/+}$) animals showed an average distal airway diameter of airway five and six of 130.02 µm (n=4), *Fltp*$^{ZV/+}$ animals showed an average distal airway diameter of airway five and six of 102.66 µm (n=7), and *Fltp*$^{ZV/ZV}$ animals showed an average distal airway diameter of airway five and six of 84.48 µm (n=6; Figure 40 G second three bars). For this analysis we used *Fltp*^{ZV} mice backcrossed to 129S2/SvPasCrlCD1 mice for four generations.

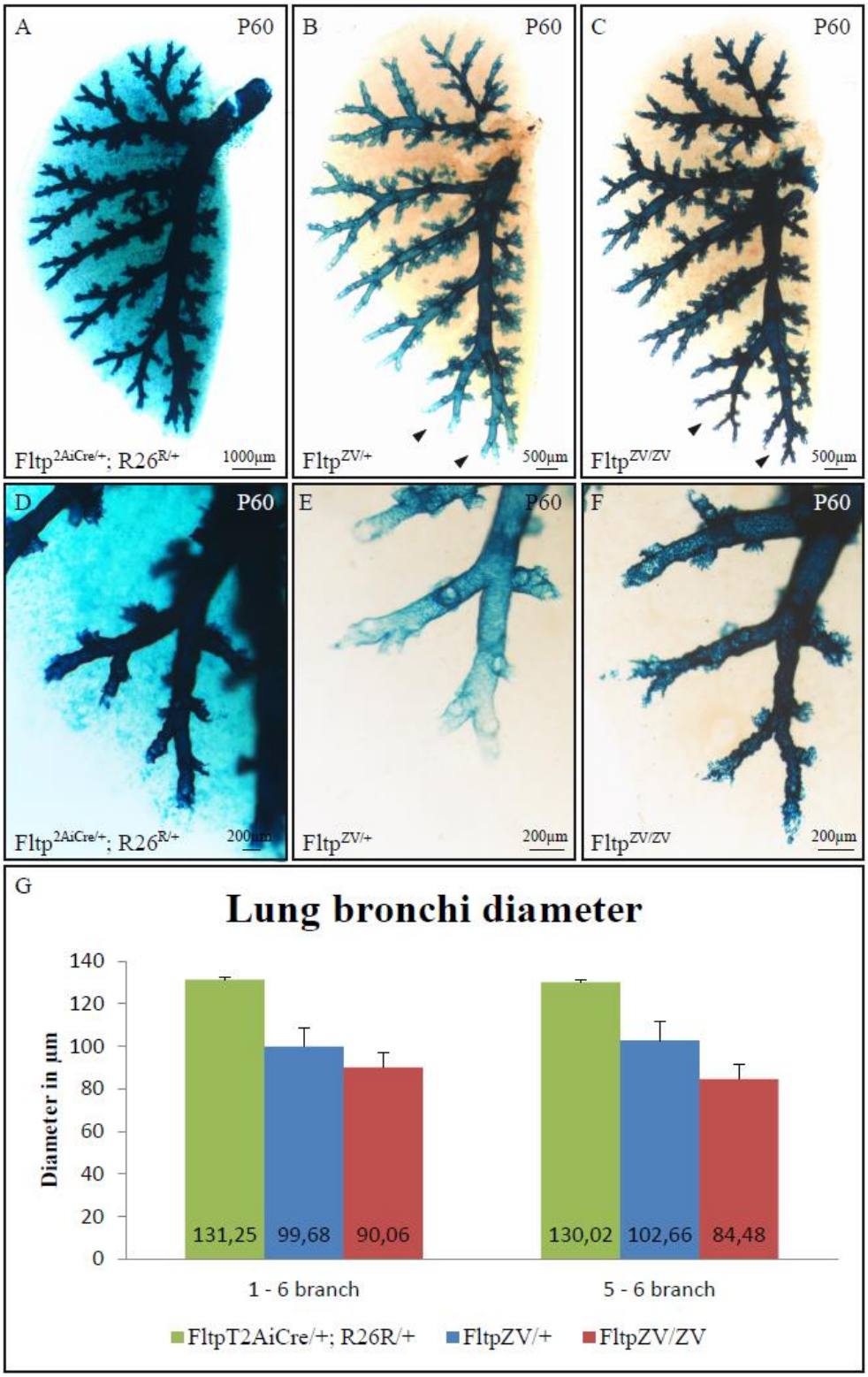

Figure 40 *Fltp*^{ZV} animals show constricted distal airways in the lung

(**A-F**) BABB cleared left lung lobes at P60 of mice with different genotypes. *Fltp*^{ZV} animals are in G4 on 129S2 background.

(**A**) The lung of *Fltp*$^{T2AiCre/+}$; *R26*$^{R/+}$ shows normal distal airways.

(**B**) The lung of *Fltp*$^{ZV/+}$ animals shows more constricted distal airways (black arrow heads).

(**C**) Severest constriction was visible in *Fltp*$^{ZV/ZV}$ animals (black arrow heads).

(**D**) Enlargement of distal airways of A.

(**E**) Enlargement of distal airways of B.

(**F**) Enlargement of distal airways of C. Note that the epithelial structure is curled.
(**G**) Measurement of lung airway diameter of all 3 genotypes introduced above. The first 3 bars show the average diameter of all most distal airways, the second 3 bars just include the most distal airways of the last 2 larger bronchi.

Taken together, the phenotype observed in the ciliated lung epithelium of *Fltp*^{ZV} mutants partially mirrors the lung airway constriction phenotype observed in the core PCP mutants *Vangl2*$^{Lp/Lp}$ and *Celsr1*$^{Crsh/Crsh}$ (Yates et al., 2010). Combined with the PCP phenotype in the IE and the neural tube defects, it is very likely that Fltp is a novel component of the PCP pathway.

3.4.2.4 *Flattop*$^{ZV/ZV}$ animals show loss of cilia in multiciliated airway epithelium

To further investigate the cell-type specific defects in the lung, we performed immunohistochemical analysis of multiciliated epithelial lung cells. Immunohistochemical analysis of the trachea revealed no obvious changes in cell composition and morphology (data not shown). Ciliated cells were present in *WT*, *Fltp*$^{ZV/+}$, and *Fltp*$^{ZV/ZV}$ animals (data not shown). The same was true for the other larger airways. Because the constricted airway phenotype was restricted to the most distal airways of *Fltp*^{ZV} mutant mice we started to analyze only airways with diameters smaller than 100 x 100 µm. The airway epithelium of adult *WT* mice showed a typical pseudostratified columnar morphology with normal multiciliated cells (Figure 41 A, D). On the contrary, cilia were difficult to detect in *Fltp*$^{ZV/ZV}$ mice. Interestingly, we could identify poorly differentiated ciliated cells with strikingly fewer ciliary projections in *Fltp*$^{ZV/+}$ and *Fltp*$^{ZV/ZV}$ littermates (Figure 41 B, C, E, F). Additionally, we noticed that some BBs were not correctly positioned and docked at the apical surface of the ciliated cells, but rather remained in the cytoplasm between the nucleus and the apical membrane (Figure 41 C, F). We analyzed lungs of mice at P7 and P30. The ciliated cells of *Fltp*$^{ZV/ZV}$ mice at P7 showed strikingly shorter cilia in comparison to *WT* and *Fltp*$^{ZV/+}$ mice as can be seen in Figure 41 G. Additionally, we found a lot of poorly differentiated ciliated cells with no cilia on their apical surface in *Fltp*$^{ZV/ZV}$ mice (Figure 41 C). Even the *Fltp*$^{ZV/+}$ animals showed shorter cilia compared to controls (Figure 41 A, B, G). Here we only found few non ciliated cells compared to homozygous animals. Similar results were obtained at P30, where we saw cells with significantly shorter cilia in *Fltp*$^{ZV/+}$ and *Fltp*$^{ZV/ZV}$ animals compared to *WT* (Figure 41 D, E, F, H). In contrast to P7 we found less non ciliated cells in homozygous animals at P30.

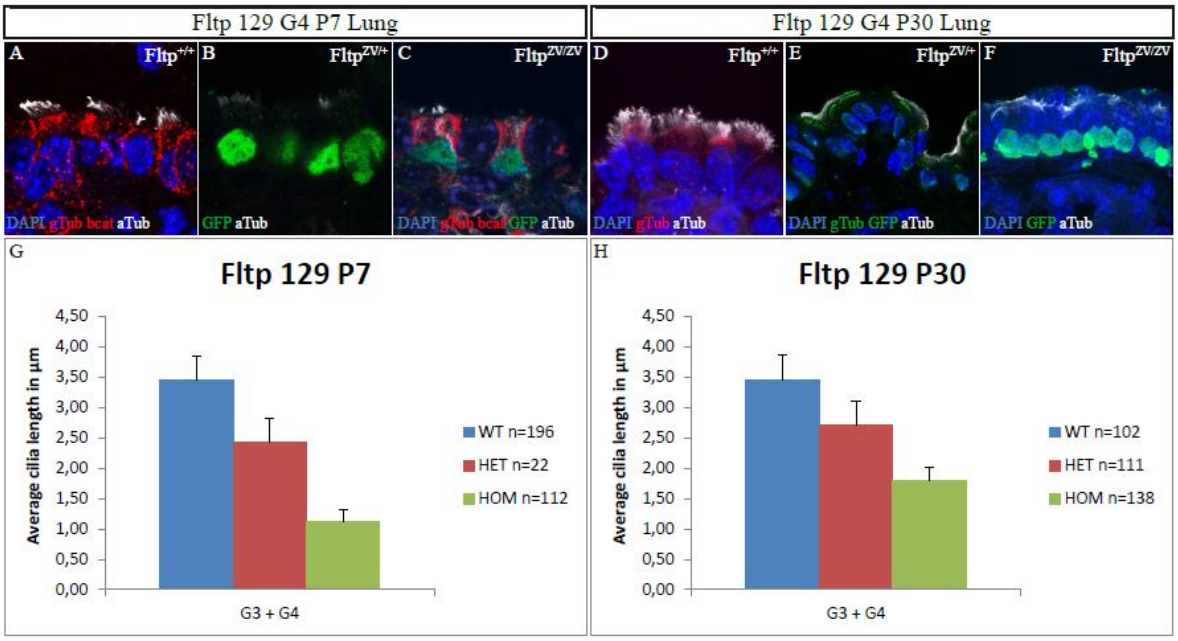

Figure 41 *Fltp*^{ZV} animals show defective ciliogenesis in epithelial lung cells

(**A-F**) Confocal images of lung distal airway epithelium of *Fltp* mice. Age and genotype as indicated. *Fltp* reporter gene expressing cells are shown in green.
(**A**) In *WT* animals at P7 the basal bodies (BBs), stained by γ-tubulin (red) project cilia (white) at the apical surface. β-catenin marks the cell membrane (red).
(**B**) In *Fltp*$^{ZV/+}$ P7 animals significantly less cilia (white) are detectable.
(**C**) At P7 *Fltp*$^{ZV/ZV}$ animals show often absence of all cilia at the apical surface. In some cells shorter cilia (white) are present. Note that only very few BBs (red) are docked at the apical surface. β-catenin marks the cell membrane (red).
(**D**) *WT* cells at P30 show BBs (red) docked at the apical surface and projecting cilia (white) into the lumen.
(**E**) *Fltp*$^{ZV/+}$ P30 animals show docked BBs (red) at the apical surface but shorter cilia (white).
(**F**) At P30 *Fltp*$^{ZV/ZV}$ animals show cells without cilia and cells with short cilia (white).
(**G, H**) Average cilia length of genotypes indicated at P7 and P30. Animals on 129S2 background in G3 +G4 were analyzed. Significant changes in cilia length can be observed between the genotypes. In total we examined 196 cells of 14 *WT* mice, 22 cells of 2 *Fltp*$^{ZV/+}$, and 112 cells of 7 *Fltp*$^{ZV/ZV}$ P7 animals. For P30 we examined 102 cells of 8 *WT* mice, 111 cells of 9 *Fltp*$^{ZV/+}$, and 138 cells of 11 *Fltp*$^{ZV/ZV}$ animals. The standard deviation was calculated by collecting the mean cilia length values of each mouse for each genotype.

Our findings indicate that Fltp is required for proper differentiation of multiciliated airway epithelial cells most likely through involvement in the apical transport and docking process of BBs to the plasma membrane, which is important for cilia formation.

3.4.2.5 Establishment of *in vitro* cultures of mouse tracheal epithelial cells

BB transport and docking are dynamic processes and can hardly be studied *in vivo*. Therefore, we made use of the mouse tracheal epithelial cell (MTEC) *in vitro* culture system (Vladar and Stearns, 2007). To differentiate ciliated epithelial cells from progenitor cells, this culture is switched to air-liquid interface (ALI) culture where the cells are supplied by medium from the basal side and the apical side is exposed to air. This culture method can be divided into three main steps: First, before

switch to ALI conditions, the cells are present in a monolayer and no ciliated cells can be observed. Second, after switch to ALI conditions, the cells start to amplify their centrosomes but cilia are not yet build. In the third phase, ciliogenesis starts and after 14 days of ALI culture 40-60% of the cells are ciliated. The development of ciliated cells in this culture closely mirrors the timing of ciliogenesis during airway development and regeneration (Rawlins et al., 2007). The process of centriole formation in these cultures can be separated into four stages. In the beginning, directly after the switch to ALI, the cells contain two separate centrosomes where one projects a primary cilium at the apical surface. At stage one, centrosomal proteins accumulate around the centrosomes and the primary cilium is elongated compared to the cells directly after ALI creation. At this stage, two days after ALI creation, the amplification of the centrosomes starts. During the second stage, the transport of the centrosomes starts resulting in their distribution to one random side of the cell. Primary cilia are no longer present. At stage three, the centrosomes move out of the cluster and are starting to be distributed at the apical surface of the cell. In stage four, shortly after the centrosomes docked at the apical surface but before the centrosomes are distributed equally at the membrane, ciliogenesis starts. In fully differentiated cells the BBs are equally distributed at the apical membrane and each BB projects a cilium (Vladar and Stearns, 2007).
Fltp reporter gene expression in cultured cells correlates with onset of ciliogenesis, BB amplification, transport, and docking and is already visible at day one after the switch to ALI. Due to the restriction of *Fltp* reporter gene expression to ciliated cells we could easily investigate BB docking in ciliated cells and Fltp deficient cells only.

3.4.2.5.1 Cultured mouse tracheal epithelial cells show basal body docking defects and therefore delay in ciliogenesis

To investigate BB docking in the MTEC cultures we performed a time series from day one till day seven after the switch to ALI differentiation conditions. Therefore, we dissected the tracheas of *WT*, $Fltp^{ZV/+}$, and $Fltp^{ZV/ZV}$ littermates backcrossed on C57BL/6NCrl in generation eight and harvested the tracheal cells. Analysis of BB position of cells of a day three ALI culture revealed that in *WT* animals the BB are docked at the apical surface as shown by a co-staining with the apical membrane marker ZO-1 (Figure 42 A, B). Cultured epithelial cells of $Fltp^{ZV/+}$ animals at day three after switch to ALI show that most BBs are located in the cytoplasm between - and around - the nucleus and the apical surface as indicated by the tight junction marker ZO-1 and the nuclear marker DAPI, respectively (Figure 42 C, D). The same BB docking phenotype can be observed in $Fltp^{ZV/ZV}$ littermates at the same time point (Figure 42 C, D). Additionally, the ZO-1 staining in these cultured cells was not present as one single ring around the cell on the apical surface, but was doubled and expanded more to the basal side of the cell (data not shown).

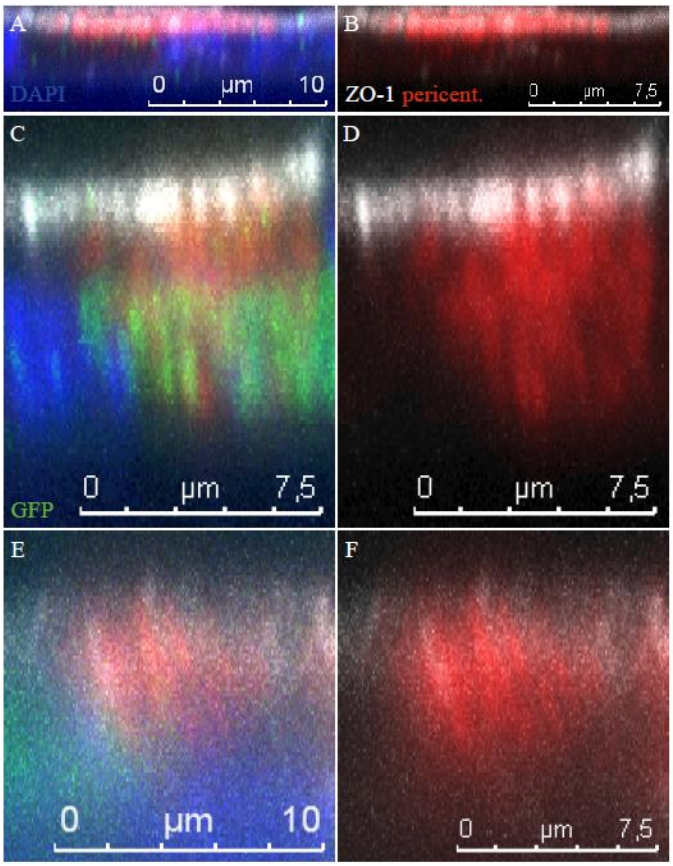

Figure 42 Isolated MTECs of *Fltp*^{ZV} animals show defective basal body docking in ALI cultures

(**A-F**) Rotated confocal pictures of murine tracheal epithelial cell (MTEC) culture of adult mice at day 3 after the switch to ALI culture. *Fltp* reporter gene expressing cells are shown in green.
(**A, B**) *WT* cells show all basal bodies (red, anti-pericentrin antibody) docked at the apical surface (white, anti-ZO-1 antibody).
(**C, D**) Cells of *Fltp*$^{ZV/+}$ animals show a majority of basal bodies (red) in the cytoplasm and not at the apical surface (white).
(**E, F**) *Fltp*$^{ZV/ZV}$ animals show basal bodies in the cytoplasm. The ZO-1 staining (white) to mark the apical tight junctions is not present as a thin line but in a broader stripe.

Failure of BB docking should result in less or even no cilia projected at the apical surface. To analyze this we used an anti-acetylated-tubulin antibody to stain for the presence of cilia in combination with an anti-pericentrin antibody to stain for the presence of BBs. Again we analyzed cells switched to ALI for three days of *Fltp*^{ZV} littermates on C57BL/6NCrl background in generation eight. As expected control cells showed perfectly docked BBs with each single one projecting a cilium into the lumen (Figure 43 A, B). ALI cultures of *Fltp*$^{ZV/+}$ animals showed that the majority of BBs were not yet docked at the apical surface and therefore did not project a cilium into the lumen. GFP antibody staining shows *Fltp Venus* reporter gene expressing cells (Figure 43 C, D). We could also detect *Fltp* reporter expressing cells with some docked BBs and cilia. In the ALI culture of *Fltp*$^{ZV/ZV}$ animals the majority of cells displayed BBs that are stuck in the cytoplasm and therefore are non-ciliated (Figure 43 E, F).

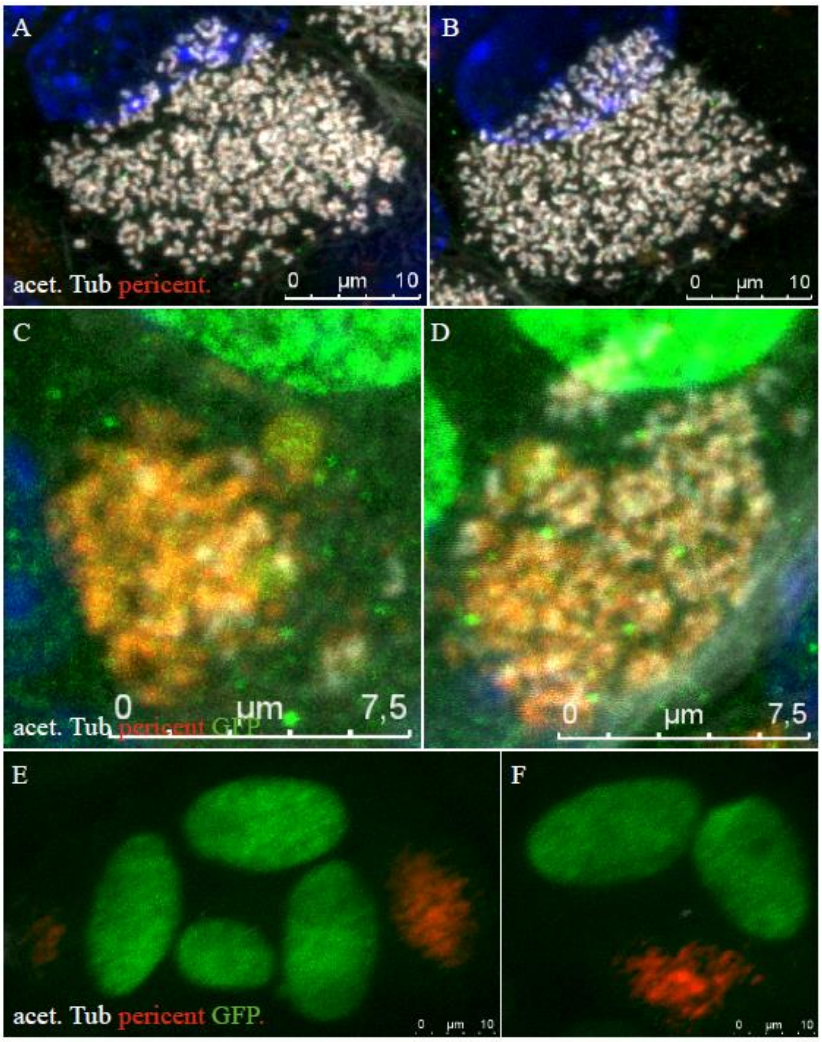

Figure 43 Isolated MTECs of *Fltp*^{ZV} animals show delayed ciliogenesis in three day ALI cultures

(**A-F**) Confocal pictures of MTEC culture of adult mice at day 3 after the switch to ALI culture. *Fltp* reporter gene expressing cells are shown in green.
(**A, B**) *WT* cells show a cilium (white, anti-acetylated tubulin antibody) projecting from each BB (red, anti-pericentrin antibody).
(**C, D**) *Fltp*$^{ZV/+}$ animals show only few docked basal bodies (red) that project a cilium (white). Most basal bodies are still in the cytoplasm.
(**E, F**) in *Fltp*$^{ZV/ZV}$ animals most cells do not have cilia. All their basal bodies (red) are in the cytoplasm.

These observations indicate that Fltp deficient cells are stuck between stage one and two of centriole assembly whereas control cells are already at stage four.
The fact that in nearly all control cells every single BB projected a cilium and BB docking decreased progressively from *Fltp*$^{ZV/+}$ to *Fltp*$^{ZV/ZV}$ cells convincingly confirms the phenotype observed *in vivo*.
To answer the question if these cells are completely unable to generate a fully differentiated multiciliated cell we analyzed the cultures at day seven after ALI creation. Again we found the majority of control cells fully ciliated with all BBs docked (Figure 44 A, B). For ALI cultures from *Fltp*$^{ZV/+}$ trachea we found cells where nearly all BBs had cilia and some that did not dock their BBs yet (Figure 44 C, D). These cells might be cells that started differentiation not at day one of ALI culture but on later days. ALI cultures of *Fltp*$^{ZV/ZV}$ animals showed clearly cells that were not able to dock all their BBs (Figure 44 E, F). Nevertheless, we found cells that were able to dock most BBs.

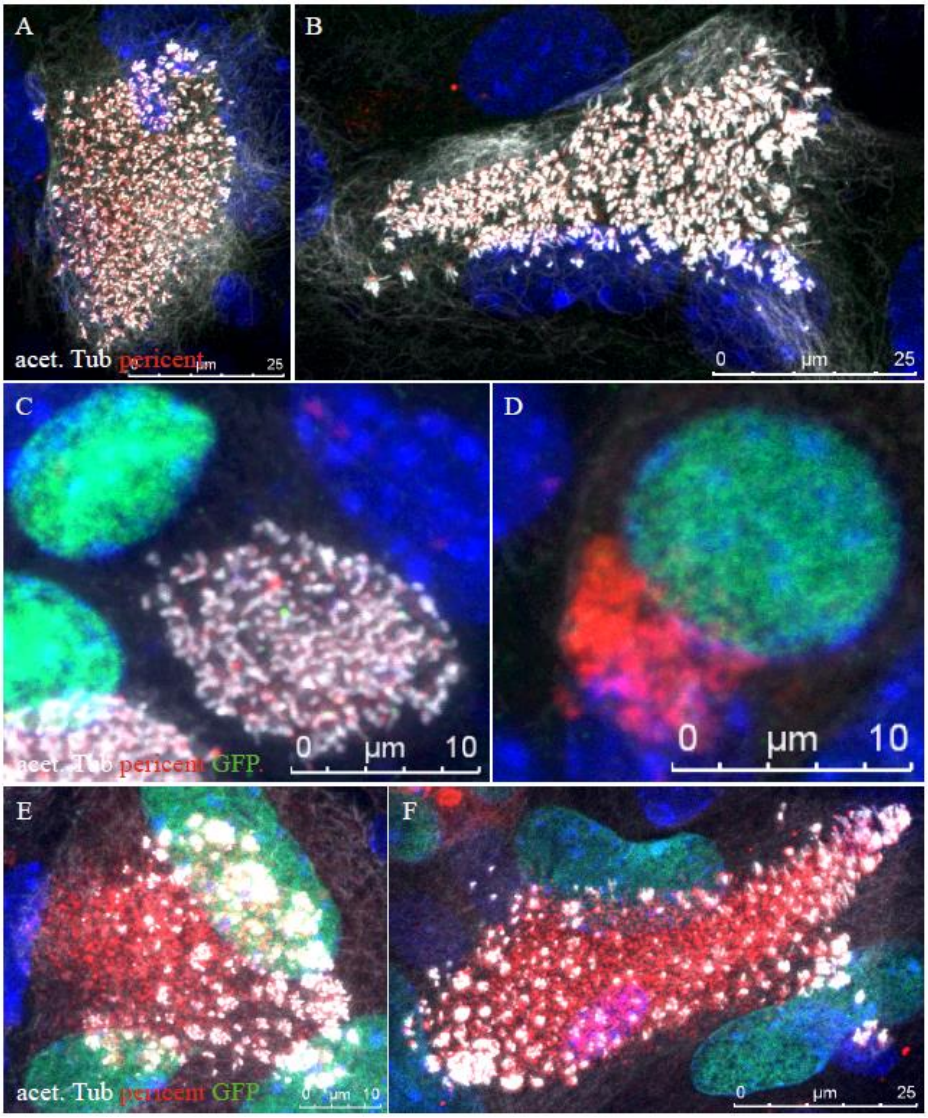

Figure 44 Isolated MTECs of *Fltp*^{ZV} animals show delayed ciliogenesis in seven day ALI cultures

(**A-F**) Confocal pictures of murine tracheal epithelial cell (MTEC) culture of adult mice at day 7 after the switch to air liquid interface (ALI) culture. *Fltp* reporter gene expressing cells are shown in green.
(**A, B**) *WT* cells show a cilium (white, anti-acetylated tubulin antibody) projecting from each BB (red, anti-pericentrin antibody).
(**C, D**) *Fltp*$^{ZV/+}$ animals sometimes show cells with docked basal bodies (red) that project a cilium (white) and some that have their basal bodies in the cytoplasm.
(**E, F**) In *Fltp*$^{ZV/ZV}$ animals most cells do not show cilia for all basal bodies suggesting that only some basal bodies are not docked.

In summary, we could show by immunohistochemistry on ALI cultures of MTECs that *Fltp*$^{ZV/+}$ and *Fltp*$^{ZV/ZV}$ cells are delayed in their apical BB transport. Directional BB transport is not completely abolished as shown by *Fltp*$^{ZV/ZV}$ cells that were able to build cilia.
Another remarkably observation could be made regarding the localization of Fltp reporter positive cells to each other. In all cultures it was very obvious that these cells always appear as duplets or as a multiple of two (Figure 43; Figure 44). Similar observations could be made for Fltp reporter positive cells in cryosections of lung airways, the testis, in the crypt stem cell compartment of the intestine, as

well as in the neurogenic regions of the brain (Figure 29; Figure 30; Figure 31; Figure 32; Figure 33). Some cells in these tissues seem to be in the process of nuclear rearrangement that is happening often after cell division. This observation suggests that *Fltp* is expressed directly after cell division in daughter cells of symmetric division of progenitor cells which will be further tested in detail.

3.4.2.6 *Flattop* genetically interacts with the core PCP gene *Celsr1*

Fltp$^{ZV/ZV}$ mice show an IE, lung, BB docking, and an open neural tube phenotype reminiscent of mice deficient for PCP molecules. The IE and open neural tube phenotype show signs of defective CE movements during neural tube closure (see 3.4.2.1; Figure 37). To directly test if Fltp is involved in PCP we investigated a possible genetic interaction of *Fltp* and the core PCP component *Celsr1* (Curtin et al., 2003). *Celsr1* encodes for a protocadherin and is one of the three mammalian homologs of *Drosophila flamingo/starry night*. *Fltp* and *Celsr1* expression overlap in the six sensory patches of the IE, the vestibular epithelium of the IE, the developing lung, the AER in the limb buds, the ventricular zone, and the whole olfactory epithelium in the vomeronasal organ (for the detailed expression pattern of *Fltp* and *Celsr1* see 3.4.1 and 2.8.6, respectively). These tissues are all possible regions for a genetic interaction. A genetic interaction is proven when the severity of the phenotype of single gene mutations increases synergistically in double mutants. For this reason we crossed *Fltp*$^{ZV/+}$ and *Celsr1*$^{crsh/+}$ animals and collected the double heterozygous *Fltp*$^{ZV/+}$; *Celsr1*$^{crsh/+}$ animals. We subsequently analyzed the offspring of the double heterozygous *Fltp*$^{ZV/+}$; *Celsr1*$^{crsh/+}$ intercrosses.
The first morphological abnormality we could observe was that the *Celsr1*^{crsh} mice show craniorachischisis and loop tail independent of the *Fltp*^{ZV} allele (Figure 45 A-C). Additionally, mutant mice show a shortened anterior-posterior body axis most likely due to CE defects during gastrulation. *Celsr1*$^{crsh/crsh}$ mice also show this shortened body axis therefore it remains to be answered to what extend the anterior-posterior body axis of *Fltp*$^{ZV/ZV}$; *Celsr1*$^{crsh/crsh}$ mice is even shorter (the difference, if any, is not very obvious) (Figure 45 A-C). Interestingly, double homozygous *Fltp*$^{ZV/ZV}$; *Celsr1*$^{crsh/crsh}$ mice show malformed hindlimbs along the proximal-distal axis (Figure 45 A-C). The hindlimbs are bent but not extremely shortened and do not lack the digits like in the *Ror2*$^{-/-}$; *Vangl2*$^{lp/lp}$ mice or in the *Wnt5a*$^{-/-}$ animals (see 2.8.3) (Gao et al., 2011). The fact that this hindlimb patterning defect is absent in *Celsr1*$^{crsh/crsh}$ mice and gets progressively worse in *Fltp*$^{ZV/ZV}$; *Celsr1*$^{crsh/crsh}$ animals suggests for a genetic interaction of *Fltp* and *Celsr1* in hindlimb patterning. This suggests that the PCP pathway is important for proper limb patterning and that a different set of PCP genes is required for fore- versus hindlimb patterning in mouse.

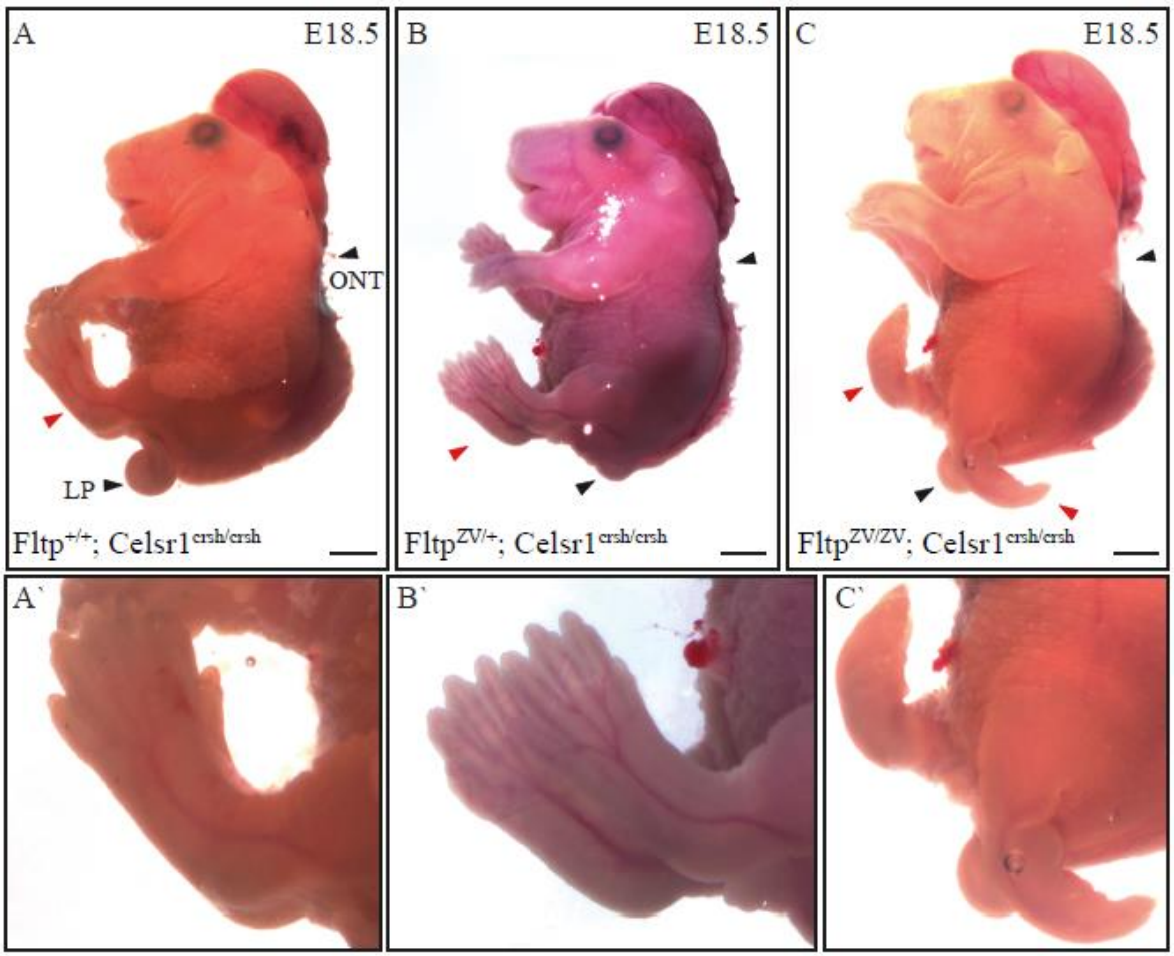

Figure 45 *Fltp^{ZV}; Celsr1^{crsh}* embryos show skeletal hindlimb malformations

(**A**) *Fltp$^{+/+}$*; *Celsr1$^{crsh/crsh}$* embryos at E18.5 show a loop tail (LP), an open neural tube (ONT), and normal hindlimbs (red arrow head).
(**A`**) Enlargement of the hindlimbs of A.
(**B**) *Fltp$^{ZV/+}$*; *Celsr1$^{crsh/crsh}$* embryos at E18.5 show a LP, an ONT, and normal hindlimbs (red arrow head).
(**B`**) Enlargement of the hindlimbs of B.
(**C**) *Fltp$^{ZV/ZV}$*; *Celsr1$^{crsh/crsh}$* embryos at E18.5 show a LP, an ONT, and abnormal hindlimbs (red arrow heads).
(**C`**) Enlargement of the hindlimbs of C.

To analyze a potential genetic interaction in other tissues we compared the Phalloidin staining in the cochlea of the IE of *Fltp$^{+/+}$*; *Celsr1$^{crsh/crsh}$*, *Fltp$^{ZV/+}$*; *Celsr1$^{crsh/crsh}$*, and *Fltp$^{ZV/ZV}$*; *Celsr1$^{crsh/crsh}$* animals. Surprisingly, the staining pattern of *Fltp$^{ZV/ZV}$* seemed to show rather mild disruption of the hair cell pattern. Phalloidin staining in *Celsr1$^{crsh/crsh}$* animals shows a rather normal alignment of hair cells from the base to the middle part of the cochlea but the alignment gets more and more disrupted closer to the apex. The organ of Corti of *Fltp$^{ZV/ZV}$*; *Celsr1$^{crsh/crsh}$* animals revealed the highest degree of misalignment of the hair cells. The quantification of the rotation of IE hair cells was performed by measuring the angle from the normal tissue polarity (measured by the medial to distal alignment of the IE hair cell rows) to the spot where the kinocilium marks the middle of the stereociliary hair bundle (Figure 38 D). This angle was grouped into 0-30°, 30-45°, 45-60°, 60-90°, and over 90° of rotation. 0-30° of rotation was accounted as WT situation because we noticed a slight rotation in some hair cells of *WT* animals, too. All hair cell rows were counted separately. This analyzes revealed a higher degree of rotation in the double homozygous animals compared to both single homozygous

animals (Figure 46 A, B). Homozygous *Celsr1*^{crsh} mice and double homozygous mice showed individual IHC that were out of row. Moreover, we found especially OHC of the third row being heavily rotated. We were also able to detect a fourth row of OHC but only in IEs of double homozygous mice and not in *Celsr1*^{crsh} homozygous mice (Figure 46 A, B). Nevertheless, this fourth row was also present in heterozygous *Fltp*^{ZV} mice independent of the *Celsr1* genotype. The rotation is always most prominent in the third outer hair cell row. This hair cell row often shows a rotation of more than 180° compared to the normal plane of orientation (Figure 46 C, D).
Taken together, the limb outgrowth defect and the IE phenotype strongly suggest that Fltp and Celsr1 act together in the PCP pathway.

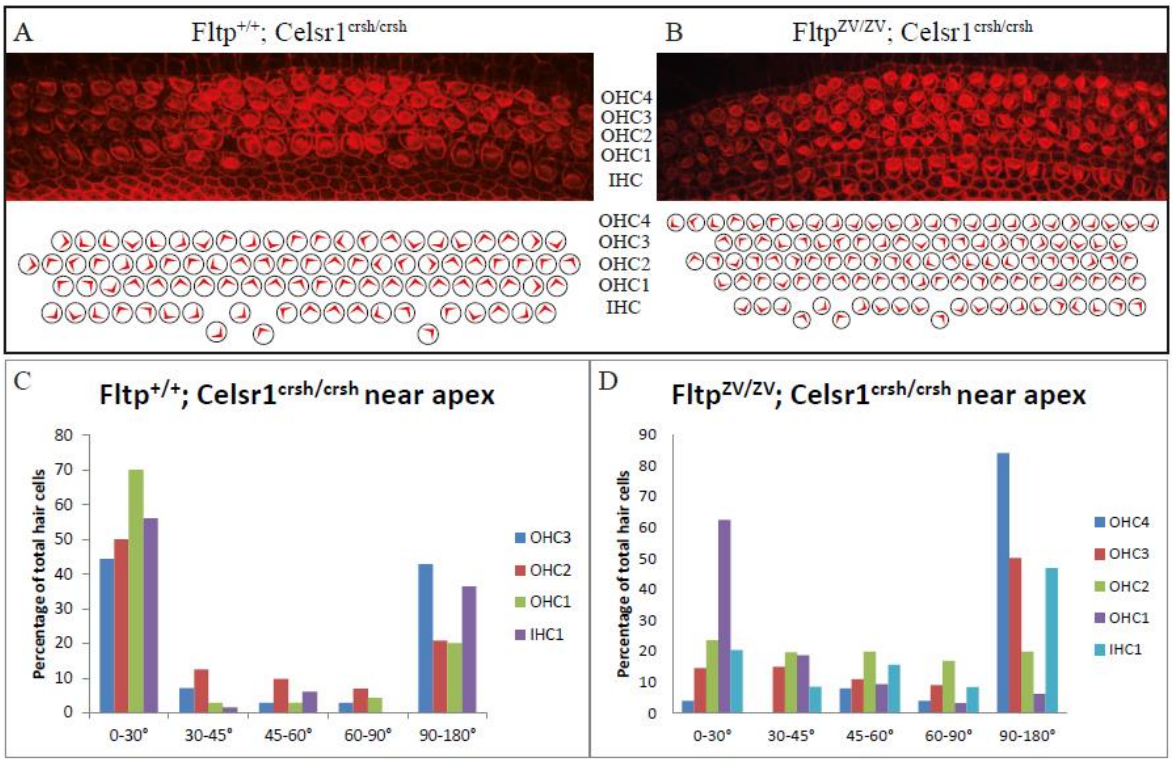

Figure 46 *Fltp* and *Celsr1* show a genetic interaction in the inner ear

(**A**) Phalloidin staining of the cochlea of a *Fltp*$^{+/+}$; *Celsr1*$^{crsh/crsh}$ embryo at E18.5 revealed rotated cells in all outer hair cell (OHC) rows as well as the inner hair cell (IHC) row. The diagram below shows the rotation of the cells.
(**B**) Phalloidin staining of the cochlea of a *Fltp*$^{ZV/ZV}$; *Celsr1*$^{crsh/crsh}$ embryo at E18.5 revealed more severely rotated cells in all outer hair cell (OHC) rows as well as the inner hair cell (IHC) row and an additional OHC row in comparison to the IE of a *Fltp*$^{+/+}$; *Celsr1*$^{crsh/crsh}$ mouse. The diagram below shows the rotation of the cells.
(**C, D**) The charts show the percentage of rotated hair cells grouped into 5 different categories.

In total we analyzed 66 cells in the IHC row, 70 in the OHC row 1, 72 in the OHC row 2, and 70 in the OHC row 3 of one *Fltp*$^{+/+}$; *Celsr1*$^{crsh/crsh}$ animal. Till now we were not able to collect more than one animal with this genotype on this background. For the *Fltp*$^{ZV/ZV}$; *Celsr1*$^{crsh/crsh}$ genotype we analyzed 482 cells in the IHC row, 489 in the OHC row 1, 485 in the OHC row 2, 488 in the OHC row 3, and 22 in the OHC row 4 of four different mice.
Mice were genotyped for *Fltp*^{ZV} according to the genotyping protocol described in the “Material and methods” section (see 5.2.4.1). Interestingly, some *Celsr1*$^{crsh/crsh}$ mice are viable and show a looptail

phenotype in addition to the headshaking behavior. Born *Celsr1*^{crsh} mice were genotyped by head-shaking behavior and looptail phenotype (*Celsr1*$^{crsh/+}$ and *Celsr1*$^{crsh/crsh}$ show head-shaking phenotype but only *Celsr1*$^{crsh/crsh}$ shows additionally the looptail phenotype) as well as by sequencing (see 5.2.4.1). Unborn embryos were genotyped by sequencing for the *Celsr1* point mutation.

3.4.3 Flattop interacts with the scaffolding protein Discs large 3

Analysis of the Fltp protein revealed that it harbors two PRRs. PRRs are known to bind to SH3 domains (Harkiolaki et al., 2009). Fortunately, we already worked on a protein called Discs large 3 (Dlg3) that is involved in apical basal polarity establishment, showed an IE defect reminiscent of PCP defects, and contains a SH3 domain in its protein sequence (see 2.6.1) (Van Campenhout et al., 2011). Therefore, this protein was a potential Fltp interaction partner, which we tested in an immunoprecipitation (IP) assay.

3.4.3.1 Flattop and Discs large 3 physically interact in ciliated cells

To test whether Fltp binds to SH3 domains via its PRRs we transfected HEK293T cells with a construct expressing Fltp-Tap, myc tagged Dlg3 as well as Fltp-Tap and Dlg3-myc together. As a control we used untransfected HEK293T cells. In the first blot we loaded the lysate from proliferating HEK293T cells and blotted against Dlg3 with an anti-c-myc antibody. As expected we detected Dlg3 protein in cells transfected with *Dlg3* (Figure 47 A, first four rows, Dlg3 band marked by asterisk). The IP was performed against Fltp-Tap and later blotted against Dlg3 to see if both proteins complex together. An interaction of both proteins could not be shown (Figure 47 A, last four rows). The next blot is loaded just as the first but this time not blotted against Dlg3 but against Fltp (2D3, monoclonal anti-Fltp antibody). Again we could detect the Fltp protein only in the lysates where we transfected *Fltp* (Figure 47 B, first four rows, Fltp band marked by asterisk). The detection of the Fltp band in the IP did not work (Figure 47 B, last four rows). Next we changed the conditions from proliferating cells to cells that exit the cell cycle by serum starvation. The first blot is blotted against Dlg3 and as expected shows the protein in the transfected cells (Figure 47 C, first four rows, Dlg3 band marked by asterisk). Using these conditions we could successfully immunoprecipitate the Dlg3 band in cells where we transfected both, *Fltp* and *Dlg3* (Figure 47 C, last four rows, Dlg3 band marked by red asterisk). The last blot was blotted against Fltp and Fltp protein could only be detected in the lysates of the transfected cells (Figure 47 D, first four rows, Fltp band marked by asterisk). Here the IP worked and we could detect Fltp protein in the IPs of the *Fltp* transfected cells (Figure 47 D, last four rows, Fltp band marked by asterisk).

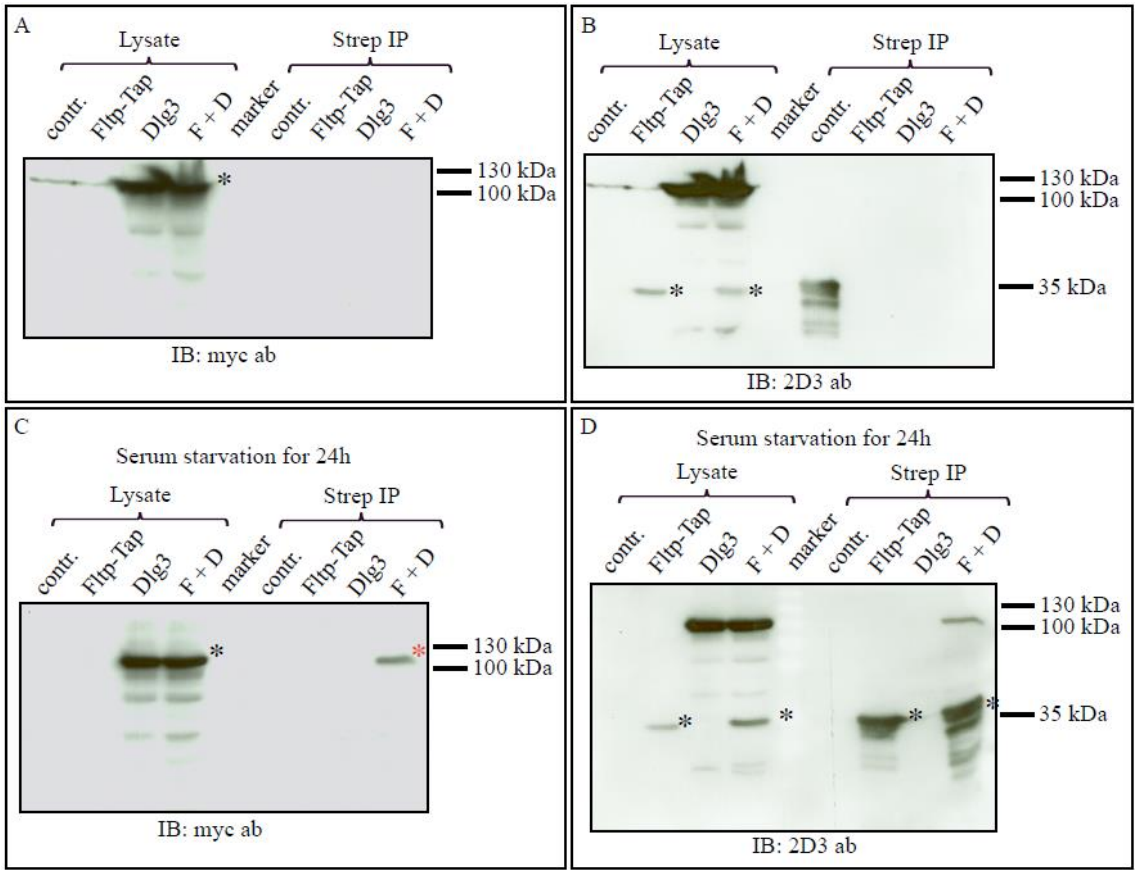

Figure 47 Fltp physically interacts with Dlg3

(**A-D**) HEK293T cells were transfected with Fltp-Tap, Dlg3-myc, and Fltp-Tap together with Dlg3-myc. As control we used untransfected HEK293T cells.
(**A**) Immunoblot against Dlg3-myc on lysate and strep immunoprecipitation (IP) of transfected HEK293T cells. A Dlg3 band could only be detected in the lysate of Dlg3-myc and Fltp-Tap together with Dlg3-myc transfected cells.
(**B**) Immunoblot against Fltp on lysate and strep IP of transfected HEK293T cells. A Fltp-Tap band could only be detected in the lysate of Fltp-Tap and the Fltp-Tap together with Dlg3-myc transfected cells. The IP did not work.
(**C**) Immunoblot against Dlg3-myc on lysate and strep IP of transfected and serum starved HEK293T cells. A Dlg3 band could be detected in the lysate of Dlg3-myc and Fltp-Tap together with Dlg3-myc transfected cells as well as in the strep IP but only when Fltp-Tap and Dlg3-myc are both transfected.
(**D**) Immunoblot against Fltp on lysate and strep IP of transfected and serum starved HEK293T cells. A Fltp-Tap band could be detected in the lysate of Fltp-Tap and Fltp-Tap together with Dlg3-myc transfected cells as well as in the strep IP but only when Fltp-Tap alone and Fltp-Tap together with Dlg3-myc are transfected.

Taken together, we convincingly showed that Fltp is able to interact with SH3 containing proteins more precisely, with Dlg3. We could only detect an interaction in serum starved conditions consistent with Fltps' function in BB transport, docking, and positioning. To map the precise interaction domains of Fltp and Dlg3 Dr. Anika Böttcher performs deletion assays of Dlg3 and Fltp. These results are in preparation.

3.4.3.2 Flattop and Discs large 3 co-localize in inner ear hair cells

As mentioned earlier we generated the *Fltp*^{T2AiCre} mouse line with the aim to do lineage tracing in distinct mono- and multiciliated tissues such as the node, the lung, the choroid plexus, and the pancreas (Lange et al., 2012). For this we fused a Strep/Flag (SF) tandem affinity purification (TAP) tag (Gloeckner et al., 2009) followed by the viral *T2A* sequence (Donnelly et al., 2001) and the *iCre* (Shimshek et al., 2002) to the ORF of *Fltp* (Lange et al., 2012). With the antibodies we generated against the T2A peptide we are able to detect the T2A tagged Fltp protein because the 2A part of the T2A peptide is fused to the Fltp protein after cleavage (Ryan and Drew, 1994). As I already showed, Fltp localization is restricted to the lateral side of IE hair cells, more precisely to the kinocilium and the apical part of the lateral membrane without localizing to the site of the BB (Figure 27 G).
To visualize the expression of *Dlg3* in IE hair cells we made use of the *Dlg3:Venus* mouse line which is a transgenic mouse line expressing a Dlg3-Venus fusion protein. For the co-localization study we crossed *Fltp*$^{T2AiCre/T2AiCre}$ animals with *Dlg3:Venus* animals. Subsequently, we intercrossed the double positive animals and analyzed the *Fltp*$^{T2AiCre/+}$; *Dlg3:Venus* animals. We could detect expression of *Dlg3*, monitored by antibody staining for the Venus protein, in a crescent at the lateral side of the apical membrane of the IHCs as well as the OHCs of the IE. Dlg3 localization overlaps at the lateral membrane with ZO-1 which marks the apical tight junction complex (Figure 48 A-C, A'-C'). Dlg3-Venus fusion protein is located directly in front of the stereociliary hair bundles marked by Phalloidin staining. Interestingly, the staining is left open exactly at the position where the BB is anchored to the lateral membrane (Figure 48 D-F). Unfortunately, we did not succeed in performing a double staining of Fltp and Dlg3.

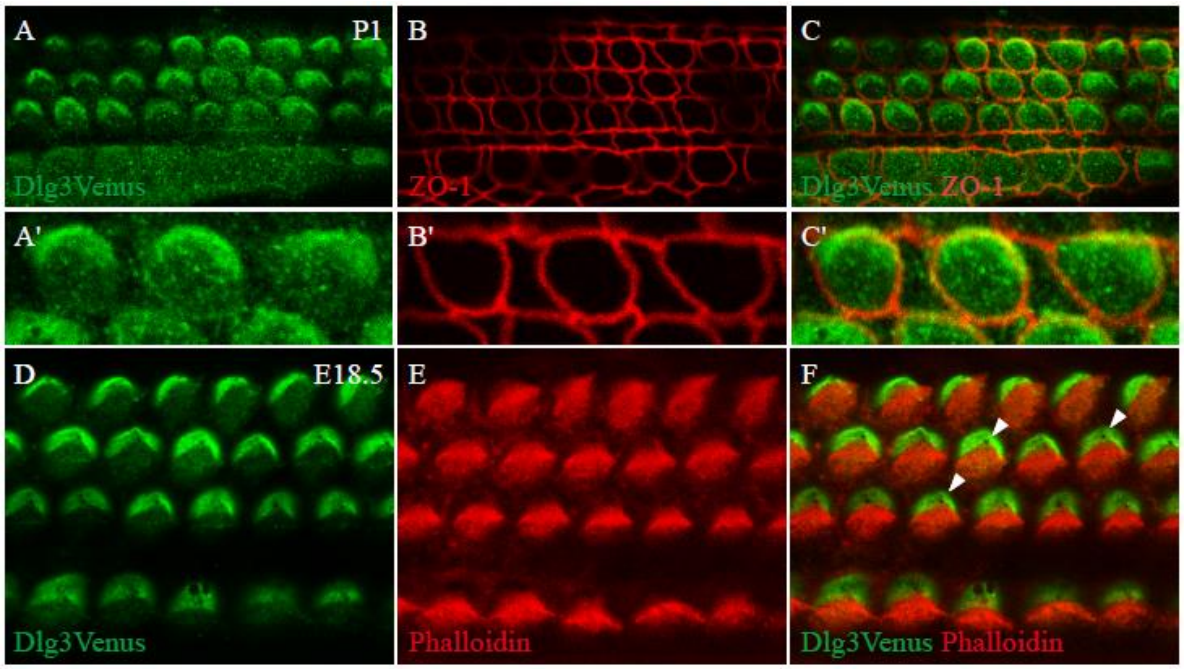

Figure 48 Fltp and Dlg3 are both localized at the lateral side of inner ear hair cells

Confocal images of the organ of Corti of *Fltp*$^{T2AiCre/+}$; *Dlg3:Venus* E18.5 animals.
(**A-C**) Dlg3-Venus fusion protein (green) is located at the apical surface (marked by ZO-1, red) of the lateral side of IE hair cells.
(**A`-C`**) Enlargement of A-C where the co-localization of Dlg3-Venus and ZO-1 at the lateral side of the hair cells is visible.
(**D-F**) Dlg3-Venus (green) is located in front of the stereociliary hair cell bundles (red) at the lateral side. Note that the BB is excluded from the Dlg3-Venus staining (white arrow heads in F).

By comparing both, Fltp and Dlg3 localization, we strongly suggest that they are co-localized at the lateral side of IE hair cells. This finding is also supported by the physical interaction in HEK293T cells (see 3.4.3.1).
To confirm our co-localization results in the IE we performed immunohistochemistry on the murine embryonic node of an E7.75 embryo. Here we were able to detect Dlg3 protein enriched at the apical surface of the node cells (data not shown). We could show that Fltp protein is localized at the same place in node cells (Figure 19; Figure 25).

3.4.3.3 Flattop influences localization of Dlg3 in inner ear hair cells

To analyze the result of absence of Fltp for Dlg3 localization we crossed the *Fltp*^{zV} mouse line into the *Dlg3:Venus* mouse line. We analyzed the offspring of double heterozygous intercrosses. Latest results indicate that Dlg3 localization is disrupted upon Fltp deletion. Animals WT for *Fltp* and positive for *Venus* expression show Dlg3-Venus localization at the lateral side of IE hair cells (Figure 49 A). The cells' cytoplasm does not show heavy Dlg3-Venus staining. The BB is excluded from the Dlg3-Venus staining. Already in animals heterozygous for *Fltp* and positive for Dlg3-Venus not as much Dlg3-Venus fusion protein as in animals WT for *Fltp* can be observed at the lateral side of the hair cells. Interestingly, the IHCs show more Dlg3-Venus protein at the lateral side than the OHCs (Figure 49 B, white arrowheads). It seems that the rest of the Dlg3-Venus fusion protein is located to the cytoplasm of the IE hair cells (Figure 49 B, red arrowheads). Upon Fltp deletion, Dlg3-Venus is not localized at the lateral side of the IE hair cells anymore (Figure 49 C).

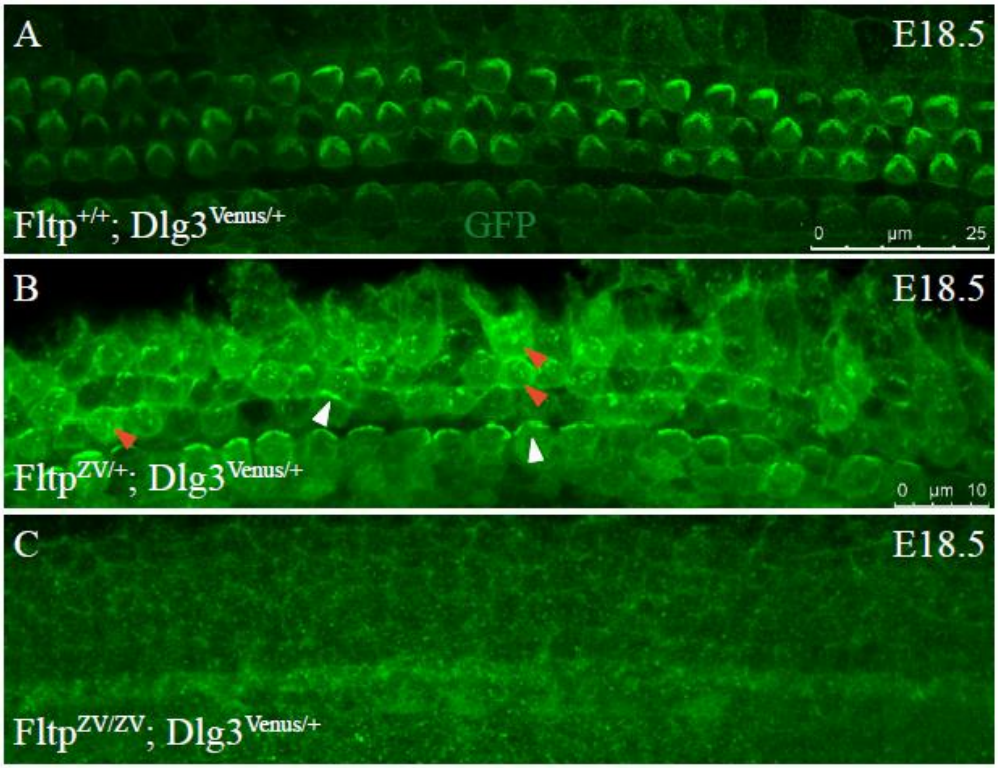

Figure 49 Fltp stabilizes Dlg3 at the apical-lateral plasma membrane of inner ear hair cells.

Confocal images of the cochlea of E18.5 animals. Genotype as indicated.
(**A**) The Dlg3-Venus protein (green) is located at the lateral side of IE hair cells in *Fltp*$^{+/+}$; *Dlg3:Venus* mice.
(**B**) It seems that the Dlg3-Venus protein is only partially localized to the lateral side of the hair cell in *Fltp*$^{ZV/+}$; *Dlg3:Venus* mice. The rest seems to be in the cytoplasm.
(**C**) In *Fltp*$^{ZV/ZV}$; *Dlg3:Venus* mice Dlg3-Venus localization is absent from the lateral side of the hair cells.

Taken together, we could show that Fltp and Dlg3 physically interact in ciliated cells, that they are co-localized in IE as well as in node cells, and that presence or absence of Fltp influences Dlg3-Venus localization. We could not only show physical interaction and co-localization but also biological evidence that both proteins interact.

4 Discussion

4.1 Advantages of the *Foxa2*^{T2AiCre} mouse line over the *Foxa2*^{iCre} mouse line

How neighboring tissue interactions pattern endodermal as well as mesodermal tissues is not completely understood. Therefore, spatial and temporal inactivation of genes specifically in the endoderm is of great interest. One of the earliest factors specifying the endodermal lineage is *Foxa2*. We generated a new *Foxa2-iCre* mouse line for the analysis of conditional gene deletions during early endoderm formation as well as in endoderm-derived organs, such as pancreas, lung, liver, and GI tract. Now, key transcription factors, growth factors, and signaling molecules can be conditionally deleted in the endoderm and endoderm-derived organs for a better understanding of endoderm development. Moreover, this mouse line can be used for genetic-lineage tracing of cells that express *Foxa2*. More precisely, progenitor cells of the endoderm as well as adult stem cells in the lung and pancreas can be analyzed in more detail.

One great advantage over the *Foxa2*^{iCre} mouse line generated by Uetzmann et al. (Uetzmann et al., 2008) is the usage of the T2A strategy, were no copy of *Foxa2* is deleted. This is important for conditional knock-out (CKO) studies, as loss of one *Foxa2* allele might influence the interpretation of the CKO results. The intention of the former *Foxa2*^{iCre} line was to delete *Foxa2* completely but instead a hypomorphic allele was generated. This happened because at that time it was unknown that beside the first promoter in front of exon one an alternative promoter in front of exon two drives expression of an alternative transcript of *Foxa2* downstream of the *iCre* knock-in. Thus, iCre recombinase activity using *R26R* animals revealed chimeric recombination efficiency in organs like the lung, the thymus, and the thyroid, which is disadvantageous for CKO studies. Likely, iCre recombinase mRNA expression driven from the upstream promoter did not reach comparable levels than endogenous mRNA driven from both promoters. Evidence for this comes from robust mRNA expression of *Foxa2* in the lung epithelium revealed via *in situ* hybridization (data not shown) and is consistent with data from the literature (Wan et al., 2004). Moreover, Foxa2 is known to function in an autoregulatory feedback loop to increase its own expression via binding to its own promoter. Thus, reduced levels of Foxa2 protein will ultimately lead to reduced *Foxa2* mRNA levels due to lack of positive feedback regulation (Odom et al., 2006).

One positive feature of this mouse line was certainly the generation of a hypomorphic allele, which allows for the generation of an epi-allelic series. By using this mouse line it is possible to reduce *Foxa2* expression not only to 0 and 50% as by analyzing knock-out and heterozygous embryos, but also to about 75 and 25% by combining the knock-out and the hypomorphic *Foxa2*^{iCre} allele. Moreover, the influence of deleting the Foxa2 transcript expressed from the first promoter in distinct tissues can be studied. This cell-type specific promoter regulation opens the possibility to study animals where *Foxa2* is deleted in one organ whereas other organs still express *Foxa2*.

To generate a Cre mouse line that circumvented all the former problems, we used a T2A strategy to separate the endogenous *Foxa2* locus from the iCre recombinase. The T2A strategy allows expression of both copies of *Foxa2* as well as the translation of equimolar amounts of the Foxa2 and iCre protein. Therefore, iCre protein amount reflects the endogenous level of Foxa2 protein most accurately. With this strategy we combined the ability of the iCre recombinase to recombine *loxP* flanked alleles with the tissue-specific and temporal properties of the *Foxa2* locus without disrupting its function. Another advantage of using the *T2A* sequence is that antibodies generated against the T2A peptide can be used to visualize Foxa2 protein in immunohisto- and cytochemistry, for

chromatin immunoprecipitation (ChIP) of Foxa2, as well as for biochemical analysis of the Foxa2 protein. With this strategy all regulatory elements should stay intact in contrast to the knock-in/knock-out strategy of the *Foxa2*^{iCre} line. Especially all the regulatory sequences of the endogenous 3'UTR are present and enhance *Foxa2* expression as well as the fully functional autoregulatory feedback mechanism positively regulates *Foxa2* expression.

4.2 Foxa2 positive cells mark an early endodermal progenitor population as well as progenitors for mesodermal derived tissues

The first detectable β-gal activity appeared at E7.0 in the posterior epiblast and the visceral endoderm (VE). It has been shown by *in situ* hybridization data that *Foxa2* mRNA is clearly expressed in the VE and the posterior epiblast earlier than E7.0 (Kinder et al., 2001). Supporting this data are experiments we performed in our lab by immunohistochemistry on E6.5 to E7.5 embryos (Burtscher and Lickert, 2009). They were able to show that epiblast cells are already fate specified at E6.5 either to the mesodermal lineage (T positive) or to the endodermal lineage (Foxa2 positive). Additionally, VE cells show Foxa2 protein in the nucleus at E6.5. One reason that we were not able to detect β-gal activity earlier than E7.0 might be the time delay in Cre mediated recombination of the *R26R* gene locus. The whole process of Cre transcription, translation, and accumulation in the cell, Cre mediated recombination of the *lacZ* locus, translation of the *lacZ*, as well as β-gal transcription and accumulation can lead to a time shift of up to 12 hours (Nagy, 2000). Additionally, a particular threshold of Cre protein is needed for recombination of the *lacZ* locus. This is the reason for β-gal detection problems in cells with low promoter activity. Nevertheless, we could detect onset of recombination earlier than in the *Foxa2*^{iCre} (Uetzmann et al., 2008) mouse line.
From E7.5 onwards, the *iCre* recombinase is expressed reliable in the anterior primitive streak (APS) region, in the node, the DE, the VE, the notochord, the floor plate, as well as the endoderm derived organs such as the lung, the liver, the intestine, and the pancreas. This expression precisely reflects earlier reported *Foxa2* mRNA expression (Ang and Rossant, 1994), is consistent with other mouse lines generated for genetic lineage tracing (Frank et al., 2007; Park et al., 2008a; Uetzmann et al., 2008), as well as immunohistochemical analyzes (Burtscher and Lickert, 2009). Taken together, these results suggest that Foxa2 marks an early progenitor population for endoderm-derived tissues.
Foxa2 positive cells are found in the early-gastrula organizer (EGO) of the early-streak embryo, in the mid-gastrula organizer (MGO) of the mid-streak embryo, as well as in the node of the late-streak embryo. Therefore, β-gal activity is expected in all tissues derived from the axial mesoderm such as parts of the head mesoderm, the prechordal plate, the floor plate, and the notochord. As expected, iCre recombinase activity was detected in mesendodermal tissues like the organizer populations from early- to late-streak embryos, the organizer derived axial mesoderm (gives rise to the notochord and the head process), as well as the heart. These observations confirm the lineage tracing experiments from Kinder et al. (Kinder et al., 2001) suggesting that the APS region gives rise to a diverse cell lineage including the axial mesoderm and the notochord.
Cells from the EGO contribute to the heart mesenchyme which also could be confirmed by β-gal activity of the *Foxa2*^{T2AiCre} mouse line and is consistent with the Cre activity in early cells of the cardiac crescent (Park et al., 2008a). The observed lacZ staining in the outflow tract (OFT), both ventricle, and partially to both of the atria suggests that Foxa2 positive cells in the cardiac crescent are progenitors for both, the primary and secondary heart field. The secondary heart field harbors the progenitors for the OFT and most of the right ventricle (RV) but it also contributes partially to

both of the atria. The primary heart field cells are the precursors for the left ventricle (LV) and contribute to most of the two atria. Cranial mesenchyme derived mostly from the EGO and only partially from the MGO is also lacZ positive in *Foxa2*$^{T2AiCre/+}$*; R26*$^{R/+}$ animals consistent with previous results from Kinder et al. (Kinder et al., 2001). We could also confirm the contribution of organizer derivatives to the more ventral regions of the neural tube.
Cells derived from the MGO and partially from the EGO are contributing to the roof of the foregut and the foregut endoderm which is consistent with iCre activity pattern. Nodal cells mostly contribute to the notochord and the floor plate which both show high β-gal activity.
Taken together, these results show that Foxa2 positive progenitor cells not only mark an early endodermal progenitor population (the endodermal stem cell) but moreover contain progenitors for mesodermal derived organs.

4.3 Foxa2 marks the potential endodermal stem cell

In contrast to the *Foxa2*^{iCre} mouse line the *Foxa2*^{T2AiCre} line shows a uniform *iCre* recombinase expression in all endoderm-derived organs. In the lung the *Foxa2*^{T2AiCre} line reflects the endogenous *Foxa2* expression most precisely (Wan et al., 2004). Additionally, we could detect lineage positive cells in the ureteric buds of the kidney which is of mesodermal origin. We could show that all endoderm-derived organs are lineage positive which might implicate that *Foxa2* expression marks an endodermal stem cell that generates all endoderm-derived tissues. Moreover, Foxa2 is the first factor that is expressed in the endodermal progenitor cells, induces endoderm formation, and is a pioneering factor that opens chromatin for other transcription factors. Additional support provides the *Foxa2* knock-out which lacks all endoderm-derived tissues and thus supports the theory of a *Foxa2* expressing precursor cell of all endodermal cells residing most likely in the epiblast (Ang and Rossant, 1994; Burtscher and Lickert, 2009; Weinstein et al., 1994).
A well described stem cell compartment is the intestinal crypt. The intestinal crypt harbors Lgr5 positive stem cells at the bottom of the crypt in close contact with Paneth cells. These cells are important to renew the whole intestinal epithelium of one villus. As already shown by Uetzmann et al. (Uetzmann et al., 2008) Foxa2 lineage positive cells can be found throughout the whole gut epithelium including the cells of the bottom of the crypt compartment including the stem cells. By immunohistochemistry as well as with a mouse line expressing the fluorescent reporter gene *Venus* under the transcriptional control of *Foxa2* we could show that only a subset of crypt cells express *Foxa2* (unpublished observation of Dr. Ingo Burtscher) suggesting that Foxa2 marks a subpopulation of the intestinal stem cells.
Another area of intensive scientific investigation is the formation of the pancreatic islet cells (endocrine pancreas) as well as the duct cells. Type I Diabetes mellitus is caused by loss of insulin producing β-cells and could potentially be cured by a β-cell transplantation. One possibility to antagonize the symptoms could be to identify a potential β-cell precursor in the islet of Langerhans or a pancreatic stem cell and differentiate these cells to functional β-cells by activating the essential transcriptional program. Till now it is not clear if the pancreas harbors adult stem cells and from which precursors the insulin producing β-cells derive. There is evidence that the duct harbors a small amount of cells that are activated after injury and might even be able to regenerate islet cells *in vivo* (Rovira et al., 2010). During embryonic development till approximately E16.0, Foxa2 and Pdx1 mark multipotent progenitors. Later on, Pdx1 gets restricted to endocrine precursors and finally to β-cells. The same seems to hold true for Foxa2 positive cells despite the fact that *Foxa2* is also expressed in

α-cells in the adult pancreas. *Foxa2* expressing cells in the pancreas are potential candidates for multipotent precursor cells. The duct and the endocrine pancreatic cells are Foxa2 lineage positive but active *Foxa2* expression can only be detected in a subset of lineage positive cells. Recently, pancreatic-derived multipotent precursor (PMP) cells have been identified and isolated in murine embryonic tissue as well as in human adult islets. These cells are able to proliferate, self-renew, and to generate different pancreatic and neural cell types (Smukler et al., 2011). Interestingly, the PMPs are insulin positive, consequently meaning that they are Pdx1 positive. Therefore it can be speculated, that these cells are Foxa2 positive because both factors are expressed during development and in adulthood in the endocrine lineage.
Foxa2 lineage could also be observed in the hair follicles of the head. Hair follicles are known to contain stem cells that are able to contribute to wound repair after injury of the epidermis (Ito et al., 2005). It remains to be answered whether *Foxa2* is expressed in these cells.
Taken together, the lineage tracing as well as the newly identified insulin positive adult PMP cells strongly suggest that *Foxa2* is expressed in cells with regenerative capacity. If the Foxa2 positive epiblast cell would be the endodermal stem cell than this cell should be able to form all endoderm derived tissues discussed above.

4.4 The *Foxa2*^{T2AiCre} mouse line is a valuable tool for conditional gene inactivation in endoderm derived tissues

It already has been shown that the *Foxa2*^{T2AiCre} mouse line is a valuable tool for conditional gene inactivation in endoderm derived tissues (Horn et al., 2012). Here, the authors used the *Foxa2*^{T2AiCre} mouse line to conditionally delete *Mind bomb 1* (*Mib1*) in the DE. *Mib1* is an E3 ubiquitin ligase essential for Notch ligand activity. Endoderm deletion of *Mib1* leads to loss of Nkx6-1^{+}Ptf1a^{-} cells and a corresponding loss of duct cells, Neurog3^{+} endocrine progenitors, and β-cells in the pancreas. Specification of the pancreas and the liver endoderm occurs normally although *Mib1* is also deleted in all other endoderm-derived organs indicating that this is a cell autonomous effect of *Mib1* in the pancreas. Nevertheless, other endodermal organs like the duodenum and the stomach show developmental defects. The advantage of the *Foxa2*^{T2AiCre} line is that the gene of interest gets deleted early and in all endoderm (including pancreatic islet) cells. The *Ptf1a-Cre* mouse line for example deletes the gene of interest earliest in the common Nkx6-1^{+}Ptf1a^{+} precursor for acinar, duct, and β-cells (Nakhai et al., 2008). Not only deletion of *Mib1* confirmed the value of this mouse line but also of *Dll1* (*Delta like 1*, encodes for a Notch ligand) and *Hes1* (a Notch target gene) were successfully deleted in the endoderm (Horn et al., 2012). In the same study, the expression of a dominant negative Maml1-EGFP fusion protein from a targeted *ROSA26* locus that functions as a specific inhibitor of all four mammalian Notch receptors was expressed under the transcriptional control of *Foxa2* in endoderm-derived tissues.
As shown by the results discussed above, this line has already proven its functionality and can be used for further studies of signals and factors directing lineage decisions in the pancreas. Care has to be taken for the analysis of the phenotypes because this line deletes the gene of interest in all endoderm cells and additionally in some mesodermal tissues which might lead to misinterpretation of the results. Effects in other tissues and organs might preclude the analysis of the candidate endoderm-derived organ.

Taken together, we successfully generated a new mouse line (*Foxa2*^{T2AiCre}) expressing the *iCre* recombinase under the transcriptional control of *Foxa2*. Moreover, we showed that the viral *T2A* sequence is able to co-translational cleave both proteins *in vivo* which was not shown when we generated this mouse line. This new mouse line is a clear improvement to the existing *Foxa2-Cre* lines because, due to the T2A strategy, iCre recombinase activity most accurately reflects *Foxa2* expression in the organizer tissues from E7.0 onwards, in all endoderm-derived organs, shows no chimerism at any time, and does not interfere with regulatory sequences especially in the 3'UTR. Therefore, this mouse line is a valuable tool for genetic lineage tracing experiments as shown by the iCre recombination activity. Moreover, it is also a functional tool for conditional gene targeting in the *Foxa2* expression domains namely in organizer tissues such as the node and the notochord as well as organs such as the lung and the pancreas. Functionality of the strategy was proven by the specific deletion of *Mib1* in the DE showing that Notch signaling is used iteratively to control cell fate choices during pancreatic development. Moreover, if we can proof that *Foxa2* expressing cells in distinct tissues have stem cell capacity this mouse line can be used for conditional gene targeting in these stem cells to further characterize the molecular identity of different stem cell compartments. Future work will address the question if Foxa2 marks crypt stem cells but lineage experiments as well as experiments with the *Foxa2-Venus* mouse line strongly suggest this. By generating an inducible *Foxa2-CreERT2* mouse line following the same targeting strategy questions regarding *Foxa2* expression in the crypt stem cell and in the basal cells of the lung as well as the question whether a mesendodermal progenitor cell does exist could be answered.

4.5 The *Flattop*^{zv} mouse line

In this thesis I report the identification and characterization of the novel PCP effector gene *Fltp* (*1700009p17RiK*). It has been shown that this gene of unknown function is exclusively expressed in the node which is a ciliated tissue with organizer function at E7.5 (Tamplin et al., 2008). Beside this the mRNA of this Riken clone was shown to be highly expressed in ciliated tissues strongly suggestive for a function during the process of ciliogenesis (McClintock et al., 2008). Endogenous Fltp protein is localized in ciliated cells and *Fltp* reporter is activated early after cell division in pre-committed postmitotic cells. Loss of *Fltp* leads to several PCP phenotypes including exencephaly, constricted distal airways in the lung, and misarrangement of IE hair cells. Further support for a role of Fltp in PCP provides the genetic interaction of *Fltp* with one of the core PCP genes *Celsr1*. This interaction is manifested in the phenotypes of the IE and the limbs. Moreover, multiciliated lung epithelial cells show defects in BB transport resulting in absence or reduction of cilia on the apical surface. This phenotype could be reproduced in *in vitro* cultures of MTECs. Our data suggests that Fltp is an important regulator for BB docking and positioning in distinct mono- and multiciliated cells. Fltp might function in a complex together with Dlg3, centrosomal proteins, proteins of the cytoskeleton, proteins important for apical transport, proteins of the tight junction complex, as well as with PCP molecules.

4.5.1 Flattop functions in ciliated tissues dependent on planar cell polarity

Reporter gene expression analysis revealed that *Fltp* is expressed in a tightly regulated spatial and temporal pattern in distinct mono- and multiciliated tissues during development and in adult mice. Ciliogenesis as well as ciliary function moves more and more into the focus of contemporary research

because it has been shown recently that primary cilia are important to sense extracellular signals and therefore play a crucial role in Ca^{2+}, Hedgehog (HH), PDGFRα, Wnt/β-catenin, and PCP signaling (Corbit et al., 2005; Eggenschwiler and Anderson, 2007; Gerdes et al., 2007; Huangfu et al., 2003; McGrath et al., 2003; Schneider et al., 2005). Most of these ciliated tissues have been shown to depend on PCP suggestive for a functional role of Fltp in PCP dependent ciliary positioning. The PCP machinery establishes defined membrane compartments of cells within the plane of an epithelium. It provides positional information for directed transport of cell organelles towards distinct sides of a cell. Some ciliated tissues depend on PCP function for ciliary positioning. In these cells, the whole BB transport and positioning machinery is tightly connected with the PCP machinery. Till now it is not fully understood how the positional information of the asymmetrically localized PCP molecules is translated into directed BB transport.

Fltp reporter gene expression in known PCP dependent tissues like the node, the IE, the limb, the ependymal cells lining the ventricle, and the olfactory sensory neurons (OSN) could be shown. In these tissues PCP is important to position the cilia on a distinct side of the cell as well as to coordinate this positioning machinery over the whole tissue surface.

The first region where *Fltp* reporter could be detected is the murine embryonic node at E7.5. Embryonic organizer tissue like the node harbor monociliated sensory cilia and depend on PCP (Santos and Reiter, 2010; Song et al., 2010) as well as ciliary signaling for proper ciliary positioning (Eggenschwiler and Anderson, 2007). The nodal cilia generate the nodal flow and are indispensable for breaking bilateral symmetry resulting in asymmetry of the body. During maturation of node cells the BBs have to be repositioned from a central position to the posterior side of the node cells (see 2.1.1) (Nonaka et al., 2005). To dissect the mechanism underlying this repositioning Hashimoto et al. analysed a mouse model where five of six *Dvl* alleles were missing and additionally a *Wnt3a* mutant mouse (Hashimoto et al., 2010). They could show that in the compound *Dvl* mutant the repositioning is disrupted whereas it is not in the *Wnt3a* mutant suggesting that this mechanism is dependent on PCP signaling but not on canonical Wnt signaling. We did not analyse the ciliary positioning on the node cells in detail which remains to be done to detect BB positioning and left-right asymmetry defects.

Ciliary positioning of the kinocilium in the IE is tightly controlled by the PCP pathway. PCP in the organ of Corti is important for the stereotypic alignment of the hair cells and PCP defects lead to misalignment of these highly ordered rows of cells. *Fltp* reporter is expressed in all six sensory regions of the IE. Loss of *Fltp* in the IE results in a PCP defect (see 4.5.4).

Another tissue that depends on PCP and where *Fltp* reporter is expressed is the developing limb (Gao et al., 2011). Gao et al. reported that Wnt dependent phosphorylation of Vangl2 through Ror2 is needed for normal limb development. Phosphorylated Vangl2 is important for PCP establishment in the chondrocytes. The proximal-distal polarization of the chondrocytes is needed for elongation of the bone cartilage. A failure in PCP signaling in the chondrocytes results in shortened limbs along the proximal-distal axis. Which role PCP signaling plays during the development of the apical ectodermal ridge (AER) is not fully understood. What is known is that *Fgf8* expression in the AER is absent in *Vangl2*$^{LP/LP}$ mice (Wang et al., 2011). Fgf8 is an important ligand expressed in the AER that keeps the underlying mesoderm proliferative. The FGFs also stimulate Shh expression in the zone of polarizing activity (ZPA) which in turn induces the expression of the BMP antagonist *Gremlin1* to keep the FGF secretion stable (Bastida et al., 2009). Deletion of *Fltp* in the limbs results in a hindlimb specific skeletal defect (see 4.5.4).

The multiciliated ependymal cells lining the cerebral ventricles beat unidirectional to generate the cerebrospinal fluid (CSF) flow. To establish this fluid flow a tightly regulated interplay of

hydrodynamic forces and PCP signaling is needed. Two types of polarity in ependymal cells are known: The rotational polarity which is important for the correct orientation of the basal foot of the BB in the direction of fluid flow as well as the translational polarity which is indispensable for the movement of the BBs towards the anterior part of the ependymal cell (Hirota et al., 2010; Mirzadeh et al., 2010; Tissir et al., 2010). The first cue is provided by the passive fluid flow of the CSF through the lateral ventricles into the foramina of Monroe where the CSF finally becomes reabsorbed by the arachnoid granulations (Grzybowski et al., 2006). It has been shown that the PCP molecules Dvl2, Vangl2, Celsr2, and Celsr3 are important for establishment of rotational polarity but translational polarity seems not to be regulated through PCP in the ependymal cells (Guirao et al., 2010; Hirota et al., 2010; Tissir et al., 2010). Translational polarity is already established in the radial glia cells (Mirzadeh et al., 2010), the precursors of ependymal cells, by the position of their primary cilia to the anterior side and inherited to the ependymal cells. *Fltp* reporter gene is expressed in the ependymal cells of the ventricle as well as on the ependymal cells of the cp. In both tissues no apparent phenotypes were observed. Whether *Fltp* is expressed in radial glia cells is not known.

The OSNs project immotile 9+2 cilia on their apical surface into the lumen. Proteins of the Bardet-Biedl syndrome (BBS) are important for formation of these cilia and BBS proteins are known to be important for PCP. BBS proteins play a role in MT organization in ciliated cells (Kulaga et al., 2004; Ross et al., 2005). By E12, the OSNs of the main olfactory epithelium initiate the centriole transport from the vicinity of the nucleus to the dendritic knob where the cilia form. It remains a task for the future to analyze the influence of Fltp on BB transport in the main olfactory epithelium.

For other *Fltp* reporter expressing tissues like the ciliated cells in the lung, the crypt stem cell compartment, the pancreas, and the floor plate it is not yet finally proven if and how PCP influences ciliary positioning in these tissues.

Ciliogenesis of the lung starts in the trachea and main bronchi at E14.0-14.5 and subsequently waves in a proximal to distal direction through the whole lung till the terminal bronchioles are finally ciliated two days later (Rock and Hogan, 2011; Toskala et al., 2005). According to this observation we could detect the first reporter positive cells in the trachea and main bronchi at E14.0-E14.5 (Figure 28 B). We could also show that the *Fltp* reporter gene is expressed in multiciliated epithelial lung cells. Endogenous Fltp protein is restricted to only a subset of cells in the lung epithelium, most likely multiciliated cells. Additionally, the localization of the protein in the cytoplasm between the nucleus and the apical surface fits to the hypothetical function of Fltp in BB transport and docking (Figure 30). Strikingly, *Fltp* reporter gene expression directly stops at the broncho-alveolar-duct junction (BADJ) where the terminal bronchiole that harbors ciliated cells descends into the alveoli which do not comprise any ciliated cells (Figure 28). Ciliated lung cells have, till now, not been reported to depend on PCP.

For the crypt stem cell compartment it is not shown whether PCP influences its composition. Nevertheless, *Fltp* reporter is expressed in cells of the Lgr5 receptor positive crypt stem cell compartment. This might indicate that *Fltp* and therefore PCP is required for normal homeostasis of the crypt stem cell compartment. Moreover, *Fltp* reporter is expressed in Paneth cells and these cells are known to secrete Wnt3 and Wnt11 which is known to activate the PCP signaling cascade (Sato et al., 2011; Zhou et al., 2007).

It is not yet clear if PCP plays a role in pancreatic development or directed BB transport in ciliated pancreatic cells. Concerning the stereotype pattern of arrangement of β- and α-cells in the middle and periphery, respectively, it is very likely that the islet of Langerhans has some kind of intrinsic tissue polarity. Recently, the Grapin-Botton lab showed that inactivation of the PCP proteins Celsr2 and 3 has no apparent influence on pancreatic morphology but results in a severe decrease in

endocrine cell differentiation (personal communication with the Grapin-Botton lab). This observation suggests that PCP is important for endocrine lineage formation. They have also shown that the PCP proteins Vangl1/2 and Fzd3 are restricted to pancreatic progenitors aligned in pancreatic ducts and that PCP is established at E11.5 at the same time as the apical-basal polarity (personal communication with the Grapin-Botton lab). We had a look at the *Fltp* reporter gene expression in the pancreas and noticed that it is expressed in insulin positive as well as glucagon positive cells (data not shown). Interestingly, it is not expressed in all insulin or glucagon positive cells. It is important to know of which molecular identity these Fltp negative cells are. Possibly, these cells are uncommitted immature pancreatic precursors. Moreover, not all Fltp reporter positive cells are ciliated indicating that a small subgroup might yet be undifferentiated. All ciliated cells are Fltp reporter positive and it is known that the Insulin-receptor 1 α is localized to the cilia upon glucose induction. It has been shown that mice deficient for the PCP gene *BBS4* show a reduced first phase insulin secretion phenotype in isolated islets stimulated with glucose. Moreover, $BBS4^{-/-}$ animals show elevated plasma insulin levels and obesity (Eichers et al., 2006). It is now important to find out if and how loss of *Fltp* influences pancreatic islet structure. In islet isolation experiment we noticed that isolated $Fltp^{zv/zv}$ islets seem to be smaller than *WT* and $Fltp^{zv/+}$ islets. In whole mount lacZ stainings of $Fltp^{zv/zv}$ pancreata we could detect also bigger islets. This might suggest that the isolated islets do not adhere as strong as the *WT* and heterozygous do and consequently are digested faster by the digestive enzymes needed for islet isolation.

Another tissue where it is not yet shown that PCP is important for ciliary positioning is the floor plate. Floor plate cells are important signaling centers for neural tube patterning and depend on their sensory cilia because Shh signaling is essential for patterning (Dessaud et al., 2008). Whether PCP is important for ciliary positioning in this tissue is not answered till now.

Taken together, we showed that *Fltp* reporter is expressed in known ciliated tissues that depend on PCP as well as in ciliated tissues where PCP has not yet been involved in tissue or cell type-specific functions. The kidney harbors ciliated cells and is known to depend on PCP for tubule morphogenesis (Karner et al., 2009). *Fltp* reporter gene expression and mRNA studies show only a low expression of *Fltp* in the kidney. Why some ciliated tissues show *Fltp* expression whereas other do not, remains unanswered. One possibility could be that Fltp modifies the PCP response towards precise ciliary positioning whereas other PCP dependent tissues do not have to position their cilia on a distinct side of the cell.

4.5.2 *Flattop* expression compared to *Flattop* lineage tracing

As mentioned earlier we also generated and analyzed a mouse line for genetic lineage tracing and conditional gene inactivation that we called $Fltp^{T2AiCre}$ (Lange et al., 2012). In this section I compare the similarities and discuss the differences of live *Fltp* reporter gene expression and genetic lineage tracing.

At E7.5 both, Fltp reporter and lineage positive cells are restricted to the murine embryonic node. One day later, expression and lineage are still visible in the same embryonic tissues. This is consistent with the idea that node cells contribute to the floor plate and the notochord (Kinder et al., 2001). From E9.5-11.5 expression and lineage overlap with the difference that neural crest cells are lineage positive but not reporter positive. These neural crest cells must therefore be descendants from Fltp reporter positive neural tube cells.

Fltp reporter is expressed in terminally differentiated cells of the choroid plexus, the IE, and the lung. Therefore lineage equals expression in these tissues. In the brain, *Fltp* is not active in multipotent stem cells because most cells that are reporter positive are terminally differentiated. Nevertheless, it cannot be excluded that a subset of Fltp reporter positive cells are progenitor cells generating only terminally differentiated ciliated cells of the ependyma and the choroid plexi. Contrary to the results of the reporter gene expression, Fltp lineage positive cells were also found in the olfactory bulb (OB). Neurons migrate through the rostro-migratory stream from the subependymal zone, where they are born, to the OB. This observation suggests that Fltp positive cells do not only give rise to terminally differentiated multiciliated ependymal cells but also to new born neurons that migrate to the OB. Unfortunately, we do not know if Fltp positive cells also locate to the rostro-migratory stream. Nevertheless, it is not possible that these cells just turn on *Fltp* when they arrive at the OB because then we would detect them by reporter gene expression. Fltp could also be cell-cycle dependently regulated and we might not see *Fltp* expression in the OB as it is only on for a very short time window.

Regarding the IE, expression perfectly correlates with lineage. *Fltp* reporter is expressed in sensory IE hair cells which are terminally differentiated cell types that do not have the potential to divide again.

Interestingly, in the lung, Fltp lineage positive cells are visible earlier than *Fltp* reporter gene expression. Fltp reporter positive cells can first be observed in the trachea and the main bronchi at E14.5 whereas lineage positive cells are already visible by E13.5 in the trachea and the left lung lobe as well as in the right accessory lobe. The reason might lie in the complete deletion of the gene including all exons and introns in the $Fltp^{ZV}$ mouse line. It is possible that we deleted important regulatory sequences for lung expression which are still present in the $Fltp^{T2AiCre}$ mouse line.

Latest results from the intestinal tract suggest that lineage differs from reporter gene expression. Fltp reporter is restricted to cells in close proximity to crypt stem cells. First we thought these cells might be Paneth cells due to their morphology. Now we think that at least some of these cells might be precursors for terminal differentiated enterocytes. Lineage tracing revealed that Fltp positive cells generate ribbons of cells from the base of the crypt till the tip of the villus (unpublished data from Dr. Anika Böttcher). This would suggest that a subpopulation of Lgr5 positive stem cells start to express *Fltp* (the expression profile of Lgr5 positive stem cells shows upregulated *Fltp* expression; personal communication with the Clever's lab) and subsequently divide symmetrically to generate only enterocytes that continually replace the villus epithelium. Now, it would be important to know which signals activate *Fltp* expression in the crypt stem cells and which role PCP in general plays for the crypt villus structure.

Reporter gene expression in the pancreas is restricted to the islets of Langerhans. Lineage tracing reveled that not only the islets of Langerhans but also the pancreatic ducts are lineage positive. This implicates that both tissues are descendants of the same precursor. *Fltp* reporter is expressed already very early at E10.5 in the pancreatic progenitor which supports the precursor theory. *Fltp* reporter expression is later only maintained in the endocrine islet lineage but not in the duct cells.

Here we showed that Fltp mostly marks differentiated cells that do not divide any more therefore expression equals lineage. In some tissues Fltp lineage differs from *Fltp* expression. This indicates that *Fltp* is expressed in progenitors that are able to generate different lineages.

4.5.3 The subcellular localization of Flattop suggests for a role in basal body transport

We investigated the subcellular localization of Fltp in IE hair cells of *Fltp*^{T2AiCre} mice by making use of the T2A antibody. In mature hair cells of the organ of Corti endogenous Fltp is localized at the kinocilium and the lateral side of the hair cell spreading along the basolateral cell membrane but excluding the BB (Figure 27 G). By using antibodies directed against Fltp, asymmetric localization of Fltp protein in mature hair cells could be shown (Figure 27 D, E, F). Additionally, we could detect endogenous Fltp protein in the cytoplasm of hair cells between the nucleus and the apical surface. We speculate that these hair cells are in the maturation process and are starting to transport their BB to the apical surface to nucleate the kinocilium and start the polarization process. Immature hair cells can be found in the region of the apex even at later time points. It is known from mice that the IE continues to develop over the first three postnatal weeks (Frolenkov et al., 2004). Supporting for this hypothesis is the fact that the hair cell does not show stereociliary hair bundles on the apical surface meaning that the BB has not docked yet and the kinocilium is not formed (Figure 27 A, B, C).
Fltp reporter expression in the lung starts at the onset of ciliogenesis, is restricted to multiciliated cells, and stops directly at the BADJ (Figure 28). Endogenous Fltp is localized in the cytoplasm between the nucleus and the apical surface of multiciliated epithelial lung cells (Figure 30).
Taken together, endogenous Fltp protein is located at the kinocilium, at the lateral membrane compartment of IE hair cells excluding the BB, in the cytoplasm of premature IE hair cells, and in the cytoplasm of multiciliated epithelial lung cells. This subcellular localization might indicate that Fltp is involved in ciliogenesis, more precisely, in BB transport, positioning, and docking.
Antibody specificity is shown on Western blot because lysate of *Fltp*$^{ZV/+}$ animals shows less protein than in the *WT* and even more strikingly the Fltp protein band is absent in the lysate of *Fltp*$^{ZV/ZV}$ animals. We also showed that the antibodies recognize overexpressed Fltp protein on Western blot (Figure 18). Moreover, different polyclonal antibodies for Fltp show the same restricted localization in the node and it is very unlikely that different antibodies generated against the same peptide recognize the same unspecific protein (Figure 19 N). This restricted node expression pattern is consistent with the mRNA expression as well as with the reporter gene expression and the lineage tracing studies (Lange et al., 2012; Tamplin et al., 2008). With these antibodies we detected the endogenous Fltp protein in the lung in *Fltp*$^{ZV/+}$ and *WT* animals but the staining is absent in *Fltp*$^{ZV/ZV}$ animals demonstrating their specificity (Figure 30). On top we show that monoclonal antibodies generated against the T2A peptide also show the same restricted expression pattern in the node. We already published the specificity for the T2A antibodies on immunohistochemistry as well as on Western blot (Lange et al., 2012). Taken together, we showed the same specific staining with different antibodies generated against different peptides suggesting that the antibodies show endogenous Fltp localization.

4.5.4 Inactivation of Flattop leads to PCP defects

We know that *Fltp* reporter is expressed in ciliated tissues depending on PCP. Therefore, we examined the loss-of-function phenotype of *Fltp* with major focus on tissues depending on PCP.
The first phenotype we observed in the *Fltp*$^{ZV/ZV}$ mutant mice was the exencephalus phenotype at E13.5. This neural tube closure defect phenocopies the phenotypes associated with genes involved in the PCP signaling pathway. It is well known that loss-of-function mutations in PCP genes are associated with neural tube defects (NTDs). *BBS4*$^{-/-}$ mice for example show an exencephalus phenotype very similar to the phenotype observed in *Fltp*$^{ZV/ZV}$ animals (Ross et al., 2005). It is known

that *BBS4* is involved in PCP because in addition to the exencephalus phenotype these mutants show misaligned stereociliary hair bundles in the organ of Corti, a phenotype specific for PCP mutants. This exencephalus phenotype, more precisely anencephaly, and in our case holoanencephaly because mid- and hindbrain regions are affected, is caused by a failure of closure two during the process of neural tube closure (Copp and Greene, 2010). NTDs in PCP mutants are most likely due to CE movement defects which lead to a broadened neural fold that is not able to close properly because of the large distance between the rims of the neural folds. The most severe form of NTDs is the craniorachischisis. Craniorachischisis only manifests in homozygous mutations of core PCP genes or double heterozygous mutations of core PCP gens with other members of the non-canonical Wnt pathway. We think that Fltp is not a novel core PCP protein but rather a PCP effector gene that interacts with proteins of the PCP network. Therefore, we do not expect craniorachischisis in $Fltp^{ZV/ZV}$ mice. Other PCP effectors like *Inturned* and *Fuzzy* do not show CE defects or craniorachischisis either (see 2.8.4). Unfortunately, we had no possibility to cross $Fltp^{ZV}$ mice into $Vangl2^{LP}$ animals to see if a more severe NTD arises in double heterozygous animals. Nevertheless, we crossed the $Fltp^{ZV}$ mouse line with the $Celsr1^{crsh}$ line but could not observe a NTD in double heterozygous mice. The exencephaly phenotype could only be observed in homozygous animals of heterozygous intercrosses of the first generation of $Fltp^{ZV}$ mice crossed into the CD1 strain. Later generations on the CD1, the 129, and the Bl6 background did not show an exencephalus phenotype or other NTD. Right now we have generated new chimeras and try to recover the right background to observe NTD. Nevertheless, this NTD prompted us to investigate $Fltp^{ZV}$ animals for additional PCP specific defects. The most sensitive organ to study PCP defects is the organ of Corti in the IE. Here, sensory hair cells are aligned in four rows with their kinocilium always located precisely at the lateral side of the hair cell which results in a highly ordered structure.

The IE phenotype can clearly be explained by defective ciliary positioning in the sensory hair cells. Ciliogenesis is a multistep process that requires interaction of transport molecules with centrosomal proteins as well as asymmetrically localized molecules that provide positional information. In the IEs of $Fltp^{ZV}$ animals we could observe mispositioning of the kinocilium on the apical surface of hair cells. This is the result of defective BB rearrangement, a well-known PCP defect. During establishment of the characteristic medial to lateral polarity in the hair cells the first step is docking of the future BB to the center of the apical surface. For this, proteins of the transport machinery have to guide the centrosome from a cytoplasmic position near the nucleus to the apical surface. During ciliogenesis the BB and the kinocilium are getting repositioned via cytoskeletal rearrangement events as a result of PCP signaling. Wnt7a and Wnt5a are known mediators of PCP signaling and the current knowledge suggests that the cilium might act as a receiver for Wnts or other unknown regulators of PCP. The BB is transported to the lateral side of the IE hair cell where asymmetrically localized proteins of the PCP pathway like Fz and Dsh are anchored to the apico-lateral membrane. The IE phenotype clearly demonstrates defective PCP. Not only that the hair cells lost their polarization but also CE movement defects could be observed, most prominent in the appearance of a fourth outer hair cell row. Shortening of the cochlear duct could not be observed and if, there is only a slight difference. We analyzed *WT*, $Fltp^{ZV/+}$, and $Fltp^{ZV/ZV}$ littermates in generation two (G2) on the 129S2 background and could identify eight different $Fltp^{ZV/+}$ animals with an obvious IE phenotype. In contrast we only identified one $Fltp^{ZV/ZV}$ animal with a short region of four hair cell rows. The rest was phenotypically normal. A possible explanation is that all homozygous animals of 129S2 G2 with severe phenotypes die during embryogenesis and the one that survive are escapers where the phenotype is not pronounced. This hypothesis is also supported by the Mendelian ratio observed in 129S2 G2 where the homozygous animals are significantly underrepresented (see 3.3.1.1).

It is not a rare event that phenotypes are background dependent. For example the *BBS* phenotypes are also low penetrance, differ from group to group, and are genetic background dependent (Ross et al., 2005; Zhang et al., 2012). Zhang et al. have shown that *BBS4*$^{-/-}$ did not show the reported phenotype neither on the 129 nor on the Bl6 background. Their mice were generated via homologues recombination whereas the mice showing a phenotype were generated via the gene trap methodology.

To analyze a possible mislocalization of PCP proteins in the IE of *Fltp*^{ZV} animals we use an anti-Scribble (Scrib) antibody. Scrib was originally identified as a protein of the Scrib-Dlg-Lgl complex important for establishment of the basolateral membrane identity. These days it is also implicated in PCP signaling. Double heterozygous *Vangl2*^{LP}; *Scrib* mice show craniorachischisis the most severe NTD that is only found in mutants with defective PCP signaling. Scrib antibody staining revealed a horseshoe like localization near the nucleus that always points towards the lateral side of the sensory hair cell in *Fltp*$^{T2AiCre/+}$ mice. In homozygous *Fltp*^{ZV} mice Scrib localization was found to be more random. We could only observe this in one mouse each genotype. The Phalloidin staining at the apical surface did not work so I cannot make any comments about the influence of Scrib localization on the orientation of the stereociliary hair bundles. Obviously, the homozygous *Fltp*^{ZV} animal did not show a fourth outer hair cell row opening the question how Scrib staining would look in animals with an obvious IE phenotype. This could not be tested because 129S2 G2 animals are lost and the phenotype of G4 is not as pronounced. Nevertheless, we could demonstrate a clear PCP phenotype in the organ of Corti of *Fltp*^{ZV} animals.

Recently, it was reported that mice defective for PCP signaling show a specific lung phenotype with constricted airways and lung branching morphogenesis defects (Yates et al., 2010). In contrast to the findings described in this publication we could not observe smaller lungs or branching defects in *Fltp*^{ZV} animals. But, consistently, we could observe constricted airways in *Fltp*^{ZV} animals most prominent in the distal airways. To quantify this phenotype I measured the distal airway diameters resulting in a significant decrease from *WT* over heterozygous to homozygous *Fltp*^{ZV} animals. In addition, we noticed that the epithelium was disorganized and sometimes multilayered. The disorganization in *Vangl*^{LP} and *Celsr1*^{crsh} mice were a result of a disruption of the cytoskeleton in these mutants (Yates et al., 2010). The narrowed lumen of the airways in these mutants was most likely the result of the disorganization of the airway epithelium. Again, *Fltp* is a PCP effector gene rather than a core PCP gene therefore we do not expect as strong phenotypes as for core PCP mutants.

As all the phenotypes observed above implicate the involvement of Fltp in PCP we tested whether *Fltp* genetically interacts with one of the core PCP genes *Celsr1*. All animals homozygous for *Celsr1*^{crsh} show craniorachischisis and the loop tail phenotype independently of *Fltp*. Double heterozygous animals did also not show craniorachischisis or the loop tail phenotype. Double homozygous *Fltp*^{ZV}*; Celsr1*^{crsh} animals show severe skeletal malformations in both hindlimbs together with severely rotated IE hair cells. Recent observations suggest that disruption of PCP signaling through mislocalization of Vangl2 in chondrocytes leads to skeletal defects in limb patterning (Gao et al., 2011). *Vangl2*$^{Lp/Lp}$; *Ror2*$^{-/-}$ double knock-out mice show malformations of the forelimbs including the digits. In contrast, double homozygous *Fltp*^{ZV}*; Celsr1*^{crsh} animals show server malformations of both hindlimbs. This suggests that *Fltp* together with *Celsr1* regulates hindlimb development and the developmental molecular program differs from fore- to hindlimbs. Where this limb deformation phenotype has its molecular origin and whether *Fltp* influences the chondrocyte function or development is not known up to now. Because the limbs are not shortened we think the defect does

not lie in elongation processes but in proper bone formation. To answer this question we will perform skeletal preparations of the hindlimbs.

The *Fltp*^{zv} phenotype in IE hair cells is not as severe as it is in core PCP mutants like *Celsr1*$^{crsh/crsh}$. Nevertheless, the phenotype of *Fltp*$^{zv/zv}$*; Celsr1*$^{crsh/crsh}$ double homozygous and double heterozygous mice is more severe than both homozygous mutations alone. We noticed a fourth outer hair cell row in double homozygous mice which clearly represents the *Fltp*^{zv} phenotype and does not occur in *Celsr1*^{crsh} animals. Additionally, we found more severely rotated hair cells in double homozygous animals. In *Celsr1*^{crsh} animals the most severe phenotype is prominent near the apex. In double homozygous animals it already starts farther away from the apex. These results suggest that *Fltp* and *Celsr1* genetically interact consequently placing *Fltp* in the PCP pathway.

Nevertheless, the problem is the genetic background of these mice. *Celsr1*^{crsh} mice are on a rather mixed background (C3H/HeH;101/H;BALB/c) whereas *Fltp*^{zv} mice were kept on a 129S2/SvPasCrlCD1 background. To what extend the phenotype would increase in an inbred strain remains unclear. Therefore, the variation of phenotypes and penetrance can be partially explained by the genetic background differences. However, the genetic interaction of *Fltp* and *Celsr1* suggests that Fltp can modify PCP signaling in the mammalian embryo.

Taken together, the identified *Fltp*^{zv} phenotypes are highly characteristic of phenotypes observed in PCP mutants. *Fltp*^{zv} animals show exencephaly, disrupted IE hair cell arrangement, constricted distal airways in the lung, as well as a genetic interaction with the core PCP gene *Celsr1* manifesting in a skeletal limb defect and IE hair cell misalignment. Moreover, we could show that ciliogenesis in the lung is impaired and endogenous Fltp protein is localized asymmetrically in IE hair cells and around the BB. These observations strongly suggest that Fltp is involved in PCP dependent BB transport and positioning.

4.5.5 Flattop functions in basal body transport, docking, and localization

Complete failure of directed BB transport can result in absence of cilia leading to severe ciliopathies including syndromes like polycystic kidney disease, hydrocephalus, *situs inversus*, blindness, chronic bronchitis, obesity, and most likely also cancer as well as diabetes. Milder forms of BB transport/positioning defects can lead to a delay in ciliogenesis or defects in ciliary positioning. In this paragraph I show a line of evidence that implicates Fltp in BB transport, docking, and localization.

Fltp reporter expression in the lung starts at the onset of ciliogenesis, is restricted to multiciliated cells, and stops directly at the BADJ (Figure 28). Moreover, endogenous Fltp is located in the cytoplasm of multiciliated epithelial lung cells between the nucleus and the apical surface (Figure 30). Additionally, we noticed that ciliogenesis in *Fltp*^{zv} animals was severely impaired. In distal airways of *Fltp*$^{zv/+}$ as well as *Fltp*$^{zv/zv}$ animals we found cells with notably shorter and misshapen cilia. We could observe cells with absolutely no cilia in *Fltp*$^{zv/zv}$ mice. In multiciliated epithelial cells of *Fltp*^{zv} mutant mice we could observe BBs stuck in the cytoplasm whereas all BBs in *WT* littermates were docked at the apical surface where they project cilia into the lumen (Figure 41). In P30 animals we could also identify cells without cilia but less than in P7 animals. This indicates that *Fltp*^{zv} mutant cells are able to form cilia but not as effective as *WT* cells. Therefore, we hypothesize that Fltp is a positive modulator for BB transport. At both stages we could identify cilia in the trachea and the main bronchi. One possibility could be that the BBs in the larger airways are already docked even in homozygous *Fltp*^{zv} mutant mice because ciliogenesis in these airways starts earlier than in the distal

airways. Another possibility might be that the distal airway epithelium is more prone to defects in BB docking. Therefore, the phenotype is restricted to distal airway epithelium.
To confirm the phenotype observed *in vivo* we performed *in vitro* MTEC cultures which we switched to ALI cultures when the cells were confluent. In a time resolved manner we analyzed the BB docking mechanism in *WT*, heterozygous and homozygous *Fltp*^{ZV} mice. *WT* cells showed a complete overlap of ZO-1, an apical membrane marker, and pericentrin suggesting that the BBs are docked at the apical surface and project cilia into the environment. Interestingly, in *Fltp*$^{ZV/+}$ as well as in *Fltp*$^{ZV/ZV}$ cells at day three after the switch to ALI the majority of BBs is in the cytoplasm and not docked at the apical surface suggesting that these cells did not form any cilia. Next, we analyzed whether these cells have cilia and how many. For the *WT* cells we saw the expected cilia at the apical surface. Each BB is docked and has assembled a cilium. No "free" BBs are detectable. In contrast, *Fltp*$^{ZV/+}$ cells showed only some cilia whereas the rest of the BBs were not yet docked. *Fltp*$^{ZV/ZV}$ cells often did not show any cilia. At day seven the *WT* shows docked BBs and cilia. The heterozygous *Fltp*^{ZV} cells sometimes showed docked BBs with cilia and some earlier stages with no docked BBs. The homozygous *Fltp*^{ZV} cells showed only a few docked BBs with cilia the rest was not docked yet. It can be argued that the cells with "free" BBs are just in the process of BB docking but if we compare mutant *Fltp*^{ZV} with *WT* cells we could observe a significantly higher amount of cells being in the BB docking phase in the mutant than in the *WT* cells. This observation strongly suggests that we observed a Fltp specific defect in the BB docking process.
By making use of the ALI culture system we could confirm the absence of cilia phenotype from the *in vivo* studies. With this *in vitro* culture system we were able to show that loss of Fltp protein leads to a delay in BB docking consequently resulting in a delay of ciliogenesis. These results suggest that Fltp functions as a positive modulator for BB transport. BB transport is not inhibited but Fltp increases the efficiency of the apical transport.
Evidence for a role of Fltp in BB transport and positioning shows the localization of Fltp protein in the IE as well as the loss of gene function phenotype in the IE. In immature hair cells we could detect endogenous Fltp protein in the cytoplasm between the nucleus and the apical surface indicating ongoing BB transport. After the transport process endogenous Fltp protein is localized asymmetrically on the lateral side of mature hair cells indicating that Fltp interacts with asymmetrically localized PCP molecules (Figure 27 D, E, F). This interaction is defective in *Fltp*^{ZV} mutant mice resulting in misorientation of the stereociliary hair bundles (Figure 38).

4.5.6 Flattop interacts with Discs large 3 to transport the basal body to the apical surface

Discs large 3 (Dlg3) is a molecule involved in apical-basal polarity as well as in PCP because we showed that loss-of-function of *Dlg3* leads to a PCP like phenotype in IE hair cells and to a NTD (Van Campenhout et al., 2011). Moreover, in *Drosophila*, Dlg3 complexes with Scrib which is involved in PCP in vertebrates (Courbard et al., 2009). Additionally, Dlg3 harbors a SH3 domain which is known to interact with PRRs. Therefore, we tested whether the two identified PRRs in the Fltp protein are functional and show the predicted interaction with SH3 domains in a candidate approach. We could show that Fltp and Dlg3 physically interact only in serum starved HEK293T cells. Serum starved cells exit the cell cycle, transport their centrosome to the apical surface, and nucleate a cilium. This is consistent with the observation that *Fltp* is only expressed in cells starting the ciliogenesis process. By deleting different parts of Fltp and Dlg3 we right now try to map the exact interaction site.

We performed immunohistochemistry to confirm the physical interaction by co-localization studies. Notably, we could show an asymmetric localization of Dlg3-Venus fusion protein in IE hair cells. Dlg3-Venus is located at the apical lateral membrane exactly like Fltp. Similar to Fltp, the staining also excludes a hole in front of the vertex of the stereocilia, the region where the BB is anchored to the apical membrane (data not shown). We could show that Fltp and Dlg3 physically interact and co-localize in IE hair cells at the lateral side. To analyze the influence of Fltp protein on Dlg3 localization we generated a *Fltp*$^{zv/zv}$; *Dlg3:Venus* mouse. We could show that upon *Fltp* deletion Dlg3 is not localized at the apical lateral membrane anymore. This would suggest that the positional information for the localization is transmitted via Fltp. Consequently, Fltp has to interact with an asymmetrically localized PCP molecule located on the lateral side of IE hair cells. Known PCP molecules establishing the lateral identity in the sensory cells of the IE are Frizzled (Fzd), Dishevelled (Dvl), and Diego (Dgo). Unfortunately we could not identify one of these PCP molecules among the interaction partner list obtained from HEK293T cells. Most likely because PCP signaling is not activated in HEK293T cells as they are not planar polarized.

4.5.7 Hypothetical molecular function of Flattop

Because of all this data presented and discussed above we tried to build a hypothetical model of Fltp protein function. We believe that Fltp regulates BB transport, docking, as well as localization. Moreover, we suggest that *Fltp* is a PCP effector gene that is important for trafficking cargo (proteins of the BB and other proteins) to their designated places in the cell.

Studies in *Drosophila* have shown that establishment of PCP relies on the transport of Fz containing vesicles to a distinct side of the cell. Vesicle transport depends on the conserved proteins of the exocyst complex like Sec6, 8, 10, as well as Rab8. Core PCP mutants exhibit defects in polarized vesicle trafficking. Strikingly, Dvl controls the recruitment of Sec8 to the BB (Park et al., 2008b), Fuzzy is essential for trafficking of cargo to BBs and to the apical tips of cilia (Gray et al., 2009), and Fritz controls septin localization and therefore is crucial for collective cell movement and ciliogenesis (Kim et al., 2010). Additionally, PTK7 is regulating membrane trafficking of Dvl in two ways: first by interacting with the downstream effector molecule, Receptor of Activated Protein Kinase C1 (RACK1), and second by interaction with Fz7 (Yen et al., 2009).

The Fltp interactome has identified different centrosomal proteins as potential interaction partners. Fltp could bind via one of the centrosomal proteins to the BB. We have shown that Fltp and Dlg3 physically interact and co-localize at the lateral side of IE hair cells. Moreover, loss of Fltp leads to mislocalization of Dlg3-Venus fusion protein. Therefore, we speculate that Dlg3 binds to the Fltp-BB complex (Figure 50). It has been shown that apical transport of BBs depends on regulated actin assembly and vesicle trafficking (Boisvieux-Ulrich et al., 1990; Dawe et al., 2007; Sorokin, 1968). Sec8, an exocyst component involved in vesicle trafficking, is involved in BB transport mediated by the core PCP protein Dvl and membrane bound vesicles. During BB docking Dvl interacts with the PCP effector Inturned to activate the Rho-GTPase specifically at the apical surface of ciliated epithelial cells (Park et al., 2008b). It has been shown previously that Dlg3 interacts with Sec8 (Sans et al., 2003). Dlg3 could possibly facilitate the recruitment of Sec8 positive exocytic vesicles for apical transport of the Fltp-BB complex similar to the function of Dvl. Moreover, we identified the motor protein Dynein, required for apical transport, and the E3 ubiquitin ligase Nedd4-2 which is involved in protein trafficking as interaction partners for Dlg3 (Van Campenhout et al., 2011). Therefore, we speculate that the BB-Fltp-Dlg3 complexes with Dynein and Sec8 to mediate BB transport to the apical cell

surface (Figure 50). We could show that Fltp co-localizes with acetylated-tubulin at the apical membrane. In mature IE hair cells the kinocilium is located precisely at the vertex of each V-shaped stereociliary bundle which is anchored to the cuticular plate. The cuticular plate is composed of a meshwork of cross-linked actin filaments and associated cytoskeletal proteins. The BB is located in a pocket at the lateral side of the hair cell and is excluded from the cuticular plate. The BB connects the actin filaments of the cuticular plate to apical MTs surrounding the periphery of the cell and spread along the lateral cell membranes. This indicates that Fltp interacts with the tubulin network to stabilize the BB at the apical-lateral surface (Figure 50). Moreover, apical actin is required for fusion of the exocytic vesicles to the plasma membrane (Lanzetti, 2007).

Additionally, the Dlg3-Fltp-BB complex could interact with the TJ complex. Sans et al. identified the TJ protein TJ-associated protein 1 (TJAP1) as an interaction partner of Dlg3 (Sans et al., 2003). The BB-Fltp-Dlg3 multiprotein complex therefore might be anchored via Dlg3 to the TJs (Figure 50). In addition, co-localization of Dlg3 and ZO-1 in hair cells has been shown. Upon Fltp deletion Dlg is not localized at the lateral side anymore suggesting that Fltp is important for the asymmetric localization. Therefore, Fltp has to interact with a PCP molecule to asymmetrically position the BB. This molecule has not been identified yet. Due to Fltp localization and function Dvl would be an interesting candidate for providing the positional information.

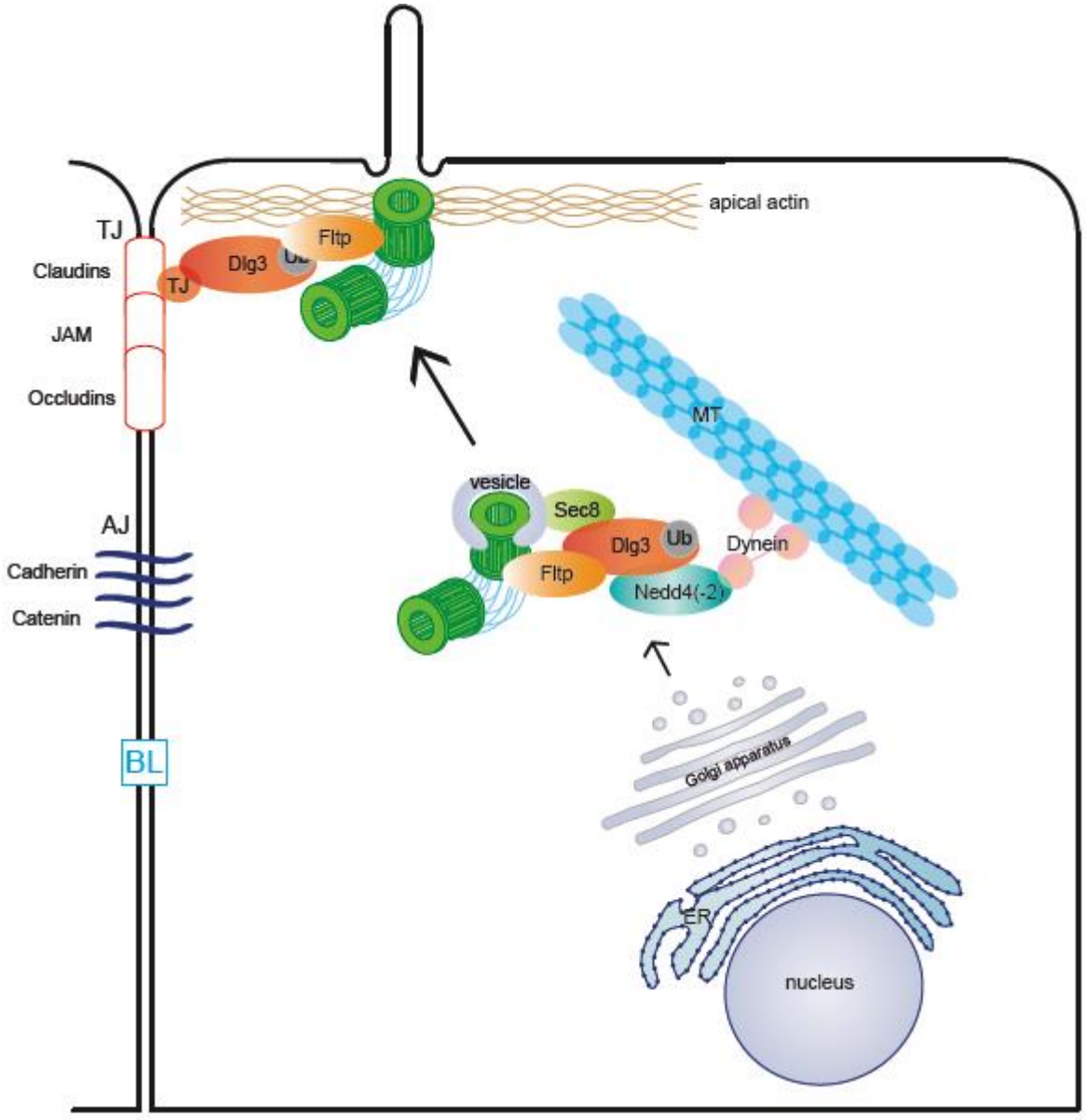

Figure 50 Hypothetical function of Fltp

Fltp binds to Dlg3 and proteins of the BB. Dlg3 associates with Sec8 and Nedd4(-2). Sec8 provides the link for the BB-Fltp-Dlg3-Nedd4(-2) complex to the vesicle important for BB transport. Nedd4(-2) associates with Dynein which allows transport of this complex to the apical surface. At the apical surface the BB-Fltp-Dlg3 complex is targeted to the tight junction (TJ) complex via TJ proteins. Fltp interacts with apical actin.
Abbreviations: basolateral (BL); adherens junction (AJ); microtubule (MT); endoplasmic reticulum (ER); junctional adhesion molecule (JAM)

These observations might suggest that the common mediator between PCP and ciliogenesis might be the proteins important for polarized transport of specific cargo.
Dvl, Inturned, Sec8, and Rho comprise the framework of BB transport and anchoring to the apical surface of ciliated cells. We identified at least one more protein (Fltp) involved in this process. The identification of Fltp as a new molecule involved in targeted BB transport is an important observation because till now it is not exactly known which molecular mechanisms are involved in positional docking of the mother centriole and how the translation from asymmetric PCP information to BB

positioning is mediated (Santos and Reiter, 2010). The BB-Fltp-Dlg3 complex might influence the Dvl, Inturned, and Sec8 mediated apical BB transport in a positive way. For the special case of the IE, Dvl is located at the lateral side of the hair cells exactly like Fltp emphasizing their potential interaction in BB transport. Additionally, this asymmetrically localized core PCP gene would be the ideal candidate for the yet unsolved asymmetric distribution of Fltp in these cells. In addition, this study adds a new molecule to the not yet fully understood molecular mechanism of multiciliated cell ciliogenesis.

4.5.8 Flattop as a marker for early postmitotic cells

We recognized that Fltp reporter positive cells in the lung epithelium often are in close contact with each other. They mostly appear as doublets. Over 90% of Fltp reporter positive cells in the lung epithelium are postmitotic multiciliated cells. Only about 10% seem not to be associated with cilia but instead are T1α positive. T1α is a marker for basal cells which are assumed to be the lung stem cells in mice. T1α positive cells are capable of self-renewal and can differentiate into the ciliated and secretory lineages (Rock and Hogan, 2011). We speculate that the T1α Fltp double positive cells undergo symmetric division in most cases, initiate the ciliogenesis program and finally differentiate into multiciliated cells. If our speculation that Fltp positive basal cells generate ciliated cells is correct, and we have evidence, than we could answer the question whether basal cells directly generate ciliated cells or if they have to go through an obligate Scgb1a1 positive intermediate stage. This question is not yet answered. To proof that basal cells expressing *Fltp* become ciliated cells all ciliated cells could be erased by naphthalene treatment and renewal of the ciliated cells over time could be analyzed. First Fltp positive basal cells should appear which repopulate the epithelium by differentiating into ciliated cells.

Further evidence comes from the MTEC and ALI cultures. Here we observe patches of Fltp reporter positive cells. In most cases two or a multiple of two cells were located next to each other suggesting that these cells arose from a common basal progenitor. Moreover, onset of *Fltp* reporter gene expression directly correlates with onset of ciliogenesis in these cultures.

Because of the location of Fltp reporter positive cells in the testis we assume that the expression is restricted to the primary spermatocytes, maybe to the secondary spermatocytes, as well as the spermatids. *Fltp* reporter gene is definitely absent in the spermatogonia which are the dividing cells that generate the primary spermatocytes via mitosis. No signal could be detected in the differentiated spermatids. After the first mitotic division of the spermatogonia two meiotic divisions follow till the haploid gametes are generated. If Fltp is cell cycle regulated and turns on after mitosis than this expression pattern would make sense. On the other hand it is not known if PCP plays a role in these cells and if they are ciliated. For *Drosophila* it is known that primary spermatocytes are ciliated.

We also analyzed *Fltp* reporter expression in the intestinal tract. We noticed that Fltp reporter positive cells could be detected in the crypt stem cell compartment of isolated crypts as well as of histological sections of intestinal tracts of adult mice. We wondered if PCP also plays a role in maintaining crypt stem cell compartment identity and if these cells are ciliated. These questions remain to be answered. Interestingly, we again could observe Fltp positive cells appearing as doublets in the crypt stem cell compartment. We speculate because of their position, their pair wise alignment, as well as their round cell shape that these cells might be right after division. Some of the reporter positive cells even lost their E-cadherin expression suggestive for loss of cell-cell adhesion complexes a theme common for cells after division. We further speculate that these are transient

amplifying cells generated from Lrg5 positive stem cells. In expression profile analysis of Lgr5 positive crypt stem cells *Fltp* is upregulated (personal communication with the Clevers lab). Lineage tracing analysis revealed that Fltp positive cells generate ribbons of cells located from the base of the crypt till the villus (unpublished data from Dr. Anika Böttcher). To which cell type Fltp positive cells give rise to in the intestine is not known till now. We speculate that these cells might be enterocytes because of their abundance in the intestinal epithelium. We could identify Fltp, Foxa2, a potential marker for crypt stem cells, double positive cells (unpublished data from Dr. Ingo Burtscher). These cells are in an intermediate stage between stem cell and differentiating cell and possibly the precursors for the enterocytic lineage. These observations indicate that intestinal crypt stem cells divide symmetrically generating two identical daughter cells that give rise to a specific, maybe enterocytic, cell lineage in the intestinal epithelium.

Analyses of the murine brain revealed that *Fltp* reporter gene expression can be detected in the ependymal cells of the ventricular wall as well as in the dentate gyrus, both neurogenic regions of the adult brain. Stem cells of the ependymal zone in the brain reside in the subependymal zone and project a single cilium into the ventricle. *Fltp* reporter expression is restricted to the most apical ciliated cells. Fltp positive stem cells could not be observed. It would be interesting to know if Fltp positive transient amplifying cells can be found that generate ciliated cells either via asymmetric or symmetric cell division. It is clear that Fltp positive cells only generate one specific postmitotic cell type in this case multiciliated ependymal and choroid plexus cells. This could also be demonstrated by lineage tracing experiments where we only find post mitotic multiciliated cells positive for the Fltp lineage. The other area where we identified strong reporter gene expression was the dentate gyrus. Regarding the position of the cells we can exclude that stem cells express the *Fltp* reporter. We rather speculate that transient amplifying cells are Fltp reporter positive. To which lineage they give rise in the dentate gyrus is unknown.

In the main olfactory epithelium *Fltp* reporter is expressed in the olfactory sensory neurons (OSN). These cells differentiate from proliferative basal cells that are located basally of the OSN (Jenkins et al., 2009). Again we can speculate that the basal cells generate OSN through an Fltp positive intermediate that divides symmetrically. The OSN are terminally differentiated cell types that harbor cilia and depend most likely on PCP.

Taken together, *Fltp* reporter is expressed in close vicinity to the stem cell compartments of the lung (basal cells), the testis (spermatogonia), the intestinal tract (crypt stem cells), the brain (subependymal zone and dentate gyrus) and the main olfactory epithelium (basal cells) in cells after division. Moreover, a small number of Fltp positive cells are in addition positive for progenitor cell markers.

4.5.9 Conclusion

The discovery and the analysis of the novel PCP effector gene *Fltp* contribute to the open question how asymmetric PCP information is translated into targeted BB transport. In this study a new piece to the mosaic of targeted BB transport has been added and this helps for more detailed elucidation of this pathway in future studies. Additionally, a new member of the small group of PCP effector molecules has been identified and Fltp might be a marker for progeny of stem cells after symmetric division differentiating into a postmitotic ciliated cell lineage depending on PCP.

Fltp^{zv} mutant mice show low penetrance exencephaly which is genetic background dependent. Upon deletion of *Fltp* in the IE stereociliary bundles are misorientated and a fourth outer hair cell row is

present. Again, this phenotype shows low penetrance and is background dependent. Fltp dysfunction in the lung can lead to abnormal epithelial cell arrangements and reduced diameter of distal airways. Moreover, we showed that loss of Fltp protein leads to a delay in BB docking *in vivo* and *in vitro*. We could also present a genetic interaction of *Fltp* and the core PCP gene *Celsr1* which allows us to integrate Fltp in the PCP pathway. This genetic interaction is manifested by defective limb patterning as well as IE hair cell arrangement. In these distinct ciliated tissues Fltp functions as a positive modulator for BB transport. Additionally, Fltp reporter most likely marks the progeny of symmetrically divided stem cells which differentiate and upregulate proteins of the ciliogenesis machinery. The involvement of Fltp during ciliogenesis can be summarized as follows: first, the prospective ciliated cells induce *Fltp* expression, second, these cells start the amplification of their BBs, third, Fltp assists to transport the BBs to the apical membrane, fourth, the BBs dock together with Fltp at the apical membrane and in some cell types get repositioned with the help of Fltp and PCP molecules, and in the end, the cells build one or more motile or immotile cilia.

Due to the restricted expression pattern of *Fltp* it might be involved in ciliopathies which are disease affecting ciliated tissues. The great spectrum of ciliopathies includes defects of left-right asymmetry, male infertility, blindness, polycystic kidney disease, hydrocephalus, chronic bronchitis, obesity, and possibly also cancer as well as diabetes (Hildebrandt et al., 2011). *Fltp* could also be involved in olfactory senses, in hearing loss as well as in diabetes. To analyze these functions in more detail $Fltp^{zV}$ mice could be crossed into other mouse lines mutant for PCP molecules or BB transport proteins. By this genetic interactions could be identified and maybe the phenotypes will enhance.

Taken together, we showed that $Fltp^{zV}$ animals show distinct PCP phenotypes, *Fltp* reporter gene is expressed in distinct mono- and multiciliated cells, and Fltp might be a marker for symmetric divisions of distinct stem cell types.

5 Material and methods

5.1 Material

5.1.1 Equipment

Centrifuges	5417 R (Eppendorf AG, Hamburg)
	5417 C (Eppendorf AG, Hamburg)
	5804 R (Eppendorf AG, Hamburg)
	Haereus Rotanta 460R (Thermo Fisher Scientific Inc., Waltham)
	Hettich Universal 30F (Andreas Hettich GmbH & Co. KG, Tuttlingen)
	1-14 (Sigma Laborzentrifugen GmbH, Osterode am Harz)
	Galaxy Mini (VWR International GmbH, Darmstadt)
Incubation systems/ovens	Shaking incubator; 37°C bacteria (Shel Lab, Sheldon Manufacturing, Cornelius)
	TH-30 and SM-30; 32°C bacteria (Edmund Bühler GmbH, Hechingen)
	65°C Southern Blot
	Thermomixer comfort (Eppendorf AG, Hamburg)
	Shake'n'Stack (ThermoHybaid, (Thermo Fisher Scientifi c Inc., Waltham)
Electroporation system	BioRad Gene Pulser Xcell (BioRad Laboratories, München)
Power suppliers	Power Pack Basic (BioRad Laboratories, München)
Agarose gel chamber	Midi 450 (Harnischmacher, Kassel)
Gel documentation system	UV-Transilluminator (Biorad, München)
	Gene Flash (Syngene Bio Imaging, Synoptics Ltd, Cambridge)
Pipettes	1000 µl / 100 µl / 20 µl / 10 µl Eppendorf Research (Eppendorf AG, Hamburg)
	Pipettboy accu-jet and accu-jet® pro (Brand GmbH & Co. KG, Wertheim)
Photometer	BioPhotometer (Eppendorf)
	ND-1000 Spectrophotometer (NanoDrop, (Thermo Fisher Scientific Inc., Waltham))
Polyacrylamid gel preparation	(BioRad)
Polyacrylamid gel chamber	Mini Trans-Blot® Cell (BioRad GmbH, Heidelberg)
Western Blot semi-dry system	Trans-Blot® SD, Semi-Dry Transfer cell (Biorad, Heidelberg)
PCR machines	Px2 ThermoHybaid (Thermo Fisher Scientific Inc., Waltham)
	PXE0.2 Thermo Cycler (Thermo Fisher Scientific Inc.Waltham)
FACS	FACS Calibur (Becton and Dickinson and Company, Franklin Lakes)
Balances	ScoutTM Pro (OHAUS)
	(Sartorius)
Vortexer	Vortexer (VWR international GmbH, Darmstadt)
Rotator/tumbler	VSR 23 (Grant BOEKEL, VWR international GmbH,Darmstadt)
Roller Mixer	SRT1 (Bibby Scientifi c (Stuart), Staffordshire, GB)
Water bath	VWR

pH meter	pH211 Microprocessor pH Meter (HANNA instruments Deutschland GmbH, Kehl am Rhein)
Pumps	LABOPORT ® (neoLab Migge Laborbedarf-Vertriebs GmbH, Heidelberg)
Hybridisation tubes	Hybridizer HB 100 (ThermoHybaid, (Thermo Fisher Scientific Inc., Waltham)
Film cassettes	Hypercassette (Amersham, GE Healthcare GmbH, München)
Developing machine	AGFA Curix 60 developing machine (AGFA HealthCare GmbH, Bonn)
Radiation monitor	Berthold LB122 radiation monitor (BERTHOLD TECHNOLOGIES GmbH & Co. KG, Bad Wildbach)
Microscopes	Axiovert 200M (Carl Zeiss AG, Göttingen) Lumar.V12 (Carl Zeiss AG, Göttingen) MS5 (Leica Microsystems GmbH, Wetzlar) TCS SP5 (Leica Microsystems GmbH, Wetzlar)
Cameras	AxioCam MRc5 (Carl Zeiss AG, Göttingen) AxioCam HRm (Carl Zeiss AG, Göttingen)
Microwave	700W (Severin Elektrogeräte GmbH, Sundern)
Stirrer	STIR (VWR international GmbH, Darmstadt)
Microtome	Microm HM 355 S rotation microtome (Thermo Fisher Scientific Inc., Waltham)
Glassware	Schott-Duran (Schott, Mainz)
Plastic ware	(VITLAB GmbH, Großostheim)
Counting chamber (cells)	Neubauer (LO - Laboroptik GmbH, Friedrichsdorf)
Freezer	-20°C (Liebherr Hausgeräte Ochsenhausen GmbH, Ochsenhausen)
Fridge	4°C (Liebherr Hausgeräte Ochsenhausen GmbH, Ochsenhausen)

5.1.2 Consumables

50 ml/ 15 ml tubes	(Becton and Dickinson and Company, Franklin Lakes; Sarstedt, Nürnbrecht)
14 ml tubes	BD Labware (Becton Dickinson GmbH, Heidelberg)
2 ml/ 1.5 ml	safe-lock reaction tubes (Eppendorf AG, Hamburg)
0.2 ml tubes	(Eppendorf AG, Hamburg)
15 cm/ 10 cm/ 6 cm dishes	nunc (Thermo Scientific Fisher, Wiesbaden)
6-well/ 12-well/ 24-well/ 48-well plates/ 96-well plates (straight/conical)	nunc (Thermo Scientific Fisher, Wiesbaden)
10 cm bacterial plates	BD FalconTM (Becton Dickinson GmbH, Heidelberg)
Embedding cassettes	(Carl Roth GmbH & Co. KG, Karlsruhe)
Embedding moulds	(Carl Roth GmbH & Co. KG, Karlsruhe)
50ml/ 25ml/ 10ml/ 5ml/ 2ml/ 1ml plastic pipettes	(Greiner bio-one, Frickenhausen)
Pasteur pipettes, plastic	transfer pipettes (Carl Roth GmbH & Co. KG, Karlsruhe)
Pasteur pipettes, glass	15cm/ 23cm (LABOR-BRAND, Gießen; Hirschmann Laborgeräte GmbH & Co. KG, Eberstadt)

Parafilm	Parafilm (Pechiney Plastic Packaging, Menasha)
PVDF membrane	Immun-Blot PVDF-Membrane (BioRad Laboratories, Hercules)
Nitrocellulose membrane	(GE Healthcare Buchler GmbH & Co. KG, München)
Blotting paper	Whatman paper (GE Healthcare Buchler GmbH & Co. KG, München)
Scalpels	surgical disposable scalpels B/Braun (Aesculap AG & Co. KG Tuttlingen)
Films	Kodak BioMax MS (Sigma-Aldrich GmbH, Hamburg), Amersham Hyperfilm ECL (GE Healthcare Buchler GmbH & Co. KG, München)

5.1.3 Kits

QIAquick PCR Purifi cation Kit (Qiagen Holding, Hilden)
QIAquick Gel Extraction Kit (Qiagen Holding, Hilden)
QIAgen Maxi Kit (Qiagen Holding, Hilden)
QIAgen Mini Kit (Qiagen Holding, Hilden)
RNeasy Mini Kit (Qiagen Holding, Hilden)
Labelling Kit (Roche Holding GmbH, Applied Science, Mannheim)
Nextract (Sigma-Aldrich GmbH, Hamburg)
ECL Detection Kit (Millipore Cooperation, Billerica, MA)

5.1.4 Chemicals

(Sigma-Aldrich GmbH, Hamburg, Merck KGaA, Darmstadt, Carl Roth GmbH & Co. KG, Karlsruhe)

A Acetic acid
Activin A, human (R&D Systems, Minneapolis)
Acrylamide/bisacrylamide
Agarose (Biozym Scientifi c GmbH, Hess. Oldendorf)
Ampicillin
APS
B BCA
BSA
Bradford reagent
bromine phenol blue
C Calcium chloride
Chloroform, 99+%
CI (Chloroform-Isoamylalcohol: 24:1)
D Diethylpyrocarbonate (DEPC), approx. 97%
Dimethylsulfoxide (DMSO), >99,9%
Dithiothreitol (DTT)
dNTPs (Fermentas GmbH, St. Leon-Rot)
E EDTA
Ethanol, 96%
Ethidiumbromide
F Formaldehyde

Formamide
G Gelatine
Glutamine
Glutaraldehyde
Glycerol
G418 (Geneticin, 50mg/ml, Gibco, InvitrogenTM Cooperation, Carlsbad, CA)
H HEPES (200mM, Gibco, InvitrogenTM Cooperation, Carlsbad, CA)
HEPES (powder)
HCl
I Isopropanol, 100%
K Kanamycin
L L-glutamine (200mM, Gibco, InvitrogenTM Cooperation, Carlsbad, CA)
M Magnesium chloride
Methanol, 100%
MEMs non essential amino acids (100x, Gibco, InvitrogenTM Cooperation, Carlsbad, CA)
Milk powder (Becton Dickinson GmbH, Heidelberg)
Mitomycin C
Mounting medium
MOPS
β-mercaptoethanol (50mM, Gibco, InvitrogenTM Cooperation, Carlsbad, CA)
N Nitrogen(l) (Linde AG, München)
Nuclear Fast Red
O Oligo-dT-primer (Promega GmbH, Mannheim)
P Paraformaldehyde
PBS (Gibco, InvitrogenTM Cooperation, Carlsbad, CA)
PCI (Phenol-Chloroform-Isoamylalcohol: 25:24:1; Carl Roth GmbH + Co. KG, Karlsruhe)
Penicillin/Streptomycin (Gibco, InvitrogenTM Cooperation, Carlsbad, CA)
Polyacrylamide
Potassium acetate
Puromycin
Q Q-Solution (Qiagen Holding, Hilden)
R RNaseZAP
Rotihistol
S Sodium chloride
Sodiumdodecylsulphate (SDS)
Sodium hydrogenic phosphate (Na2HPO4)
Sodium hydroxide
T TEMED
TWEEN20
Tris
Triton X-100
Trizol Reagent (Gibco, InvitrogenTM Cooperation, Karlsruhe)
X X-Gal
Xylene

5.1.5 Buffer and solutions

Isolation of genomic DNA

Proteinase K lysis buffer:	100 mM Tris, pH8.0-8.5
	5 mM EDTA, pH8.0
	2% SDS
	200 mM Sodium chloride

Plasmid preparation

P1 buffer:	50 mM Tris HCl, pH 8.0
	10 mM EDTA
	100 µg/ml RNase A
P2 buffer:	200 mM Sodium hydroxide
	1% SDS
P3 buffer:	3 M Potassium acetate, pH 5.5
QBT buffer:	750 mM Sodium chloride
	50 mM MOPS, pH 7.0
	15% Isopropanol (v/v)
	0.15% Triton X-100 (v/v)
QC buffer:	1 M Sodium chloride
	50 mM MOPS, pH 7.0
	15% Isopropanol (v/v)
QF buffer:	1.25 M Sodium chloride
	50 mM Tris HCl, pH 8.5
	15% Isopropanol
TE buffer:	10 mM Tris HCl, pH 8.0
	0.1 mM EDTA
EB buffer:	10 mM Tris HCl, pH 8.0

DNA/RNA agarose gels

TAE buffer (50x stock):	2 M Tris
	50 mM Glacial acetic acid
	50 mM EDTA
Loading buffer DNA:	100 mM EDTA
	2% SDS
	60% Glycerol
	0.2% Bromine phenol blue
	Loading buffer RNA (2x): 95% Formamide
	0.025% SDS
	0.025% Bromine phenol blue
	0.025% Xylene cyanol FF
	0.025% Ethidium bromide
	0.5mM EDTA

Southern blot

Depurination

(fragments >=10 kb):	1.1% HCl in H_2O
Denaturation (all gels):	87.66 g Sodium chloride
	20.00 g NaOH
	1000 ml H_2O (final volume)
Neutralization (all gels):	87.66 g Sodium chloride
	60.50 g Tris
	1000 ml H_2O (final volume)
	pH7.5 with HCl conc. (approx. 11 ml)
Transfer, 20x SSC (all gels):	88.23 g Tri-sodium-citrat
	175.32 g Sodium chloride
	1000 ml H_2O (final volume)
	pH7-8
Hybridisation buffer:	1 M Sodium chloride
	50 mM Tris, pH7.5 (at 37°C)
	10% Dextransulfate
	1% SDS
	250 µg/ml Salmon Sperm DNA sonificated
	store aliquots à 30 ml at -20°C
Washing buffers:	a) 2x SSC / 0.5% SDS
	b) 1x SSC / 0.5% SDS
	c) 0.1% SSC / 0.5% SDS
stock solutions:	a) 20x SSC 175.3 g Sodium chloride
	88.2 g sodium citrate
	pH7.0
	b) 20% SDS 200 g SDS
	1000 ml H_2O (final volume)

Western blot

Lysisbuffer:	50 mM Tris/HCl, pH7.4
	150 mM Sodium chloride
	2 mM EDTA, pH8
	1% Nonidet P-40
	filtrate sterile
APS:	10% APS (in dest. H_2O)
4x Tris/SDS pH8.8:	1.5 M Tris (pH8.8)
	0.4% SDS
4x Tris/SDS pH6.8:	0.5 M Tris (pH6.8)
	0.4% SDS
10x Tris-Glycine	
(Running buffer):	1.0% SDS
	0.25 M Tris
	1.92 M Glycine
4x SDS-loading dye:	(2 M DTT add freshly: 40 µl to 160 µl buffer)
	200 mM Tris/HCl, pH6.8
	8% SDS
	40% Glycerol

	0.4% bromine phenol blue
Buffer cathode:	25 mM Tris/HCl, pH9.4
	40 mM Glycine
	10% Methanol
Buffer anode I:	300 mM Tris/HCl, pH10.4
	10% Methanol
Buffer anode II:	25 mM Tris/HCl, pH10.4
	10% Methanol
Ponceau-solution:	0.2% PonceauS
	3% TCA
10x TBST:	(washing buffer, add Tween20 freshly)
	100 mM Tris/HCl, pH7.4
	1.5 M Sodium chloride
	1.0% Tween20
Blocking solution:	1:10 (v/v) milk powder
	1 g BSA
	in 1x TBST
ECL-solution:	mix directly before usage
	Solution A and B mix: 1:1

LacZ-staining

Fixation buffer:	0.02% NP-40
	5 mM EGTA, pH8.0
	2 mM MgCl2 x $6H_2O$
	1% Formaldehyde
	0.2% Glutaraldehyde
	in PBS
Washing buffer:	0.02% NP-40
	in PBS
Staining buffer:	0.02% NP-40
	2 mM $MgCl_2$ x $6H_2O$
	5 mM $K_3[Fe(CN)_6]$
	5 mM $K_4[Fe(CN)_6]$ x $6H_2O$
	0.01% Natriumdesoxycholat
	1 mg/ml X-Gal
	in PBS

Transfections

2x HBS buffer:	0.27 M Sodium chloride
	0.054 M HEPES
	0.001 Sodium hydrogenic phosphate (Na_2HPO_4)
	pH7.05

Immunostainings

Permeabilisation:	0.1% TritonX-100,
	100 mM Glycin
	in H_2O
Blocking solution:	10% FCS

	1% BSA
	3% serum (goat, donkey)
	in PBST (0.1% Tween20 in PBS)

Immunoprecipitation

TBS:	30 mM Tris-HCl pH 7.4
	150 mM NaCl
Lysis buffer:	TBS buffer
	0.5% Nonidet-P40
	Protease inhibitor cocktail (Roche)
	Phosphatase inhibitors (Sigma)
Wash buffer:	TBS buffer
	0.1% Nonidet-P40
	Protease inhibitor cocktail

5.1.6 Enzymes

Proteinase inhibitors	(Sigma-Aldrich GmbH, Seelze)
Superscript II	(Fermentas GmbH, St. Leon-Rot)
RNase inhibitors	(Fermentas GmbH, St. Leon-Rot)
Restriction enzymes	(NEB GmbH, Frankfurt a. M.; Fermentas GmbH, St. Leon-Rot)
DNA-Polymerases	(DNA Polymerase I, Large (Klenow) Fragment, NEB GmbH, Frankfurt a. M.; M0210; *Taq* DNA Polymerase recombinant, Fermentas GmbH, St. Leon-Rot, EP0402; *Taq* DNA Polymerase; Qiagen, Hilden; 201203; *Pfu* DNA Polymerase, Stratagene, La Jolla)
RNase	(Promega GmbH, Mannheim)
RNase-free DNase I	(Promega GmbH, Mannheim)
Ligase	(T4 DNA ligase; NEB GmbH, Frankfurt a. M.; M0202)
Phosphatase	(T4 Polynucleotide Kinase, NEB GmbH, Frankfurt a. M.; Antarctic phosphatase NEB GmbH, Frankfurt a. M.)

5.1.7 Antibodies and sera

Primary antibodies:

ID	name	generated in	dilution	company	Order Number
5	E-Cadherin	mouse	WB 1:2.500, IF 1:2.000	BD	610181
15	Par 6	goat	WB 1:100	Santa Cruz	sc14405
17	anti-SAP102	goat	WB 1:4.000	abcam	ab12086
18	anti-SAP102	rabbit	WB 1:400	LifeSpan	LS-C93/AN-03
20	anti-SAP102	mouse	WB 1:1.000	Calbiochem	573902
22	anti-beta-catenin	rabbit	IF 1:2.000	Sigma	C2206
23	HNf-3ß (Foxa2) M-20	goat	WB 1:800, IF 1:1.000	Santa Cruz	sc-6554
27	C-Nap1	mouse	WB 1:250, IF: 1:500	BD	611374
30	anti-Acetylated tubulin	mouse	IF 1:250	Sigma	T7451

31	Anti Flag M2	mouse	WB 1:10.000, IF 1:500	Sigma	F1804
32	Anti-Flag	rabbit	IF 1:500	Sigma	F7425
33	anti-SAP102	rabbit	WB 1:3.000	Synaptic sytems	124202
37	anti-ZO1	mouse	IF 1:200	Invitrogen	33-9100
48	chicken anti-GFP	chicken	WB 1:5.000 IF 1:1.000	Aves Labs	GFP-1020
51	anti-Flag	rabbit	WB 1:800 IP 1:200 IF 1:160	Sigma	F7425
54	anti-Centrin 1	rabbit	IF 1:200 WB 1:2.000	abcam	ab11257
56	Foxa2	rabbit	WB 1:5.000, IF 1:1.000	abcam	ab40874
66	g tubulin	mouse	WB 1:1.000, IF 1:250	Sigma	T5326
68	anti-beta-Tubulin	mouse	WB 1:1.000, IF 1:200	Sigma	T4026
84	Ep-CAM (G8.8-c)	rat	IF 1:500	DSHB Hybridoma	4G1
88	c-Myc clone 9E10	mouse	WB 1:10.000	Sigma	M4439
91	anti-GM130	mouse	WB 1:500, IF 1:250	BD	610822
96	Anti-Gamma-Tubulin	rabbit	WB 1:250, IF 1:1.000	Sigma	T5192
105	Anti-Frizzled-3	rabbit	IF 1:250	Sigma	F3179
106	Prickle	rabbit	IF 1:200	abcam	ab15577
107	CELSR1 (N-17)	goat	WB 1:1.000, IF 1:100, IP 1-2µg	Santa Cruz	sc-46841
127	rat anti-KRT8 TROMA-I	rat	IF 1:500	DSHB Hybridoma	TROMA-I
128	hamster anti-T1alpha	hamster	IF 1:200	DSHB Hybridoma	Clone 8.1.1.
136	Scrib (H-300)	rabbit	IF 1:200	Santa Cruz	sc-28737
153	Arl13B (L-15)	goat	IF 1:250, WB 1:200	Santa Cruz	sc-102318
172	anti Centrin 1	rabbit	WB 1:2.000, IF 1:200	abcam	ab11257
174	Pericentrin	rabbit	WB 1:300, IF 1:500	covance	PRB-432C
236	CD133 (Prominin-1)	rat	IF 1:250	eBioscience	14-1331
	FltpI	rabbit	WB 1:4.000, IF 1:250		
	FltpII	rabbit	WB 1:4.000, IF 1:250		
	FltpIII	guinea pig	WB: 1:250, IF 1:50		
	Rat-EGR 1G8-G1+2a+2c	rat	IF 1:250		
	Rat-EGR 5E6-G1+2a	rat	IF 1:250		

Table 5 Primary antibodies

A list of all primary antibodies used in this thesis. Abbreviations: WB: Western Blot, IC: immunohistochemistry

Secondary antibodies:

ID	name	conjugated	dilution	company	order number
4	rabbit anti-goat IgG 488	Fluorescent	IC 1:800	Invitrogen	A-11078
5	rabbit anti-goat IgG 555	Fluorescent	IC 1:800	Invitrogen	A-21431
6	goat anti-rat IgG	FITC	IC 1:800	South. Biot.	3030-02
7	goat anti-mouse 488	Fluorescent	IC 1:800	Invitrogen	A11029
8	goat anti-rabbit 594	Fluorescent	IC 1:800	Invitrogen	A11037
9	goat anti-rat 594	Fluorescent	IC 1:800	Invitrogen	A11007
10	goat-anti-guinea pig	HRP	WB 1:10.000	Santa Cruz	sc2903
11	Alexa Fluor 546 phalloidin	Fluorescent	IC 1:40	Invitrogen	A22283
12	goat anti-mouse IgG 546	Fluorescent	IC 1:800	Invitrogen	A11030
13	goat anti-rabbit IgG 488	Fluorescent	IC 1:800	Invitrogen	A11034
14	goat anti-mouse IgG Cy3	Fluorescent	IC 1:800	Dianova	115-165-003
17	goat anti-mouse IgG 405	Fluorescent	IC 1:800	Invitrogen	A31553
18	donkey anti-goat IgG 633	Fluorescent	IC 1:800	Invitrogen	A21082
19	goat anti-rabbit IgG	HRP	WB 1:20.000	Dianova	111-036-045

20	donkey *anti-chicken IgY*	Cy5	IC 1:800	Dianova	703-175-155
23	donkey anti-mouse IgG 488	Fluorescent	IC 1:800	Invitrogen	A21202
24	donkey anti-rabbit IgG 555	Fluorescent	IC 1:800	Invitrogen	A31572
25	donkey anti-goat IgG 488	Fluorescent	IC 1:800	Invitrogen	A11055
26	donkey anti-rabbit IgG 488	Fluorescent	IC 1:800	Invitrogen	A21206
27	donkey *anti-chicken IgY*	Cy3	IC 1:800	Dianova	703-165-155
28	donkey *anti-chicken IgY*	Cy2	IC 1:800	Dianova	703-545-155
29	*goat anti-rabbit IgG*	Cy5	IC 1:400	Dianova	111-175-144
30	goat *anti-chicken IgY*	*DyLight 488*	IC 1:800	Dianova	103-485-155
32	donkey anti-mouse IgG 555	Fluorescent	IC 1:800	Invitrogen	A31570
33	goat anti-guinea pig IgG 633	Fluorescent	IC 1:800	Invitrogen	A21105
34	goat anti-mouse IgG 633	Fluorescent	IC 1:800	Invitrogen	A21052
35	donkey anti-goat IgG 555	Fluorescent	IC 1:800	Invitrogen	A21432
37	donkey anti-mouse IgG 649	DyLight 649	IC 1:800	Dianova	715-495-151
40	goat anti-Syrian Hamster	*DyLight 549*	IC 1:800	Dianova	107-505-142
41	donkey anti-rat IgG 549	*DyLight 549*	IC 1:800	Dianova	712-505-153
44	donkey anti-rabbit IgG 649	Fluorescent	IC 1:400	Dianova	711-605-152
45	donkey anti-rat IgG 649	*DyLight 649*	IC 1:400	Dianova	712-495-150
46	donkey anti-guineapig 649	*DyLight 649*	IC 1:400	Dianova	706-495-148
48	donkey anti-mouse DyLight	DyLight 405	IC 1:200	Dianova	715-475-150

Table 6 Secondary antibodies

Secondary antibodies used in this thesis. Abbreviations: WB: Western Blot, IC: immunohistochemistry

Sera:

Sheep serum (Sigma-Aldrich GmbH, Hamburg)
Goat serum (Sigma-Aldrich GmbH, Hamburg)
Donkey serum (Sigma-Aldrich GmbH, Hamburg)

5.1.8 Vectors and BACs

The PL-452 vector contains a *loxP* site flanked *neo* resistance gene under the control of a hybrid promoter consisting of the very efficient phosphoglycerate kinase (PGK) - to allow expression in eukaryotic cells - and EM7 - for prokaryotic expression - promoter followed by the strong bovine growth hormone polyadenylation (bGHpA) signal.

Vectors:

pBluescript
PL-452

BACs:

RPCI22-254-G2 (RZPD; 129Sv Foxa2-BAC; Bacterial artificial chromosome libraries for mouse sequencing and functional analysis.)

RP23-333P11 (RZPD; DNA source: C57BL/6L kidney & brain Vector: pBACe3.6; BAC for Fltp; Bacterial artificial chromosome libraries for mouse sequencing and functional analysis.)

5.1.9 Oligonucleotides

5.1.9.1 Oligonucleotides for genotyping

This is the list of oligonucleotides used for genotyping; all oligonucleotides are displayed in 5’ to 3’ direction.

EP180: 5’-*GTGAACCGCATCGAGCTGAAGG*-3’
EP181: 5’-*GAACTCCAGCAGGACCATGTG*-3’
EP418: 5’-*AGCCATACCACATTTGTAGAGG*-3’
EP397: 5’-*CTACTACCAAGGAGTGTACTCC*-3’
EP398: 5’-*CTGTGGCCCATCTATTTAGGG*-3’
EP534: 5’-*GGTCTCTGATGAAGCAGTGATTTTT*-3’
EP535: 5’-*TGATGACCCATAGACAGTAGGATCA*-3’
EP536: 5’-*CTAAAGCGCATGCTCCAGAC*-3’
EP564: 5’-*GATCTATGGTGCCAAGGATGAC*-3’
EP565: 5’-*CAGCATGGCATAGATCTGGAC*-3’
EP566: 5’-*GAGGCTGACTGGGAACAATC*-3’
EP568: 5’-*GCTGGTGGCTGGACCAATGTG*-3’
EP779: 5’-*ACAACCTTTGGGCTCTCG*-3’
EP780: 5’-*TATAGTCCCTCCGGACCTC*-3’

5.1.9.2 Oligonucleotides for cloning

This is the list of oligonucleotides used for cloning; restriction enzyme sites are underlined; the oligonucleotides are displayed in 5’ to 3’ direction.

2A_fwd:
5’-*GGCCGCACGCGTTTGAAGGTAGAGGCTCTTTACTAACATGCGGCGACGTTGAGGAAAACCCAGGACC*-3’
2A_rev:
5’-*GGCCTGGTCCTGGGTTTTCCTCAACGTCGCCGCATGTTAGTAAAGAGCCTCTACCTTCAAACGCGTGC*-3’
5’ Southern Fltp FWD: 5’-*NNNCTCGAGGAGCCCTTACGCACACTTAAG*-3’
5’ Southern Fltp REV: 5’-*NNNTCTAGACGGGACATTAACTGCATCTTATCTGAGGTTG*-3’
EP011: 5’-*NNNACTAGTAGGTAAGTGTACCCAATTCGCCCTATAG*-3’
EP012: 5’-*NNNGGATCCACGCGTTAAGATACATTGATGAGTTTGGAC*-3’
EP013: 5’-*NNNTCTAGAATGGTGAGCAAGGGCGAGGAGCTGTTC*-3’
EP014: 5’-*NNNACTAGTTTACTTGTACAGCTCGTCCATGCCGAGAG*-3’
EP019: 5’-*NNNGAGCTCGTGAGAAGCAACTGGCACTGAAGGAAG*-3’
EP020: 5’-*NNNTCTAGAGGATGAGTTCATAATAGGCCTGGAGTAC*-3’
EP021: 5’-*NNNAAGCTTGAAGATGGCTTTCAGGCCCTGCTAGCTC*-3’
EP022: 5’-*NNNCTCGAGCTTTCTCCTGGTCCGGTACACCAGACTC*-3’
EP025: 5’-*NNNGCGGCCGCGCCACCATGCCAGAGCCAGCG*-3’
EP026: 5’-*NNNTCTAGACTTAGCGCTGGTGTACTTGGTGATGG*-3’
EP322: 5’-*NNNAAGCTTGCCTGAAATGTGTTTCATTATC*-3’

EP323: 5'-*NNNCTCGAGGGGAGGCAATATAATATCTGTG*-3'
EP324: 5'-*NNNGGCGCGCCCCGTCTGTATTGAGCAAAGCAGATGAG*-3'
EP325: 5'-*NNNAAGCTTATGCAGAGCTGTTGATGGCAATCAC*-3'
EP326: 5'-*NNNAAGCTTCATATGAGGCATCAGAGGTGTTTCTAC*-3'
EP327: 5'-*NNNACTAGTCCCTCCTCCTTCAATTTCTCTTC*-3'
EP340: 5'-*NNNGCGGCCGCGCCACCATGAACCTTGAAGCTCGAAAAACAAAG*-3'
EP341: 5'-*NNNGGCGCGCCTTTTTGACACCAGACCAACTGGTAATGGTAGC*-3'
EP449: 5'-*NNNGGCGCGCCAGTCAGGAAGTGGAAGAGAAGAACACAG*-3'
EP450: 5'-*NNNAAGCTTACTAGTGTGGTGGAGTGCCTGTCTACATGTG*-3'
EP451: 5'-*NNNAAGCTTCACGACAGTCAAAGCTGCAATAGAAC*-3'
EP452: 5'-*NNNGGATCCGGTAATTTGGCAATTATAGAACTCAGGC*-3'
EP453: 5'-*NNNCCGCGGAGCAGACTTAACTATGTTGGGGAAACAGC*-3'
EP454: 5'-*NNNGTCGACGCGGCCGCTGTTTACACTTGTTGCCTGGCAACTG*-3'
EP455: 5'-*NNNGTCGACGGTCCTAGTCTAGCTGAGGTCCAGATC*-3'
EP456: 5'-*NNNGGTACCATGCTGTGGGAGTCACTGACATTCTTG*-3'

5.1.10 Southern probes

Foxa2 3' Southern probe (730 bp)
Primer for generation: EP322 and EP323 (see 5.1.9.2)

5'−GGTCACCTCTATAAACATGGCATTCCCTGTATATATACCAATAGAAATAGATTTGCCAAATGGGTAAGAATA
TATAACCCCACCTCCATTGTCACTGATAATATTGAAACAAATTGTGTGGAGCTATTCTGTGTTTATATCGAGCCA
CTGGTTGACTTTGAAATGGAAACTAAGAAGCTAAGACCACTTCCCAAGCCTCACATTTGAACCCCAGGCCTTGC
TGCCTTGTGCCAGCTCTCCACATTGCTCAATGCCTCACTGCTTCTTATATATTGGTAGGACATTTGCTTATCCCAC
AGGTGGTCAGTGGTTCCGCAGATCCAATGGAATTCCCTCCAAATCTGCTACCCAAGTAACACAGAGAAAAGAA
ATGCTCAGAGTCTGTGAGTGGCTTCTCTGGACTGCTATCTTTCATGAAGTTCACCATTTATCTGGTTGGCAGGA
ATATCAGTTATTTCTCCCAAGAACAGCATGCAAATGAATATAGAAGCTCCCAGGGTCACAGATGTAGGTGTGT
CTACTTTAAGCATCCCTCAGCAGAGACTTTCCTCCTCACGGTTCTCTGTTGTTATTGCTACCATGAGTTGTTATCT
TTTATTTTCATCTCTTGCAATTATTTTAATCCTGCTGTAAGAGCTTCACACACCAGAAACATGCTAAAAGTGCAA
GAATTGTGGATGAGATGTTAAGCATGTCTCAGAAATATTCCTCAACTTCTCAACCCAAGTGG−3'

Fltp 5' Southern probe (608 bp)
Primer for generation: 5' Southern Fltp FWD and 5' Southern Fltp REV (see 5.1.9.2)

5'−GAGCCCTTACGCACACTTAAGTATGCCTTTTTCTTTCCCTAGTCTCTCTTTCTCTTAACCTTCTTGTGTAAAGT
TTGTCAGAAGTGTTCTTCAGGAGCCGGAGAGACGGCAAGTACTGGCACTTAACCTCCTGAGTACCGGTTTTCA
TTGTAGGTGTAGATGCCACCTTGTTTAATACAGATTTAAGGACAAATACTGAAAGATAGAGAGCAGCTTAGGA
AAATGCAGGAAACACATTACAAACCTGAGGGTGGGTACGGATGTCTCAAAAGAGTAAGACCAGACACTTAAC
TGAAGTCACTGAATAGCTTCCAGTCATTACCCTTTATTATGCTATTTCTGTGTACTCACTTGAGCAACGTAGCCT
ATATCTCCTCCTTGGGAGAAACTGACTAAAGAGGAAATGTCACCGGTTTCATTATACAAGGTGACACACCTTCC
TCTTCATTGTCTTGGGATACACTTAGAACCCACCATCCTGAACATGCTAATTAAAATGCCCTGATAGCAAAATAA
CTAAGTAAAATTCATTTTTTTTAAAAGATATCTTCTGAGAGGCCACACGAGACTGCTCCTGCAACCTCAGATAA
GATGCAGTTAATGTCCCG−3'

5.1.11 Molecular weight markers

DNA ladder:	100 bp ladder; 1 kb ladder (NEB GmbH, Frankfurt a. M.)
Protein ladder:	SeeBlueR Plus2 Pre-Stained Standard (Gibco, Invitrogen™ Cooperation, Carlsbad, CA)
RNA ladder:	RNA ladder high range (Fermentas GmbH, St. Leon-Rot)

5.1.12 Bacteria and culture media

Bacteria

E.coli K12 EL250	(Lee et al., 2001)
E.coli K12	XL-1 Blue endA1 gyrA96(nalR) thi-1 recA1 relA1 lac glnV44 F`[:: Tn10 proAB + laclq ∆(lacZ)M15]hsdR17(rK-mK+) (Stratagene, LaJolla)
E.coli K12 DH5α	F-.lacl-recA1, endA1, D(lacZY A-argF), U169, F80dlacZDM15, supE44, thi-1, gyrA96, relA1 (Hanahan et al., 1985)

Culture media

LB Medium	(Lysogeny broth; (Bertani, 1951)
LB Agar	(Lysogeny broth; (Bertani, 1951) Optionally with 100 µg/ml Ampicillin 25 µg/ml Kanamycin 12.5 µg/ml Chloramphenicol

5.1.13 Cell lines and culture media

Cell lines

HEK293T	human embryonic kidney cells stably expressing the T-large antigen of SV40 (Graham et al., 1977)
NIH3T3	murine embryonic fibroblast cell line (Todaro and Green, 1963)
IDG3.2	murine ES cell line (F1); genetic background 129S6/SvEvTac x C57BL/6J (Hitz et al., 2007)
TBV2	murine ES cell line; background: 129Sv (Wiles et al., 2000)
MEF	primary murine embryonic fibroblasts isolated on E13.5

Culture media

HEK293T/NIH3T3	DMEM (Gibco, Invitrogen™ Cooperation, Carlsbad, CA), supplemented with 2 mM L-glutamine (200 mM Gibco, Invitrogen™ Cooperation, Carlsbad, CA), 10% FCS (PAA Laboratories Gesellschaft mbH, Pasching, Österreich)

MEF	DMEM (Gibco, Invitrogen™ Cooperation, Carlsbad, CA), supplemented with 2 mM L-glutamine (200 mM Gibco, Invitrogen™ Cooperation, Carlsbad, CA), 15% FCS (PAN Biotech GmbH, Aidenbach), 0.1 mM β-mercaptoethanol (50 mM, Gibco, Invitrogen™ Cooperation, Carlsbad, CA), 1x MEM (non-essentiell amino acids, 100x; Gibco, Invitrogen™ Cooperation, Carlsbad, CA)
TBV2	DMEM (Gibco, Invitrogen™ Cooperation, Carlsbad, CA), supplemented with 2 mM L-glutamine (200 mM Gibco, Invitrogen™ Cooperation, Carlsbad, CA), 15% FCS (PAN, Biotech GmbH, Aidenbach), 0.1 mM β-mercaptoethanol (50 mM, Gibco, Invitrogen™ Cooperation, Carlsbad, CA), ESGRO® (LIF) (107 U/ml; Chemicon, Millipore, Schwalbach), 1x MEM (non-essentiell amino acids, 100x; Gibco, Invitrogen™ Cooperation, Carlsbad, CA)
IDG3.2	DMEM (Gibco, Invitrogen™ Cooperation, Carlsbad, CA), supplemented with 2 mM L-glutamine (200x, Gibco, Invitrogen™ Cooperation, Carlsbad, CA), 15% FCS (PAN Biotech GmbH, Aidenbach), 0.1 mM β-mercaptoethanol (50 mM, Gibco, Invitrogen™ Cooperation, Carlsbad, CA), ESGRO® (LIF) (107 U/ml; Chemicon, Millipore, Schwalbach), 1x MEM (non-essential amino acids, 100x; Gibco, Invitrogen™ Cooperation, Carlsbad, CA), 2 mM HEPES (200 mM, Gibco, Invitrogen™ Cooperation, Carlsbad, CA)
MTEC basic	DMEM F12 (Invitro #21331-020), 15 mM HEPES (1M stock), 3.6 mM sodium bicarbonate, 4 mM L-Glut (200 mM stock), P/S (100x stock), Fungizone (500x stock)
MTEC/plus	MTEC basic, 10 µg/ml Insulin (5 mg/ml stock), 5 µg/ml Transferrin (5 mg/ml stock), 0.1 µg/ml cholera toxin (100 µg/ml stock), 25 ng/ml EGF (25 µg/ml stock), 30 µg/ml BPE, 5% FBS, 0.01 µM RA

Solutions for cell culture

1x PBS without Mg^{2+}/Ca^{2+}	(Gibco, Invitrogen™ Cooperation, Carlsbad, CA)
1x trypsin-EDTA	(0.05 % Trypsin, 0.53 mM EDTA•4Na, Gibco, Invitrogen™ Cooperation, Carlsbad, CA)

5.1.14 Mouse lines

129S6/SvEvTac these mice were obtained from the company Taconic. Progenitors of this strain used extensively to establish embryonic stem (ES) cell lines (e.g.,

	IDG3.2) for the production of targeted mutation (knockout) mice. For further information please visit http://www.taconic.com/wmspage.cfm?parm1=809
129S2/SvPasCrlCD1	these mice were obtained from Charles River. For further information please visit http://www.criver.com/en-US/ProdServ/ByType/ResModOver/ResMod/Pages/129Mouse.aspx
C57BL/6NCrl	these mice were obtained from Charles River. For further information please visit http://www.criver.com/en-US/ProdServ/ByType/ResModOver/ResMod/Pages/C57BL6Mouse.aspx
CD1	outbred strain (Helmholtz Zentrum München)
Flp-e	(Dymecki, 1996)
$R26^{R/R}$	(Soriano, 1999)
R26Cre	(Soriano, 1999)
CAG-CAT-EGFP	(Kawamoto et al., 2000)
$Celsr1^{Crsh}$	(Curtin et al., 2003)
$Foxa2^{T2AiCre}$	mouse line generated in this thesis (Bl6 background)
$Fltp^{ZV}$	mouse line generated in this thesis (129S2, Bl6, CD1 background)
$Fltp^{ZV}$; $Celsr1^{Crsh}$	$Fltp^{ZV}$ mouse line crossed into $Celsr1^{Crsh}$ mouse line (Curtin et al., 2003)
$Fltp^{T2AiCre}$	mouse line generated in this thesis (background CD1, Bl6) (Lange et al., 2012)
$Fltp^{ZV}$; *Dlg3:Venus*	$Fltp^{ZV}$ mouse line crossed into *Dlg3:Venus* mouse line (Van Campenhout et al., 2011)
$Fltp^{T2AiCre}$; *Dlg3:Venus*	$Fltp^{T2AiCre}$ mouse line (Lange et al., 2012) crossed into *Dlg3:Venus* mouse line (Van Campenhout et al., 2011)

5.2 Methods

5.2.1 Cell culture

5.2.1.1 Embryonic stem cell culture

To keep murine embryonic stem (ES) cells in culture and to prevent spontaneous differentiation a murine embryonic fibroblast layer (MEF, feeder cells) and medium supplemented with LIF (leukemia inhibitory factor) are needed.

5.2.1.1.1 Culture of primary murine embryonic fibroblasts

Depending on their growth, speed, and density MEFs were split every 3 to 5 days 1:4 – 1:6. Therefore, 15 cm dishes of confluent MEFs were washed with at least 10 ml PBS (-$MgCl_2$) and afterwards treated with 7 ml trypsin-EDTA at 37°C for 5 min. To stop the reaction 7 ml MEF medium was added. A single cell suspension was accomplished by pipetting up and down at least 10 times. The single cell suspension was transferred to a 15 or 50 ml Falcon tube and centrifuged at 250xg for 5 min. The supernatant was discarded and the cells were resuspended in a suitable volume of MEF medium and plated on 5-6 new 15 cm dishes.

5.2.1.1.2 Treatment of murine embryonic fibroblasts with mitomycin C

To inhibit the growth of the MEFs in co-culture with ES cells they are incubated with mitomycin C (MMC). MMC is an inhibitor of mitosis.
To treat MEFs with MMC dishes were grown confluent and trypsinized. Then the cells of five 15 cm dishes were transferred to a 50 ml Falcon tube in 20 ml MEF medium, treated with 200 µl MMC (1 mg/ml) and incubated at 37°C for 45 min. The tube was inverted every 15 min to prevent cells from attaching to the plastic of the tube. The cells were pelleted by centrifugation at 250xg for 5 min. The supernatant was discarded and the cells were washed twice with MEF medium to remove remaining MMC. Afterwards the cells were plated on cell culture plates or dishes for direct use as a feeder layer for ES cells or they were frozen for later use.

5.2.1.1.3 Thawing of ES cells

Before thawing ES cells a falcon tube with 10 ml pre-warmed ES medium was prepared. Under careful shaking a cryovial of ES cells was thawed fast in a 37°C water bath. The thawed cells were transferred into a prepared falcon tube and pelleted at 250xg for 4 min. The pellet was resuspended in a suitable volume of ES cell medium (e.g. 5 ml for one 6 cm dish) and cultured on feeder cells (MEF) at 37°C and 5-7% CO_2 in a humid incubator.

5.2.1.1.4 Passaging of ES cells

ES cells need to be split after two days in culture to prevent differentiation and to expand them. Therefore, the medium was removed and the cells were washed with a suitable volume of PBS (-Mg^{2+}/Ca^{2+}). The PBS was removed and the cells were incubated with trypsin-EDTA (1 ml per 6 cm dish

or 3 ml per 10 cm dish) for 5 min at 37°C and 5-7% CO_2 in a humid incubator. The dissociation of the cells was controlled under the microscope and the reaction was stopped using at least the same amount of medium like trypsin (4 ml for one 6 cm dish). A single cell suspension was generated by pipetting up and down for at least 10 times. The cells were transferred to a new falcon tube and centrifuged for 4 min at 250xg. The supernatant was discarded and the cells were resuspended in fresh ES cell medium. They can be split from 1:2 to 1:30 depending on their division rate. Dilutions of cells were plated on new feeder cells according to the splitting ratio determined before. Cells were incubated at 37°C and 5-7% CO_2 in a humid incubator till they need to be split again (approximately 48 h).

5.2.1.1.5 Cryopreservation of ES cells

For long term storage ES cells are cryopreserved in liquid nitrogen ($N_{2(l)}$). Therefore, the cells are trypsinized as described above (see 5.2.1.1.4) and centrifuged. Now, the cells were resuspended in pre-cooled freezing medium and transferred into cryovials. These cryovials were put into freezing boxes and stored at –80°C for at least four hours to cool the cells slowly down to –80°C. When cells are frozen the vials were transferred into $N_{2(l)}$.

5.2.1.2 Homologous recombination in ES cells

To generate knock in mice the method of homologous recombination is needed. Therefore, ES cells are electroporated with the linearized targeting vector, integration is controlled via selection, and the positive cells are picked and expanded.

5.2.1.2.1 Transformation of ES cells by electroporation

For one electroporation half a 10 cm dish ES cells (70-80% confluent) was trypsinized as described before (see 5.2.1.1.4). The single cell suspension was then transferred to a Falcon tube and pelleted at 250xg for 5 min. Cells were then washed with 10 ml PBS (-Mg^{2+}/Ca^{2+}) at room temperature (RT) and centrifuged under latter conditions. The cell pellet was resuspended in 1.5 ml ice-cold PBS (-Mg^{2+}/Ca^{2+}). 0.7 ml of this cell suspension was mixed with 100 µl vector (25 µg) and transferred into a pre-cooled cuvette. The electroporation was carried out under the following conditions.

(2 pulses, stored on ice in between for 1 min)
Program: 220 V
500 µF
Resistance: ∞

After electroporation the cuvette was kept on ice for additional 5 min and transferred into a pre-warmed dish with feeder cells and supplemented with ES cell medium (0.4 ml of the cell suspension was put on one 10 cm dish). The medium had to be exchanged daily. After 24 h of growth the selection was started with neomycin (G418; 300 µg/ml). After 6-8 days clones could be picked.

5.2.1.2.2 Picking of ES cell clones

For picking of ES cell clones one conical 96-well plate with 60 µl PBS (-Mg^{2+}/Ca^{2+}) per well and two normal 96-well plates, one coated with gelatin (0.1%) and one with a feeder layer both filled with 100 µl ES selection medium are prepared.
After discarding the medium of one 10 cm dish with ES cell clones 10 ml PBS (-Mg^{2+}/Ca^{2+}) were added. Clones that looked compact and round were picked under the stereo microscope in 20 µl PBS. The clones were detached, sucked, and transferred into one well of the prepared 96-well dishes filled with PBS (-Mg^{2+}/Ca^{2+}). It was taken care not to mix clones by detached cells. After one 96-well plate was filled 30 µl trypsin-EDTA were added per well and the cells were incubated at 37°C for 15 min. After incubation a single cell suspension was generated by pipetting 10 times up and down with a multi-channel pipette. 50 µl were transferred to each of the two prepared 96-well plates (one with feeder layer which is the master plate for freezing, one with gelatin which is the template for DNA preparation).

5.2.1.2.3 Expansion of ES cell clones

After 2-4 days of incubation at 37°C and 6% CO_2 in a humid incubator the cells were dense enough and the master plate was frozen. When the medium of the DNA plate turned yellow in just one day the cells were ready to prepare the DNA (see 5.2.2.1.2).

5.2.1.2.4 Cryopreservation of ES cell clones in 96-well-plates

For the cryopreservation of ES cell clones in 96-well plates 2x freezing medium (10 ml per 96-well plate) was prepared and cooled down to 4°C.

2x ES freezing medium:

- 4 ml ES cell medium
- 4 ml FCS
- 2 ml DMSO

The cells were washed once with 200 µl PBS (-Mg^{2+}/Ca^{2+}). 40 µl trypsin-EDTA per well were added and cells were incubated at 37°C for 5 min. The reaction was stopped with 60 µl cold medium and the cells were resuspended by pipetting up and down 10 times. 100 µl 2x freezing medium were added to each well as fast as possible. The plates were closed with parafilm, put in napkins and stored at – 80°C for 6-8 weeks.

5.2.1.3 Generation of the *Foxa2^{T2AiCre}* targeting vector

The objective of our cloning strategy was to create a mouse line where the T2A and iCre are fused to the N-terminus of *Foxa2* by removing its stop codon, followed by the endogenous *Foxa2* UTR.
The knock-in construct was designed as shown in Figure 8.
5’ and 3’ homology regions (HR) for the *Foxa2* gene were amplified by PCR (EP324 fwd 5’ HR *AscI*, EP325 rev 5’ HR *HindIII*, EP326 fwd 3’ HR *HindIII-NdeI*, EP327 rev 3’ HR *SpeI*; for all following primers see 5.1.9.2) using a 129Sv BAC (bacterial artificial chromosome; RPCI22-254-G2) as a template and

subcloned into 5'-*AscI* and 3'-*SpeI* sites of the pL254 vector (Copeland et al., 2001; Liu et al., 2003). Using gap repair a 10 kb genomic fragment was retrieved from the aforementioned BAC via homologous recombination in EL350 bacteria as described previously (Copeland et al., 2001; Liu et al., 2003), resulting in pL254 Foxa2. *HindIII* and *NdeI* sites were used as single cutters for linearization prior to gap repair. For cloning of the knock-in cassette in pBluescript KS- (pBKS-) 5' and 3' HR for the knock-in into exon three of *Foxa2* were generated by PCR (EP19 fwd 5' HR *SacI*, EP21 rev 5' HR *HindIII*, EP20 fwd 3' HR *XbaI*, EP22 rev 3' HR *XhoI*) using the previously mentioned BAC as a template and subcloned into pBKS- using the introduced restriction sites, resulting in pBKS- Foxa2-Ex3-HR. The pKS-T2A-iCre-FRT-Neo-FRT (Engert et al., 2009) was cloned between homology arms of the pBKS-Foxa2-Ex3-HR resulting in the final targeting construct (pL254 Foxa2-iCre).

5.2.1.4 Generation of the *Fltp*^{zv} targeting vector

The knock-in/knock-out construct was designed as shown in Figure 23. 5' and 3' HR for the *Fltp* gene were amplified by PCR (EP449 fwd 5' HR *AscI*; EP450 rev 5' HR *HindIII*, *SpeI*; EP451 fwd 3' HR *HindIII*; EP452 rev 3' HR *BamHI*; for all following primers see 5.1.9.2) using a C57BL/6J BAC clone (RP23-333P11) as template. These two PCR products were subcloned into the pL254 vector (Liao et al., 2009) using *AscI* and *BamHI.* The resulting vector was digested with *HindIII*, *SpeI* and electroporated into electrocompetent EL350 bacteria containing the *Fltp* BAC clone to retrieve the *WT* sequence between PCR homology arms resulting in the *Fltp* retrieval vector.
For cloning of the knock-in/knock-out cassette in pBKS$^-$ 5' and 3' HR for the knock-in into the ATG of exon two of *Fltp* were generated by PCR (EP453 fwd 5' HR *SacII*; EP454 rev 5' HR *SalI*, *NotI*; EP455 fwd 3' HR *SalI*; EP456 rev 3' HR *KpnI*) using the previously mentioned BAC as a template and subcloned into pBKS$^-$ using the introduced restriction sites, resulting in pBKS$^-$-Fltp-HomArms.
The first step to generate the targeting vector was to construct the pBKS$^-$-H2B-Venus-intron-SV40pA plasmid by subcloning an oligonucleotide for the H2B (histone 2B) that introduces a 5' *NotI* and a perfect Kozak sequence (EP025) and a 3' *XbaI* site (EP026). This PCR product was ligated into pBKS$^-$ (both cut with *NotI*, *XbaI*) resulting in pBKS$^-$-H2B. The next step was to introduce the *Venus* reporter gene (yellow fluorescent protein) also via PCR with the forward (fwd) primer containing an *XbaI* site (EP013) and a reverse (rev) primer containing a *SpeI* site (EP014). This PCR and the vector pBKS$^-$-H2B were digested with *XbaI* and *SpeI* and ligated resulting in pBKS$^-$-H2B-Venus. To complete the construct an intron-SV40pA oligonucleotide was generated by using the fwd primer containing *SpeI* (EP011) and the rev primer containing *BamHI* (EP012). This oligonucleotide was subcloned into pBKS$^-$-H2B-Venus by cutting both with *SpeI* and *BamHI* resulting in the pBKS$^-$-H2B-Venus-intron-SV40pA plasmid.
The next step was to introduce the *loxP* flanked *neomycin* (*neo*) resistance cassette by digesting the PL-452 vector (Liu et al., 2003) with *SalI* and *BamHI*. The digested vector was ligated into the pBKS$^-$-H2B-Venus-intron-SV40pA plasmid opened by cutting with *SalI* and *BamHI* resulting in pBKS$^-$-H2B-Venus-intron-SV40pA-loxP-bGHpA-neo-EM7-PGK-loxP (pBKS$^-$-H2B-Venus-neo).
For following cloning steps it was necessary to destroy the *MluI* site located in the SV40pA by cutting with *MluI*, filling up the 5' overhang with Klenow polymerase and religating the vector.
The T2A sequence from *Thosea asigna* virus was introduced into the *NotI* site of pBKS$^-$-H2B-Venus-neo by annealing the following oligos 2A_fwd; 2A_rev, which created a *NotI* compatible overhang resulting in pBKS$^-$-2A-H2B-Venus-neo.

To clone the NLS-lacZ (nuclear localisation signal-β-galactosidase fusion protein) in front of the H2B-Venus construct we amplified the NLS-lacZ by PCR out of a NLS-lacZ containing vector. We used the fwd primer EP340 with a *NotI* site at the 5' end and the rev primer EP341, containing an *AscI* site at the 3' end. The PCR product was digested with *NotI* and *AscI* and ligated into the *NotI* and *MluI* digested pBKS$^-$-2A-H2B-Venus- neo vector resulting in pBKS$^-$-NLS-lacZ-2A-H2B-Venus-neo.
For finishing the minitargeting construct we cloned pBKS$^-$-NLS-lacZ-2A-H2B-Venus-neo into pBKS$^-$-Fltp-HomArms (both cut with *NotI* and *SalI*). The minitargeting construct was cut out by *SacII* and *KpnI*, electroporated in EL350 bacteria and introduced into PL254 via bacterial homologues recombination resulting in the final targeting construct (PL254-Fltp-NLS-lacZ-2A-H2B-Venus-intron-SV40pA-loxP-bGHpA-neo-EM7-PGK-loxP) which was confirmed by sequencing and is ready for electroporating into ES cells (after linearization by *AscI*).

5.2.1.5 Generation of the *Fltp^{T2AiCre}* targeting vector

The *Fltp^{T2AiCre}* targeting construct was designed as published in Lange et al. 2012 (Lange et al., 2012).

5.2.1.6 Transfection of HEK293T and NIH3T3 cells

To introduce expression plasmids into NIH3T3 and HEK293T cells the cells were transfected with Lipofectamine™ 2000 (Invitrogen). The cells were split in such a ration that the cells were 80-90% confluent the next day (3x 10^6 cells for a 6-well plate). 2 µg DNA and 4 µg Lipofectamine are filled up to 500 µl with Optimem in two different tubes. After 5 min incubation step at RT both tubes are mixed and incubated additional 20 min at RT before the solution is pipetted drop wise onto the cells. On the next day the medium is changed and the transfection efficiency is controlled by a transfection control mostly a fluorescent protein.

5.2.1.7 Isolation of mouse tracheal epithelial lung cells

To isolate mouse tracheal epithelial cells the mice were sacrificed and the trachea dissected out. The trachea was put into ice cold HamF12 medium supplemented with penicillin/streptomycin (P/S). Tissue surrounding the trachea was removed under the dissecting microscope in HamF12 medium. The trachea was digested in HamF12 medium supplemented with 1.5 mg/ml pronase (protease 14) at 4°C ON. On the next day the tube was put on ice, FBS (fetal bovine serum) was added to a concentration of 10%, and the tube was inverted at least 12x. Now the tracheas were transferred into a new tube with HamF12 P/S 10% FBS medium and again inverted 12x. Tracheas of the same genotype can now be pooled and centrifuged for 10 min at 4°C at 400 g. 200 µl HamF12 P/S per trachea were supplemented with 0.5 mg/ml DNaseI and 10 mg/ml BSA (bovine serum albumin), the trachea were resuspended and incubated for 5 min on ice. Subsequently, the tubes were centrifuged for 5 min at 4°C at 400 g. The cells were resuspended in MTEC basic medium (see 5.1.12) with 10% FBS and incubated for 3-4 h at 37°C. The supernatant was collected, centrifuged for 5 min at 400 g, and resuspended in 100-200 µl MTEC plus medium for counting. 75.000 cells per cm^2 were seeded on a transwell filter in MTEC plus medium. Medium was changed every two days. When the cells were confluent the MTEC culture was changed to an ALI culture by removing the medium on top of the filter and providing only medium supply from the bottom.

5.2.2 Molecular biology

5.2.2.1 DNA extraction

5.2.2.1.1 Plasmid and BAC preparations

Plasmid preparation is needed to isolate plasmid DNA from a bacterial suspension. The bacterial cells are separated from the medium and solubilized by addition of special lysis buffers. Addition of detergents lyses the cell and DNA denaturing solutions are added. Afterwards, the medium is being neutralized and RNases are added and the DNA is getting renatured. Plasmid DNA renatures faster than chromosomal DNA therefore chromosomal DNA is pelleted by centrifugation whereas plasmid DNA stays in solution. Plasmid DNA is now precipitated by adding isopropanol, washed with ethanol, and resuspended in water. For long term storage the DNA can be resuspended in TE (Tris, EDTA) buffer and stored at -20°C.

Plasmid preparations according to the QIAGEN Plasmid Kits To isolate plasmids out of a bacterial culture we used the QIAGEN Mini Kit. In the end the plasmid DNA pellet was resuspended in up to 50 µl Milli Q H_2O, TE buffer, or EB (elution buffer). For larger amounts of DNA the QIAGEN Maxi Kit is used and the DNA is resuspended in 150-300 µl TE buffer.

BAC mini preparation according to Copeland The preparation of BAC DNA is similar to the preparation of plasmid DNA. The protocol is adopted from an existing protocol (Warming et al., 2005). The obtained yield of BAC DNA lies at around 1-1.5 µg.
5 ml of a bacterial overnight (ON) culture (LB (lysogeny broth) medium supplemented with appropriate antibiotic in our case 25 µg/ml chloramphenicol) were centrifuged at 5000 rpm in a 15 ml Falcon tube for 5 min (centrifuge: 5804 R; Eppendorf). The supernatant was discarded, the pellet resuspended in 250 µl P1 buffer, and transferred to an Eppendorf tube. 250 µl of P2 buffer were added and the reaction tube was carefully inverted. Afterwards, incubation at RT for a maximum 5 min followed. 250 µl of P3 buffer were added and the tube was subsequently incubated for 5 min on ice. The protein precipitate was collected by centrifugation at 13.500 rpm for 5 min (centrifuge: 5417 R; Eppendorf) and the DNA containing supernatant was transferred to a new Eppendorf reaction tube. This procedure was repeated once again to completely eliminate the precipitate. To precipitate the BAC DNA 750 µl of isopropanol were added to the clean supernatant, mixed, and incubated on ice for 10 min. After the incubation the DNA was pelleted at 13.000 rpm for 10 min (centrifuge: 5417 R; Eppendorf), the supernatant was removed, and the DNA pellet was washed using 1 ml 70% ethanol. Following this step, the DNA was centrifuged again at 13.200 rpm for 5 min. The ethanol was removed carefully; the pellet was air-dried up to 10 min, and dissolved in 50 µl TE while incubating at 37°C and 500 rpm (Thermomixer comfort; Eppendorf) for 1 h. Subsequent restriction digests were carried out in a volume of at least 60 µl.

BAC maxi preparation Preparations of BAC DNA in a large scale were done according to the NucleoBond BAC Purification Maxi Kit. Finally, the BAC DNA pellet was resuspended in a suitable volume of TE buffer.

5.2.2.1.2 Isolation of genomic DNA from cells and tissues

Isolation of genomic DNA from cells in 96-well plates The freshly picked ES cell clones were incubated for 2-3 days till they were confluent and the media (100 µl/well) turns yellow within a day. Proteinase K was added to the prepared lysis buffer directly before use in a concentration of 100 µg/ml to avoid self-digestion. Before applying the lysis buffer the cells were washed two times with PBS (-Mg^{2+}/Ca^{2+}) to completely remove the medium. After discarding the PBS 50 µl/well of lysis buffer were added and the 96-well plate was sealed with parafilm and incubated at 55°C ON in a humid chamber. The next day 150 µl 5 M sodium chloride were mixed with 10 ml 100% ice-cold ethanol and 100 µl of this mixture was added to each well for precipitation. The plate was incubated at RT for 30 min without moving. After this step the plate was inverted carefully and slowly on a paper towel to decant the liquid. Now the DNA is being washed three times in 150 µl 70% ice-cold ethanol per well. At this point the DNA can be stored in 70% ethanol at -20°C. After the last washing step the DNA was dried at RT for 10-15 min. Then 25 µl TE buffer or autoclaved water were added to the pellet and the DNA was dissolved at 4°C ON or at 37°C, shaking, for 1 h in a humid chamber.

Isolation of genomic DNA from cells in cell culture dishes Before applying the lysis buffer the cells were washed two times with PBS (-Mg^{2+}/Ca^{2+}) to completely remove the medium. Proteinase K was added to the prepared lysis buffer directly before use in a concentration of 100 µg/ml to avoid self-digestion. After discarding the PBS 5 ml of lysis buffer were added per 10 cm plate. The cells were detached by making use of a cell scraper and subsequently transferred into a 50 ml Falcon tube. The cells in the lysis buffer were incubated at 55°C ON. On the next day Phenol-chloroform-isoamylalcohol (25:24:1, PCI) was added 1:1 to the cell solution and was mixed well by vortexing. Now the phases were separated by centrifugation for 10 min at 4.500xg and RT. The upper phase was removed without the protein-containing interphase and mixed 1:1 with PCI again. After centrifugation the upper phase was transferred to a new tube and the DNA precipitated by adding 10 ml ethanol:sodium-acetate (25:1). To pellet the DNA the tube was centrifuged at 4.500xg and 4°C for 10 min. Now the supernatant was discarded and the pellet washed with minimum 7.5 ml of 70% ice-cold EtOH. Afterwards, the tube was centrifuged at 4.500xg and 4°C for 5 min. After centrifugation the supernatant was discarded and the DNA pellet was dried at RT until it appears glassy. After that, the pellet was dissolved in a suitable volume TE buffer at 4°C ON or for 1 h at 37°C in the shaker and can be stored at 4°C.

Isolation of genomic DNA from mouse tail biopsy This technique provides the basis for genotyping mice. The approximately 4 mm long mouse tail-clips were put into a single Eppendorf tube with the corresponding mouse number written on it. If the tail-clips were not lysed the same day, they can be stored at -20°C till processing. The lysis buffer was supplemented with fresh proteinase K in a concentration of 100 µg/ml, 500 µl lysis buffer per mouse tail was added and incubated ON at 55°C. On the next day the digested mouse tails were vortexed and centrifuged at 14.000 rpm for 10 min to pellet the hair and the other insoluble fragments. The supernatant was transferred into a new tube with 500 µl isopropanol, inverted 3-4 times and centrifuged for 20 min at 14.000 rpm at RT. The supernatant was discarded and the pellet washed with 300 µl 70% EtOH for 10 min at 14.000 rpm. The pellet was air dried and resuspended in 300 - 500 µl H_2O or for long term storage in 300 – 500 µl TE buffer. Usually 1 µl is used for genotyping of mouse lines.

Hot shot method for isolation of genomic DNA from mouse tail biopsy This method works most efficient with embryonic tissues but is also applicable to adult tail biopsies. It is very fast and uses NaOH to denature the mouse tails under temperatures of 98°C.
The chopped mouse tails were covered with 100 µl 50 mM NaOH, boiled 20 min at 98°C, cooled down on ice for 5 min, and then neutralized with 30 µl of Tris pH 7.5. 1 µl of DNA can directly be used for genotyping.

5.2.2.2 RNA preparation

For RNA work it is of great importance to work fast and especially RNase free. The use of RNase inhibitors is highly recommended. β-mercaptoethanol can be added to the lysis buffer to solubilize the cells and inhibit the RNases. Solutions should be prepared with diethylpyrocarbonate (DEPC) because this inactivates the RNases. Extracted RNA should be stored at -80°C.
To isolate RNA from embryonic or adult tissue we used 1 ml TRIZOL per 50-100 mg of tissue. The tissue was homogenized with the help of a pipet tip and incubated 5 min at RT. Now chloroform was added and the tube was vortexed well. To separate the phases the tube was centrifuged at 12.000 rpm for 10 min at 4°C. Afterwards, the RNA containing upper phase was transferred into a new reaction tube. For RNA precipitation, 400 µl isopropanol were added and the tube was centrifuged at 12.000 rpm for 10 min at 4°C. The supernatant was discarded and the pellet washed with 70% EtOH for 10 min at 12.000 rpm at 4°C. The pellet was dried shortly and resuspended in 10-50 µl of DEPC water. Immediately use the RNA or store it at -80°C.

5.2.2.3 Determination of DNA or RNA concentration in solutions

The concentration of DNA or RNA in solution can be determined by measuring the extinction at 260 nm with a photometer (NanoDrop). The quotient E_{260nm}/E_{280nm} should be between 1.9-2.0 for clean RNA solutions and between 1.8-1.9 for clean DNA solutions.

5.2.2.4 Reverse transcription

During reverse transcription RNA is transcribed into cDNA. Before the reverse transcription can start, DNA has to be removed from the RNA sample by DNase digestion. After the digestion the RNA solution proteins and chemicals have to be removed by LiCl precipitation.

For cDNA preparation we used the following mixture:

2.0 µl RNA
1.0 µl Oligo-dT-primer (500 ng/µl)
11.0 µl filled up with DEPC-treated H_2O

The solution was incubated at 70°C for 10 min to denature the RNA and allow for the annealing of the primers. Afterwards, the mixture was put on ice and the following components were added:

4.0 µl 5x transcriptase buffer
2.0 µl DTT (0.1 M > 10 mM)

1.0 µl dNTPs (10 mM > 0.8 mM each)
1.0 µl RNA inhibitor (40 U/µl > 40 U)

The mixture was incubated for 2 min at 42°C. Afterwards 200 U SuperScript (200 U/µl > 1 µl) was added and subsequently incubated at 42°C for 50 min. To stop the reaction the enzyme was inactivated at 70°C for 15 min. The cDNA was stored at -20°C.

5.2.2.5 Restriction analysis of DNA

Restriction analysis of DNA is based on the ability of bacterial derived enzymes (restriction endonucleases) to cut DNA at enzyme specific recognition nucleotide sequences called restriction sites. These endonucleases originally served the purpose to defend the bacteria against foreign DNA (e.g. phages) and are now used in molecular biology. To prevent digestion of the own DNA, the specific restriction site in the bacterial genome are methylated. There are three classes of restriction endonucleases; class one cuts the DNA approximately 100 bp away from the recognition site, class two cuts exactly at the restriction site and class three cuts at a defined distance from the recognition site. After cutting, these endonucleases leave either sticky ends with 3' or 5' overhangs or blunt ends with plain ends.

Analytical or preparative restriction digest of plasmid or BAC DNA A typical reaction for a restriction digest for plasmid or BAC DNA is as follows:

DNA from mini preparation (ca. 500-100 ng)	5.0 µl
10x buffer	2.0 µl
10x BSA (optional)	2.0 µl
enzyme (5.000 U)	0.5 µl
dist. H_2O	10.5 µl
Σ	20.0 µl

The digest was incubated in 1.5 ml Eppendorf tubes at 37°C or 25°C for 1.5 h.

Restriction digests of genomic DNA basically, the restriction digest of genomic DNA used for Southern blot analysis and the restriction analysis of plasmid DNA are the same. The suitable enzyme buffer and BSA, if necessary, are added to the reaction. To complete the digest spermidine (in a final concentration up to 2 mM) is added. The completeness of the digest is controlled visually on an agarose gel before blotting. The DNA should appear on a lower molecular level and repetitive sequences should emerge in a distinct band.

Restriction digests of genomic DNA for Southern blot analysis A typical mix for a restriction digest of genomic DNA was carried out as follows:

25 µl genomic DNA
1x restriction buffer
(1x BSA)
1x spermidine (1 mM)

50-100 µg/ml RNaseH
H_2O to fill up
approx. 50 U restriction enzyme

The reaction was incubated ON at the optimal working temperature of the specific enzyme. Before loading, samples were partially evaporated to obtain a smaller volume.

Restriction digests of genomic DNA from (ES-) cells in 96-well plates for Southern blot analysis
A typical mix for a restriction digest of genomic DNA in 96-well plates was carried out as follows:

25.0 µl DNA (whole DNA preparation of one well)	
0.40 µl 100x BSA	c_{end} = 1x BSA
0.40 µl 100 mM spermidine	c_{end} = 1 mM spermidine
0.25 µl RNase A 1 mg/ml	c_{end} = 6.25 µg RNase
4.00 µl 10x enzyme buffer	c_{end} = 1x enzyme buffer
2.50 µl enzyme (10 U/µl)	c_{end} = 25 U enzyme/reaction
7.45 µl H_2O	
40.0 µl	

The restriction digest was performed in a 96-well plate sealed with parafilm to prevent evaporation and incubated in a humid chamber at the enzymes optimal temperature ON.

5.2.2.6 Gelelectrophoresis

Analytical agarose gelelectrophoresis Negatively charged DNA/RNA fragments move with different speed, depending on their size, through agarose gels. Small fragments move faster and large fragments slower.
A typical agarose gel was prepared with agarose in a concentration between 0.8 and 2%. The agarose TAE (Tris-acetate, EDTA) buffer solution was prepared in the microwave, cooled down, 5 µl EtBr were added, mixed through swaying, and poured into a gel tray. Finally, the combs were added and the gel was ready to use when it was solid. Prior to loading the gel was putt into a TAE filled gel chamber, loaded with the DNA loading buffer mixture, and voltage was applied for a variable time (usually 30-40 min). To detect the band pattern a UV lamp is needed.
The same procedure was applied for RNA gels despite that the gel chamber, the tray, and the combs were washed with NaOH platelets or with RNAZap. To prevent degradation of RNA the running-time of the gel was shortened to 10 min.

Preparative agarose gelelectrophoresis For DNA purification via gel extraction preparative gel electrophoresis was carried out. Gels were prepared according to the latter section but the bands of the right size were cut out and documented under UV-light with less intensity to avoid UV-light induced damage of DNA.

5.2.2.7 Dephosphorylation of linearized DNA

When a cloning vector is linearized by restriction endonuclease digestion, for the purpose of integrating another DNA fragment, and the resulting overhangs are compatible, the DNA has to be dephosphorylated otherwise the vector will religate. This will influence the efficiency of the ligation because self-ligation is preferred and the insert will not be integrated very efficiently.
A typical mix for the dephosphorylation of linearized plasmid DNA carried out as follows:

1.0 µg DNA	
1.0 µl 10x enzyme buffer	c_{end} = 1x enzyme buffer
1.0 µl alkaline phosphatase (1 U/µl)	c_{end} = 1 U enzyme/reaction (1 µg DNA)
7.0 µl H_2O	
10.0 µl add at	

5.2.2.8 Ligation

Ligations are used to insert DNA fragments of interest into plasmid vectors. First the vector has to be linearized by a restriction enzyme. It does not matter if the DNA fragments have a 3' or 5' overhang or if they are is a blunt ended. The enzyme used for ligating DNA is the T4 DNA ligase isolated from the T4 phage. Ligation depends on ATP which is supplied in the buffer.
Vector and Insert should be used in a 1:3 ratio for best results for a ligation with sticky DNA ends. For a blunt end ligation a 1:1 ratio of vector and insert is recommended.

A typical mix for the ligation of vector with insert is the following:

1.0 µl vector DNA (e.g.; see below)	
0.5 µl insert DNA (e.g.; see below)	
1.0 µl 10x T4 ligation buffer	c_{end} = 1x enzyme buffer
0.5 µl T4 ligase (10 U/µl ; NEB)	c_{end} = 5 U enzyme/reaction
7.0 µl dist. H_2O (add at 10 µl with dist. H_2O)	
10.0 µl	

The used volume of insert can be calculated with the following equation:

Ratio: vector/insert = 1/3

vector concentration:	c(v) [ng/µl] = x ng/µl	size (v) [bp] = y bp
insert concentration:	c(i) [ng/µl] = a ng/µl	size (i) [bp] = b bp
used amount of vector-DNA:	100-400 ng	> used for ligation: v ng / w µl
used amount of insert-DNA:	intron [ng] = 3 * (b bp / y bp) * w µl	> intron DNA [µl]

5.2.2.9 Generation of competent bacteria

Generation of electro-competent bacteria (E. coli K-12 XL1-Blue)
recA1 endA1 gyrA96 thi-1 hsdR17 supE44 relA1 lac [F´ proAB lacIqZΔM15 Tn10 (Tetr)]

Out of a 2 ml pre-culture, bacteria were plated on LB plates with kanamycin (30 µg/ml), tetracycline, ampicillin (40 µg/ml), and with antibiotics as controls and incubated at 37°C ON. The following day, if the control plates have proven that there cannot be found any adapted resistance, a 50 ml preculture was set up for the next day using a single colony and incubated ON at 37°C while shaking. All material that will be used should be washed carefully with clean water. Any detergent that is left will reduce the efficiency of competence. The following day 500 ml LB medium were inoculated with 5 ml bacterial preculture at 37°C until OD_{600} = 0.5 (~3 h).
The following steps were all carried out on ice or at 4°C to prevent the bacteria from warming. Every material used should be precooled. First the bottles with the bacterial suspension were put in ice water for at least 15 min to cool down. The bacteria were then pelleted in clean centrifugation bottles (2x 250 ml) by spinning them for 15 min at 4.000xg in the precooled centrifuge. The pellets were resuspended in 250 ml ice-cold water each and pelleted at 6.000xg for 15 min. Increasing g is necessary to avoid losing a lot of bacteria. After centrifugation each pellet was again resuspended in 125 ml ice-cold water and centrifuged under latter conditions. After this centrifugation step the bacteria were resuspended in 5 ml pre-cooled 10% glycerol solution per pellet and transferred to pre-cooled 30 ml Correx-tubes. The cells were centrifuged at 8.000xg for 15 min. Finally, the pellets were resuspended in 0.5 ml fresh pre-cooled 10% glycerol solution. Aliquots à 40 µl were made and immediately frozen down on dry ice. The bacteria were kept on –80°C.

5.2.2.10 Transformation of bacteria

To transfer foreign DNA into bacteria two methods are used: Transformation of bacteria using electroporation and transformation of bacteria using heat shock.

Transformation of bacteria using electroporation First the competent bacteria were thawed on ice and later 1-2 µl of DNA was added. The mixture was transferred into a pre-cooled electroporation cuvette (0.1 cm) without bubbles. Electroporation was carried out with a tension of U=2.5 kV. After the pulse the bacteria were immediately transferred into a 1.5 ml tube (Eppendorf) using 1 ml LB medium. To allow amplification and regeneration the transformed bacteria were kept shaking (850 rpm; Eppendorf shaker) at 37°C for 30-60 min. Subsequently, the bacteria were put on LB plates supplemented with appropriate antibiotics in a suitable dilution and incubated at 37°C ON.

Transformation of bacteria using heat shock For the transformation of bacteria with heat shock Dh5α cells were thawed on ice. 4 µl of vector DNA was mixed with the bacteria and incubated on ice for 30 min. For the heat shock the mixture was put on 42°C for 90 s, immediately after stored on ice, diluted with 1 ml LB medium, and incubated for regeneration for 30-60 min at 37°C (850 rpm, Eppendorf shaker).

5.2.2.11 Bacterial homologues recombination

Bacteria from a glycerol stock of EL-250/350 were incubated with 2-4 ml LB medium at 32°C ON. On the next day the ON culture was diluted 1:50–1:100 and grown in 50 ml LB medium to OD_{600}=0.6. The culture was split at the appropriate density: 25 ml were left in a Falcon tube at RT (recombineering control), the other 25 ml were kept shaking at 42°C for 15 min. Afterwards both cultures were kept on ice for 5 min and cooled from now on. Bacteria were centrifuged at 5.000 rpm and 4°C for 5-10

min (Eppendorf 5804 R). The bacterial pellets were resuspended in 1.8 ml of ice-cold 10% glycerol and transferred into 2 ml tubes. The suspensions were centrifuged at 14.000 rpm (Eppendorf 5417 R) and 4°C for 20 s. The pellet was resuspended in 1.8 ml 10% ice-cold glycerol (vortexing). This washing step was repeated 3 more times before the pellet was resuspended in 10% glycerol to a total volume of 100 µl. 50 µl of the bacterial suspension were used for each electroporation. 15 ng of the linearized PL-254 vector with retrieval PCRs (e.g.) was mixed with 50 µl of competent cells, left on ice for 5 min and subsequently electroporated.

5.2.2.12 DNA sequencing

To sequence a specific part of the DNA a PCR with only one primer per reaction and fluorescence coupled dideoxynucleotides has to be performed. In principle, each base is linked to a unique color and the integration of one of these labeled bases into the elongating DNA strand stops the elongation reaction. In the end DNA strands of all possible length with the last base being a fluorescent tagged dideoxynucleotide are generated. The master mix for one of these reactions contains:

0.5 µl	BigDye
2.0 µl	BigDye-Puffer
10 pM	Primer (sense/antisense)
(n) bp/100 = x ng	
Σ	5,0 µl

The PCR program used to amplify the sequencing products:

96°C 1 min	
96°C 10 s	35x
50°C 5 s	
60°C 4 min	
16°C ∞	

For subsequent precipitation of the DNA fragments 0.5 µl 125 mM EDTA, 2.0 µl 3 M NaAc, and 50 µl 100% EtOH were applied, mixed, and incubated for 15 min at RT. The DNA was centrifuged at 15.000 rpm at 4°C for 30 min, washed with 70% EtOH, centrifuged again, air dried, and resuspended in 25 µl HPLC water.

5.2.2.13 Southern blot

The Southern blot technique, developed by Edwin Southern, is used to identify a distinct genomic sequence among the pool of DNA present in an organism. The DNA is cut into pieces with the help of restriction enzymes (see 5.2.2.5) and separated by gel electrophoresis (see 5.2.2.6). These restriction fragments are blotted onto a membrane and the sequence of interest is marked by a radioactive or fluorescent labeled specific complementary DNA probe. The radioactive DNA fragment can be visualized by transferring the signal on a film. The Southern blot technique is often used to verify the proper integration of the vector into the host genome.

Gel electrophoresis The digested DNA was applied to a 0.8% gel and separated slowly (30V) ON. On the next day the gel was photographed under UV-light and a ruler, placed next to the DNA ladder, was used for reference length. If the digest is complete, repetitive sequences can be easily detected by a distinct band under UV-light.

Blot The gel was depurinized by incubating it in 989 ml H_2O + 11 ml HCl (conc.) for 15-20 min while shaking. This was followed by a denaturation step in 0.4 M sodium hydroxide and 0.6 M sodium chloride for 30 min again while shaking. For neutralization the gel was incubated in a solution of 0.5 M Tris and 1 M sodium chloride (pH 7.2) for 30 min again while shaking. The blot was built up in 20x SSC (saline-sodium citrate) as follows and the transfer was carried out ON. 2 sheets of 20x SSC soaked blotting paper with contact to a 20x SSC reservoir were placed on a glass plate. 3 additional 20x SSC blotting papers with perfect size of the gel were placed bubble free on top of the first papers. Now the gel was applied upside down to the blot. The nitrocellulose membrane was placed on top. A few layers of blotting paper and paper towels closed the blot. The next day, the blot was taken apart and the slots of the gel were marked on the membrane with a pen. Afterwards, the membrane was dried and cross-linked for 30 min at 80°C or treated in the cross-linker (UV Stratalinker 1800; Stratagene) for 1 min.

Hybridization The hybridization involves the three following steps.

Prehybridization 30 ml hybridization buffer were preheated to 65°C in a water bath. The membrane was rolled and put into the hybridization tube (Hybridizer HB 100; ThermoHybaid, Thermo Electron Cooperation) and the preheated buffer was poured into the tube. The membrane was prehybridized in an oven at 65°C for at least 1.5-2 h.

Radioactive labeling of the probe 100 ng of the linearized DNA probe was diluted with dist. H_2O to a final volume of 24 µl in an Eppendorf reaction tube. 10 µl of random oligonucleotides were added and the mixture was boiled for denaturation in a water bath for 5 min. Subsequently, the tube was put on ice, centrifuged, and put back on ice. 10 µl 5x buffer (d*CTP-buffer for 32P labeled CTP) was added. The next steps were carried out in the radioactive lab. Radioactive labeled dCTP (50 Cu) and 5 U Klenow-enzyme (Exo(-) Klenow, 1 µl, 5 U/µl) were added, the mixture well-mixed, shortly centrifuged, and labeled at 37-40°C for 2-10 min. For completion of the labeling 2 µl STOPmix were added.
For the purification (removal of proteins and residual nucleotides) the reaction mixture was loaded on a prepared column (centrifuged without sample for 2 min at 400 g) and centrifuged at 400 g for 2 min. Afterwards, 1 µl of the sample was used to measure the activity. For denaturation of the probe 500 µl salmon sperm DNA (10 mg/ml) were denatured at 100°C in a water bath for 10 min, put in a 50 ml Falcon tube, and stored on ice. The labeled probe was added in a final concentration of $1x10^6$ counts per 1 ml hybridization buffer. By adding 50 µl 10 N sodium hydroxyl the sample was denatured while the tube was swung carefully to mix. Further on swinging, 300 µl 2 M Tris, pH8.0, and afterwards 475 µl 1 M HCl were pipetted drop wise into the tube for neutralization.

Hybridization After the prehybridization step the 10 ml hybridization buffer were discarded and the radioactive-labeled DNA probe was pipetted into the hybridization tube. The tube was put back into the oven on 65°C rotating for 12-24 h. The following day the probe was decanted from the

glass tube and the membranes were washed with 2x SSC/0.5% SDS (approx. 250 ml, RT) for 5 min at RT. After the 5 min washing step the buffer was discarded. The membranes were washed with 500 ml fresh 2x SSC/0.5% SDS preheated to 65°C up to 30 min while shaking in a 65°C water bath. Replace the washing buffer as necessary. If the probe was used the first time control measurements were carried out every 5 min. If the signal was approximately 100-200x10^2 counts the washing step was simply repeated. The stringency of the washing steps could be raised by lowering the concentration of SSC (1x SSC 0.5% SDS or 0.1x SSC/0.5% SDS) if higher signals were measured (> 200x10^2 counts). Finally, at approximately 35x10^2 counts, the membrane was wrapped tightly in saran wrap and fixed in a film cassette. A film (Kodak, BioMax) was applied, stored at –80°C ON and developed the following day (AGFA Curix 60).

5.2.3 Protein biochemistry

5.2.3.1 Protein extraction

To prevent proteins from degradation quick and work on low temperature is required. Proteins of the whole cell or of single compartments can be isolated depending on the used lysis buffer. Protease inhibitors and working on ice keeps the proteins intact.

Whole cell lysate After washing the cells with ice-cold PBS 50-100 µl lysis buffer supplemented with protease inhibitor cocktail was applied to one well of a 6-well plate. Cells were released using a cell scraper and transferred to a 1.5 ml reaction tube (Eppendorf) with a pipette. Cells were now rocked at 4°C in a shaker (Thermomixer comfort, Eppendorf) for 10 min. After this incubation step the lysed cells were centrifuged at 14.000 rpm (centrifuge: 5417R, Eppendorf) and 4°C for 10 min to precipitate insoluble constituents like nuclei and parts of the membrane. The supernatant contains the proteins. It was transferred to a new pre-cooled tube and stored on –80°C or used immediately. 1 µl was kept separately for the determination of the protein concentration with Bicinchoninic acid (BCA; see 5.2.3.2).

5.2.3.2 Determination of protein concentrations

BCA is a chromogenic reagent specific for Cu(I) because it forms in a violet complex with Cu(I) that has its absorption maximum at 562 nm. Proteins are able to reduce alkaline Cu(II) to Cu(I) in a concentration dependent manner. To determine the protein concentration of a sample the protein solution was compared to a standard row with known concentrations in a photometer. This is possible because the absorption of the BCA Cu(I) complex is directly proportional to the protein concentration.
The standard row was prepared with the following dilutions of BSA in lysis buffer: 25 µg/ml, 125 µg/ml, 250 µg/ml, and 500 µg/ml. The protein samples were diluted with lysis buffer 1:50. 50 µl null control (only lysis buffer), standard row, and samples were mixed 1:20 with BCA solution (+1 ml). The mixtures were incubated at 50°C for 15-30 min till the color changed to violet. The null control, the standard dilutions, and the protein samples were cooled down to RT and measured in an Eppendorf photometer. Then the dilution factor for the samples (1 in 49) was entered and the absorptions and concentrations of the samples were determined.

5.2.3.3 Western blot

With the Western blot method proteins are separated by their size via electrophoreses on a denaturing polyacrylamide gel. Sodiumdodecylsulfate (SDS) covers the proteins and thereby gives all proteins a negative charge according to their size. The proteins are then transferred onto a membrane using electric tension in a wet or semi-dry blot. Proteins bound to this membrane can be detected with specific antibodies. These primary antibodies are detected by specific secondary antibodies coupled to horseradish peroxidase (HRP). This enzyme catalyzes the reaction of a substrate into a gloomy product that can be exposed to a film. For saturation of unspecific binding sides of (mostly) the secondary antibody milk powder is used for blocking.

Denaturing SDS-polyacrylamide gelectrophorese (SDS-PAGE)
For four separating gels (10% - or see list below) the following mixture was used:

10.0 ml acrylamide/bisacrylamide-mixture (ready-to-use)
7.5 ml 4x Tris/SDS buffer, pH8.8
12.5 ml H_2O
40.0 µl TEMED
300.0 µl APS

The mixture was immediately filled between two glass plates with a 10 ml pipette and covered with water or ethanol to exclude air and achieve a sharp and straight border without bubbles. After polymerization of the gel the water/ethanol was decanted and completely suck off with a paper towel.
For 4 collecting gels (approximately 1 cm deep underneath the pockets) the following mixture was prepared:

1.3 ml acrylamide/bisacrylamide-mixture (ready-to-use)
2.5 ml 4x Tris/SDS buffer, pH6.8
6.2 ml H_2O
20.0 µl TEMED
100.0 µl APS

The mixture was immediately filled between the two glass plates with a 10 ml pipette till the upper rim was reached then the comb was inserted.
The samples were mixed 1:3 with 4x SDS loading buffer mixed with dithiothreitol (DTT). This mixture was denatured at 95°C for 4 min and afterwards stored on ice. The comb was removed and the pockets were rinsed with H_2O. Gels were put into the gel chamber filled with 1x Tris glycine running buffer. The gel pockets were rinsed again to remove remaining gel filaments. The samples were applied into the gel pockets (20 µl protein weight marker) and separated at 20 mA for approximately 45 min.
Acrylamide concentration (in %) linear range of separation (kDa)

%	kDa
15.0	12 – 43
10.0	16 – 68

7.0	36 – 94
5.0	57 – 212

Immunoblot: Semi-dry Blot
The glass plates were separated, the gels taken out, and equilibrated in KP buffer for 10 min. The PVDF membrane was activated in methanol for 15 s, incubated in H_2O for 2 min, and afterwards in APII buffer for 5 min.

The blot was built up as follows:

Anode
1x blotting paper (thick) wet with API
1x blotting paper (thin) wet with APII
PVDF- membrane
gel
1x blotting paper (thick) wet with KP
Cathode

The gel was blotted at 220 mA (per small gel) for 20 min then the blot was broken up and the membrane was (optionally) put into Ponceau-S solution for 5 min to confirm successful blotting. The membrane was washed or de-stained with H_2O.

Immunostaining After the proteins were blotted on the membrane the membrane was blocked with blocking solution (1x TBST buffer + 5% milk powder (w/v) + 1 g BSA (per 50 ml)) for 2 h. The primary antibody in blocking solution was added and incubated for at least 2 h at RT (or ON at 4°C). Now the membrane was washed 3x with 1x TBST for 15 min. Afterwards, it was incubated with the secondary antibody in blocking solution at RT for 1-2 h. The membrane was rinsed 3x using 1x TBST and washed 3x for 15 min while shaking. After washing the membrane was put on a glass plate. For the enzymatic reaction ECL (enhanced chemiluminescence) solution one and two was mixed immediately before it was applied on the membrane on the glass plate. Then the membranes were wrapped in foil and exposed to a film for 1 s to 10 min. After exposure the film was developed.

5.2.3.4 Immunoprecipitation

Immunoprecipitation is a method that enables the purification of a specific protein from a cell lysate or extract. To analyze protein-protein interactions under native conditions we used the tandem affinity purification (TAP) method. Here we pulled out the TAP-tagged Fltp protein and its interaction partners by Strep-Tactin superflow resin beads. Through this the protein of interest is physically isolated from the rest of the sample. The sample can later be separated by SDS-PAGE and Western blot analysis can be carried out to identify interaction partners.
For the interaction analysis we used HEK293T cells transfected with Fltp-TAP-TAG and as a control HEK293T cells only transfected with TAP-TAG.
The first step was to remove the medium from the culture dishes. The cells were then rinsed with warm PBS. To lyse the cells they were incubated with 1 ml ice cold lysis buffer (see 5.1.5) per 10 cm dish on ice. The nuclei and the cell debris was spinned down for 10 min at 10.000 xg at 4°C. The

lysates were cleaned by filtration through syringe filters (MILLEX GP, 0.22 µm, Millipore). 1 mg of the filtered lysate was incubated with 50 µl Strep-Tactin superflow resin (IBA) in 1 ml of lysis buffer for 1 h at 4°C in an overhead tumbler. The protein-Strep-Tactin solution was spinned down for 30 s at 7.000 xg and transferred to microspin columns (GE-Healthcare). The supernatant was spinned down for 5 s at 100 xg, washed 3 times with 500 µl wash buffer (see 5.1.5) (centrifuge 5 s, 100 xg). The protein was eluted by 500 µl desthiobiotin elution buffer (IBA) and incubated for 10 min while mixing the resin for several times. The elute can now be used for Western blot analysis.

5.2.3.5 Immunohistochemistry

Cryosections Dissected tissues were fixed in 4% paraformaldehyde (PFA) and cryoprotected by incubation in a sucrose gradient for at least 1 h each (5%, 15%, 30%). Tissues were frozen in OCT (optimal cutting temperature) after which immunohistochemical staining was carried out on 8 to 12 µm-thick sections, mounted on glass slides. Briefly, sections were rehydrated in PBS, permeabilised for 10 min in 0.1 M glycine/0.1% TritonX100 in PBS, and blocked for 1 h in 5% donkey serum/PBS-Tween 0.1% (PBS-T). Finally, the sections were incubated with the primary antibody in blocking solution ON at 4°C. The next day, the slides were washed with PBS-T, incubated with the secondary antibody in PBS for 2 h at RT, washed with PBS, and incubated with DAPI and finally mounted with ProLong Gold antifade reagent (Invitrogen, P36930).

Whole mount stainings Immunofluorescence whole-mount stainings were performed as previously described (Nakaya et al., 2005). Briefly, embryos were isolated, fixed for 20 min in 2% PFA in PBS, and then permeabilized in 0.1% Triton X-100 in 0.1 M glycine pH 8.0. After blocking in 10% FCS, 3% goat serum, 0.1% BSA, 0.1% Tween 20 for 2 h, embryos were incubated with the primary antibody ON at 4°C in blocking solution. After several washes in PBS containing 0.1% Tween-20 (PBST) embryos were incubated with secondary antibodies in blocking solution for 3 h. During the final washes with PBST, embryos were stained with 4',6-diamidino-2-phenylindole, dihydrochloride (DAPI), transferred into 40% glycerol, and embedded between two coverslips using 120 µm Secure-Seal spacers (Invitrogen, S24737) and ProLong Gold antifade reagent (Invitrogen, P36930).
Image acquisition was performed on a Leica DMI 6000 confocal microscope and image analysis was carried out using Leica LAS AF software.

5.2.4 Embryology

5.2.4.1 Genotyping of mice and embryos

Mice at weaning age were genotyped using the method **Isolation of genomic DNA from mouse tail biopsy** (see 5.2.2.1.2). Embryos were genotyped using the **Hot shot method** (see 5.2.2.1.2).

Genotyping of *Foxa2*^{T2AiCre} mouse line Mice were genotyped by PCR analysis of tail tip DNA. Genotyping of the *Foxa2*$^{T2AiCre/+}$ intercrosses (after Flp-e mediated excision of the *neomycin* selection cassette) was performed using either a forward primer in exon 3 of the *Foxa2* locus (EP397, for all following primers see 5.1.9.1) or a forward primer in the *iCre* (EP564) in combination with a reverse primer in the 3' UTR (EP398). Using 35 cycles at an annealing temperature of 55°C, this PCR yields products of 207 bp and 457 bp for the *WT* and for the targeted allele, respectively.

Genotyping of *Fltp^{zv}* mouse line Genotyping of this mouse line (after Cre mediated excision of the *neomycin* selection cassette) was performed using a forward primer located in exon 6 of *Fltp* (EP566, for all following primers see 5.1.9.1) and a forward primer located in the artificial *SV40-polyA* sequence (EP418) as well as a reverse primer located in the 3' UTR (EP565). With an annealing temperature of 57°C and 35 cycles this PCR amplified a *WT* product of 317 bp and a targeted allele band of 387 bp.

Genotyping of the *Fltp^{T2AiCre}* mouse line Genotyping of this mouse line (after Flp-e mediated excision of the *neomycin* selection cassette) was performed using a forward primer in the *Fltp* locus, in exon six (EP566, for all following primers see 5.1.9.1) and a forward primer in the *iCre* (EP568) in combination with the reverse primer in the 3' UTR (EP565). Using 35 cycles at an annealing temperature of 57°C, this PCR yields products of 317 bp and 229 bp for the *WT* and for the targeted allele, respectively.

Genotyping of *Dlg3:Venus* mouse line Here we used a forward primer located in the *Venus* reporter gene (EP180, for all following primers see 5.1.9.1) and a reverse primer also located in the *Venus* (EP181). A PCR performed with an annealing of 60°C and 32 cycles amplifies a product of 312 bp.

Genotyping of *SAP-102* mouse line was performed using a forward primer EP534 (for all following primers see 5.1.9.1) upstream of the selection cassette integration site and a reverse primer EP535 in the *WT* sequence deleted by the targeted mutation as well as a reverse primer EP536 within the selection cassette. Amplification of 33 cycles with an annealing of 58°C yielded a *WT* product of 535 bp and a 215 bp product for the targeted allele.
The gene trap clone P038A02 (R1 on a pure 129Sv6 genetic background) was obtained from the German Gene Trap Consortium. *Dlg3$^{tm1Grnt/Y}$* male and *Dlg3$^{tm1Grnt/+}$* female mice on a C57Bl/6 background were genotyped as previously described (Cuthbert et al., 2007).

Genotyping of *Fltp^{zv}; Celsr1^{Crsh}* mouse line First we performed a PCR with the forward primer EP779 (for all following primers see 5.1.9.1) and the reverse primer EP780 resulting in a 321 bp band. Next we purified the PCR product via the PCR purification kit and sequenced the product in both directions. The adenine in the *WT* was replaced by a guanine in the mutated sequence. For the *Fltp^{zv}* genotyping we used the protocol described above.

Genotyping of *R26R* mouse line Genotyping of *R26R Cre* reporter strain (background C57Bl/6) was performed by PCR as described (Soriano, 1999).

5.2.4.2 PCR Programs for genotyping

***Foxa2^{T2AiCre}* PCR program**

94°C 10 min		
94°C 45 sec	}	35x
59°C 45 sec		
72°C 45 sec		
72°C 10 min		
16°C ∞		

***Fltp*^{ZV} PCR program**	95°C 4 min 95°C 30 sec 57°C 45 sec 72°C 1 min } 35x 72°C 10 min 16°C ∞
***Fltp*^{T2AiCre} PCR program**	95°C 4 min 95°C 30 sec 57°C 45 sec 72°C 1 min } 35x 72°C 10 min 16°C ∞
***Venus* PCR program**	95°C 10 min 95°C 45 sec 60°C 45 sec 72°C 50 sec } 35x 72°C 10 min 16°C ∞
***SAP-102* PCR program**	94°C 5 min 94°C 30 sec 58°C 40 sec 72°C 1:30 min } 33x 72°C 10 min 16°C ∞
***Fltp*^{ZV}*; Celsr1*^{Crsh} PCR program**	94°C 4 min 94°C 30 sec 56°C 1 min 72°C 1 min } 35x 72°C 10 min 16°C ∞

5.2.4.3 Isolation of embryos and organs

Dissections of embryos and organs were carried out according to Nagy and Behringer („Manipulating the mouse embryo: a laboratory manual“). Embryos were staged according to Downs and Davies (Downs and Davies, 1993).

5.2.4.4 X-gal (5-bromo-4-chloro-3-indolyl β-D-galactoside) staining

β-gal staining of whole-mount embryos and organs were performed as previously described (Liao et al., 2009). Some tissues were further processed (see 5.2.4.5). Not BABB treated whole-mount embryos/organs were fixed, washed in PBS, and photographed on a Zeiss Lumar.V12 Stereo microscope using an AxioCam MRc5 camera. BABB treated embryos/organs were left in BABB for photographing.

5.2.4.5 Tissue clearing with BABB

Tissues were dehydrated through a methanol/H_2O series: 2 h in 25% methanol/H_2O, 2 h in 50% methanol/H_2O, 2 h in 75% methanol/H_2O and ON in 100% methanol. Finally the tissue was transferred to a clearing solution, a 1:2 mixture of benzyl alcohol and benzyl benzoate (BABB) and photographed on a Zeiss Lumar.V12 Stereo using an AxioCam MRc5 camera.

5.2.4.6 Whole-mount *in situ* hybridization

To visualize gene expression patterns in mouse, embryos, or organs whole-mount *in situ* hybridization was used. Complementary RNA probes labeled with digoxygenin are recognized by an antibody that can be visualized by an enzymatic reaction with BM-purple. For the *in situ* hybridization embryos have to be dissected fast and sterile. Next they were fixed 1 h at 4°C and dehydrated in an increasing methanol series. Embryos can be stored at -20°C.

Day 1
First embryos were rehydrated in a decreasing methanol/PBST gradient for 5 min each step and washed twice in PBST for 10 min. To clear the embryos an incubation in 3% H_2O_2 in PBST at RT followed by 3x washing in PBST for 5 min. Now the embryos were fixed in 4% PFA/0.2% glutaraldehyd for 20 min followed by 3x washing for 5 min in PBST. Prehybridization is carried out for 2 h at 70°C. Afterwards, the solution is changed and the labeled RNA probes are applied in hybridization juice and incubated ON at 70°C.

PBST: 1x PBS, 0.1% Tween-20
Prehybridization: 50% Formamid, 5x SSC pH4.5, 1% SDS, 50 µg/ml yeast tRNA, 50 µg/ml Heparin
Hybridization: Prehybridization, 1 µg/ml probe

Day 2
Solution I was preheated on 70°C. The embryos were washed at 70°C for 30 min and subsequently in TNT solution 3x for 5 min at RT. To digest the remaining RNA probes a RNase digest was performed at 37°C (0.1 mg/ml in TNT). Now the embryos were washed 3x 30 min in solution II followed by 3x 5 min in MAB. Blocking was performed in blocking solution for 2 h. Antibody incubation was done ON at 4°C

Solution I:	50% Formamid, 5x SSC pH4.5, 1% SDS
Solution II:	50% Formamid, 5x SSC pH4.5, 0.2% SDS
TNT:	10 mM Tris HCl pH7.5, 0.5 M NaCl, 0.1% Tween-20

MAB:	100 mM Maleic Acid, 150 mM NaCl, 2 mM Levamisole, 0.1% Tween20, pH7.5 with NaOH
Blocking solution:	MAB, 2% BM Blocking reagent
Antibody solution:	Embryo powder was incubated for 30 min in 5 ml blocking solution at 70°C and cooled down on ice. 50 µl sheep serum was added and 4 µl anti-DIG-alkaline-phosphatase-antibody (1:5.000). After 1 h incubation on ice the solution was centrifuge at 5.000 rpm at 4°C. The supernatant was transferred into a new Falcon tube and 15 ml blocking solution with 1% sheep serum was added.

Day 3

The embryos were washed with MAB every hour at RT while shaking and ON at 4°C.

Day 4

On the next day the embryos were washed 2x for 10 min in NTMT at RT and transferred to BM-purple. For the chromogenic reaction handle the embryos in darkness. Depending on the probe a chromogenic reaction could be observed between 1 h and 4 days. Afterwards, the embryos were washed in PBST and fixed in 4% PFA.

NTMT:	100 mM Tris HCl pH9.5, 50 mM $MgCl_2$, 100 mM NaCl, 0.1% Tween20

5.2.5 Histology

5.2.5.1 Paraffin sections

After *in situ* hybridization or lacZ staining the embryos were dehydrated via a methanol series (25%, 50%, 75%, and 2x100%) for 10 min per step. To make the embryos transparent they were cleared 2x in xylol for 5-10 min (depending on the thickness of the specimen). For tissue penetration of the paraffin the specimen was left in paraffin at 65°C ON. On the next day they were transferred into fresh paraffin and incubated at 65°C ON. Now the embryos can be orientated and embedded into a mold. The cooled down paraffin blocks were mounted onto a grid and could be sectioned on a microtome. The sections were mounted on glass slides, dried ON at 37°C, dewaxed in xylol (2x 15 min), fixed with mounting medium, and covered with a cover slip. After one night at 4°C the sections were ready for microscopical analyses.

Histological staining of paraffin sections using Nuclear Fast Red (NFR) First, paraffin sections on glass slides were dewaxed twice for 15 min in xylene. An alcohol row (100%, 90%, 80%, 70%, 1 min each) for rehydration followed and ended in H_2O. Afterwards, the slides were dipped into NFR for 1 min and thoroughly washed with dist. H_2O. Then a dehydration step followed within an afferent alcohol row (70-100%, see above). Finally, the slides were incubated twice in xylene for 15-30 min and once in Rotihistol for 15-30 min. After incubation in Rotihistol slides were put on a paper towel, sprinkled with a few drops mounting medium, and covered with a cover slip.

5.2.5.2 Cryosections

Freshly isolated embryos or organs were fixed from 30 min (RT) up to ON (4°C) in 4% PFA. After 3x 10 min washes in PBS the embryos/organs were incubated in 5%, 15%, 30% sucrose in PBS until they sunk on the bottom of the tube. Now the solution was exchanged to a 50:50 solution of 30% sucrose in PBS and OCT embedding medium. The specimen was incubated until it sunk to the bottom of the tube. Afterwards, it was washed in 100% OCT, embedded in a mold, and orientated. To freeze the tissue the molds were placed on dry ice and stored at -80°C until use. Before sectioning the specimen was put on -20°C for an hour and 10-12 µm thick sections were cut of using a cryostat.

6 Literature

Adams, C.L., Chen, Y.T., Smith, S.J., and Nelson, W.J. (1998). Mechanisms of epithelial cell-cell adhesion and cell compaction revealed by high-resolution tracking of E-cadherin-green fluorescent protein. The Journal of cell biology *142*, 1105-1119.

Adler, P.N., and Lee, H. (2001). Frizzled signaling and cell-cell interactions in planar polarity. Current opinion in cell biology *13*, 635-640.

Ahn, S., and Joyner, A.L. (2004). Dynamic changes in the response of cells to positive hedgehog signaling during mouse limb patterning. Cell *118*, 505-516.

Anderson, C.T., and Stearns, T. (2009). Centriole age underlies asynchronous primary cilium growth in mammalian cells. Curr Biol *19*, 1498-1502.

Ang, S.L., Conlon, R.A., Jin, O., and Rossant, J. (1994). Positive and negative signals from mesoderm regulate the expression of mouse Otx2 in ectoderm explants. Development *120*, 2979-2989.

Ang, S.L., and Rossant, J. (1994). HNF-3 beta is essential for node and notochord formation in mouse development. Cell *78*, 561-574.

Angers, S., and Moon, R.T. (2009). Proximal events in Wnt signal transduction. Nature reviews Molecular cell biology *10*, 468-477.

Barald, K.F., and Kelley, M.W. (2004). From placode to polarization: new tunes in inner ear development. Development *131*, 4119-4130.

Bastida, M.F., Sheth, R., and Ros, M.A. (2009). A BMP-Shh negative-feedback loop restricts Shh expression during limb development. Development *136*, 3779-3789.

Beddington, R.S. (1994). Induction of a second neural axis by the mouse node. Development *120*, 613-620.

Beddington, R.S., and Robertson, E.J. (1998). Anterior patterning in mouse. Trends in genetics : TIG *14*, 277-284.

Belo, J.A., Bouwmeester, T., Leyns, L., Kertesz, N., Gallo, M., Follettie, M., and De Robertis, E.M. (1997). Cerberus-like is a secreted factor with neutralizing activity expressed in the anterior primitive endoderm of the mouse gastrula. Mechanisms of development *68*, 45-57.

Bertani, G. (1951). A Method for Detection of Mutations, Using Streptomycin Dependence in Escherichia Coli. Genetics *36*, 598-611.

Bilder, D., Li, M., and Perrimon, N. (2000). Cooperative regulation of cell polarity and growth by Drosophila tumor suppressors. Science *289*, 113-116.

Bilder, D., and Perrimon, N. (2000). Localization of apical epithelial determinants by the basolateral PDZ protein Scribble. Nature *403*, 676-680.

Bloodgood, R.A. (2010). Sensory reception is an attribute of both primary cilia and motile cilia. Journal of cell science *123*, 505-509.

Blum, M., Gaunt, S.J., Cho, K.W., Steinbeisser, H., Blumberg, B., Bittner, D., and De Robertis, E.M. (1992). Gastrulation in the mouse: the role of the homeobox gene goosecoid. Cell *69*, 1097-1106.

Boisvieux-Ulrich, E., Laine, M.C., and Sandoz, D. (1990). Cytochalasin D inhibits basal body migration and ciliary elongation in quail oviduct epithelium. Cell and tissue research *259*, 443-454.

Brody, S.L., Yan, X.H., Wuerffel, M.K., Song, S.K., and Shapiro, S.D. (2000). Ciliogenesis and left-right axis defects in forkhead factor HFH-4-null mice. American journal of respiratory cell and molecular biology *23*, 45-51.

Burtscher, I., and Lickert, H. (2009). Foxa2 regulates polarity and epithelialization in the endoderm germ layer of the mouse embryo. Development *136*, 1029-1038.

Carney, P.R., and Silver, J. (1983). Studies on cell migration and axon guidance in the developing distal auditory system of the mouse. The Journal of comparative neurology *215*, 359-369.

Chen, J., Knowles, H.J., Hebert, J.L., and Hackett, B.P. (1998). Mutation of the mouse hepatocyte nuclear factor/forkhead homologue 4 gene results in an absence of cilia and random left-right asymmetry. The Journal of clinical investigation *102*, 1077-1082.

Cizmecioglu, O., Arnold, M., Bahtz, R., Settele, F., Ehret, L., Haselmann-Weiss, U., Antony, C., and Hoffmann, I. (2010). Cep152 acts as a scaffold for recruitment of Plk4 and CPAP to the centrosome. The Journal of cell biology *191*, 731-739.
Conduit, P.T., Brunk, K., Dobbelaere, J., Dix, C.I., Lucas, E.P., and Raff, J.W. (2010). Centrioles regulate centrosome size by controlling the rate of Cnn incorporation into the PCM. Curr Biol *20*, 2178-2186.
Copeland, N.G., Jenkins, N.A., and Court, D.L. (2001). Recombineering: a powerful new tool for mouse functional genomics. Nature reviews Genetics *2*, 769-779.
Copp, A.J., and Greene, N.D. (2010). Genetics and development of neural tube defects. The Journal of pathology *220*, 217-230.
Copp, A.J., Greene, N.D., and Murdoch, J.N. (2003). Dishevelled: linking convergent extension with neural tube closure. Trends in neurosciences *26*, 453-455.
Corbit, K.C., Aanstad, P., Singla, V., Norman, A.R., Stainier, D.Y., and Reiter, J.F. (2005). Vertebrate Smoothened functions at the primary cilium. Nature *437*, 1018-1021.
Courbard, J.R., Djiane, A., Wu, J., and Mlodzik, M. (2009). The apical/basal-polarity determinant Scribble cooperates with the PCP core factor Stbm/Vang and functions as one of its effectors. Developmental biology *333*, 67-77.
Curtin, J.A., Quint, E., Tsipouri, V., Arkell, R.M., Cattanach, B., Copp, A.J., Henderson, D.J., Spurr, N., Stanier, P., Fisher, E.M.*, et al.* (2003). Mutation of Celsr1 disrupts planar polarity of inner ear hair cells and causes severe neural tube defects in the mouse. Curr Biol *13*, 1129-1133.
Cuthbert, P.C., Stanford, L.E., Coba, M.P., Ainge, J.A., Fink, A.E., Opazo, P., Delgado, J.Y., Komiyama, N.H., O'Dell, T.J., and Grant, S.G. (2007). Synapse-associated protein 102/dlgh3 couples the NMDA receptor to specific plasticity pathways and learning strategies. The Journal of neuroscience : the official journal of the Society for Neuroscience *27*, 2673-2682.
Dabdoub, A., and Kelley, M.W. (2005). Planar cell polarity and a potential role for a Wnt morphogen gradient in stereociliary bundle orientation in the mammalian inner ear. Journal of neurobiology *64*, 446-457.
Dawe, H.R., Farr, H., and Gull, K. (2007). Centriole/basal body morphogenesis and migration during ciliogenesis in animal cells. Journal of cell science *120*, 7-15.
Deans, M.R., Antic, D., Suyama, K., Scott, M.P., Axelrod, J.D., and Goodrich, L.V. (2007). Asymmetric distribution of prickle-like 2 reveals an early underlying polarization of vestibular sensory epithelia in the inner ear. The Journal of neuroscience : the official journal of the Society for Neuroscience *27*, 3139-3147.
Dessaud, E., McMahon, A.P., and Briscoe, J. (2008). Pattern formation in the vertebrate neural tube: a sonic hedgehog morphogen-regulated transcriptional network. Development *135*, 2489-2503.
Dietrich, J.E., and Hiiragi, T. (2007). Stochastic patterning in the mouse pre-implantation embryo. Development *134*, 4219-4231.
Donnelly, M.L., Hughes, L.E., Luke, G., Mendoza, H., ten Dam, E., Gani, D., and Ryan, M.D. (2001). The 'cleavage' activities of foot-and-mouth disease virus 2A site-directed mutants and naturally occurring '2A-like' sequences. The Journal of general virology *82*, 1027-1041.
Downs, K.M., and Davies, T. (1993). Staging of gastrulating mouse embryos by morphological landmarks in the dissecting microscope. Development *118*, 1255-1266.
Dymecki, S.M. (1996). Flp recombinase promotes site-specific DNA recombination in embryonic stem cells and transgenic mice. Proceedings of the National Academy of Sciences of the United States of America *93*, 6191-6196.
Dzhindzhev, N.S., Yu, Q.D., Weiskopf, K., Tzolovsky, G., Cunha-Ferreira, I., Riparbelli, M., Rodrigues-Martins, A., Bettencourt-Dias, M., Callaini, G., and Glover, D.M. (2010). Asterless is a scaffold for the onset of centriole assembly. Nature *467*, 714-718.
Eggenschwiler, J.T., and Anderson, K.V. (2007). Cilia and developmental signaling. Annual review of cell and developmental biology *23*, 345-373.
Eichers, E.R., Abd-El-Barr, M.M., Paylor, R., Lewis, R.A., Bi, W., Lin, X., Meehan, T.P., Stockton, D.W., Wu, S.M., Lindsay, E.*, et al.* (2006). Phenotypic characterization of Bbs4 null mice reveals age-dependent penetrance and variable expressivity. Human genetics *120*, 211-226.

Engert, S., Liao, W.P., Burtscher, I., and Lickert, H. (2009). Sox17-2A-iCre: a knock-in mouse line expressing Cre recombinase in endoderm and vascular endothelial cells. Genesis *47*, 603-610.
Etheridge, S.L., Ray, S., Li, S., Hamblet, N.S., Lijam, N., Tsang, M., Greer, J., Kardos, N., Wang, J., Sussman, D.J.*, et al.* (2008). Murine dishevelled 3 functions in redundant pathways with dishevelled 1 and 2 in normal cardiac outflow tract, cochlea, and neural tube development. PLoS genetics *4*, e1000259.
Formstone, C.J., and Little, P.F. (2001). The flamingo-related mouse Celsr family (Celsr1-3) genes exhibit distinct patterns of expression during embryonic development. Mechanisms of development *109*, 91-94.
Frank, D.U., Elliott, S.A., Park, E.J., Hammond, J., Saijoh, Y., and Moon, A.M. (2007). System for inducible expression of cre-recombinase from the Foxa2 locus in endoderm, notochord, and floor plate. Developmental dynamics : an official publication of the American Association of Anatomists *236*, 1085-1092.
Frolenkov, G.I., Belyantseva, I.A., Friedman, T.B., and Griffith, A.J. (2004). Genetic insights into the morphogenesis of inner ear hair cells. Nature reviews Genetics *5*, 489-498.
Gangar, A., Rossi, G., Andreeva, A., Hales, R., and Brennwald, P. (2005). Structurally conserved interaction of Lgl family with SNAREs is critical to their cellular function. Curr Biol *15*, 1136-1142.
Gao, B., Song, H., Bishop, K., Elliot, G., Garrett, L., English, M.A., Andre, P., Robinson, J., Sood, R., Minami, Y.*, et al.* (2011). Wnt signaling gradients establish planar cell polarity by inducing Vangl2 phosphorylation through Ror2. Dev Cell *20*, 163-176.
Gerdes, J.M., Liu, Y., Zaghloul, N.A., Leitch, C.C., Lawson, S.S., Kato, M., Beachy, P.A., Beales, P.L., DeMartino, G.N., Fisher, S.*, et al.* (2007). Disruption of the basal body compromises proteasomal function and perturbs intracellular Wnt response. Nature genetics *39*, 1350-1360.
Glinka, A., Wu, W., Delius, H., Monaghan, A.P., Blumenstock, C., and Niehrs, C. (1998). Dickkopf-1 is a member of a new family of secreted proteins and functions in head induction. Nature *391*, 357-362.
Gloeckner, C.J., Boldt, K., and Ueffing, M. (2009). Strep/FLAG tandem affinity purification (SF-TAP) to study protein interactions. Current protocols in protein science / editorial board, John E Coligan [et al] *Chapter 19*, Unit19 20.
Goetz, S.C., and Anderson, K.V. (2010). The primary cilium: a signalling centre during vertebrate development. Nature reviews Genetics *11*, 331-344.
Goss, A.M., Tian, Y., Tsukiyama, T., Cohen, E.D., Zhou, D., Lu, M.M., Yamaguchi, T.P., and Morrisey, E.E. (2009). Wnt2/2b and beta-catenin signaling are necessary and sufficient to specify lung progenitors in the foregut. Dev Cell *17*, 290-298.
Graham, F.L., Smiley, J., Russell, W.C., and Nairn, R. (1977). Characteristics of a human cell line transformed by DNA from human adenovirus type 5. The Journal of general virology *36*, 59-74.
Gray, R.S., Abitua, P.B., Wlodarczyk, B.J., Szabo-Rogers, H.L., Blanchard, O., Lee, I., Weiss, G.S., Liu, K.J., Marcotte, E.M., Wallingford, J.B.*, et al.* (2009). The planar cell polarity effector Fuz is essential for targeted membrane trafficking, ciliogenesis and mouse embryonic development. Nat Cell Biol *11*, 1225-1232.
Grzybowski, D.M., Holman, D.W., Katz, S.E., and Lubow, M. (2006). In vitro model of cerebrospinal fluid outflow through human arachnoid granulations. Investigative ophthalmology & visual science *47*, 3664-3672.
Guirao, B., Meunier, A., Mortaud, S., Aguilar, A., Corsi, J.M., Strehl, L., Hirota, Y., Desoeuvre, A., Boutin, C., Han, Y.G.*, et al.* (2010). Coupling between hydrodynamic forces and planar cell polarity orients mammalian motile cilia. Nat Cell Biol *12*, 341-350.
Habas, R., and Dawid, I.B. (2005). Dishevelled and Wnt signaling: is the nucleus the final frontier? Journal of biology *4*, 2.
Habas, R., Kato, Y., and He, X. (2001). Wnt/Frizzled activation of Rho regulates vertebrate gastrulation and requires a novel Formin homology protein Daam1. Cell *107*, 843-854.
Harkiolaki, M., Tsirka, T., Lewitzky, M., Simister, P.C., Joshi, D., Bird, L.E., Jones, E.Y., O'Reilly, N., and Feller, S.M. (2009). Distinct binding modes of two epitopes in Gab2 that interact with the SH3C domain of Grb2. Structure *17*, 809-822.

Hashimoto, M., Shinohara, K., Wang, J., Ikeuchi, S., Yoshiba, S., Meno, C., Nonaka, S., Takada, S., Hatta, K., Wynshaw-Boris, A.*, et al.* (2010). Planar polarization of node cells determines the rotational axis of node cilia. Nat Cell Biol *12*, 170-176.
Hatch, E.M., Kulukian, A., Holland, A.J., Cleveland, D.W., and Stearns, T. (2010). Cep152 interacts with Plk4 and is required for centriole duplication. The Journal of cell biology *191*, 721-729.
Haycraft, C.J., Banizs, B., Aydin-Son, Y., Zhang, Q., Michaud, E.J., and Yoder, B.K. (2005). Gli2 and Gli3 localize to cilia and require the intraflagellar transport protein polaris for processing and function. PLoS genetics *1*, e53.
Hendrickx, A., Beullens, M., Ceulemans, H., Den Abt, T., Van Eynde, A., Nicolaescu, E., Lesage, B., and Bollen, M. (2009). Docking motif-guided mapping of the interactome of protein phosphatase-1. Chemistry & biology *16*, 365-371.
Hensen, V. (1876). Beobachtungen über die Befruchtung und Entwicklung des Kaninchens und Meerschweinchens. Z Anat Entw-Gesch *1*, 213.
Hildebrandt, F., Benzing, T., and Katsanis, N. (2011). Ciliopathies. The New England journal of medicine *364*, 1533-1543.
Hirota, Y., Meunier, A., Huang, S., Shimozawa, T., Yamada, O., Kida, Y.S., Inoue, M., Ito, T., Kato, H., Sakaguchi, M.*, et al.* (2010). Planar polarity of multiciliated ependymal cells involves the anterior migration of basal bodies regulated by non-muscle myosin II. Development *137*, 3037-3046.
Hitz, C., Wurst, W., and Kuhn, R. (2007). Conditional brain-specific knockdown of MAPK using Cre/loxP regulated RNA interference. Nucleic Acids Res *35*, e90.
Horikoshi, Y., Suzuki, A., Yamanaka, T., Sasaki, K., Mizuno, K., Sawada, H., Yonemura, S., and Ohno, S. (2009). Interaction between PAR-3 and the aPKC-PAR-6 complex is indispensable for apical domain development of epithelial cells. Journal of cell science *122*, 1595-1606.
Horn, S., Kobberup, S., Jorgensen, M.C., Kalisz, M., Klein, T., Kageyama, R., Gegg, M., Lickert, H., Lindner, J., Magnuson, M.A.*, et al.* (2012). Mind bomb 1 is required for pancreatic beta-cell formation. Proceedings of the National Academy of Sciences of the United States of America *109*, 7356-7361.
Hoyer-Fender, S. (2010). Centriole maturation and transformation to basal body. Seminars in cell & developmental biology *21*, 142-147.
Huangfu, D., Liu, A., Rakeman, A.S., Murcia, N.S., Niswander, L., and Anderson, K.V. (2003). Hedgehog signalling in the mouse requires intraflagellar transport proteins. Nature *426*, 83-87.
Hurd, T.W., Gao, L., Roh, M.H., Macara, I.G., and Margolis, B. (2003). Direct interaction of two polarity complexes implicated in epithelial tight junction assembly. Nat Cell Biol *5*, 137-142.
Ito, M., Liu, Y., Yang, Z., Nguyen, J., Liang, F., Morris, R.J., and Cotsarelis, G. (2005). Stem cells in the hair follicle bulge contribute to wound repair but not to homeostasis of the epidermis. Nature medicine *11*, 1351-1354.
Izumi, Y., Hirose, T., Tamai, Y., Hirai, S., Nagashima, Y., Fujimoto, T., Tabuse, Y., Kemphues, K.J., and Ohno, S. (1998). An atypical PKC directly associates and colocalizes at the epithelial tight junction with ASIP, a mammalian homologue of Caenorhabditis elegans polarity protein PAR-3. The Journal of cell biology *143*, 95-106.
Jenkins, P.M., McEwen, D.P., and Martens, J.R. (2009). Olfactory cilia: linking sensory cilia function and human disease. Chemical senses *34*, 451-464.
Jessen, J.R., Topczewski, J., Bingham, S., Sepich, D.S., Marlow, F., Chandrasekhar, A., and Solnica-Krezel, L. (2002). Zebrafish trilobite identifies new roles for Strabismus in gastrulation and neuronal movements. Nat Cell Biol *4*, 610-615.
Jones, C., and Chen, P. (2008). Primary cilia in planar cell polarity regulation of the inner ear. Current topics in developmental biology *85*, 197-224.
Jones, C., Roper, V.C., Foucher, I., Qian, D., Banizs, B., Petit, C., Yoder, B.K., and Chen, P. (2008). Ciliary proteins link basal body polarization to planar cell polarity regulation. Nature genetics *40*, 69-77.

Karner, C.M., Chirumamilla, R., Aoki, S., Igarashi, P., Wallingford, J.B., and Carroll, T.J. (2009). Wnt9b signaling regulates planar cell polarity and kidney tubule morphogenesis. Nature genetics *41*, 793-799.

Kawamoto, S., Niwa, H., Tashiro, F., Sano, S., Kondoh, G., Takeda, J., Tabayashi, K., and Miyazaki, J. (2000). A novel reporter mouse strain that expresses enhanced green fluorescent protein upon Cre-mediated recombination. FEBS letters *470*, 263-268.

Kelley, M.W. (2006). Regulation of cell fate in the sensory epithelia of the inner ear. Nature reviews Neuroscience *7*, 837-849.

Khodjakov, A., Rieder, C.L., Sluder, G., Cassels, G., Sibon, O., and Wang, C.L. (2002). De novo formation of centrosomes in vertebrate cells arrested during S phase. The Journal of cell biology *158*, 1171-1181.

Kikuchi, A., Yamamoto, H., and Sato, A. (2009). Selective activation mechanisms of Wnt signaling pathways. Trends in cell biology *19*, 119-129.

Kim, S.K., Shindo, A., Park, T.J., Oh, E.C., Ghosh, S., Gray, R.S., Lewis, R.A., Johnson, C.A., Attie-Bittach, T., Katsanis, N.*, et al.* (2010). Planar cell polarity acts through septins to control collective cell movement and ciliogenesis. Science *329*, 1337-1340.

Kimura-Yoshida, C., Tian, E., Nakano, H., Amazaki, S., Shimokawa, K., Rossant, J., Aizawa, S., and Matsuo, I. (2007). Crucial roles of Foxa2 in mouse anterior-posterior axis polarization via regulation of anterior visceral endoderm-specific genes. Proceedings of the National Academy of Sciences of the United States of America *104*, 5919-5924.

Kinder, S.J., Tsang, T.E., Wakamiya, M., Sasaki, H., Behringer, R.R., Nagy, A., and Tam, P.P. (2001). The organizer of the mouse gastrula is composed of a dynamic population of progenitor cells for the axial mesoderm. Development *128*, 3623-3634.

Kinzel, D., Boldt, K., Davis, E.E., Burtscher, I., Trumbach, D., Diplas, B., Attie-Bitach, T., Wurst, W., Katsanis, N., Ueffing, M.*, et al.* (2010). Pitchfork regulates primary cilia disassembly and left-right asymmetry. Dev Cell *19*, 66-77.

Klein, T.J., and Mlodzik, M. (2005). Planar cell polarization: an emerging model points in the right direction. Annual review of cell and developmental biology *21*, 155-176.

Kohjima, M., Noda, Y., Takeya, R., Saito, N., Takeuchi, K., and Sumimoto, H. (2002). PAR3beta, a novel homologue of the cell polarity protein PAR3, localizes to tight junctions. Biochemical and biophysical research communications *299*, 641-646.

Kulaga, H.M., Leitch, C.C., Eichers, E.R., Badano, J.L., Lesemann, A., Hoskins, B.E., Lupski, J.R., Beales, P.L., Reed, R.R., and Katsanis, N. (2004). Loss of BBS proteins causes anosmia in humans and defects in olfactory cilia structure and function in the mouse. Nature genetics *36*, 994-998.

Lafont, F., Burkhardt, J.K., and Simons, K. (1994). Involvement of microtubule motors in basolateral and apical transport in kidney cells. Nature *372*, 801-803.

Lai, E., Prezioso, V.R., Smith, E., Litvin, O., Costa, R.H., and Darnell, J.E., Jr. (1990). HNF-3A, a hepatocyte-enriched transcription factor of novel structure is regulated transcriptionally. Genes & development *4*, 1427-1436.

Lai, E., Prezioso, V.R., Tao, W.F., Chen, W.S., and Darnell, J.E., Jr. (1991). Hepatocyte nuclear factor 3 alpha belongs to a gene family in mammals that is homologous to the Drosophila homeotic gene fork head. Genes & development *5*, 416-427.

Lange, A., Gegg, M., Burtscher, I., Bengel, D., Kremmer, E., and Lickert, H. (2012). Fltp(T2AiCre): a new knock-in mouse line for conditional gene targeting in distinct mono- and multiciliated tissues. Differentiation; research in biological diversity *83*, S105-113.

Lanzetti, L. (2007). Actin in membrane trafficking. Current opinion in cell biology *19*, 453-458.

Lawrence, P.A., Struhl, G., and Casal, J. (2007). Planar cell polarity: one or two pathways? Nature reviews Genetics *8*, 555-563.

Lee, E.C., Yu, D., Martinez de Velasco, J., Tessarollo, L., Swing, D.A., Court, D.L., Jenkins, N.A., and Copeland, N.G. (2001). A highly efficient Escherichia coli-based chromosome engineering system adapted for recombinogenic targeting and subcloning of BAC DNA. Genomics *73*, 56-65.

Lemmers, C., Michel, D., Lane-Guermonprez, L., Delgrossi, M.H., Medina, E., Arsanto, J.P., and Le Bivic, A. (2004). CRB3 binds directly to Par6 and regulates the morphogenesis of the tight junctions in mammalian epithelial cells. Molecular biology of the cell *15*, 1324-1333.
Liao, W.P., Uetzmann, L., Burtscher, I., and Lickert, H. (2009). Generation of a mouse line expressing Sox17-driven Cre recombinase with specific activity in arteries. Genesis *47*, 476-483.
Liu, P., Jenkins, N.A., and Copeland, N.G. (2003). A highly efficient recombineering-based method for generating conditional knockout mutations. Genome Res *13*, 476-484.
Lock, L.S., Royal, I., Naujokas, M.A., and Park, M. (2000). Identification of an atypical Grb2 carboxyl-terminal SH3 domain binding site in Gab docking proteins reveals Grb2-dependent and -independent recruitment of Gab1 to receptor tyrosine kinases. The Journal of biological chemistry *275*, 31536-31545.
Logan, C.Y., and Nusse, R. (2004). The Wnt signaling pathway in development and disease. Annual review of cell and developmental biology *20*, 781-810.
Luders, J., and Stearns, T. (2007). Microtubule-organizing centres: a re-evaluation. Nature reviews Molecular cell biology *8*, 161-167.
Ma, D., Yang, C.H., McNeill, H., Simon, M.A., and Axelrod, J.D. (2003). Fidelity in planar cell polarity signalling. Nature *421*, 543-547.
Marlow, F., Topczewski, J., Sepich, D., and Solnica-Krezel, L. (2002). Zebrafish Rho kinase 2 acts downstream of Wnt11 to mediate cell polarity and effective convergence and extension movements. Curr Biol *12*, 876-884.
Marshall, W.F., and Kintner, C. (2008). Cilia orientation and the fluid mechanics of development. Current opinion in cell biology *20*, 48-52.
Martin, G.R. (1981). Isolation of a pluripotent cell line from early mouse embryos cultured in medium conditioned by teratocarcinoma stem cells. Proceedings of the National Academy of Sciences of the United States of America *78*, 7634-7638.
Mathew, D., Gramates, L.S., Packard, M., Thomas, U., Bilder, D., Perrimon, N., Gorczyca, M., and Budnik, V. (2002). Recruitment of scribble to the synaptic scaffolding complex requires GUK-holder, a novel DLG binding protein. Curr Biol *12*, 531-539.
McClintock, T.S., Glasser, C.E., Bose, S.C., and Bergman, D.A. (2008). Tissue expression patterns identify mouse cilia genes. Physiological genomics *32*, 198-206.
McGrath, J., Somlo, S., Makova, S., Tian, X., and Brueckner, M. (2003). Two populations of node monocilia initiate left-right asymmetry in the mouse. Cell *114*, 61-73.
McMahon, A.P., Ingham, P.W., and Tabin, C.J. (2003). Developmental roles and clinical significance of hedgehog signaling. Current topics in developmental biology *53*, 1-114.
Medina, E., Lemmers, C., Lane-Guermonprez, L., and Le Bivic, A. (2002). Role of the Crumbs complex in the regulation of junction formation in Drosophila and mammalian epithelial cells. Biology of the cell / under the auspices of the European Cell Biology Organization *94*, 305-313.
Merte, J., Jensen, D., Wright, K., Sarsfield, S., Wang, Y., Schekman, R., and Ginty, D.D. (2010). Sec24b selectively sorts Vangl2 to regulate planar cell polarity during neural tube closure. Nat Cell Biol *12*, 41-46; sup pp 41-48.
Metzger, R.J., Klein, O.D., Martin, G.R., and Krasnow, M.A. (2008). The branching programme of mouse lung development. Nature *453*, 745-750.
Mirzadeh, Z., Han, Y.G., Soriano-Navarro, M., Garcia-Verdugo, J.M., and Alvarez-Buylla, A. (2010). Cilia organize ependymal planar polarity. The Journal of neuroscience : the official journal of the Society for Neuroscience *30*, 2600-2610.
Mitchell, B., Stubbs, J.L., Huisman, F., Taborek, P., Yu, C., and Kintner, C. (2009). The PCP pathway instructs the planar orientation of ciliated cells in the Xenopus larval skin. Curr Biol *19*, 924-929.
Mombaerts, P. (2004). Genes and ligands for odorant, vomeronasal and taste receptors. Nature reviews Neuroscience *5*, 263-278.
Monaghan, A.P., Kaestner, K.H., Grau, E., and Schutz, G. (1993). Postimplantation expression patterns indicate a role for the mouse forkhead/HNF-3 alpha, beta and gamma genes in determination of the definitive endoderm, chordamesoderm and neuroectoderm. Development *119*, 567-578.

Montcouquiol, M., Rachel, R.A., Lanford, P.J., Copeland, N.G., Jenkins, N.A., and Kelley, M.W. (2003). Identification of Vangl2 and Scrb1 as planar polarity genes in mammals. Nature *423*, 173-177.
Montcouquiol, M., Sans, N., Huss, D., Kach, J., Dickman, J.D., Forge, A., Rachel, R.A., Copeland, N.G., Jenkins, N.A., Bogani, D.*, et al.* (2006). Asymmetric localization of Vangl2 and Fz3 indicate novel mechanisms for planar cell polarity in mammals. The Journal of neuroscience : the official journal of the Society for Neuroscience *26*, 5265-5275.
Morrisey, E.E., and Hogan, B.L. (2010). Preparing for the first breath: genetic and cellular mechanisms in lung development. Dev Cell *18*, 8-23.
Murillas, R., Simms, K.S., Hatakeyama, S., Weissman, A.M., and Kuehn, M.R. (2002). Identification of developmentally expressed proteins that functionally interact with Nedd4 ubiquitin ligase. The Journal of biological chemistry *277*, 2897-2907.
Nagai-Tamai, Y., Mizuno, K., Hirose, T., Suzuki, A., and Ohno, S. (2002). Regulated protein-protein interaction between aPKC and PAR-3 plays an essential role in the polarization of epithelial cells. Genes to cells : devoted to molecular & cellular mechanisms *7*, 1161-1171.
Nagy, A. (2000). Cre recombinase: the universal reagent for genome tailoring. Genesis *26*, 99-109.
Nakaya, M.A., Biris, K., Tsukiyama, T., Jaime, S., Rawls, J.A., and Yamaguchi, T.P. (2005). Wnt3a links left-right determination with segmentation and anteroposterior axis elongation. Development *132*, 5425-5436.
Nakhai, H., Siveke, J.T., Klein, B., Mendoza-Torres, L., Mazur, P.K., Algul, H., Radtke, F., Strobl, L., Zimber-Strobl, U., and Schmid, R.M. (2008). Conditional ablation of Notch signaling in pancreatic development. Development *135*, 2757-2765.
Navarro, C., Nola, S., Audebert, S., Santoni, M.J., Arsanto, J.P., Ginestier, C., Marchetto, S., Jacquemier, J., Isnardon, D., Le Bivic, A.*, et al.* (2005). Junctional recruitment of mammalian Scribble relies on E-cadherin engagement. Oncogene *24*, 4330-4339.
Niwa, H., Toyooka, Y., Shimosato, D., Strumpf, D., Takahashi, K., Yagi, R., and Rossant, J. (2005). Interaction between Oct3/4 and Cdx2 determines trophectoderm differentiation. Cell *123*, 917-929.
Nonaka, S., Tanaka, Y., Okada, Y., Takeda, S., Harada, A., Kanai, Y., Kido, M., and Hirokawa, N. (1998). Randomization of left-right asymmetry due to loss of nodal cilia generating leftward flow of extraembryonic fluid in mice lacking KIF3B motor protein. Cell *95*, 829-837.
Nonaka, S., Yoshiba, S., Watanabe, D., Ikeuchi, S., Goto, T., Marshall, W.F., and Hamada, H. (2005). De novo formation of left-right asymmetry by posterior tilt of nodal cilia. PLoS biology *3*, e268.
Odom, D.T., Dowell, R.D., Jacobsen, E.S., Nekludova, L., Rolfe, P.A., Danford, T.W., Gifford, D.K., Fraenkel, E., Bell, G.I., and Young, R.A. (2006). Core transcriptional regulatory circuitry in human hepatocytes. Molecular systems biology *2*, 2006 0017.
Oishi, I., Suzuki, H., Onishi, N., Takada, R., Kani, S., Ohkawara, B., Koshida, I., Suzuki, K., Yamada, G., Schwabe, G.C.*, et al.* (2003). The receptor tyrosine kinase Ror2 is involved in non-canonical Wnt5a/JNK signalling pathway. Genes to cells : devoted to molecular & cellular mechanisms *8*, 645-654.
Okubo, T., and Hogan, B.L. (2004). Hyperactive Wnt signaling changes the developmental potential of embryonic lung endoderm. Journal of biology *3*, 11.
Park, E.J., Sun, X., Nichol, P., Saijoh, Y., Martin, J.F., and Moon, A.M. (2008a). System for tamoxifen-inducible expression of cre-recombinase from the Foxa2 locus in mice. Developmental dynamics : an official publication of the American Association of Anatomists *237*, 447-453.
Park, T.J., Mitchell, B.J., Abitua, P.B., Kintner, C., and Wallingford, J.B. (2008b). Dishevelled controls apical docking and planar polarization of basal bodies in ciliated epithelial cells. Nature genetics *40*, 871-879.
Paudyal, A., Damrau, C., Patterson, V.L., Ermakov, A., Formstone, C., Lalanne, Z., Wells, S., Lu, X., Norris, D.P., Dean, C.H.*, et al.* (2010). The novel mouse mutant, chuzhoi, has disruption of Ptk7 protein and exhibits defects in neural tube, heart and lung development and abnormal planar cell polarity in the ear. BMC developmental biology *10*, 87.

Pazour, G.J., Dickert, B.L., Vucica, Y., Seeley, E.S., Rosenbaum, J.L., Witman, G.B., and Cole, D.G. (2000). Chlamydomonas IFT88 and its mouse homologue, polycystic kidney disease gene tg737, are required for assembly of cilia and flagella. The Journal of cell biology *151*, 709-718.
Perea-Gomez, A., Vella, F.D., Shawlot, W., Oulad-Abdelghani, M., Chazaud, C., Meno, C., Pfister, V., Chen, L., Robertson, E., Hamada, H.*, et al.* (2002). Nodal antagonists in the anterior visceral endoderm prevent the formation of multiple primitive streaks. Dev Cell *3*, 745-756.
Phillips, B.T., Gassei, K., and Orwig, K.E. (2010). Spermatogonial stem cell regulation and spermatogenesis. Philosophical transactions of the Royal Society of London Series B, Biological sciences *365*, 1663-1678.
Piccolo, S., Agius, E., Leyns, L., Bhattacharyya, S., Grunz, H., Bouwmeester, T., and De Robertis, E.M. (1999). The head inducer Cerberus is a multifunctional antagonist of Nodal, BMP and Wnt signals. Nature *397*, 707-710.
Plant, P.J., Fawcett, J.P., Lin, D.C., Holdorf, A.D., Binns, K., Kulkarni, S., and Pawson, T. (2003). A polarity complex of mPar-6 and atypical PKC binds, phosphorylates and regulates mammalian Lgl. Nat Cell Biol *5*, 301-308.
Pringle, F.M., Gordon, K.H., Hanzlik, T.N., Kalmakoff, J., Scotti, P.D., and Ward, V.K. (1999). A novel capsid expression strategy for Thosea asigna virus (Tetraviridae). The Journal of general virology *80 (Pt 7)*, 1855-1863.
Qian, D., Jones, C., Rzadzinska, A., Mark, S., Zhang, X., Steel, K.P., Dai, X., and Chen, P. (2007). Wnt5a functions in planar cell polarity regulation in mice. Developmental biology *306*, 121-133.
Que, J., Choi, M., Ziel, J.W., Klingensmith, J., and Hogan, B.L. (2006). Morphogenesis of the trachea and esophagus: current players and new roles for noggin and Bmps. Differentiation; research in biological diversity *74*, 422-437.
Rawlins, E.L., Clark, C.P., Xue, Y., and Hogan, B.L. (2009a). The Id2+ distal tip lung epithelium contains individual multipotent embryonic progenitor cells. Development *136*, 3741-3745.
Rawlins, E.L., Okubo, T., Xue, Y., Brass, D.M., Auten, R.L., Hasegawa, H., Wang, F., and Hogan, B.L. (2009b). The role of Scgb1a1+ Clara cells in the long-term maintenance and repair of lung airway, but not alveolar, epithelium. Cell stem cell *4*, 525-534.
Rawlins, E.L., Ostrowski, L.E., Randell, S.H., and Hogan, B.L. (2007). Lung development and repair: contribution of the ciliated lineage. Proceedings of the National Academy of Sciences of the United States of America *104*, 410-417.
Rock, J.R., and Hogan, B.L. (2011). Epithelial progenitor cells in lung development, maintenance, repair, and disease. Annual review of cell and developmental biology *27*, 493-512.
Rock, J.R., Onaitis, M.W., Rawlins, E.L., Lu, Y., Clark, C.P., Xue, Y., Randell, S.H., and Hogan, B.L. (2009). Basal cells as stem cells of the mouse trachea and human airway epithelium. Proceedings of the National Academy of Sciences of the United States of America *106*, 12771-12775.
Rock, J.R., Randell, S.H., and Hogan, B.L. (2010). Airway basal stem cells: a perspective on their roles in epithelial homeostasis and remodeling. Disease models & mechanisms *3*, 545-556.
Rodrigues-Martins, A., Bettencourt-Dias, M., Riparbelli, M., Ferreira, C., Ferreira, I., Callaini, G., and Glover, D.M. (2007). DSAS-6 organizes a tube-like centriole precursor, and its absence suggests modularity in centriole assembly. Curr Biol *17*, 1465-1472.
Rosenbaum, J.L., and Witman, G.B. (2002). Intraflagellar transport. Nature reviews Molecular cell biology *3*, 813-825.
Ross, A.J., May-Simera, H., Eichers, E.R., Kai, M., Hill, J., Jagger, D.J., Leitch, C.C., Chapple, J.P., Munro, P.M., Fisher, S.*, et al.* (2005). Disruption of Bardet-Biedl syndrome ciliary proteins perturbs planar cell polarity in vertebrates. Nature genetics *37*, 1135-1140.
Rovira, M., Scott, S.G., Liss, A.S., Jensen, J., Thayer, S.P., and Leach, S.D. (2010). Isolation and characterization of centroacinar/terminal ductal progenitor cells in adult mouse pancreas. Proceedings of the National Academy of Sciences of the United States of America *107*, 75-80.
Rubel, E.W., and Fritzsch, B. (2002). Auditory system development: primary auditory neurons and their targets. Annual review of neuroscience *25*, 51-101.

Ryan, M.D., and Drew, J. (1994). Foot-and-mouth disease virus 2A oligopeptide mediated cleavage of an artificial polyprotein. The EMBO journal *13*, 928-933.
Sans, N., Prybylowski, K., Petralia, R.S., Chang, K., Wang, Y.X., Racca, C., Vicini, S., and Wenthold, R.J. (2003). NMDA receptor trafficking through an interaction between PDZ proteins and the exocyst complex. Nat Cell Biol *5*, 520-530.
Santos, N., and Reiter, J.F. (2010). Tilting at nodal windmills: planar cell polarity positions cilia to tell left from right. Dev Cell *19*, 5-6.
Sasaki, H., and Hogan, B.L. (1993). Differential expression of multiple fork head related genes during gastrulation and axial pattern formation in the mouse embryo. Development *118*, 47-59.
Sasaki, H., Hui, C., Nakafuku, M., and Kondoh, H. (1997). A binding site for Gli proteins is essential for HNF-3beta floor plate enhancer activity in transgenics and can respond to Shh in vitro. Development *124*, 1313-1322.
Sato, T., van Es, J.H., Snippert, H.J., Stange, D.E., Vries, R.G., van den Born, M., Barker, N., Shroyer, N.F., van de Wetering, M., and Clevers, H. (2011). Paneth cells constitute the niche for Lgr5 stem cells in intestinal crypts. Nature *469*, 415-418.
Schneider, L., Clement, C.A., Teilmann, S.C., Pazour, G.J., Hoffmann, E.K., Satir, P., and Christensen, S.T. (2005). PDGFRalphaalpha signaling is regulated through the primary cilium in fibroblasts. Curr Biol *15*, 1861-1866.
Shih, J., and Fraser, S.E. (1996). Characterizing the zebrafish organizer: microsurgical analysis at the early-shield stage. Development *122*, 1313-1322.
Shima, Y., Copeland, N.G., Gilbert, D.J., Jenkins, N.A., Chisaka, O., Takeichi, M., and Uemura, T. (2002). Differential expression of the seven-pass transmembrane cadherin genes Celsr1-3 and distribution of the Celsr2 protein during mouse development. Developmental dynamics : an official publication of the American Association of Anatomists *223*, 321-332.
Shimada, Y., Yonemura, S., Ohkura, H., Strutt, D., and Uemura, T. (2006). Polarized transport of Frizzled along the planar microtubule arrays in Drosophila wing epithelium. Dev Cell *10*, 209-222.
Shimshek, D.R., Kim, J., Hubner, M.R., Spergel, D.J., Buchholz, F., Casanova, E., Stewart, A.F., Seeburg, P.H., and Sprengel, R. (2002). Codon-improved Cre recombinase (iCre) expression in the mouse. Genesis *32*, 19-26.
Shin, K., Fogg, V.C., and Margolis, B. (2006). Tight junctions and cell polarity. Annual review of cell and developmental biology *22*, 207-235.
Shinohara, K., Kawasumi, A., Takamatsu, A., Yoshiba, S., Botilde, Y., Motoyama, N., Reith, W., Durand, B., Shiratori, H., and Hamada, H. (2012). Two rotating cilia in the node cavity are sufficient to break left-right symmetry in the mouse embryo. Nature communications *3*, 622.
Smukler, S.R., Arntfield, M.E., Razavi, R., Bikopoulos, G., Karpowicz, P., Seaberg, R., Dai, F., Lee, S., Ahrens, R., Fraser, P.E*., et al.* (2011). The adult mouse and human pancreas contain rare multipotent stem cells that express insulin. Cell stem cell *8*, 281-293.
Song, H., Hu, J., Chen, W., Elliott, G., Andre, P., Gao, B., and Yang, Y. (2010). Planar cell polarity breaks bilateral symmetry by controlling ciliary positioning. Nature *466*, 378-382.
Soriano, P. (1999). Generalized lacZ expression with the ROSA26 Cre reporter strain. Nature genetics *21*, 70-71.
Sorokin, S.P. (1968). Reconstructions of centriole formation and ciliogenesis in mammalian lungs. Journal of cell science *3*, 207-230.
Sotillos, S., Diaz-Meco, M.T., Caminero, E., Moscat, J., and Campuzano, S. (2004). DaPKC-dependent phosphorylation of Crumbs is required for epithelial cell polarity in Drosophila. The Journal of cell biology *166*, 549-557.
Spemann, H., and Mangold, H. (1924). über Induktion von Embryonalanlagen durch Implantation artfremder Organisatoren. Development genes and evolution *100*, 599-638.
Strutt, D.I., Weber, U., and Mlodzik, M. (1997). The role of RhoA in tissue polarity and Frizzled signalling. Nature *387*, 292-295.
Supp, D.M., Witte, D.P., Potter, S.S., and Brueckner, M. (1997). Mutation of an axonemal dynein affects left-right asymmetry in inversus viscerum mice. Nature *389*, 963-966.

Tam, P.P., Steiner, K.A., Zhou, S.X., and Quinlan, G.A. (1997). Lineage and functional analyses of the mouse organizer. Cold Spring Harbor symposia on quantitative biology *62*, 135-144.
Tamplin, O.J., Kinzel, D., Cox, B.J., Bell, C.E., Rossant, J., and Lickert, H. (2008). Microarray analysis of Foxa2 mutant mouse embryos reveals novel gene expression and inductive roles for the gastrula organizer and its derivatives. BMC Genomics *9*, 511.
Tarpey, P., Parnau, J., Blow, M., Woffendin, H., Bignell, G., Cox, C., Cox, J., Davies, H., Edkins, S., Holden, S.*, et al.* (2004). Mutations in the DLG3 gene cause nonsyndromic X-linked mental retardation. American journal of human genetics *75*, 318-324.
Tissir, F., De-Backer, O., Goffinet, A.M., and Lambert de Rouvroit, C. (2002). Developmental expression profiles of Celsr (Flamingo) genes in the mouse. Mechanisms of development *112*, 157-160.
Tissir, F., Qu, Y., Montcouquiol, M., Zhou, L., Komatsu, K., Shi, D., Fujimori, T., Labeau, J., Tyteca, D., Courtoy, P.*, et al.* (2010). Lack of cadherins Celsr2 and Celsr3 impairs ependymal ciliogenesis, leading to fatal hydrocephalus. Nature neuroscience *13*, 700-707.
Todaro, G.J., and Green, H. (1963). Quantitative studies of the growth of mouse embryo cells in culture and their development into established lines. The Journal of cell biology *17*, 299-313.
Toskala, E., Smiley-Jewell, S.M., Wong, V.J., King, D., and Plopper, C.G. (2005). Temporal and spatial distribution of ciliogenesis in the tracheobronchial airways of mice. American journal of physiology Lung cellular and molecular physiology *289*, L454-459.
Traweger, A., Wiggin, G., Taylor, L., Tate, S.A., Metalnikov, P., and Pawson, T. (2008). Protein phosphatase 1 regulates the phosphorylation state of the polarity scaffold Par-3. Proceedings of the National Academy of Sciences of the United States of America *105*, 10402-10407.
Tsou, M.F., and Stearns, T. (2006). Mechanism limiting centrosome duplication to once per cell cycle. Nature *442*, 947-951.
Tsukita, S., Katsuno, T., Yamazaki, Y., Umeda, K., and Tamura, A. (2009). Roles of ZO-1 and ZO-2 in establishment of the belt-like adherens and tight junctions with paracellular permselective barrier function. Annals of the New York Academy of Sciences *1165*, 44-52.
Uetzmann, L., Burtscher, I., and Lickert, H. (2008). A mouse line expressing Foxa2-driven Cre recombinase in node, notochord, floorplate, and endoderm. Genesis *46*, 515-522.
Van Campenhout, C.A., Eitelhuber, A., Gloeckner, C.J., Giallonardo, P., Gegg, M., Oller, H., Grant, S.G., Krappmann, D., Ueffing, M., and Lickert, H. (2011). Dlg3 trafficking and apical tight junction formation is regulated by nedd4 and nedd4-2 e3 ubiquitin ligases. Dev Cell *21*, 479-491.
Vladar, E.K., and Stearns, T. (2007). Molecular characterization of centriole assembly in ciliated epithelial cells. The Journal of cell biology *178*, 31-42.
Waddington, C.H., and Waterman, A.J. (1933). The Development in vitro of Young Rabbit Embryos. Journal of anatomy *67*, 355-370.
Wallingford, J.B. (2006). Planar cell polarity, ciliogenesis and neural tube defects. Hum Mol Genet *15 Spec No 2*, R227-234.
Wallingford, J.B., and Mitchell, B. (2011). Strange as it may seem: the many links between Wnt signaling, planar cell polarity, and cilia. Genes & development *25*, 201-213.
Wallingford, J.B., Rowning, B.A., Vogeli, K.M., Rothbacher, U., Fraser, S.E., and Harland, R.M. (2000). Dishevelled controls cell polarity during Xenopus gastrulation. Nature *405*, 81-85.
Wan, H., Xu, Y., Ikegami, M., Stahlman, M.T., Kaestner, K.H., Ang, S.L., and Whitsett, J.A. (2004). Foxa2 is required for transition to air breathing at birth. Proceedings of the National Academy of Sciences of the United States of America *101*, 14449-14454.
Wang, B., Sinha, T., Jiao, K., Serra, R., and Wang, J. (2011). Disruption of PCP signaling causes limb morphogenesis and skeletal defects and may underlie Robinow syndrome and brachydactyly type B. Hum Mol Genet *20*, 271-285.
Wang, J., Mark, S., Zhang, X., Qian, D., Yoo, S.J., Radde-Gallwitz, K., Zhang, Y., Lin, X., Collazo, A., Wynshaw-Boris, A.*, et al.* (2005). Regulation of polarized extension and planar cell polarity in the cochlea by the vertebrate PCP pathway. Nature genetics *37*, 980-985.

Wang, Y., Guo, N., and Nathans, J. (2006). The role of Frizzled3 and Frizzled6 in neural tube closure and in the planar polarity of inner-ear sensory hair cells. The Journal of neuroscience : the official journal of the Society for Neuroscience *26*, 2147-2156.
Wansleeben, C., Feitsma, H., Montcouquiol, M., Kroon, C., Cuppen, E., and Meijlink, F. (2010). Planar cell polarity defects and defective Vangl2 trafficking in mutants for the COPII gene Sec24b. Development *137*, 1067-1073.
Warming, S., Costantino, N., Court, D.L., Jenkins, N.A., and Copeland, N.G. (2005). Simple and highly efficient BAC recombineering using galK selection. Nucleic Acids Res *33*, e36.
Weinstein, D.C., Ruiz i Altaba, A., Chen, W.S., Hoodless, P., Prezioso, V.R., Jessell, T.M., and Darnell, J.E., Jr. (1994). The winged-helix transcription factor HNF-3 beta is required for notochord development in the mouse embryo. Cell *78*, 575-588.
Wetzel, R. (1925). Untersuchungen am Hühnerkeim. Development genes and evolution *106*, 463-468.
Wiles, M.V., Vauti, F., Otte, J., Fuchtbauer, E.M., Ruiz, P., Fuchtbauer, A., Arnold, H.H., Lehrach, H., Metz, T., von Melchner, H*., et al.* (2000). Establishment of a gene-trap sequence tag library to generate mutant mice from embryonic stem cells. Nature genetics *24*, 13-14.
Woods, D.F., Hough, C., Peel, D., Callaini, G., and Bryant, P.J. (1996). Dlg protein is required for junction structure, cell polarity, and proliferation control in Drosophila epithelia. The Journal of cell biology *134*, 1469-1482.
Yamanaka, T., Horikoshi, Y., Sugiyama, Y., Ishiyama, C., Suzuki, A., Hirose, T., Iwamatsu, A., Shinohara, A., and Ohno, S. (2003). Mammalian Lgl forms a protein complex with PAR-6 and aPKC independently of PAR-3 to regulate epithelial cell polarity. Curr Biol *13*, 734-743.
Yates, L.L., Schnatwinkel, C., Murdoch, J.N., Bogani, D., Formstone, C.J., Townsend, S., Greenfield, A., Niswander, L.A., and Dean, C.H. (2010). The PCP genes Celsr1 and Vangl2 are required for normal lung branching morphogenesis. Hum Mol Genet *19*, 2251-2267.
Yen, W.W., Williams, M., Periasamy, A., Conaway, M., Burdsal, C., Keller, R., Lu, X., and Sutherland, A. (2009). PTK7 is essential for polarized cell motility and convergent extension during mouse gastrulation. Development *136*, 2039-2048.
Zhang, Q., Seo, S., Bugge, K., Stone, E.M., and Sheffield, V.C. (2012). BBS proteins interact genetically with the IFT pathway to influence SHH-related phenotypes. Hum Mol Genet *21*, 1945-1953.
Zhou, W., Lin, L., Majumdar, A., Li, X., Zhang, X., Liu, W., Etheridge, L., Shi, Y., Martin, J., Van de Ven, W*., et al.* (2007). Modulation of morphogenesis by noncanonical Wnt signaling requires ATF/CREB family-mediated transcriptional activation of TGFbeta2. Nature genetics *39*, 1225-1234.
Zimmermann, K.W. (1898). Beiträge zur Kenntnis einiger Drüsen und Epithelien.

7 Supplement

7.1 Abbreviations

aa	amino acid
AB	apico-basolateral
ADE	anterior definitive endoderm
AEC	alveolar epithelial cells
Aer	apical ectodermal ridge
AJ	adherens junctions
AJC	apical junctional complex
ALI	air liquid interface
AME	anterior mesendoderm
aPKC	atypical protein kinase C
AVE	anterior visceral endoderm
BAC	bacterial artificial chromosome
BADJ	broncho-alveolar-duct junction
BB	basal body
BBS	Bardet-Biedl syndrome
BCA	Bicinchoninic acid
β-gal	β-galactosidase
BMP	bone morphogenetic protein
bp	base pair
BSA	bovine serum albumin
C	Celsius
CDC	cell division control
Cdx	caudal-related homeobox
CE	convergent extension
Cer	Cerberus
COP	coat protein complex
Cp	choroid plexus
Crb	Crumbs
CSF	cerebrospinal fluid
DE	definitive endoderm
Dkk	Dickkopf
Dlg	Discs large
DNA	deoxyribonucleic acid
DTT	Dithiothreitol
DVE	distal visceral endoderm
E	embryonic day
E1	exon one
EB	elution buffer
ECL	enhanced chemiluminescence
eGFP	enhanced green fluorescent protein
EMT	epithelial-mesenchymal transition

ENU	N-ethyl-N-nitrosourea
ER	endoplasmic reticulum
ES	embryonic stem
eYFP	enhanced yellow fluorescent protein
FACS	fluorescent activated cell sorting
FBS	fetal bovine serum
FGF	fibroblast growth factor
Flp-e	enhanced flippase
Fltp	Flattop
Fmi	Flamingo
Foxa2	forkhead box transcription factor a 2
fp	floorplate
FRT	Flp recombination target
Fwd	forward
Fz	Frizzled
G	generation
GGT	G1-G2 tether
GI	gastrointestinal
Gli	glioma
GUK	guanylate kinase-like
H2B	histone 2B
HEK	human embryonic kidney
Hex	haematopoetically expressed homeobox gene
HH	hedgehog
HNF	hepatocyte nuclear factor
HR	homology regions
HRP	horseradish peroxidase
ICM	inner cell mass
iCre	improved Cre recombinase
IE	inner ear
IFT	intraflagellar transport
IHC	inner hair cell
IMCD	inner medullary collecting duct
Inv	Inversin
IP	immunoprecipitation
IRES	internal ribosomal entry site
iv	inversus viscerus
JAM	junctional adhesion molecules
JAMA	junctional adhesion molecule A
kb	kilo base
LB	lysogeny broth
Lefty	left right determination factor
Lgl	Lethal giant larvae
LIF	leukemia inhibitory factor
LLB	left lung lobe
Lrd	left-right dynein

LRP	low-density lipoprotein receptor-related protein
LSM	laser scanning microscopy
MAGUK	membrane associated guanylate kinase
MDCK	Madin Darby canine kidney
MEF	murine embryonic fibroblast
MMC	mitomycin C
MOE	main olfactory epithelium
MT	microtubule
MTEC	murine tracheal epithelial cell
N_{2l}	liquid nitrogen
NC	notochord
Neo	neomycin
NFR	nuclear fast red
NLS	nuclear localization signal
NVP	nodal vesicular parcel
OCT	optimal cutting temperature
OHC	outer hair cell
ON	over night
ORF	open reading frame
OSN	olfactory sensory neuron
P	postnatal day
Par	partitioning-defective
pBKS	pBluescriptKS
PCM	pericentriolar material
PCP	planar cell polarity
PCR	polymerase chain reaction
PDGFR	platelet derived growth factor receptor
PDZ	postsynaptic density-95/Dlg/zonula occludens-1
PE	primitive endoderm
PFA	paraformaldehyde
Pifo	Pitchfork
PGK	phospho-glycerate kinase
PLK	polo like kinase
PMP	pancreatic-derived multipotent precursor
PRR	proline rich repeat
PS	primitive streak
R26R	ROSA26 reporter
RA	retinoic acid
Rev	reverse
RFLP	restriction length polymorphism
RMB	right main bronchus
RT	room temperature
SAG	statoacoustic ganglion
Scrib	scribble
SH3	SRC homology 3
Shh	sonic hedgehog

SJ	septate junctions
SML	S-M linker
Smo	Smoothened
SSC	saline-sodium citrate
SV40pA	Simian Virus 40 polyadenylation signal sequence
T2A	a 2A-like
T	brachyury
TAE	Tris-acetate, EDTA
TaV	*Thosea asigna* virus
TE	trophectoderm
TE	Tris, EDTA
TJ	tight junction
TSS	transcriptional start site
UTR	untranslated region
Vang	Van Gogh
VE	visceral endoderm
WISH	whole mount *in situ* hybridization
WT	wild type

7.2 Figures

7.3 Tables

8 Publications

Gegg, M., Böttcher, A., Burtscher, I., Hasenöder, S., Lickert, H.
Fltp is a novel planar cell polarity effector regulating inner ear and lung development.
Manuscript in preparation.

David, R., Jarsch, V.B., Schwarz, F., Nathan, P., Gegg, M., Lickert, H., and Franz, W.M. (2011). Induction of MesP1 by Brachyury(T) generates the common multipotent cardiovascular stem cell. Cardiovascular research.

Horn, S., Kobberup, S., Jorgensen, M.C., Kalisz, M., Klein, T., Kageyama, R., Gegg, M., Lickert, H., Lindner, J., Magnuson, M.A.*, et al.* (2012). Mind bomb 1 is required for pancreatic beta-cell formation. Proceedings of the National Academy of Sciences of the United States of America *109*, 7356-7361.

Lange, A., Gegg, M., Burtscher, I., Bengel, D., Kremmer, E., and Lickert, H. (2012). Fltp(T2AiCre): a new knock-in mouse line for conditional gene targeting in distinct mono- and multiciliated tissues. Differentiation; research in biological diversity *83*, S105-113.

Van Campenhout, C.A., Eitelhuber, A., Gloeckner, C.J., Giallonardo, P., Gegg, M., Oller, H., Grant, S.G., Krappmann, D., Ueffing, M., and Lickert, H. (2011). Dlg3 trafficking and apical tight junction formation is regulated by nedd4 and nedd4-2 e3 ubiquitin ligases. Dev Cell *21*, 479-491.